ISBN 92-64-01070-X NEA/WPEC-19

International Evaluation Co-operation

Volume 19

NEUTRON ACTIVATION CROSS-SECTION MEASUREMENTS FROM THRESHOLD TO 20 MEV FOR THE VALIDATION OF NUCLEAR MODELS AND THEIR PARAMETERS

A REPORT BY THE WORKING PARTY ON
INTERNATIONAL EVALUATION CO-OPERATION
OF THE NEA NUCLEAR SCIENCE COMMITTEE

Co-ordinator

A.J.M. Plompen
European Commission, Joint Research Centre, Institute for Reference Materials and Measurements, Retieseweg 111, 2440 Geel, Belgium

Monitors

M.B. Chadwick
Theoretical Division, Group T16, Los Alamos National Laboratory, Los Alamos, NM 87545, USA

A.J. Koning
Nuclear Research and Consultancy Group NRG, Westerduinweg 3, NL-1755 ZG Petten, The Netherlands

NUCLEAR ENERGY AGENCY
ORGANISATION FOR ECONOMIC CO-OPERATION AND DEVELOPMENT

ORGANISATION FOR ECONOMIC COOPERATION AND DEVELOPMENT

The OECD is a unique forum where the governments of 30 democracies work together to address the economic, social and environmental challenges of globalisation. The OECD is also at the forefront of efforts to understand and to help governments respond to new developments and concerns, such as corporate governance, the information economy and the challenges of an ageing population. The Organisation provides a setting where governments can compare policy experiences, seek answers to common problems, identify good practice and work to co-ordinate domestic and international policies.

The OECD member countries are: Australia, Austria, Belgium, Canada, the Czech Republic, Denmark, Finland, France, Germany, Greece, Hungary, Iceland, Ireland, Italy, Japan, Korea, Luxembourg, Mexico, the Netherlands, New Zealand, Norway, Poland, Portugal, the Slovak Republic, Spain, Sweden, Switzerland, Turkey, the United Kingdom and the United States. The Commission of the European Communities takes part in the work of the OECD.

OECD Publishing disseminates widely the results of the Organisation's statistics gathering and research on economic, social and environmental issues, as well as the conventions, guidelines and standards agreed by its members.

* * *

This work is published on the responsibility of the Secretary-General of the OECD. The opinions expressed and arguments employed herein do not necessarily reflect the official views of the Organisation or of the governments of its member countries.

NUCLEAR ENERGY AGENCY

The OECD Nuclear Energy Agency (NEA) was established on 1^{st} February 1958 under the name of the OEEC European Nuclear Energy Agency. It received its present designation on 20^{th} April 1972, when Japan became its first nonEuropean full member. NEA membership today consists of 28 OECD member countries: Australia, Austria, Belgium, Canada, the Czech Republic, Denmark, Finland, France, Germany, Greece, Hungary, Iceland, Ireland, Italy, Japan, Luxembourg, Mexico, the Netherlands, Norway, Portugal, the Republic of Korea, the Slovak Republic, Spain, Sweden, Switzerland, Turkey, the United Kingdom and the United States. The Commission of the European Communities also takes part in the work of the Agency.

The mission of the NEA is:

- to assist its member countries in maintaining and further developing, through international co-operation, the scientific, technological and legal bases required for a safe, environmentally friendly and economical use of nuclear energy for peaceful purposes, as well as
- to provide authoritative assessments and to forge common understandings on key issues as input to government decisions on nuclear energy policy and to broader OECD policy analyses in areas such as energy and sustainable development.

Specific areas of competence of the NEA include safety and regulation of nuclear activities, radioactive waste management, radiological protection, nuclear science, economic and technical analyses of the nuclear fuel cycle, nuclear law and liability, and public information. The NEA Data Bank provides nuclear data and computer program services for participating countries.

In these and related tasks, the NEA works in close collaboration with the International Atomic Energy Agency in Vienna, with which it has a Cooperation Agreement, as well as with other international organisations in the nuclear field.

Members of subgroup 19

A.J.M. Plompen, P. Reimer, A. Fessler
European Commission, DG Joint Research Centre, Institute for Reference Materials and Measurements, Retieseweg 111, 2440 Geel, Belgium

D.L. Smith
Special Term Appointee, Nuclear Data Program, Nuclear Engineering Division, Argonne National Laboratory, 1710 Avenida del Mundo #1506, Coronado, California 92118-3073, U.S.A.

V. Semkova
Institute for Nuclear Research and Nuclear Engineering, Bulgarian Academy of Sciences, 72 Tzarigradsko chaussee, Blvd., BG-1784 Sofia, Bulgaria

S.M. Qaim
Insitut für Nuklearchemie, Forschungszentrum Jülich GmbH, D-52425 Jülich, Germany

A.J. Koning
Nuclear Research and Consultancy Group NRG, Westerduinweg 3, NL-1755 ZG Petten, The Netherlands

M. Baba
Graduate School of Quantum Science & Energy Engineering, Tohoku University, 980-8579, Sendai, Japan

K. Shibata
Nuclear Data Center, Japanese Atomic Energy Research Institute, Tokai-mura, Naka-gun, Ibaraki-ken 319-1195, Japan

P. Oblozinsky and M. Herman
National Nuclear Data Center, Brookhaven National Laboratory, Upton, NY 11973-5000

M. Avrigeanu, V. Avrigeanu
"Horia Hulubei" National Institute for Nuclear Physics and Nuclear Engineering, PO Box MG-6, 76900 Bucharest, Romania

G. Csikai, F. Cserpák, R. Doczi, S. Sudár
Institute of Experimental Physics, University of Debrecen, H-4001 Debrecen, Hungary

R. Forrest
Culham Science Center, UKAEA, OX14 3DB, Abingdon, Oxfordshire, United Kingdom

J. Kopecky
Juko Research, Kalmanstraat 4, 1817 HX Alkmaar, The Netherlands

R. Capote Noy
Nuclear Data Section, International Atomic Energy Agency, Vienna, Austria

Table of Contents

Part A

Summary Report

1. INTRODUCTION

1.1 Neutron-induced activation cross-sections

Accurate knowledge of neutron-induced activation cross-sections is of interest to many fields of nuclear science. As neutron-induced activation cross-sections govern the rate of production of isomers and radioactive isotopes, these cross-sections are of immediate interest in estimating radiation levels and decay heat of materials that have been exposed to radiation fields with a strong neutron component [1]. Other prominent direct applications concern reactor, environmental and space dosimetry, material analysis and isotope production (e.g. [1–5] and references therein).

A rather large number of target nuclides exists for which measurements of cross-sections with the activation technique provide easy access to a variety of reaction channels. This allows for a quick experimental survey of the dominant reaction channels on many isotopes [6, 7]. However, any such survey necessarily contains gaps, for instance because reactions may lead to stable nuclei, or the reaction products have unfavourable decay properties, or a neutron energy range can not be addressed by the available irradiation facilities. The survey is therefore most valuable as a source of benchmark data to assess the quality and improve the performance of nuclear model codes and of evaluated cross-section data libraries. Thus, activation cross-section measurements may contribute significantly to our knowledge of scattering, neutron production and hydrogen and helium gas production cross-sections. As such, the range of applications includes, in addition to the abovementioned areas, also reactor safety, shielding and radiation damage.

The activation technique is selective for the residual nucleus. For ground state reaction products typically (but not always) total production cross-sections of the residual nucleus are determined, whereas isomeric state production cross-sections in addition probe our understanding of the level and decay structure of the residual nucleus. Often, samples that are irradiated contain a mix of isotopes of a given element so that selectivity for the residual nucleus implies a sum over different reaction channels. Examples are the ^{127}I$(n,\gamma)^{128}$I and ^{129}I$(n,2n)^{128}$I reactions for isotopes of iodine and for instance the ^{96}Mo$(n,p)^{96}$Nb and ^{97}Mo$(n,x)^{96}$Nb reactions for isotopes of molybdenum. Such a sum can be decomposed by combining measurements on two samples of different enrichments, eg. a natural Mo sample and a sample enriched in ^{96}Mo. Such a sum may also occur because

of a common decay daughter. This is the case for the ^{52}Cr$(n,2n)^{51}$Cr and ^{54}Cr$(n,\alpha)^{51}$Ti reactions in which both products decay to an excited state of ^{51}V that decays in turn by emission of a gamma ray with an energy of 320 keV. Here again two samples of different enrichments may be used, but since the residual nuclei differ, the difference in half lives or a weaker non-common decay radiation may be used to disentangle the contributions of the two reaction channels. Finally, reactions on isotopes of different elements may lead to the same residual nucleus, emphasising the need for high purity and well characterised samples (e.g. the ^{58}Ni$(n,p)^{58m}$Co and ^{59}Co$(n,2n)^{58m}$Co reactions).

Application of the activation technique is particularly fruitful if cross-sections are 1 mb or more, the radioactive product has a half life of several minutes to several days and its decay is accompanied by the emission of a gamma-ray in the range from 100 keV to several MeV and an intensity of 10% or more. In such cases the overall irradiation time, the total counting time and the sample transfer time between irradiation and activity determination are very favourable, allowing relatively large scale measurement programmes in a short span of time. Furthermore, the easy-to-use, highly selective and well established method of high-purity germanium (HPGe) spectrometry can then be used as the method of choice for the determination of the activity [8, 9].

The range of application of the activation technique may be widened to cover half lives from several seconds to several minutes by use of a pneumatic transport system that speeds up the transfer of the sample between the irradiation position and the counting position. In this case, automated repetition of the irradiation-counting cycle greatly enhances the number of accessible reactions. Radiochemical separation and thin sample preparation techniques extend the technique to characteristic decay gamma-rays with energies below 100 keV, the use of X-rays and the use of beta emission in combination with low energy germanium (LEGe), X-ray and beta spectrometry [10].

In the above, the energy range of the incident neutrons was not specified, and indeed the discussion so far applies to a very wide range of incident neutron energies. However, the subject of this report is the study of threshold reactions using neutrons in the range from 1 MeV to 60 MeV, exclusively, and with a strong focus on the range from 13 to 21 MeV. The main neutron source reaction is therefore the ^{3}H$(d,n)^{4}$He reaction. For the work that was done below 12 MeV the ^{2}H$(d,n)^{3}$He and ^{3}H$(p,n)^{3}$He reactions were used and for energies above 21 MeV the ^{7}Li(p,n) reaction was used. Specificities of these neutron source reactions are reported in Refs. [11–13].

The available database above 14 MeV is very limited, reflecting the lack of need for such data from traditional fission and fusion reactor development. Around 14 MeV many measurements were performed, as a result of the wide-spread use

of neutron generators, but often these data show discrepancies and/or large scatter. Below 14 MeV, the range that is traditionally of interest, the number of available measured data is significantly less than at 14 MeV, but is typically larger than above 14 MeV.

Since, the early 1980s several large and excellent measurement campaigns were conducted around 14 MeV to ameliorate the knowledge of cross-sections that are relevant for the fusion community [14–20]. For higher energies, the interest in the range above 14 MeV and up to several GeV is a consequence of the study of accelerator driven systems (since early 1990s [21]) and more recently of the design of the IFMIF materials irradiation facility for study of radiation damage in fusion reactors (maximum energy 55 MeV [22, 23]). Even for such systems the main energy range of relevance in a large part of the facility is below 20 MeV [21,24,25].

1.2 Model calculations and evaluations

Fig. 1.1 captures the essence of the subgroup using the ^{57}Fe$(n, x)^{56}$Mn reaction as an example. All evaluations that are shown, originate from the time that the only available data were those around 14 MeV. Clearly, it was essential to resort to model calculations in order to be able to determine the cross-sections up to 20 MeV for these evaluations. All these model calculations are more or less in agreement with the measured values around 14 MeV, a fact which is partly facilitated by the large spread and some large uncertainties in the measured data. The spread in predictions above 15 MeV by the various models is seen to be tremendous, ranging from values corresponding to about 60% of the Geel data to values that are more than twice as large. Clearly, the ENDF/B-VI evaluation that provides the best description of the most recent and consistent data around 14 MeV appears to be the most reasonable estimate. However, above 15 MeV it is 60% larger than the Geel data and in fact is not much better than the JENDL-3.3 estimates in this energy range.

All this illustrates that model predictions, essential for evaluations in areas where data are scarce, can vary greatly in the absence of a sufficient number of good quality measured data. In addition, the example shows that there appears to be no favoured approach that can be expected to out-perform other approaches. Therefore, a large body of new experimental data is needed and these new data should be used to benchmark models, so that future evaluations can benefit from enhanced descriptive and predictive power of model calculations. This also requires an understanding of the underlying origins of the problem, parameter uncertainties and model choices, and how to handle cross-section information to improve such uncertainties and arbitrate between different model options. Initiatives for improvement of the database for measured activation cross-sections

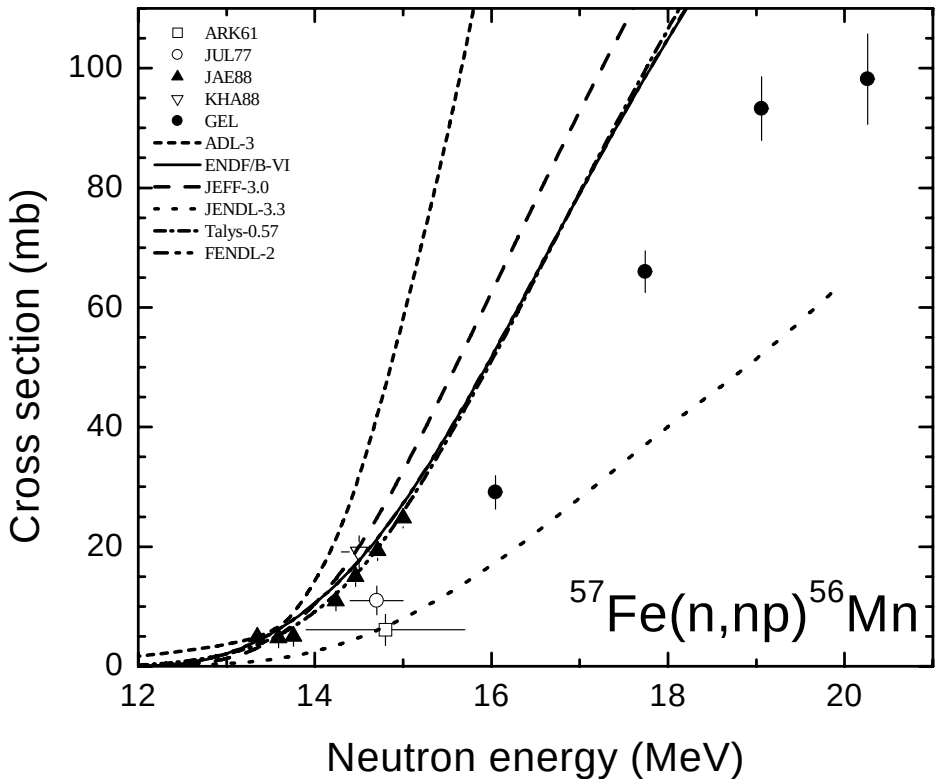

Figure 1.1: *The $^{57}Fe(n,x)^{56}Mn$ reaction compared to recent evaluations and the* TALYS-0.57 *model calculation. The IRMM data are labelled "GEL".*

are stimulated greatly by current active programmes in model code and evaluated data library development. Such initiatives guarantee timely use of measured data to improve evaluations. Recently published libraries include JENDL-3.3 [26], JEFF-3.0 [27] and EAF-2003 ([28]), and several new releases are scheduled for the near future (JEFF3.1, ENDF/B-VII, IRDF-2002, EAF-2005). Model calculations in the interest of evaluations are advancing rapidly through major code development projects (e.g. TALYS-0.57, MCGNASH, EMPIRE-II [29]) that emphasise code reliability, standardisation, interfacing with all relevant databases and libraries, code-readability, and documentation. At least one code can now generate a calculated database for all stable isotopes of the elements from carbon to bismuth based on an actual 'best' parameter set in ENDF-6 format. Also, a systematic automatically generated comparison between evaluations and/or model code predictions and the available measured data in the EXFOR database is now

feasible [1, 28].

The standardisation of model code predictions was greatly enhanced by the RIPL and RIPL2 initiatives that proposed recommended parameters for the description of all nuclear quantities in the various model approaches that are relevant for the description of neutron-induced reaction cross-sections in the low and intermediate energy range [30, 31]. The IAEA RIPL3 Co-ordinated Research Project and the WPEC MODLIB initiative attempt to achieve further standardisation by creating a pool of recommended software modules that each treat a particular aspect of a model calculation [29, 32].

Despite these efforts a full assessment of the predictive power of model calculations is difficult to make. This is both a consequence of the impact of important choices for the model calculations, e.g. concerning optical model and level densities, and of the lack of sufficient experimental data to benchmark the model codes, in particular away from 14 MeV.

1.3 Scope of the subgroup

The scope of the subgroup was defined in the original proposal consisting of a justification, objectives, project definition, specification of relevance to evaluated data files and a list of expected deliverables. These are given below.

1.3.1 Justification for the subgroup

Reliable nuclear models and their associated parameters are needed for computation of physical quantities that cannot be easily measured. Examples of these are reaction processes on radioactive targets and comprehensive particle-emission cross-sections, angular distributions, and energy spectra associated with incident neutrons in the range of several MeV to several tens of MeV. In accordance with the NEA High-Priority Request List (HPRL [33]), such data are essential for the design of advanced nuclear energy production systems such as fusion reactors and ADS as well as for analysis of the performance of ATW systems intended to reduce the inventory of long-lived radioisotopes in nuclear waste.

The necessity of improved model calculations became apparent from recent measurements of a large number of reaction cross-sections using the activation technique at IRMM and FZ Jülich [6, 10, 34]. Often evaluated data from JEFF-3.0, ENDF/B-VI and JENDL-3.3 were discrepant with each other and with the measured data, especially when measured data are scarce or previously non-existent. On the other hand it was shown that statistical model calculations (including pre-equilibrium emission) with carefully determined model parameters lead to much better results. This latter approach should be undertaken in a

systematic fashion addressing all reaction channels and the available experimental data with an internally consistent model description. Additional experimental data are required to further benchmark these nuclear models.

1.3.2 Objective of this subgroup

The unifying objectives of this subgroup are the validation of nuclear modelling by benchmarking model calculations to new and recent measurements and the development of a means to define data needs for nuclear energy applications in a more systematic fashion than was done in the past. The following subdivision is made:

1. to generate a large collection of pertinent experimental nuclear data that can be used for validation of these nuclear models;

2. to determine those nuclear model parameters that yield the best agreement with these data and compare them to the RIPL parameter set from the IAEA, and certain recent proposals for level density, optical model, pre-equilibrium and complex particle emission descriptions.

3. to provide reliable evaluations for a large number of neutron activation reactions and the competing channels of interest for the above-mentioned applications;

4. to perform nuclear-model sensitivity studies for specific reactions selected from the HPRL in order to identify those important future experiments that should be performed in order to satisfy well substantiated and documented data requirements for the above-mentioned nuclear energy technologies.

1.3.3 Definition of the project

Neutron activation cross-sections will be measured for a large number of threshold neutron-induced activation reactions in the energy range below 65 MeV. Measurements at the IRMM Van de Graaff accelerator facility will concentrate on the 16-20 MeV range, whereas for certain reactions complementary measurements will be performed at FZ Jülich below 12 MeV. Above 21 MeV selected measurements at the Cyric Laboratory of Tohoku University are included. These measurements will be carried out using existing experimental apparatus and techniques and on available elemental samples as well as isotopically enriched samples obtained on loan from JAERI. The work will also benefit by access to chemical separation technologies practiced at FZ-Jülich. The data produced by this project, along with

complementary results compiled from the literature, will be used to validate statistical, pre-compound nuclear model calculations performed with contemporary codes (e.g., STAPRE-H and/or GNASH). These calculated results will, in turn, be used to generate reliable evaluations for the studied reactions and competing reaction channels from threshold to 20 MeV. A comparison will then be made between the model parameters that lead to the best agreement with experimental data and the existing RIPL parameter set compiled by the IAEA. The details of this investigation will be thoroughly documented. Furthermore, calculations will be performed with these model codes to ascertain the sensitivity of the derived physical quantities, such as cross-sections at different neutron energies, to the nuclear model parameters. This information will serve to guide future measurement programmes and will help to clarify the prospects for satisfying developing nuclear data needs for fusion, ADS, and ATW neutronic systems through the approach of relying on nuclear model calculations validated by means of comparisons to available microscopic experimental data.

1.3.4 Relevance to evaluated data files

This project will generate a large number of evaluated excitation functions for the specific reactions studied. Evaluations will be obtained as consistent model descriptions of all reaction channels using all available cross-section, level, level density and, where necessary, scattering information. Consistency will justify the use of these evaluations in libraries intended for all neutron physics applications (transport, neutron damage, gas-production, decay-heat,...). At the same time they will be of use to dedicated activation files. These results will be provided in the ENDF-6 format so that they can be employed in such libraries as ENDF/B-VI, JEFF-3.0, JENDL-3.3, FENDL-2, EAF-2003, etc.[1]

1.3.5 Deliverables

- A new set of measured activation cross-sections for incident neutrons below 65 MeV. The emphasis is on the mass regions of Si to Zn (structural /materials), from Sr to Mo (structural materials/fission products) and on Pb (moderator/coolant/shielding material).

[1] It was later decided to discard delivery of calculated results in ENDF-6 format. Data calculated by the subgroup concern cross-sections only and even those with focus on measured activation cross-sections, or other channels for which data exist. This implies that an ENDF-6 formatted file would necessarily be incomplete due to missing channels and lack of emission spectra and angular distributions. Activation libraries would use the data tables for the individual cross-sections, whereas evaluators would require the model parameters. The latter will be provided in individual publications. The calculated excitation curves are largely provided in Part C of this report.

- Evaluated cross-sections for a large number of activation cross-sections. Consistent description of all reaction channels taking into account all pertinent experimental data. A complete picture for each target nucleus should emerge in agreement with the needs for files like JEFF-3.0, ENDF/B-VI, FENDL-2, and JENDL-3.3. Evaluated data will also be offered to the compilers of dedicated activation libraries such as EAF-2003 and IRDF.

- Results from a detailed comparison of best-fit nuclear model parameters with the RIPL set. Certain recent proposals of level density, optical model, pre-equilibrium, and complex particle emission approaches will be tested.

- A collection of sensitivity parameters that relate the physical quantities studied by this subgroup to the most significant nuclear model parameters. Recommendations for high-priority new measurements and estimates of the uncertainties, which could be expected in calculating unmeasurable physical quantities, needed for contemporary applications by means of nuclear models validated with experimental data.

2. MEASUREMENTS

Measurements have been carried out at five different laboratories, the Van de Graaff laboratory of the Institute for Reference Materials and Measurements, the Institut für Nuklearchemie of the Forschungszentrum Jülich, the Cyric cyclotron laboratory of the University of Tohoku, the Institute for Experimental Physics of the University of Debrecen and the ATOMKI cyclotron laboratory of the Hungarian Academy of Sciences in Debrecen.

2.1 The facilities

At IRMM extensive use was made of the ^{3}H$(d,n)^{4}$He reaction to address the neutron energy range from 14 to 21 MeV. In addition, for selected reactions with a low threshold the ^{3}H$(p,n)^{3}$He reaction provided neutrons in the range from 0.5 to 6 MeV. In both cases, the 7 MV Van de Graaff accelerator produced proton and deuteron beams of 10 to 50 W impinging on a 2 mg/cm^2 titanium tritide target. For the irradiations, low mass target and sample holder constructions were employed in a low-scatter environment. The neutron fields are quasi mono-energetic and low energy contributions to the reaction rates were carefully estimated using a spectral index method based on activation reactions with different thresholds. Both a manually operated and a fully automated pneumatic transport system were used to access activities with half lives of several seconds only. In all cases, gamma-ray yields were measured with HPGe detectors in order to measure the induced activity. Further details concerning these measurements may be found in Refs. [6, 7, 10, 34–40].

Measurements at FZ Jülich were made with neutrons in the energy range from 7.5 to 12.5 MeV. The ^{2}H$(d,n)^{3}$He reaction was employed with deuterons accelerated by the CV28 Compact Cyclotron incident on a deuterium gas-cell. Background was subtracted by the gas-in/gas-out technique and the low energy continuous break-up spectrum that accompanies the primary quasi mono-energetic neutrons was corrected for using the data of Cabral *et al.* [41]. In most cases HPGe's were used to determine the induced activity by gamma-ray spectrometry. However, in several instances, radiochemistry was used to extract the activity from the irradiated samples and produce thin-layer samples suitable for X-ray or beta spectrometry. For further details see Refs. [10, 34, 36].

In Debrecen the neutron generator laboratory of the Institute for Experimental Physics was used to study selected reactions at 14.6 MeV. The need for these

additional measurements arose from work at IRMM at higher energies indicating problems with the data at 14.6 MeV. Furthermore, for the determination of cross-sections in the 8-13 MeV range neutrons were produced by the variable energy MGC-20 cyclotron of ATOMKI using a D_2 gas target, applying techniques similar to those in use at FZ Jülich. Elemental samples were employed and HPGe spectrometry was used for the activity determinations. Further details may be found in Refs. [42–44].

At the Cyric laboratory of Tohoku university the $^7\mathrm{Li}(p,n)$ reaction was used to study neutron-induced cross-sections in the range from 30 to 65 MeV incident energy. The quasi mono-energetic neutrons are accompanied by a low energy tail that carries up to 50% of the total neutron fluence. Thus, deconvolution of the primary and low energy contribution to the reaction rates is essential to obtain accurate results. A collaboration between Tohoku and Debrecen universities has studied several charged-particle induced activation cross-sections, which are reported elsewhere. HPGe spectrometry is used for the activity determinations. For further details see Ref. [13].

2.2 Results of the measurements

In the course of subgroup operation new measurements were performed for 73 reactions resulting in 385 new data points. Most of this work has been published in either refereed journal paper of in publicly accessible conference proceedings and reports. References may be found with the aid of Tab. 2.1. A complete numerical and graphical presentation of these measured data is given in Part C of this report together with an additional 37 reactions (225 data points) for which data have been obtained by the IRMM-ANL-FZ-Jülich collaboration since 1997. Part C also presents a detailed comparison of all these data with earlier data available from the EXFOR database, the most recent evaluations and with TALYS-0.57 and selected EMPIRE-II model calculations. Here, some graphs, highlighting the work that was performed, are taken from Part C for illustration.

Fig. 2.1 shows an example of a systematic study of $\Delta Z = 1$ reactions on a chain of Zr isotopes that was performed at IRMM, in collaboration with ANL and INRNE. Both total and isomer production cross-sections have been measured. Enriched samples, on loan from Drs. Y. Ikeda and Y. Kasugai of JAERI, were used in order to separate the different channels leading to the same activity. Other elements for which such systematic experimental studies were carried out at IRMM are chromium, iron, nickel, molybdenum and lead. The example shows a typical case where almost no experimental data are available above 15 MeV. For the six reactions the new measurements clearly establish the excitation curves above 15 MeV. These excitation curves are joined smoothly at 14 MeV and below

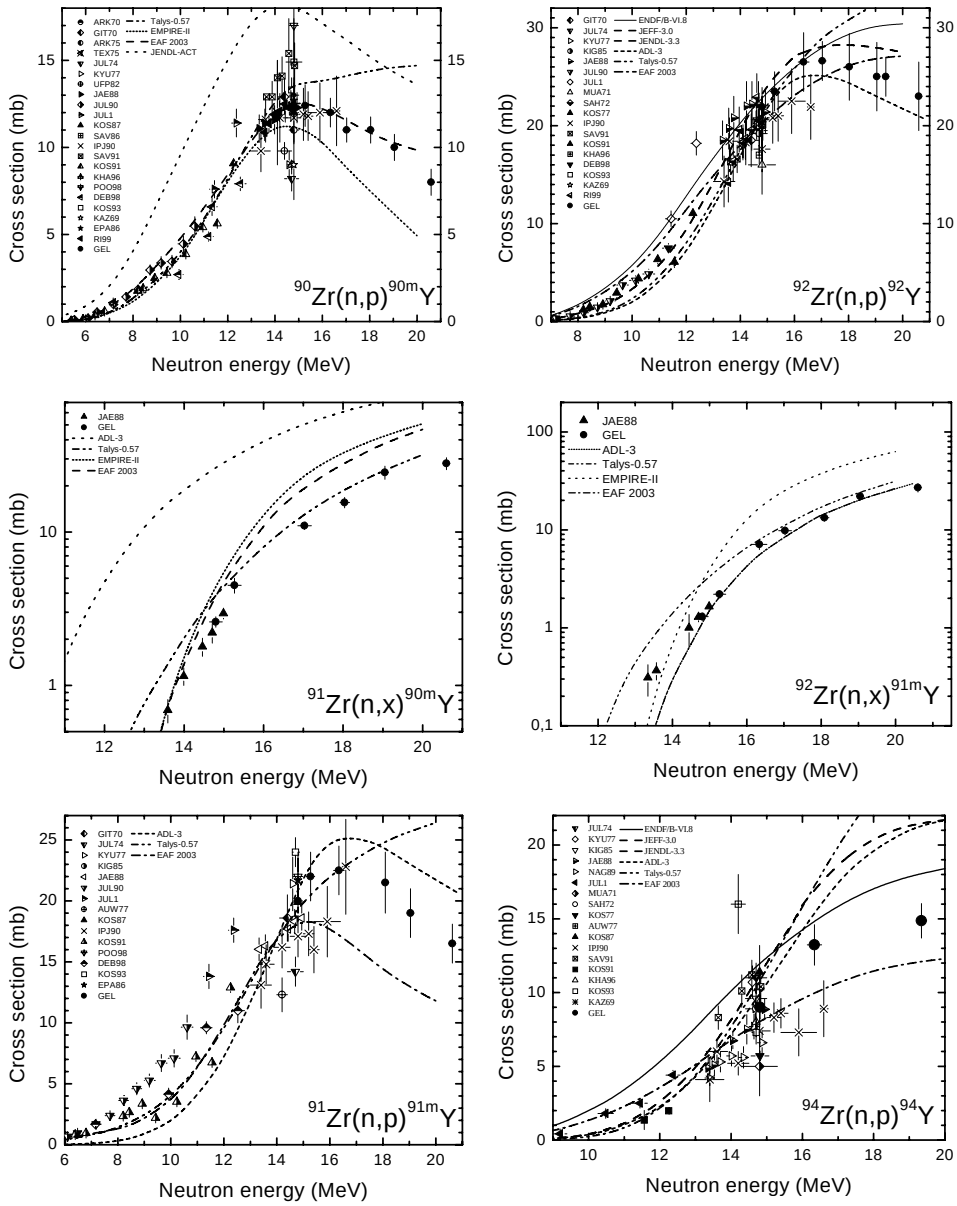

Figure 2.1: *Measurements for $\Delta Z = 1$ reactions on $^{90,91,92,94}Zr$ performed at the Geel Van de Graaff laboratory. The IRMM data are labelled "GEL".*

with the existing data. However, in some cases the spread around 14 MeV is such that the data below 13 and above 15 MeV are required to establish the curve in the region from 13 to 15 MeV, unambiguously. Below 15 MeV, with one obvious exception, the agreement between evaluations and the blind TALYS-0.57 model calculations on the one hand and the measured data on the other hand is quite reasonable. However, above 15 MeV the level of agreement amongst predictions and between predictions and the data varies strongly.

In Fig. 2.2 results are shown for the measurements that were done at FZ Jülich and the Atomki laboratory in Debrecen at the respective cyclotrons, using the ^{2}H$(d,n)^{3}$He neutron source reaction. Also shown are some examples of the new data that were obtained with the ^{3}H$(d,n)^{4}$He reaction using the neutron generator of the Institute of Experimental Physics of the University in Debrecen. As is shown in the graphs, these data were all measured for cases where new results have also been obtained at the IRMM, above 13 MeV. For the ^{28}Si$(n,p)^{28}$Al and ^{100}Mo$(n,2n)^{99}$Mo reactions the data obtained at the Atomki cyclotron cover the problem area from 10 to 13 MeV, where few data exist. Excellent agreement is obtained with the work of Mannhart *et al.*, performed at the PTB cyclotron laboratory for the ^{28}Si$(n,p)^{28}$Al reaction and in both cases the excitation curve is now well determined by the experimental data from threshold to 20 MeV.

Examples of new measurements at Debrecen University at 14.6 MeV are given for the ^{28}Si$(n,p)^{28}$Al and ^{208}Pb$(n,p)^{208}$Tl reactions. For the ^{28}Si$(n,p)^{28}$Al reaction the data point is in excellent agreement with all other recent accurate measurements (1986, onwards), so that the large spread of earlier measurements can clearly be discarded. In the case of the ^{208}Pb$(n,p)^{208}$Tl reaction, the 14.6 MeV data point is in excellent agreement with the new result from Geel, and the recent results of Ryves *et al.* (NPL90) and Begun *et al.* (KGU1). Thus, clearly all recent measurements favour the higher cross-section values at this energy, contrary to most evaluations and the TALYS-0.57 model calculation.

The contributions of FZ-Jülich that are highlighted here, all concern the collaboration with IRMM. These involve measurements below 13 MeV at the CV Compact cyclotron for the ^{nat}V$(n,x\alpha)^{47}$Sc and ^{99}Tc$(n,\alpha)^{96}$Nb reactions, the target sample preparation in the case of ^{99}Tc, and the separation and thin sample preparation of the ^{204}Tl residual nucleus in the interest of the activity determination using β-counting. All cases presented in Fig. 2.2 are characterised by the absence of reliable data prior to the new measurements, aside from recent results near 14 MeV. Also shown is the mixed success with which evaluations based on model calculations are able to predict the data. The level of agreement ranges from good to very discrepant.

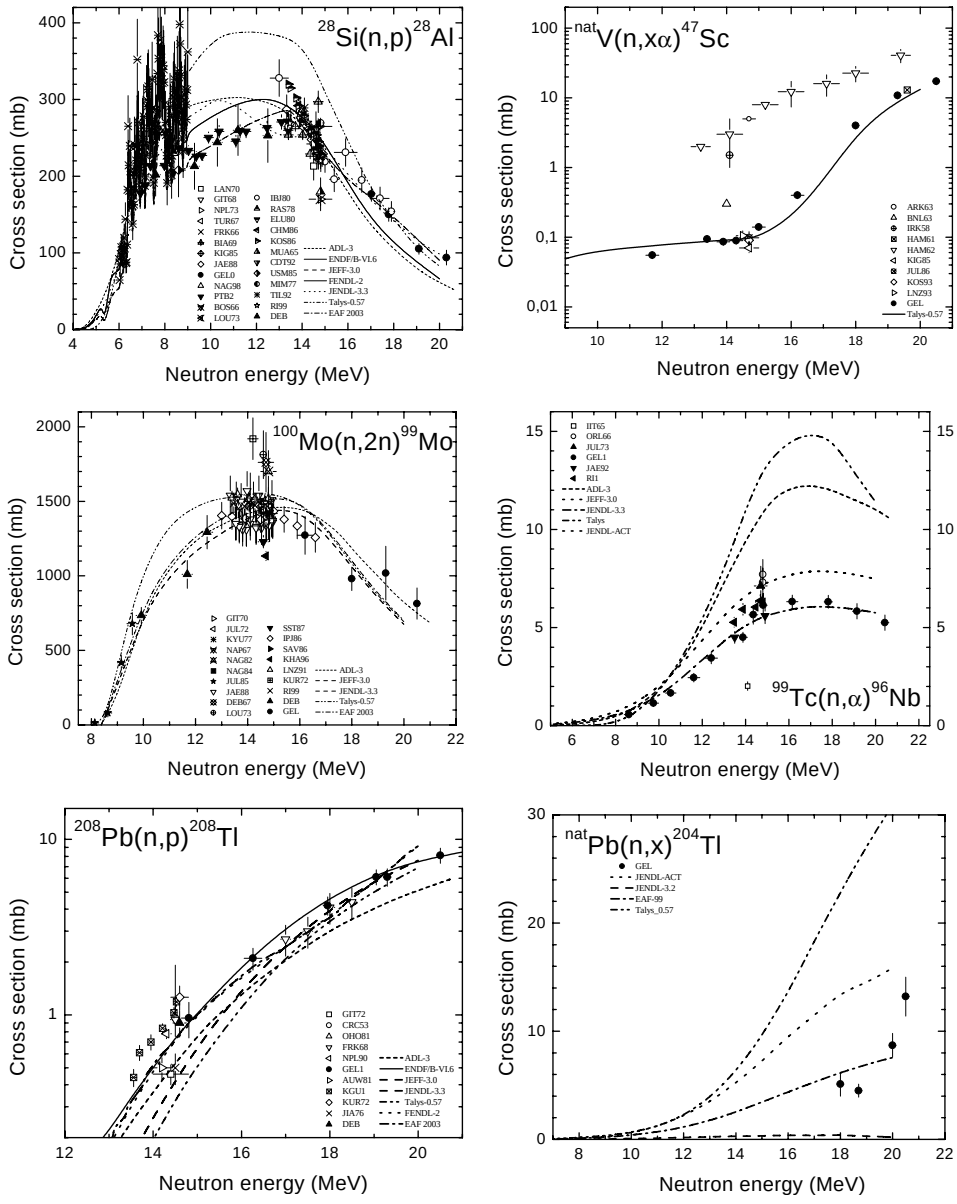

Figure 2.2: *Examples of measured data obtained at the Debrecen cyclotron and neutron generator (left) and the FZ Jülich Compact CV cyclotron (right). Sample preparation for the ^{99}Tc target as well as activity separation and thin target preparation for ^{204}Tl were performed at the Institute for Nuclear Chemistry of FZ Jülich.*

2.3 EXFOR compilation and availability of numerical data

Nearly all the measured data have been compiled in EXFOR format and the files were submitted to NEA. This compilation effort completely covers the measured data resulting from the IRMM-ANL-FZ Jülich collaboration that started in 1997 and for which the results were finalised before the start of the subgroup's activities. Only the most recent data are still being compiled and will appear in EXFOR format, shortly. As noted above, all measured data are presented numerically and graphically in Part C of this report. The status of the EXFOR compilation effort is summarised in Tab. 2.1. When available, this table gives the EXFOR entry number together with the form of and reference to the publication(s) that form the basis of the EXFOR entry. In some cases, numerical data have appeared in one or more written reports before being published in a refereed journal paper. In almost all cases this has not led to conflicts, however, some differences occur between what subgroup members consider the final results and what is actually compiled. In addition, some reactions appeared in EXFOR twice when they were measured only once. The relevant compilations differ by the status of the analysis at the time the underlying reports were written. Efforts are being made to ensure that only the numerical values considered final by the authors appear in EXFOR and that no double entries appear.

Table 2.1: *Status of data compilation*
List of abbreviations; MQ: measured quantity, j: journal paper, c: conference proceedings, r: report, x: published EXFOR *entry, xs: submitted* EXFOR *entry, xc: published* EXFOR *entry to be corrected, CS: cross-section, IR: Isomer Ratio, RCS: Re-normalised cross-section.*

Reaction	**MQ**	**Energies (MeV)**	**Nr. of points**	**Data Status**	**Ref.**	**Accession Number**
^{19}F$(n,p)^{19}$O	CS	16-20	5	j,c,x	[6]	22414.002
^{19}F$(n,p)^{19}$O	CS	14.6	1	c	[42]	
^{23}Na$(n,p)^{23}$Ne	CS	16-20	5	j,c,x	[6]	22414.003
^{23}Na$(n,\alpha)^{20}$F	CS	16-20	5	j,c,x	[6]	22414.004
^{25}Mg$(n,p)^{25}$Na	CS	16-20	5	j,c,x	[6]	22414.005
^{27}Al$(n,p)^{27}$Mg	CS	16-20	5	j,c,x	[6]	22414.006
^{28}Si$(n,p)^{28}$Al	CS	16-20	4	j,c,x	[6]	22414.007
^{28}Si$(n,p)^{28}$Al	CS	7-15	6	c	[42]	
^{29}Si$(n,p)^{29}$Al	CS	16-20	5	j,c,x	[6]	22414.008
^{29}Si$(n,x)^{28}$Al	CS	16-20	5	j,c,x	[6]	22414.009
^{31}P$(n,\alpha)^{28}$Al	CS	16-20	5	j,c,x	[6]	22414.010

Table 2.1: *Status of data compilation*
List of abbreviations; MQ: measured quantity, j: journal paper, c: conference proceedings, r: report, x: published EXFOR *entry, xs: submitted* EXFOR *entry, xc: published* EXFOR *entry to be corrected, CS: cross-section, IR: Isomer Ratio, RCS: Re-normalised cross-section.*

Reaction	**MQ**	**Energies (MeV)**	**Nr. of points**	**Data Status**	**Ref.**	**Accession Number**
^{31}P$(n,\alpha)^{28}$Al	CS	14.6	1	c	[42]	
^{35}Cl$(n,2n)^{34m}$Cl	CS	16-20	5	j,c,x	[6]	22414.011
^{37}Cl$(n,p)^{37}$S	CS	16-20	5	j,c,x	[6]	22414.012
^{45}Sc$(n,\alpha)^{42}$K	CS	11.7	1	c	[42]	
^{46}Ti$(n,p)^{46m}$Sc	CS	16-20	5	j,c,x	[6]	22414.013
^{50}Ti$(n,p)^{50}$Sc	CS	16-20	5	j,c,x	[6]	22414.014
^{50}Ti$(n,p)^{50}$Sc	CS	14.6	1	c	[42]	
^{51}V$(n,p)^{51}$Ti	CS	17-20	4	j,c,x	[6]	22414.015
^{51}V$(n,p)^{51}$Ti	CS	15.0-16.1	2	j,c,x	[36]	22656.004
^{51}V$(n,p)^{51}$Ti	CS	9.9	1	c	[42]	
^{51}V$(n,\alpha)^{48}$Sc	CS	11.7-20.5	9	j,c,x	[36]	22656.003
^{nat}V$(n,x\alpha)^{47}$Sc	CS	11.7-20.5	9	j,c,x	[36]	22656.002
^{50}Cr$(n,x)^{49}$V	CS	14-20	4	j,x	[10]	22465.002
^{52}Cr$(n,2n)^{51}$Cr	CS	14-20	4	j,x	[34]	22406.002
^{52}Cr$(n,p)^{52}$V	CS	9.3-22	22	j,x	[34]	22406.003
^{53}Cr$(n,p)^{53}$V	CS	12-22	19	j,x	[34]	22406.004
^{53}Cr$(n,x)^{52}$V	CS	16-20	5	j,x	[34]	22406.005
^{54}Cr$(n,p)^{54}$V	CS	16-20	5	j,x	[34]	22406.006
^{54}Cr$(n,p)^{54}$V	CS	14.6	1	c	[42]	
^{54}Cr$(n,x)^{53}$V	CS	16-20	5	j,x	[34]	22406.007
^{54}Cr$(n,\alpha)^{51}$Ti	CS	16-20	5	j,x	[34]	22406.008
^{55}Mn$(n,\alpha)^{52}$V	CS	16-20	5	j,x	[34]	22414.016
^{54}Fe$(n,2n)^{53}$Fe	CS	15-21	12	r,x	[35]	22440.002
^{54}Fe$(n,x)^{52}$Mn	CS	16-21	5	r,x	[35]	22440.003
^{54}Fe$(n,2n)^{53m,g}$Fe	IR	19-21	5	r	[35]	
^{54}Fe$(n,x)^{52m,g}$Mn	IR	16-20	3	r	[35]	
^{56}Fe$(n,p)^{56}$Mn	CS	16-21	4	j,r,c,x	[6]	22414.017
^{57}Fe$(n,p)^{57}$Mn	CS	16-21	5	j,r,c,x	[6]	22414.019
^{57}Fe$(n,x)^{56}$Mn	CS	16-21	4	j,r,c,x	[6]	22414.018
^{59}Co$(n,2n)^{58}$Co	CS	13-20	12	j,r,c,xc	[40]	22684.009
^{59}Co$(n,2n)^{58m}$Co	CS	15-19	5	j,r,c,xc	[40]	22684.010
^{59}Co$(n,2n)^{58m,g}$Co	IR	15-19	5	j,r,c,xc	[40]	22684.011

Table 2.1: *Status of data compilation*
List of abbreviations; MQ: measured quantity, j: journal paper, c: conference proceedings, r: report, x: published EXFOR *entry, xs: submitted* EXFOR *entry, xc: published* EXFOR *entry to be corrected, CS: cross-section, IR: Isomer Ratio, RCS: Re-normalised cross-section.*

Reaction	**MQ**	**Energies (MeV)**	**Nr. of points**	**Data Status**	**Ref.**	**Accession Number**
^{59}Co$(n,p)^{59}$Fe	CS	14.8-20.6	4	c	[45]	
^{58}Ni$(n,p)^{58}$Co	CS	1.3-21	13	j,r,c,xc	[40]	22684.002
^{58}Ni$(n,p)^{58m}$Co	CS	1.3-19	7	j,r,c,xc	[40]	22684.004
^{58}Ni$(n,p)^{58m,g}$Co	IR	1-19	10	j,r,c,xc	[40]	22684.003
^{58}Ni$(n,x)^{57}$Co	CS	15-20	12	j,r,c,xc	[40]	22684.005
^{58}Ni$(n,2n)^{57}$Ni	CS	15-20	9	j,r,c,xc	[40]	22684.006
^{58}Ni$(n,\alpha)^{55}$Fe	CS	7.4-20	11	j,r,x	[10]	22465.003
^{58}Ni$(n,\alpha)^{55}$Fe	RCS	5.4-9.5	9	j,r,x	[10]	22465.006
^{58}Ni$(n,x\alpha)^{54}$Mn	CS	14-19	4	j,r,x	[10]	22465.004
^{58}Ni$(n,t)^{56}$Co	CS	17.8-19.3	2	c	[45]	
^{60}Ni$(n,p)^{60}$Co	CS	13-20	7	j,r,c,xc	[40]	22684.007
^{60}Ni$(n,p)^{60m}$Co	CS	15-19	4	j,r,c,xc	[40]	22684.008
^{60}Ni$(n,p)^{60m,g}$Co	IR	15	1	j,r,c	[40]	
^{61}Ni$(n,x)^{60m}$Co	CS	19	1	j,r,c	[40]	22820.009
^{61}Ni$(n,p)^{61}$Co	CS	15-19	5	j,r,c	[40]	22820.010
^{62}Ni$(n,p)^{62m}$Co	CS	14.6	1	c	[42]	
^{62}Ni$(n,x)^{61}$Co	CS	15-19	4	j,r,c	[40]	22820.011
^{62}Ni$(n,\alpha)^{59}$Fe	CS	13-19	5	j,r,c,x	[10]	22465.005
^{62}Ni$(n,\alpha)^{59}$Fe	RCS	6.4-9.5	5	j,r,c,x	[10]	22465.007
^{63}Cu$(n,\alpha)^{60}$Co	CS	13-20	9	j,r,c,x	[46]	22684.012
^{90}Zr$(n,p)^{90m}$Y	CS	15-21	7	r,c	[39]	22822.003
^{90}Zr$(n,\alpha)^{87m}$Sr	CS	15-21	7	r,c	[39]	22822.002
^{91}Zr$(n,p)^{91m}$Y	CS	15-21	6	r,c	[39]	22822.004
^{91}Zr$(n,x)^{90m}$Y	CS	15-21	6	r,c	[39]	22822.005
^{92}Zr$(n,p)^{92}$Y	CS	15-21	8	r,c	[39]	22822.006
^{92}Zr$(n,x)^{91m}$Y	CS	15-21	7	r,c	[39]	22822.007
^{94}Zr$(n,p)^{94}$Y	CS	15-19.5	3	c	[47]	
^{94}Zr$(n,\alpha)^{91}$Sr	CS	15-19.5	3	c	[47]	
^{93}Nb$(n,2n)^{92m}$Nb	CS	16-20	5	j,c,x	[6]	22414.021
^{93}Nb$(n,\alpha)^{90m}$Y	CS	16-20	5	j,c,x	[6]	22414.020
^{nat}Mo$(n,x)^{94}$Nb	CS	16-20	3	j,c,r,xs	[37]	22818.003
^{92}Mo$(n,p)^{92m}$Nb	CS	16-21	4	j,c,r,xs	[7, 38]	22818.002

Table 2.1: *Status of data compilation*
List of abbreviations; MQ: measured quantity, j: journal paper, c: conference proceedings, r: report, x: published EXFOR *entry, xs: submitted* EXFOR *entry, xc: published* EXFOR *entry to be corrected, CS: cross-section, IR: Isomer Ratio, RCS: Re-normalised cross-section.*

Reaction	**MQ**	**Energies (MeV)**	**Nr. of points**	**Data Status**	**Ref.**	**Accession Number**
^{92}Mo$(n,\alpha)^{89m}$Zr	CS	16-21	4	j,c,r,xs	[7, 38]	22818.013
^{92}Mo$(n,2n)^{91m}$Mo	CS	16-21	4	j,c,r,xs	[7, 38]	22818.015
^{94}Mo$(n,2n)^{93m}$Mo	CS	16-21	4	j,c,r,xs	[7, 38]	22818.016
^{95}Mo$(n,p)^{95m}$Nb	CS	16-21	4	j,c,r,xs	[7, 38]	22818.005
^{96}Mo$(n,p)^{96}$Nb	CS	16-21	3	j,c,r,xs	[7, 38]	22818.007
^{96}Mo$(n,x)^{95m}$Nb	CS	16-21	3	j,c,r,xs	[7, 38]	22818.006
^{97}Mo$(n,p)^{97}$Nb	CS	16-21	4	j,c,r,xs	[7, 38]	22818.010
^{97}Mo$(n,p)^{97m}$Nb	CS	16-21	4	j,c,r,xs	[7, 38]	22818.009
^{97}Mo$(n,x)^{96}$Nb	CS	16-21	3	j,c,r,xs	[7, 38]	22818.008
^{98}Mo$(n,p)^{98m}$Nb	CS	16-21	4	j,c,r,xs	[7, 38]	22818.004
^{98}Mo$(n,x)^{97m}$Nb	CS	16-21	4	j,c,r,xs	[7, 38]	22818.011
^{98}Mo$(n,x)^{97}$Nb	CS	16-21	2	j,c,r,xs	[7, 38]	22818.012
^{100}Mo$(n,\alpha)^{97}$Zr	CS	16-21	4	j,c,r,xs	[7, 38]	22818.014
^{100}Mo$(n,2n)^{99}$Mo	CS	16-21	4	j,c,r,xs	[7, 38]	22818.017
^{100}Mo$(n,2n)^{99}$Mo	CS	9.9-12.4	3	c	[42]	
^{99}Tc$(n,n'\gamma)^{99m}$Tc	CS	0.5-21	20	c,r,x	[38]	22655.004
^{99}Tc$(n,p)^{99}$Mo	CS	8.5-20	12	c,r,x	[38]	22655.003
^{99}Tc$(n,\alpha)^{96}$Nb	CS	8.5-20	12	c,r,x	[38]	22655.002
^{115}In$(n,n'\gamma)^{115m}$In	CS	2.1-12.4	10	c	[42]	
^{115}In$(n,\gamma)^{116}$In	CS	0.02-12.4	19	c	[42]	
^{119}Sn$(n,p)^{119m}$In	CS	16-20	5	j,c,x	[6]	22414.022
^{127}I$(n,2n)^{126}$I	CS	16-21	4	c	[48]	
^{129}I$(n,2n)^{128}$I	CS	16-21	4	c	[48]	
^{129}I$(n,p)^{129g}$Te	CS	16-21	4	c	[48]	
^{129}I$(n,p)^{129m}$Te	CS	16-21	4	c	[48]	
^{129}I$(n,\alpha)^{126g}$Sb	CS	16-21	4	c	[48]	
^{129}I$(n,\alpha)^{126m}$Sb	CS	16-21	4	c	[48]	
^{138}Ba$(n,2n)^{137m}$Ba	CS	16-20	5	j,c,x	[6]	22414.023
^{nat}Pb$(n,x)^{204}$Tl	CS	18-21	4	r,xc	[7, 38]	22680.009
^{204}Pb$(n,n'\gamma)^{204m}$Pb	CS	3.5-21	6	j,c,r,xc	[7, 39]	22680.005
^{204}Pb$(n,2n)^{203}$Pb	CS	18-21	6	j,c,r,xc	[7, 38]	22680.007
^{204}Pb$(n,2n)^{203m}$Pb	CS	18-21	4	j,c,r,xc	[7, 39]	22680.006

Table 2.1: *Status of data compilation*
List of abbreviations; MQ: measured quantity, j: journal paper, c: conference proceedings, r: report, x: published EXFOR *entry, xs: submitted* EXFOR *entry, xc: published* EXFOR *entry to be corrected, CS: cross-section, IR: Isomer Ratio, RCS: Re-normalised cross-section.*

Reaction	**MQ**	**Energies (MeV)**	**Nr. of points**	**Data Status**	**Ref.**	**Accession Number**
^{204}Pb$(n,3n)^{202m}$Pb	CS	18-21	5	j,c,r,xc	[7, 38]	22680.008
^{206}Pb$(n,\alpha)^{203}$Hg	CS	16-21	6	j,c,r,xc	[7, 38]	22680.003
^{206}Pb$(n,3n)^{204m}$Pb	CS	18-21	3	j,c,r,xc	[7, 38]	22680.004
^{208}Pb$(n,p)^{208}$Tl	CS	15-21	6	j,c,r,xc	[7, 39]	22680.002
^{208}Pb$(n,p)^{208}$Tl	CS	14.6	1	c	[42]	

3. MODEL CALCULATIONS

3.1 Local approach

Model calculations were performed for reactions on Na, V, ^{59}Co, ^{99}Tc and ^{127,129}I and the stable isotopes of Ni, Mo, Pb. These calculations used either the STAPRE-H95 code with several enhancements, the STAPRE, or the EMPIRE-II code. In the case of sodium the TNG code was used and the results were employed for the JENDL3.3 evaluation [49].

These calculations consist of locally optimised phenomenological approaches to a coherent physics description of the available experimental information. As a starting point well established data bases are used such as RIPL (Reference Input Parameter Library) and RIPL-2 [30, 31]. Fine tuning the most relevant model parameters one typically finds good agreement with the measured cross-sections by adjustments that are within the respective parameter uncertainties.

For V, Co, Ni and Mo calculations by V. Avrigeanu followed the method proposed by Delaroche *et al.* [50] of using the available s- and p-wave resonance experimental information, as well as the measured reaction and total cross-sections to obtain the best choices for optical model and level spacings (SPRT approach). Level density parameters were determined by fitting the discrete levels and the s-wave spacing at the binding energy. Level density parameters for nuclei without experimental s-wave spacings were obtained by smooth interpolation and extrapolation. For the level densities the Back-Shifted Fermi-Gas model (BSFG) was used together with the Ignatyuk approach to include the washing out of shell effects. Furthermore, based on experimental evidence for ^{51}V and ^{40}K, an energy dependent spin cutoff parameter was smoothly varying from 0.5 at the lowest energies to 0.75 at the neutron binding energy and 1 above 15 MeV. Several optical models applied in earlier works were tested and when necessary the best choice was modified (see above). The calculations that used the Stapre-H95 code involve the geometry dependent hybrid model for estimates of pre-equilibrium contributions. In addition, the Avrigeanu α-particle optical model was used. Very successful descriptions of the measured cross-sections have been obtained that were published in Refs. [36, 40, 51]. In the case of reactions on Mo-isotopes the calculations preceded the appearance of the measured data and were found in good agreement once confronted with the measurement results [7]. This shows that the method followed to extract the first guess for the parameters can be very successful.

For technetium, iodine and lead, STAPRE and EMPIRE-II were used by

Table 3.1: *Observed differences between* TALYS-0.57 *default calculations and measured data for the reactions shown in Part C of this report.* TALYS-0.57 *results were available for 94 of the 101 reactions.*

Relative difference (%)	Number of cases (%)
< 15	39
$15 - 30$	34
$30 - 50$	18
> 50	8

S. Sudár with level density parameters for the BSFG model from the IAEA Plyaskin data base [52]. The conventional one-component exciton model was used and optical model parameters were chosen from the literature based on their agreement with the total cross-section and available reaction cross sections. Results were presented at conferences and in EUR and JEFF reports [7, 39, 46, 53, 54].

3.2 Global approach

In Part C of this report one further finds an extensive comparison with TALYS-0.57 default calculations. The latter is of interest as it demonstrates the quality of phenomenological nuclear model calculations using parameter databases obtained by global optimisation. No fine tuning was done to optimise the description of the cases at hand. As is further highlighted by the summary table 3.1 the basic level of agreement is nevertheless remarkable from the point of view of nuclear physics model calculations. Some calculations with the EMPIRE-II code by R. Capote Noy are shown as well to further illustrate this point (Part C). Although for the purpose of this subgroup, TALYS-0.57 and EMPIRE-II were used in a global approach, they may also successfully be used for calculations in the local approach. This is demonstrated elsewhere.

3.3 Recommendations

As mentioned, the various calculations that were performed were compared to existing evaluations and the measured data in a systematic way in Part C of this report. From this comparison one may learn which calculation or evaluation

provides for the best agreement with the experimental data. The conclusions of such a survey are presented in Tab. 3.2. In many cases the calculations in the local approach improve on existing calculations, as expected from the special attention devoted to the nuclei that were studied. It may furthermore be noted that in 20% of the cases TALYS-0.57 default calculations may contribute to improved evaluated data files. Thus, the comparison provides for a qualitative statement about the relative importance of studies in the local and in the global approach.

Table 3.2: *Evaluation or model calculations agreeing best with the available measured data.*

Reaction	Recommendation
^{19}F$(n,p)^{19}$O	ENDF/B-VI, JEFF-3.0, EAF-2003, FENDL-2; > 15 MeV ADL-3
^{23}Na$(n,p)^{23}$Ne	EAF-2003, JENDL-3.3, JEFF-3.0; > 15 MeV ADL-3
^{23}Na$(n,\alpha)^{20}$F	EAF-2003; > 15 MeV 0.5 (TALYS-0.57+EAF-2003)
^{25}Mg$(n,p)^{25}$Na	EAF-2003+10-15% (>10 MeV);
^{27}Al$(n,p)^{27}$Mg	(>13 MeV) ADL-3, EAF-2003, JENDL-3.3, ENDF/B-VI
^{28}Si$(n,p)^{28}$Al	(>13 MeV) EAF-2003, (JENDL-3.3)
^{29}Si$(n,x)^{28}$Al	TALYS-0.57
^{31}P$(n,\alpha)^{28}$Al	EAF-2003
^{35}Cl$(n,2n)^{34m}$Cl	TALYS-0.57, EAF-2003
^{37}Cl$(n,p)^{37}$S	ADL-3(>15 MeV), new modelling needed
^{45}Sc$(n,\alpha)^{42}$K	EAF-2003
^{46}Ti$(n,p)^{46m}$Sc	EAF-2003
^{50}Ti$(n,p)^{50}$Sc	JENDL-3.3
^{51}V$(n,p)^{51}$Ti	[36], EAF-2003
^{51}V$(n,\alpha)^{48}$Sc	[36] (EAF-2003, JENDL-3.3, ENDF/B-VI)
^{nat}V$(n,x\alpha)^{47}$Sc	[36] (JENDL-3.3-act)
^{50}Cr$(n,x)^{49}$V	TALYS-0.57, JEFF-3.0, ENDF/B-VI, FENDL-2
^{52}Cr$(n,2n)^{51}$Cr	<14 MeV EAF-2003, JENDL-3.3; >14 MeV ENDF/B-VI, FENDL-2
^{52}Cr$(n,p)^{52}$V	EAF-2003, JENDL-3.3, FENDL-2, ADL-3 (ENDF/B-VI)
^{53}Cr$(n,p)^{53}$V	<18 MeV EAF-2003(TALYS-0.57, ENDF/B-VI, JENDL-3.3, FENDL-2); >18MeV JENDL-3.3, ADL-3

Table 3.2: *Evaluation or model calculations agreeing best with the available measured data.*

Reaction	Recommendation
^{53}Cr$(n,x)^{52}$V	<18 MeV TALYS-0.57; >18 MeV JENDL-3.3
^{54}Cr$(n,p)^{54}$V	<18 MeV EAF-2003
^{54}Cr$(n,p)^{54}$V	EAF-2003, TALYS-0.57
^{54}Cr$(n,x)^{53}$V	TALYS-0.57(EAF-2003)
^{54}Cr$(n,\alpha)^{51}$Ti	EAF-2003, JENDL-3.3
^{55}Mn$(n,\alpha)^{52}$V	EAF-2003, TALYS-0.57(>12 MeV)
^{54}Fe$(n,2n)^{53}$Fe	JEFF-3.0, ENDF/B-VI
^{54}Fe$(n,x)^{52}$Mn	TALYS-0.57
^{56}Fe$(n,p)^{56}$Mn	EAF-2003, JEFF-3.0, JENDL-3.3(ADL-3, ENDF/B-VI)
^{57}Fe$(n,p)^{57}$Mn	ENDF/B-VI, FENDL-2
^{57}Fe$(n,x)^{56}$Mn	
^{59}Co$(n,2n)^{58}$Co	[40] (EAF-2003)
^{59}Co$(n,2n)^{58m}$Co	[40] (EAF-2003)
^{59}Co$(n,p)^{59}$Fe	EAF-2003, JEFF-3.0, ENDF/B-VI
^{58}Ni$(n,p)^{58}$Co	[40] (ENDF/B-VI, TALYS-0.57, JENDL-3.3)
^{58}Ni$(n,p)^{58m}$Co	[40], ADL-3
^{58}Ni$(n,x)^{57}$Co	TALYS-0.57, EMPIRE-II, ENDF/B-VI, FENDL-2
^{58}Ni$(n,2n)^{57}$Ni	[40] (EAF-2003, JEFF-3.0, ENDF/B-VI, FENDL-2)
^{58}Ni$(n,\alpha)^{55}$Fe	[40], JENDL-3.3
^{58}Ni$(n,x\alpha)^{54}$Mn	EAF-2003
^{58}Ni$(n,t)^{56}$Co	<15 MeV JEFF-3.0; >18 MeV JENDL-3.3
^{60}Ni$(n,p)^{60}$Co	[40], EAF-2003, JENDL-3.3, TALYS-0.57
^{60}Ni$(n,p)^{60m}$Co	[40], EAF-2003; <10 MeV TALYS-0.57
^{61}Ni$(n,x)^{60m}$Co	[40]
^{61}Ni$(n,p)^{61}$Co	<10 MeV TALYS-0.57, EAF-2003, JEFF-3.0, ENDF/B-VI; >13 MeV [40]
^{62}Ni$(n,p)^{62m}$Co	EAF-2003, ADL-3
^{62}Ni$(n,x)^{61}$Co	EAF-2003, [40]
^{62}Ni$(n,\alpha)^{59}$Fe	[40], JENDL-3.3
^{63}Cu$(n,\alpha)^{60}$Co	EAF-2003, JEFF-3.0, ENDF/B-VI, FENDL-2
^{90}Zr$(n,p)^{90m}$Y	<15 MeV TALYS-0.57
^{90}Zr$(n,\alpha)^{87m}$Sr	<15 MeV EAF-2003

Table 3.2: *Evaluation or model calculations agreeing best with the available measured data.*

Reaction	Recommendation
^{91}Zr$(n,p)^{91m}$Y	<16 MeV TALYS-0.57
^{91}Zr$(n,x)^{90m}$Y	<15 MeV EAF-2003, EMPIRE-II; > 15 MeV TALYS-0.57
^{92}Zr$(n,p)^{92}$Y	<13 MeV JEFF-3.0, JENDL-3.3; >13 MeV ADL-3
^{92}Zr$(n,x)^{91m}$Y	EAF-2003
^{94}Zr$(n,p)^{94}$Y	
^{94}Zr$(n,\alpha)^{91}$Sr	<15 MeV EAF-2003; >15 MeV JEFF-3.0, JENDL-3.3
^{93}Nb$(n,2n)^{92m}$Nb	IRDF
^{93}Nb$(n,\alpha)^{90m}$Y	<15 MeV EAF-2003; >15 MeV ADL-3+20%
^{nat}Mo$(n,x)^{94}$Nb	[51], TALYS-0.57
^{92}Mo$(n,p)^{92m}$Nb	[51], TALYS-0.57
^{92}Mo$(n,\alpha)^{89m}$Zr	[51]
^{92}Mo$(n,2n)^{91m}$Mo	[51]
^{94}Mo$(n,2n)^{93m}$Mo	[51], ADL-3, EAF-2003
^{95}Mo$(n,p)^{95m}$Nb	[51], EAF-2003
^{96}Mo$(n,p)^{96}$Nb	[51], ADL-3
^{96}Mo$(n,x)^{95m}$Nb	EAF-2003
^{97}Mo$(n,p)^{97}$Nb	[51]
^{97}Mo$(n,p)^{97m}$Nb	EAF-2003
^{97}Mo$(n,x)^{96}$Nb	<15 MeV [51]; >15 MeV EAF-2003
^{98}Mo$(n,p)^{98m}$Nb	[51] (TALYS-0.57)
^{98}Mo$(n,x)^{97m}$Nb	[51]
^{98}Mo$(n,x)^{97}$Nb	[51]
^{100}Mo$(n,\alpha)^{97}$Zr	[51]
^{100}Mo$(n,2n)^{99}$Mo	[51], TALYS-0.57, EAF-2003, JEFF-3.0, JENDL-3.3, ADL-3
^{99}Tc$(n,n'\gamma)^{99m}$Tc	5-14 MeV [53]; <5, >14 MeV TALYS-0.57
^{99}Tc$(n,p)^{99}$Mo	[53] (JEFF-3.0, JENDL-3.3)
^{99}Tc$(n,\alpha)^{96}$Nb	[53] (JENDL-3.3)
^{115}In$(n,n'\gamma)^{115m}$In	EAF-2003, JENDL-3.3, JEFF-3.0, (ENDF/B-VI)
^{115}In$(n,\gamma)^{116}$In	ENDF/B-VI, JENDL-3.3, IRDF
^{119}Sn$(n,p)^{119m}$In	EAF-2003
^{127}I$(n,2n)^{126}$I	EAF-2003

Table 3.2: *Evaluation or model calculations agreeing best with the available measured data.*

Reaction	Recommendation
^{129}I$(n,2n)^{128}$I	EAF-2003
^{129}I$(n,p)^{129g}$Te	JENDL-3.3
^{129}I$(n,p)^{129m}$Te	
^{129}I$(n,\alpha)^{126g}$Sb	
^{129}I$(n,\alpha)^{126m}$Sb	
^{138}Ba$(n,2n)^{137m}$Ba	TALYS-0.57, EAF-2003
^{nat}Pb$(n,x)^{204}$Tl	EAF-2003
^{204}Pb$(n,n'\gamma)^{204m}$Pb	[55] (EAF-2003)
^{204}Pb$(n,2n)^{203}$Pb	TALYS-0.57, EAF-2003, [55]
^{204}Pb$(n,2n)^{203m}$Pb	ADL-3, TALYS-0.57, [55]
^{204}Pb$(n,3n)^{202m}$Pb	[55]
^{206}Pb$(n,\alpha)^{203}$Hg	[55] (EAF-2003, JEFF-3.0, JENDL-3.3)
^{206}Pb$(n,3n)^{204m}$Pb	
^{208}Pb$(n,p)^{208}$Tl	ENDF/B-VI, [55]

4. PARAMETER SENSITIVITY AND PREDICTIVE POWER

In the course of the subgroup several calculations were made to provide further insight into the predictive power of model calculations. Furthermore, insights in the predictive power of approaches with different degrees of underpinning in fundamental nuclear physics were obtained from experts at the subgroup's workshop (See the proceedings in Part B). Some suggestions are presented of how further improvements in predictive power and in the determination of covariance information may be obtained.

4.1 Parameter sensitivity

Following Ref. [56] sensitivity coefficients $S_{\alpha,i}$ were defined as the ratio of the relative change of cross-section σ_α to the relative change in a model parameter p_i.

$$S_{\alpha,i} = \frac{\delta\sigma_\alpha/\sigma_\alpha}{\delta p_i/p_i} = \frac{p_i}{\sigma_\alpha}\frac{\delta\sigma_\alpha}{\delta p_i} \tag{4..1}$$

Fessler and Smith applied this method to the Cr [57] reactions for which measurements had been performed at IRMM and FZ Jülich by Fessler *et al.* [10, 34] while Sudár applied this method to reactions on Tc, Ag and Pb, studied experimentally (Tab. 2.1) by the subgroup. Both these works focussed on the level density parameter a and the back-shift Δ of the back-shifted Fermi-gas model as well as the effective matrix element of the exciton model. In an earlier OECD-NEA study [58] Shibata investigated sensitivity coefficients for neutron-induced reactions on ^{56}Fe including also the optical model parameters, i.e. the real and imaginary potential radii, well depths and diffusenesses. These works that were limited to neutron energies below 20 MeV are summarised in Tab. 4.1.

4.2 Cross-section uncertainty

It was found that typically two level density parameters show sensitivities well in excess of one. These represent competing channels and their sensitivities range from 2 to 8 depending on channel and energy range. Only in the case of inelastic scattering on ^{56}Fe and of the ^{52}Cr$(n,2n)^{51}$Cr reaction were all sensitivities found to be less than one. In both these cases there is no substantial competition from

Table 4.1: *Summary of sensitivity calculations.*
For the level density, only the level density parameter a is implied, whereas for the pre-equilibrium process, the effective matrix element of the exciton model is considered. The sensitivity coefficient for the backshift parameter of the BSFG model is typically (well) below 1.

Parameter type	Typical uncertainties (%)	Impact	
		Energy range (MeV)	Sensitivity
Optical model	0.5-10	thr.-20	0.1-4
Level density	5-20	Continuum	0.1-8
Pre-equilibrium	10-40	$>$12	0.5-2

other channels. On the contrary, for charged particle emission reactions one always observes this situation.

In the case of optical model parameters, Shibata found [58] that in the case of ^{56}Fe most parameters have sensitivities between 0 and 1 for what concerns the compound nucleus formation , the inelastic, the (n,p) and the (n,α) cross-sections. Only for (n,p) and (n,α) cross-sections values of 2 and 4 were found for the real potential radius and a value of 2 for the real potential diffuseness in case of the (n,α) reaction.

With reasonable guesses for parameter uncertainties and their correlations, sensitivity coefficients can be used to obtain the relative uncertainty of predicted cross-sections

$$\frac{\langle \delta\sigma_\alpha \rangle^2}{\sigma_\alpha^2} = \sum_{i,j} S_{\alpha,i} S_{\alpha,j} \frac{\langle \delta p_i \delta p_j \rangle}{p_i p_j} \tag{4..2}$$

and, more generally, of the relative covariance matrix

$$\frac{\langle \delta\sigma_\alpha \delta\sigma_\beta \rangle}{\sigma_\alpha \sigma_\beta} = \sum_{i,j} S_{\alpha,i} S_{\beta,j} \frac{\langle \delta p_i \delta p_j \rangle}{p_i p_j} \tag{4..3}$$

although the latter was not evaluated by members of the subgroup.

It was shown that for $(n,2n)$ reactions that make up a sizeable part of the total reaction cross-section (absence of significant competition) predicted uncertainties were small ($< 20\%$) whereas for charged particle reactions uncertainties of 50% are no exception. An illustration of these findings is given in Fig. 4.1

in the case of the ^{99}Tc$(n,p)^{99}$Mo and ^{99}Tc$(n,\alpha)^{96}$Nb reactions using model calculations by S. Sudár with the STAPRE code. Here, the parameter covariance matrix was assumed to be diagonal. It is evident that the uncertainty bands thus calculated neither include feedback from the measured cross-section uncertainties and correlations nor from residual modelling deficiencies. Therefore, in the face of the measurements that have taken place these uncertainties appear excessive. This conclusion is only partially offset by the lack of correlations in the parameter uncertainties. Clearly a mechanism of feedback between cross-section uncertainties and residual modelling deficiencies to the parameter uncertainties is needed. Only then effective use is made of the database of measured cross-sections to resolve the need for covariance information in nuclear data evaluations. The interest in covariance information for evaluations is currently an important topic (See e.g. Aliberti *et al.* [59]). It is therefore worthwhile to investigate this point further.

Current practice is that parameters are adjusted to obtain a more or less optimal description of the pertinent reactions. Without further effort this does not result in feedback to the parameter uncertainties and correlations. With such a method all one can deliver is a statement about the observed differences between the optimised model calculations and the measured data. The correlations between the model parameters are not only of academical interest (i.e. insight in the physics of the model). Parameters that are falsely varied in an uncorrelated manner may yield too large uncertainty estimates.

4.2.1 Recent developments

Recently, Bauge *et al.* have used observed differences between experiments and calculations with an optimised optical model potential to determine judiciously the diagonal elements of the five underlying parameters of a semi-microscopic approach to the optical model [60]. Sampling this five dimensional parameter space with the Monte Carlo technique cross-section distributions were obtained. The method provides the full distribution with the added advantage of automatically including correlations between cross-sections and securing their positive character.

This Monte Carlo approach has been proposed and elaborated mathematically by D.L. Smith [61] and it was implemented, recently, as a driver for the TALYS code [62]. The essential idea is to assume that each nuclear model parameter has its own uncertainty, where the uncertainty distribution is assumed Gaussian. The basis of the method is then formed by running TALYS K times, with e.g. $K = 1000$, whereby each time all elements of the parameter vector are sampled *randomly* from a Gaussian distribution with a specific width for each parameter. After performing the K calculations, all statistical information is available and a full covariance matrix is produced. Fig. 4.2 shows an example

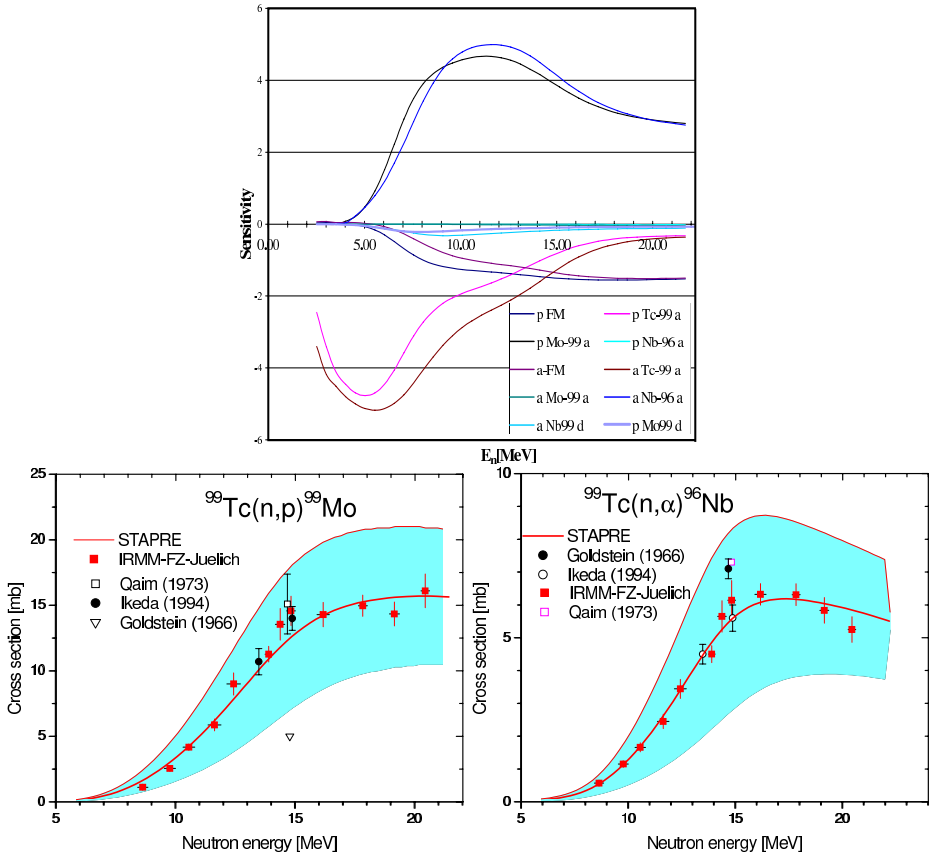

Figure 4.1: *Sensitivity coefficients (top) and uncertainty bands (bottom) for the* $^{99}Tc(n,p)^{99}Mo$ *and* $^{99}Tc(n,\alpha)^{96}Nb$ *reactions. With "p Mo-99 a" we denote the level density parameter* a *for the nucleus* ^{99}Mo *in the case of the* $^{99}Tc(n,p)^{99}Mo$ *reaction, whereas "a Nb-96 d" is the backshift parameter* Δ *for* ^{96}Nb *in case of the* $^{99}Tc(n,\alpha)^{96}Nb$ *reaction, etc. Uncertainty bands correspond to* $\Delta a/a$ *of 10% for* ^{99}Tc, ^{99}Mo, ^{96}Nb, $\Delta\sigma_{\rm abs}/\sigma_{\rm abs} = 5\%$, *an absolute change of* Δ *of 0.2 MeV and a relative change of the exciton effective matrix element of 10%.*

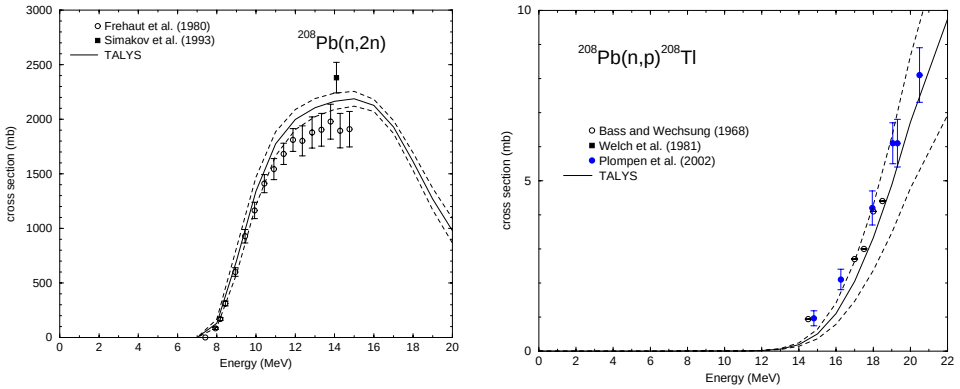

Figure 4.2: *Cross-sections and uncertainty bands as calculated with TALYS using a Monte Carlo approach for input parameter sampling, (left)* ^{208}*Pb*$(n, 2n)$ *(right)* ^{208}*Pb*$(n, p)^{208}$*Tl.*

of this method, for the ^{208}Pb$(n, 2n)$ cross-section. Note that the figure merely shows the uncertainty band, while every possible correlation between channels and energies are produced. The practicability of this approach was demonstrated only recently at the ND2004 conference in fall 2004, and further research is needed to determine realistic uncertainties of the model parameters. The first calculations indicate that the uncertainties listed in Table 4.1 are reasonable, in the sense that they lead to realistic calculated uncertainties for the cross-sections.

An assessment of parameter uncertainties and correlations is the key difficulty in any approach. Few attempts have been made to address this problem systematically for Hauser-Feshbach type calculations. Bayesian parameter estimation using the generalised least-squares technique is the standard approach in the resolved resonance region. For this region one has a theory, the Reich-Moore approximation to the R-matrix, that is sufficiently exact to allow perfect fits to the data when all experimental information has been fixed and multiple scattering is accounted for. Thus, the SAMMY code is able to provide fitted resonance parameters with full parameter covariances [63]. F. Fröhner developed the code FITACS for Bayesian parameter estimation in the unresolved resonance region using the Hauser-Feshbach-Moldauer theory [64]. Again this leads to parameter uncertainties (and in principle covariances) on quantities such as the strength functions, scattering radii, mean radiation widths and mean level spacings. FITACS is implemented as a subroutine in the SAMMY code [63].

For the energy range above the unresolved resonance region no general systematic approach was developed and only scattered examples are found where

parameter fitting was applied and parameter uncertainties and correlations could be extracted at least in principle. Kawano *et al.* implemented Bayesian parameter estimation for the analysis of ^{58}Ni$(n,\alpha)^{55}$Fe cross-sections [65]. Soukhovitskii *et al.*, applied a least-squares fit to obtain optical model parameters for ^{232}Th [66]. Recently, Leeb *et al.* presented a method that provides covariance information for cross-sections in the situation where optimisations were done 'by eye' and/or where model deficiencies do not allow a complete description of the measured data [67]. Here too, sensitivity coefficients feature.

4.3 Non-parametric changes

Sensitivity coefficients may be applied to continuous parameters of nuclear models. A workshop that was held in the context of this subgroup further confirmed that besides these continuous parameter contributions to the uncertainty there are also considerable variations to be expected when different model assumptions would enter into play. This confirms an earlier study with regard to level densities that was carried out for WPEC by Fu [68].

At the workshop an overview was given of the status of modelling based on microscopic nuclear theory by S. Goriely. E. Bauge and M. Avrigeanu presented studies highlighting the support that may be obtained from (semi-)microscopic nuclear theory for the evaluation of the optical model potential. These results are very promising in particular when no experimental information is available and moderate accuracy is adequate or in the case of complex particle emission. Furthermore, important guidance is derived from theory for the parameterisations of empirical approaches to the optical model such as the recent evaluation by Koning and Delaroche [69]. For more details see the workshop contributions of M. Avrigeanu *et al.*, E. Bauge *et al.*, and S. Goriely *et al.*

As a general conclusion, the best description of measured data is obtained in the more empirical approaches with a suitably optimised database of parameters. For specific cases when a fair amount of experimental data is available, the best results are obtained by correlating all available experimental data in the relevant region of the nuclear chart (see e.g. the previous chapter). An empirical approach with globally optimised parameter sets such as those used in the TALYS code can lead to rather good results that are typically within 50% from the data and in many cases even within 20%. On the other hand, the more microscopic the approach the less accurate the prediction. However, one may expect that the predictive power of a fully microscopic approach is much more constant over the whole mass and Z range from drip-line to drip-line. Mass, optical model, γ-strength function and level density variations are constrained by the best available underpinning in nuclear physics (workshop proceedings, S. Goriely). Critical tests of physics away

from the line of stability are underway at several laboratories, e.g. at RIA, CERN-ISOLDE, GANIL, GSI, ... These will be of importance for the development of basic theory with a primary impact on nuclear astrophysics. For nuclear energy such developments will be of less concern since most isotopes of interest are on the line of stability with fission products as a notable exception.

4.4 Potential for improvements

To facilitate cross-section evaluations and to enable the propagation of uncertainties from the measurements to the calculated and hence the evaluated cross-sections, it seems natural to explore further the possibility of least squares fitting. The comments in this section address some aspects of the problem that will certainly need to be investigated in more detail and judged on their merit by a future implementation. It similarly has to be judged by experience what will be the role of the formalism proposed by Leeb *et al*. [67]. On the one hand it may be applied if in the fitting process residual modelling discrepancies exceed the standard uncertainties associated with the data. On the other hand one may choose to apply it to the fit-by-eye process, mentioned above. This choice is open and will be left to the evaluator.

4.4.1 Least squares

Least squares fitting constitutes the minimisation of a suitably defined χ^2 to find the parameters that result in the best description of the data. Methods routinely employed for least squares minimisation include Marquardt-Levenberg, Powell, simulated annealing, the simplex method [70] or the methods of Bayesian minimisation [63, 71, 72]. Suitably initiated and adapted to the analytic form of χ^2 given below these will all find the correct minimum value for χ^2 and thus the optimum parameter set. At the minimum a suitable additional step will lead to the covariances for the parameters. Several options exist such as the determination of the inverse of the curvature matrix which involves the sensitivity coefficients, the Monte Carlo bootstrap method (computationally intensive) and the determination of contours of constant $\Delta\chi^2$ [70, 71]. From the parameters and their covariances one may then evaluate cross-sections and their covariance by either the Monte Carlo technique discussed in the previous section or by Eq. 4..3. In the latter case the sensitivity coefficients (4..1) are required.

A rather general form for χ^2 is given by

$$\chi^2 = \chi^2_D + \chi^2_P \qquad (4..4)$$
$$\chi^2_D = \frac{1}{2}[\mathbf{y} - \mathbf{f}(\mathbf{p})]^T \mathbf{V_D^{-1}} [\mathbf{y} - \mathbf{f}(\mathbf{p})]$$
$$\chi^2_P = \frac{1}{2}[\mathbf{p} - \mathbf{p_0}]^T \mathbf{V_P^{-1}} [\mathbf{p} - \mathbf{p_0}]$$

where $\mathbf{y}$ is the vector with all the relevant data, $\mathbf{f}$ is the model function that provides an estimate for each of the measured data points, $\mathbf{p}$ are the parameters on which the model depends, $\mathbf{p_0}$ is the prior guess for these parameters, $\mathbf{V_D}$ is the covariance information for the data $\mathbf{y}$ and $\mathbf{V_P}$ is the covariance information for the prior distribution of the parameters $\mathbf{p}$. The only assumption in Eq. 4..4 is that no correlations between parameters and cross-sections are included. This corresponds to the situation where none of the measurements relies on model calculations involving some of the components of the parameter vector $\mathbf{p}$ for the determination of the final results that enter the data vector $\mathbf{y}$.

4.4.2 The data vector

Specifically, $\mathbf{y}$ of Eq. 4..4 contains all relevant measured data. This implies a list of data for many different observables, taken with a great variety of measurement techniques by various authors over sometimes 10s of years. If we were to implement the local approach of the previous chapter, say for ^{51}V, this would include besides the measured $(n, x\alpha)$, (n, α) and (n, p) activation cross-sections from various authors, all other experimental information used in the analysis: the measured neutron-induced total cross-section on ^{51}V, the measured proton and alpha induced reaction cross-sections on the residual nuclei (or on nearby nuclei), s- and p-wave spacings, strength functions, mean decay widths, potential radii, the transition point between discrete and continuum levels, angle and energy differential scattering/emission data, ...

The equivalent of the global approach would need a correspondingly larger data vector requiring the quantities used in the local approach for a (large) number of nuclei in the mass table.

The apparent complexity of such an all encompassing minimisation would benefit from elimination of any potential complications. It seems therefore an essential requirement to limit the data to be included to those that are free of measurement error. This implies prior assessment of the status of the measurements in the database is essential. Such an approach has been adopted for instance in the evaluation of the activation standards published jointly by the OECD-NEA and the IAEA in 1992.

4.4.3 Weights

The natural question is how each of the components of the data vector $\mathbf{y}$ receives an appropriate weight. The answer according to probability theory is provided in Eq. 4..4. Ideally a full covariance matrix $\mathbf{V_D}$ must be constructed. In practice such a construction is probably beyond hope. Information about past measurements is incomplete and not all past measurements can be discarded. Complete covariance information for current day measurements can be pursued only within certain limits and requires dedicated expertise of the evaluator. Gauging the extent of inter-experiment correlations, for instance as a result of a common standard or even a common system of standards is a problem that is not even dealt with fully for the standards themselves.

What is needed is a sensible approach to the determination of $\mathbf{V_D}$ that duly respects the importance of each data component so that it may determine the parameters to which it is most sensitive and that also duly respects the relative merits of different measurements. Unfortunately, the simplest expression for χ^2 is fatally flawed for the purpose of this type of nuclear data evaluation. In the simplest approach one assumes $\mathbf{V_D}$ diagonal with the square of the standard uncertainty σ_i of the data point i on the diagonal $(\mathbf{V_D})_{i,i} = \sigma_i^2$.

Three examples illustrate key problems with the simplest approach to the determination of χ^2. First, suppose one single measurement of a cross-section was performed by one group at 14 MeV with 10% standard uncertainty and that in the range from threshold to 20 MeV ten measurements were done by another group with about 10% standard uncertainty for each point. In the simplest approach the latter measurement outweighs the first ten fold. That is fine unless there is a dominating common source of uncertainty for the ten points (eg. the normalisation factor). Then the relative weight of the two measurements for the normalisation of the calculated excitation curve should be equal. In such a case the importance of the ten points lies in the information about the shape of the curve, much less its normalisation. An appropriate covariance matrix for the ten points provides this essential piece of information. Second, suppose double differential emission spectra have been measured from which angle integrated energy differential spectra and energy and angle integrated channel cross-sections were determined. Clearly, the only independent data are the double differential spectra. However, indiscriminate use of a database such as EXFOR would not reveal such a point and also the differential energy spectra and the channel cross-sections would enter the expression of χ^2 as independent data. Thus, the weight of such a data set would be higher than justified. Elimination of the derived data from the fit or a full covariance matrix for the double differential data set together with the deduced data sets would result in the appropriate weight for the overall

measurement. Third, two different measurements with dominating normalisation uncertainty taken relative to the same standard cross-section really act as two points from the same author, i.e. a strong off-diagonal correlation between different measurements ought to be taken into account.

In practice, in a situation where little or no correlation information for experimental data is available a pragmatic first order approach is required. For such a first approach, it will be natural to assume no correlation between measurements, or at least limit the number of measurements that are cross correlated for obvious reasons to a few groups. Thus, χ^2_D will break down in the sum of contributions $\chi^2_{D_i}$ for measurement (group) i. As indicated, for independent measurement sets a main difficulty is when both small data sets and large data sets are present. When all the points in one data set are expected to have one common dominating source of uncertainty, an example presented below suggests that as contribution of the set to χ^2_D (Eq. 4..4) the conventional χ^2 divided by the number of data points should be used. Thus, the whole data set is weighted as if it were one point, but of course the information on the shape of, for instance, an excitation curve that is contained in the data set is preserved and will act to minimise the appropriate parameters.

When groups of measurements are taken relative to the same standard or set of standards the main point will be to ensure that the cross-section values used for the standard are the same. In such a case, the correlation of uncertainties plays a secondary role.

A large data set with dominating normalisation uncertainty.

Assume a measurement vector $\mathbf{m}$ representing for instance data points from a single measurements of an excitation curve, an angular distribution or an emission spectrum. Suppose that the measurement model is $\mathbf{m} = \lambda\mathbf{d}$ with λ a normalisation factor and $\mathbf{d}$ a sequence of raw data points that have uncorrelated standard errors σ_λ and σ_d and identical errors for all measured points ($\mathrm{Var}(\mathbf{d}) = \sigma_d^2\mathbf{I}$). The covariance matrix $\mathbf{V}$ of $\mathbf{m}$ and its inverse are given by

$$\mathbf{V} = \lambda^2\sigma_d^2\mathbf{I} + \sigma_\lambda^2\mathbf{d}\mathbf{d}^T \quad \text{and} \quad \mathbf{V}^{-1} = \frac{1}{\lambda^2\sigma_d^2}\left(\mathbf{I} - \frac{\sigma_\lambda^2}{\sigma_\lambda^2\left\|\mathbf{d}\right\|^2 + \lambda^2\sigma_d^2}\mathbf{d}\mathbf{d}^T\right)$$

or with $r_\lambda = \sigma_\lambda/\lambda$ and $r_d = \sigma_d/\left\|\mathbf{d}\right\|$

$$\mathbf{V} = \left\|\mathbf{m}\right\|^2 r_d^2\mathbf{I} + r_\lambda^2\mathbf{m}\mathbf{m}^T \quad \text{and}$$
$$\mathbf{V}^{-1} = \frac{1}{\left\|\mathbf{m}\right\|^2 r_d^2}\left(\mathbf{I} - \frac{r_\lambda^2}{\left(r_\lambda^2 + r_d^2\right)}\frac{\mathbf{m}\mathbf{m}^T}{\left\|\mathbf{m}\right\|^2}\right)$$

Thus χ^2_m is obtained from

$$\begin{aligned} 2\chi^2_m &= (\mathbf{m}-\mathbf{f})^T \mathbf{V}^{-1} (\mathbf{m}-\mathbf{f}) \\ &= \frac{1}{\|\mathbf{m}\|^2 r_d^2} \left(\|\mathbf{m}-\mathbf{f}\|^2 - \frac{r_\lambda^2}{\left(r_\lambda^2 + r_d^2\right)} \frac{(\mathbf{m}, \mathbf{m}-\mathbf{f})^2}{\|\mathbf{m}\|^2} \right) \end{aligned}$$

and, for fixed parameters $\mathbf{p}$, is seen to have values between the following limits

$$\frac{1}{r_d^2 + r_\lambda^2} \frac{\|\mathbf{m}-\mathbf{f}\|^2}{\|\mathbf{m}\|^2} \leq 2\chi^2_m \leq \frac{1}{r_d^2} \frac{\|\mathbf{m}-\mathbf{f}\|^2}{\|\mathbf{m}\|^2}$$

The right hand limit corresponds to the value for negligible normalisation error, whereas the left hand side corresponds to the minimum value to be regarded for χ^2_m for this data set. The right hand side also corresponds to the simplest approximation for χ^2 when $r_\lambda \ll r_d$, since then $r_d^2 \|\mathbf{m}\|^2 = \sigma_d^2 \approx \langle \sigma_m \rangle^2$. For the left hand side $r_\lambda \gg r_d$ yields an N times smaller value as $r_\lambda^2 \|\mathbf{m}\|^2 \approx N\sigma_m^2$. Thus one finds,

$$\frac{1}{N} \frac{\|\mathbf{m}-\mathbf{f}\|^2}{2\langle \sigma_m \rangle^2} \leq \chi^2_m \leq \frac{\|\mathbf{m}-\mathbf{f}\|^2}{2\sigma_m^2}$$

with σ_m the standard uncertainty of a single data point and N the number of data points in $\mathbf{m}$.

From the pragmatic point of view, if one suspects strongly correlated uncertainties between many data points obtained from a single measurement campaign, the least weight one must attribute to the measurement in the χ^2_D of Eq. 4..4 is the left hand expression of the last inequality given above.

4.4.4 Prior uncertainties

Prior values and uncertainties may naturally be used to constrain parameter variations through the term χ^2_P in Eq. 4..4 to ranges that are consistent with physical insights. Such insight may have been obtained from previous analysis of data sets not included in the current fit or from basic restrictions imposed by nuclear theory. Here too, the evaluator has the means to impose his physics intuition on the minimisation process. Note that χ^2_P has the effect of rendering an under-determined minimisation problem, over-determined. That is if fewer data points are available in $\mathbf{y}$ than there are parameters in $\mathbf{p}$, the prior knowledge of the parameters given by $\mathbf{p}_0$ and $\mathbf{V}_P$ renders the minimisation problem well determined. In general, this contribution to χ^2 will enhance the stability of the problem.

5. SUMMARY

Subgroup 19 has provided a large number of newly measured activation cross-sections. Most of these measurements were performed in the range from 15 to 21 MeV. Important additional measurements were made at 14 MeV and in the problem region from threshold to 12 MeV. Measured data are presented in tabular form and in graphical form in Part C of this report. A large fraction of the measured data was compiled in EXFOR format. An overview table is presented in this report together with a list of references where further details may be found.

Model calculations in a local approach have been performed for reactions on (isotopes of) Na, V, Ni, Co, Tc, Mo, I, and Pb. References to these works are presented and for many cases numerical results are given in Part C.

Comparisons of the newly measured results with the calculations in the local approach, calculations with TALYS-0.57, some calculations with EMPIRE-II and with a large number of evaluations are presented in graphical form in Part C. The calculations with the code TALYS-0.57 constitute blind calculations with parameters predetermined from global analyses over the mass table. From this graphical inter-comparison recommendations were made stating which curve reproduces the data best. Generally, the calculations of the local approach are preferred when they are available. TALYS default calculations may improve on existing evaluations in about 20% of the cases.

Sensitivity coefficients were introduced and determined for reactions on Cr, Tc, Ag and Pb. Together with an earlier OECD-NEA study on ^{56}Fe by Shibata the calculated coefficients provide valuable insight into required uncertainties of model parameters, if predefined target uncertainties for cross-sections are to be met. With a predetermined uncertainty of model parameters uncertainty bands were constructed and compared to the cross-sections.

Clearly, very large uncertainties can be expected for important reactions when model calculations use a database of parameters that have been determined with no reference to measured cross-sections. As such, it seems of interest to develop a systematic method for incorporating the database of measured cross-sections and their uncertainties into such parameter databases. This requires tools for systematic comparisons of model calculations with data as well as a strategy for (automated) adjustment of model parameters to describe the data. The latter is routine (because essential) in resonance shape analysis but is only in its exploratory phase for reaction cross-sections such as considered here. The problem of least squares fitting of data for the purpose of evaluations was discussed briefly.

Bibliography

[1] R.A. Forrest, J. Kopecky, and J.C. Sublet. Development of the European activation system. *J. of Nucl. Sci. and Technol.*, S2:96–99, 2002.

[2] E.M. Zsolnay and R. Paviotti de Corcuera. Development and status of the new International Reactor Dosimetry File IRDF-2002. Proc. of the Workshop on Neutron Measurement, Evaluations and Applications, 5-8 November, Budapest, Hungary, EUR Report 21110 EN, ISBN 92-894-6041-5, 2003.

[3] R.S. Dybczyński. Very accurate (definitive) methods by radiochemical NAA and their significance for quality assurance in trace analysis. Proc. of the Workshop on Neutron Measurement, Evaluations and Applications, 5-8 November, Budapest, Hungary, EUR Report 21110 EN, ISBN 92-894-6041-5, 2003.

[4] J. Blomgren. Nuclear data for single-event effects. Proc. of the Workshop on Neutron Measurement, Evaluations and Applications, 5-8 November, Budapest, Hungary, EUR Report 21110 EN, ISBN 92-894-6041-5, 2003.

[5] S.M. Qaim. Some applications of neutron in biology and medicine. Proc. of the Workshop on Neutron Measurement, Evaluations and Applications, 5-8 November, Budapest, Hungary, EUR Report 21110 EN, ISBN 92-894-6041-5, 2003.

[6] A. Fessler, A.J.M. Plompen, D.L. Smith, J.W. Meadows, and Y. Ikeda. Neutron activation cross-Section measurements from 16 to 20 MeV for isotopes of F, Na, Mg, Al, Si, P, Cl, Ti, V, Mn, Fe, Nb, Sn, and Ba. *Nucl. Sci. Eng.*, 134:171–200, 2000.

[7] A.J.M. Plompen, D.L. Smith, P. Reimer, V. Semkova, F. Cserpák, S.M. Qaim, V. Avrigeanu, and S. Sudár. Neutron activation cross-section measurements at Geel. *J. of Nucl. Sci. and Technol.*, S2:192, 2002.

[8] G.F. Knoll. *Radiation detection and measurement*. John Wiley and Sons, Inc., New York, USA, third edition, 2000.

[9] K. Debertin and R.G. Helmer. *Gamma- and X-ray spectrometry with semiconductor detectors*. North Holland Publishers, Amsterdam, Netherlands, 1988.

[10] A. Fessler and S.M. Qaim. Excitation functions of ^{50}Cr(n,np+pn+d)^{49}V, ^{58}Ni(n,α)^{55}Fe, ^{58}Ni(n,αp+pα)^{54}Mn, ^{62}Ni(n,α)^{59}Fe Reactions. *Radiochem. Acta*, 84:1, 1999.

[11] M. Drosg. DROSG-2000: Neutron source reactions. Report IAEA-NDS-87, v. 2.2, Rev. 8, IAEA, Vienna, Austria, www-nds.iaea.org, 2003.

[12] H. Schuhmacher, H.J. Brede, V. Dangendorff, M. Kuhfuss, J.P. Meulders, W.D. Newhauser, and R. Nolte. Quasi-monoenergetic neutron beams with energies from 25 to 70 MeV. *Nucl. Instrum. Methods Phys. Res.*, A421:284–295, 1999.

[13] M. Baba, Y. Nauchi, T. Iwasaki, T. Kiyosumi, M. Yoshioka, S. Matsuyama, N. Hirakawa, T. Nakamura, Su. Tanaka, S. Meigo, H. Nakashima, Sh. Tanaka, and N. Nakao. Charaterization of a 40-90 MeV ^{7}Li(p,n) neutron source at TIARA using a proton recoil telescope and a TOF method. *Nucl. Instrum. Methods Phys. Res.*, A428:454–465, 1999.

[14] Y. Ikeda, C. Konno, K. Oishi, T. Nakamura, H. Miyade, K. Kawade, H. Yamamoto, and T. Katoh. Activation cross-section measurements for fusion reactor structural materials at energies from 13.3 to 15.0 MeV using FNS facility. JAERI-1312, 1988.

[15] Y. Ikeda and C. Konno. Measurements of the cross-sections for ^{94}Mo(n,p)& ^{95}Mo(n,np)^{94}Nb, ^{158}Dy(n,p)^{158}Tb, ^{182}W(n,nα)^{178m2}Hf and ^{187}Re(n,2n)^{186m}Mo reactions at 14 MeV region. INDC(NDS)-286, 27-31, 1993.

[16] Y. Ikeda, C. Konno, Y. Oyama, K. Kosako, K. Oishi, and H. Maekawa. Absolute measurements of activation cross-sections of ^{27}Al(n,p)^{27}Mg, ^{27}Al(n,α)^{24}Na, ^{56}Fe(n,p)^{56}Mn, ^{90}Zr(n,2n)$^{89m+g}$Zr and ^{93}Nb(n,2n)^{92m}Nb at energy range of 13.3-14.9 MeV. *J. of Nucl. Sci. and Technol.*, 30:870–880, 1993.

[17] Y. Kasugai, H. Yamamoto, K. Kawade, and T. Iida. Measurement of (n,p) cross-sections for short-lived products by 13.4-14.9 MeV neutrons. *Ann. Nucl. Energy*, 25:23–45, 1998.

[18] Y. Kasugai, Y. Ikeda, H. Yamamoto, and K. Kawade. Systematics for (n,α) excitation functions in then neutron energy range between 13.3-15.0 MeV. *Ann. Nucl. Energy*, 25:421–435, 1998.

[19] A.A. Filatenkov, S.V. Chuvaev, V.A. Jakovlev, A.V. Malyshenkov, and S.K. Vasiljev. Systematic measurement of cross-sections at neutron energies of 13.4-14.9 MeV. In A. Ventura G. Reffo and C. Grandi, editors, *Proceedings of the International Conference on Nuclear Data for Science and Technology*, pages 598–602, Trieste, Italy, May 19-24 1997. Editrice Compositori, 40128 Bologna, Italy.

[20] A.A. Filatenkov, S.V. Chuvaev, V.N. Aksenov, V.A. Yakovlev, A.V. Malyshenkov, S.K. Vasil'ev, M. Avrigeanu, V. Avrigeanu, D.L. Smith, Y. Ikeda, A. Wallner, W. Kutschera, A. Priller, P. Steiner, H. Vonach, G. Mertens, and W. Rochow. Systematic Measurement of Activation cross-sections at Neutron Energies from 13.4 to 14.9 MeV. IAEA Report INDC(CCP)-402, Vienna, 1997; Khlopin Radium Institute Report RI-252, St Petersburg, 1999.

[21] M. Salvatores. Accelerator Driven Systems (ADS), physics principles and specificities. *J. de Phys. IV*, 9:Pr7.17, 1998. *Proceedings of the Workshop on Innovative Options in the Field of Nuclear Fission Energy*, April 27 - May 1, Les Houches, France, ed. J.-P. Schapira, EDP Sciences, 91499 Les Ulis, France.

[22] Y.A. Korovin, A.Y. Konobeyev, P.E. Pereslavtsev, A.Y. Stankovsky, U. Fischer, and U. von Möllendorf. Data library IEAF-2001 to study of activation of irradiated materials. *J. of Nucl. Sci. and Technol.*, S2:68, 2002.

[23] IFMIF International team. IFMIF Comprehensive Design Report. insdell.-tokai.jaeri.go.jp/IFMIFHOM/, 2004.

[24] S. Leray, F. Borne, A. Boudard, F. Brochard, S. Crespin, D. Drake, J.C. Duchazeaubeneix, J.M. Durand, J. Fréhaut, F. Hanappe, L. Kowalski, C. Le Brun, F.R. Lecolley, J.F. Lecolley, X. Ledoux, F. Lefebvres, R. Legrain, M. Louvel, E. Martinez, S.I. Meigo, S. Ménard, G. Milleret, Y. Patin, E. Petibon, P. Pras, Y. Terrien, J. Thun, C. Varignon, D.M. Whittal, and W. Wlazlo. Spallation neutron studies at Saturne. Proc. 3^{rd} Int. Conf. on Accelerator Driven Transmutation Technologies and Applications, Praha, 7-11 June, 1999.

[25] S. Leray, F. Borne, S. Crespin, J. Fréhaut, X. Ledoux, E. Martinez, Y. Patin, E. Petibon, P. Pras, A. Boudard, R. Legrain, Y. Terrien, F. Brochard, D. Drake, J.C. Duchazeaubeneix, J.M. Durand, S.I. Meigo, G. Milleret, D.M. Whittal, W. Wlazlo, D. Durand, C. Le Brun, F.R. Lecolley, F. Lefebvres, C. Varignon, F. Hanappe, S. Ménard, L. Stuttge, and J. Thun.

Spallation neutron production by 0.8, 1.2 and 1.6 GeV protons on various targets. *Phys. Rev. C*, 65:044621, 2002.

[26] K. Shibata, T. Kawano, T. Nakagawa, O. Iwamoto, J. Katakura, T. Fukahori, S. Chiba, A. Hasegawa, T. Murata, H. Matsunobu, T. Ohsawa, Y. Nakajima, T. Yoshida, A. Zukeran, M. Kawai, M. Baba, M. Ishikawa, T. Asami, T. Watanabe, Y. Watanabe, M. Igashira, N. Yamamuro, H. Kitazawa, N. Yamano, and H. Takano. Japanese Evaluated Nuclear Data Library Version 3 Revision-3: JENDL-3.3. *J. of Nucl. Sci. and Technol.*, 39:1125, 2002.

[27] The JEFF project. The JEFF-3.0 Nuclear Data Library. www.nea.fr/html/-dbdata/projects/nds_jef.htm#library, OECD-Nuclear Energy Agency, Issy-les-Moulineaux, France, 2002.

[28] R.A. Forrest, J. Kopecky, and J.C. Sublet. The European Activation File: EAF-2003 cross-section library. UKAEA Report FUS 486, Culham Science Center, Abingdon, OX14 3DB, UK, 2002.

[29] P. Talou, M.B. Chadwick, F. Dietrich, M. Herman, T. Kawano, A. Koning, and P. Oblozinsky. Subgroup A: Nuclear Model Codes. Report to the Sixteenth meeting of the WPEC, 26-28 May, Aix-en-Provence, www.nea.fr/html/science/docs/nsc-wpec-doc2004-312.pdf, OECD-NEA WPEC, Issy-les-Moulineaux, France, 2004.

[30] IAEA-NDS. Handbook for calculations of nuclear reaction data: Starter file, Reference Input Parameter Library. IAEA-TECDOC-1034, IAEA, Vienna, Austria, available online at www-nds.iaea.org/ripl, 1998.

[31] IAEA-NDS. Handbook for calculations of nuclear reaction data: RIPL-2. IAEA, Vienna, Austria, available online at www-nds.iaea.org/RIPL-2, 2005.

[32] IAEA-NDS. Parameters for Calculation of Nuclear Reactions of Relevance to Non-energy Applications (RIPL-3), Summary Report of the First RCM, INDC(NDS)-462, Vienna, Austria 2004. IAEA, Vienna, Austria, available online at http://www-nds.iaea.org/reports/indc-nds-462.pdf.

[33] Working Party on International Evaluation Co-operation. The High Priority Nuclear Data Request List. NEA Nuclear Science Committee, www.nea.fr/-html/dbdata/hprl/hprlmain.cgi, 2001.

[34] A. Fessler, E. Wattecamps, D.L. Smith, and S.M. Qaim. Excitation functions of (n,2n), (n,p), (n,np+pn+d), and (n,α) reactions on isotopes of chromium. *Phys. Rev. C*, 58(2):996–1004, 1998.

[35] A. Fessler. Activation cross-sections and Isomeric cross-section Ratios in Neutron Induced Reactions on Cr-, Fe-, and Ni-Isotopes in the Energy Range 9 to 21 MeV. Forschungszentrum Jülich GmbH, Report No. Jül-3502, ISSN 0944-2952, 1998.

[36] P. Reimer, V. Avrigeanu, A.J.M. Plompen, and S.M. Qaim. Reaction mechanisms of fast neutrons on ^{51}V below 21 MeV. *Phys. Rev. C*, 65:014604, 2001.

[37] P. Reimer, M. Hult, A.J.M. Plompen, P.N. Johnston, V. Avrigeanu, and S.M. Qaim. Measurement of the ^{nat}Mo(n,x)^{94}Nb cross-section using ultra low-level γ-ray spectrometry at HADES. *Nucl. Phys. A*, 705:265–278, 2002.

[38] P. Reimer. Fast neutron induced reactions leading to activation products: selected cases relevant to development of low activation materials, transmutation and hazard assessment of nuclear wastes. Forschungszentrum Jülich GmbH, Report No. Jül-3980, ISSN 0944-2952, 2002.

[39] V. Semkova, V. Avrigeanu, A.J.M. Plompen, P. Reimer, D.L. Smith, S. Sudár, A. Koning, and A. Forrest. Neutron activation cross-sections for safety of nuclear power plants. EUR Report 20820 EN, ISBN 92-894-6095-4, European Communities, JRC-IRMM, Geel, Belgium, 2003.

[40] V. Semkova, V. Avrigeanu, T. Glodariu, A.J. Koning, A.J.M. Plompen, D.L. Smith, and S. Sudár. A systematic investigation of reaction cross-sections and isomer ratios for neutrons up to 20 MeV on Ni-isotopes and ^{59}Co by measurements with the activation technique and new model studies of the underlying reaction mechanisms. *Nucl. Phys. A*, 730:255, 2004.

[41] S. Cabral, G. Börker, H. Klein, and W. Mannhart. Neutron Production from the Deuteron Breakup Reaction on Deuterium. *Nucl. Sci. Eng.*, 106:308–317, 1990.

[42] R. Dóczi, S. Sudár, A. Fenyvesi, S. Szegedi, M. Fayez-Hassan, S.M. Qaim, and J. Csikai. Validation of neutron reference activation libraries. Proc. Workshop of Subgroup 19 on Activation cross-sections, Final Report, Part B, OECD-NEA, NSC-WPEC, Issy-les-Moulineaux, France, 2004.

[43] Á. Grallert, J. Csikai, S.M. Qaim, and J. Knieper. Recommended target materials for D-D neutron sources. *Nucl. Instrum. Methods Phys. Res.*, A334:154–159, 1993.

[44] Á. Grallert, J. Csikai, and S.M. Qaim. Improved gas-cell D-D neuron sources. *Nucl. Instrum. Methods Phys. Res.*, A337:615–618, 1994.

[45] V. Semkova, A.J.M. Plompen, and D.L. Smith. Measurement of ^{58}Ni$(n,t)^{56}$Co, ^{59}Co$(n,p)^{59}$Fe and ^{63}Cu$(n,\alpha)^{60m+g}$Co Reaction cross-sections from 14 to 20 MeV. Proc. Int. Conf. on Nuclear Data for Science and Technology, September 27- October 1 2004, Santa Fe, NM, USA, to be published.

[46] V. Semkova and A.J.M. Plompen. Recent cross-section studies with the activation technique for Ni, Co and Cu. EFF-DOC-806, JEFF Project, OECD-NEA, Issy-les-Moulineaux, unpublished, 2001.

[47] V. Semkova, A.J.M. Plompen, and D.L. Smith. Light Charged-Particle Production Activation cross-sections of Zr isotopes from 14 to 20 MeV. Proc. Int. Conf. on Nuclear Data for Science and Technology, September 27- October 1 2004, Santa Fe, NM, USA, to be published.

[48] F. Cserpák, S. Sudár, and A.J.M. Plompen. Measurements and nuclear model calculations for neutron induced reactions on ^{127}I, ^{129}I isotopes up to 21 MeV. Proc. Workshop of Subgroup 19 on Activation cross-sections, Final Report, Part B, OECD-NEA, NSC-WPEC, Issy-les-Moulineaux, France, 2004.

[49] K. Shibata. *J. of Nucl. Sci. and Technol.*, 39:1065, 2002.

[50] J.P. Delaroche, Ch. Lagrange, and J. Salvy. Report IAEA-190, IAEA, Vienna, 1976.

[51] P. Reimer, V. Avrigeanu, S.V. Chuvaev, A.A. Filatenkov, T. Glodariu, A. Koning, A.J.M. Plompen, S.M. Qaim, D.L. Smith, and H. Weigmann. Reaction mechanisms of fast neutrons on stable Mo isotopes below 21 MeV. *Phys. Rev. C*, 2005.

[52] V.I. Plyaskin and R.A. Kosilov. Level Density Parameters for the Back-Shifted Fermi Gas Model in the Mass Range 24$\leq$A$\leq$250. Report INDC(CCP)-424, IAEA, Vienna, Austria, 2000.

[53] P. Reimer, A.J.M. Plompen, V. Avrigeanu, S.M. Qaim, and S. Sudár. Activation cross-section for the ^{nat}V(n,xα)^{47}Sc, ^{99}Tc(n,p)^{99}Mo, and ^{99}Tc(n,α)^{96}Nb reactions: New Measurements and their Interpretation. ISINN-8, 17-20 May, Dubna, Russia, 2000.

[54] A.J.M. Plompen. Neutron-induced reaction cross-sections from threshold to 20 MeV. In N. Janeva, editor, *Proceedings of the XV Int. School on Nuclear Physics, Neutron Physics and Nuclear Energy*, page 131. Bulgarian Nuclear Society, September 27-October 1 2003.

[55] V. Semkova et al. In preparation, 2005.

[56] D.L. Smith. *Nucl. Instrum. Methods Phys. Res.*, A 339:626, 1993.

[57] A. Fessler and D.L. Smith. Parameter sensitivities in nuclear reaction cross-section calculations. *Ann. Nucl. Energy*, 29:363, 2002.

[58] K. Shibata. Sensitivities of calculated cross-sections of ^{56}Fe to model parameters. NEA Report OECD/GD(94)21, OECD, Paris, 1994.

[59] G. Aliberti, G. Palmiotti, M. Salvatores, and C.G. Stenberg. Impact of nuclear data uncertainties on transmutation of actinides in accelerator-driven assemblies. *Nucl. Sci. Eng.*, 146:13, 2004.

[60] E. Bauge. Assessment of the uncertainties associated with the optical model potential in evaluations. Proc. Int. Conf. on Nuclear Data for Science and Technology, September 27- October 1 2004, Santa Fe, NM, USA, to be published.

[61] D.L. Smith. Covariance matrices for nuclear cross-sections derived from nuclear model calculations. Nuclear Data Measurements Series, ANL-Report ANL/NDM-159, Argonne National Laboratory, 9700 South Cass Avenue, Argonne IL 60439, USA, 2004.

[62] A. Koning. Private communication, 2004.

[63] N.M. Larson. Sammy-M6-Beta, A code system for Multilevel R-matrix fits to neutron data using Bayes' equations. PSR-158, Peripheral Shielding Routine Collection, Radiation Safety Information Computational Center, ORNL, Oak Ridge, TN, USA, 2002.

[64] F.H. Fröhner. Evaluation of the unresolved resonance region of ^{238}U. *Nucl. Sci. Eng.*, 103:119, 1989.

[65] T. Kawano, T. Sanami, M. Baba, and H. Nakashima. *J. of Nucl. Sci. and Technol.*, 36:256, 1999.

[66] E.Sh. Soukhovitskii, R. Capote, J.M. Quesada, and S. Chiba. Dispersive coupled channel analysis of nucleon scattering from ^{232}Th up to 200 MeV. submitted for publication; J.M. Quesada *et al.*, n_BANT workshop, 22-23 March, CERN, Geneve, CH, 2005.

[67] H. Leeb, M.T. Pigni, and I. Raskinyte. Covariance for evaluations based on extensive modelling. Proc. Int. Conf. on Nuclear Data for Science and

Technology, September 27- October 1 2004, Santa Fe, NM, USA, to be published.

[68] C.Y. Fu and D.C. Larson. Effects of shape differences in the level densities of three formalisms on calculated cross-sections. Report NEA/WPEC-16, OECD, Paris, 1998.

[69] A.J. Koning and J.P. Delaroche. *Nucl. Phys. A*, 713:231, 2003.

[70] W.H. Press, S.A. Teukolsky, W.T. Vetterling, and B.P. Flannery. *Numerical Recipes in C*. Cambridge University Press, Cambridge, NY, USA, second edition edition, 1992.

[71] D.L. Smith. *Probability, Statistics and Data Uncertainties in Nuclear Science and Technology*. American Nuclear Society, La Grange Park, IL, USA, 1991.

[72] F.H. Fröhner. *Evaluation and analysis of nuclear resonance data*. OECD-NEA, Issy-les-Moulineaux, France, 2000.

[73] EXFOR. Nuclear reaction data. EXFOR was accessed on line at www.nndc.bnl.gov/nndc/exfor, www.nea.fr or www-nds.iaea.or.at/exfor, 2001.

[74] V. McLane. Evaluated Nuclear Data File, Section B, Version VI (ENDF/B-VI). National Nuclear Data Center, Brookhaven National Laboratory, 1998. available online at www.nndc.bnl.gov/nndc/endf.

[75] M.R. Bhat. Evaluated Nuclear Structure Data File. www.nndc.bnl.gov, NNDC, Brookhaven, USA, 2003.

Part B

Workshop Proceedings

Workshop summary

A.J.M. Plompen

EC-JRC-IRMM, Retieseweg 111, 2440 Geel, Belgium

Abstract:
January 2003, a subgroup workshop was held at IRMM, Geel, Belgium. The workshop served to bring together the subgroup members, interested parties and specialists. At the time of the workshop, experimental activities at IRMM, FZ-Jülich and U. Debrecen/Atomki-HAS were largely completed, as well as the model calculations in the local approach. Sensitivity calculations had been made for several nuclides within a particular nuclear model. Since, model choices had not been addressed in detail by subgroup members several specialists were invited to cover the various aspects of recent nuclear theory and code developments. Developers of the European Activation File project provided background on the status and process of the evaluation of activation cross-sections and expressed their interest in a continued effort along the lines of the subgroup's activities. Some measurements carried out in the context of the EURATOM fusion programme were presented. The status of data compilation for measurements by the subgroup was reviewed.

Compilation

Table 1 shows the agenda of the workshop. A general overview of the subgroup's aims, activities and achievements was presented (see chapter 1, Part A). A major point of the work concerned measurement of pertinent activation reaction cross-sections and to make these available to applications. To achieve this goal measured data must be readily available to evaluators. D.L. Smith compiled measured data in EXFOR format and submitted them to the NEA Data Bank. His slide show highlights the role of EXFOR, some of the tools available to extract information from this database and some of the technicalities an EXFOR compiler must respect in order to produce a file that is readily retrieved by the available search tools. (See Ref. [1] for details).

Table 1: *Workshop Agenda*
Agenda of the workshop of Subgroup 19, held on 13 and 14 January 2003 in Geel, Belgium.

time	Speaker	Title/Activity
13 January		
Morning Session		
9:00	E. Anklam	Opening
9:05	A. Plompen	Subgroup goals, activities and schedule
9:45	D.L. Smith(AP)	Compilation of measured activation cross-sections
10:15		Coffee Break
10:30	R.A. Forrest	Using experimental data to improve EAF-2001
11:00	J. Kopecky	Integral experiments for EAF-2003
11:30	J.Ch. Sublet	EAF Decay Power Experimental Validation
12:00	P. Reimer	Excitation functions for neutron-induced reactions on Mo, Tc and Pb in the energy range from 0.5 to 20.4 MeV
12:30		Lunch Break
13 January		
Afternoon Session		
14:00	V. Semkova	Measurements of neutron-induced activation reaction cross-sections on different isotopes of Co, Ni, Cu, Zr, and Pb from threshold to 20 MeV
15:00	D.L. Smith(AP)	Corrections for low energy neutrons by spectral indexing
15:30		Coffee break
15:45	R. Dóczi	Validation of neutron reference activation libraries
16:15	F. Cserpák	Excitation functions of (n,2n), (n,p) and (n,a) reactions on iodine isotopes
16:45	A. Filatenkov	Activation cross-section measurements at KRI: Yesterday, Today and ...?
14 January		
Morning Session		
9:00	A. Fessler	Neutron activation cross-section measurements, calculations and parameter sensitivities for Chromium isotopes, - A review
9:30	V. Avrigeanu	Report on EAF related tools
10:00	S. Sudár	Model calculations and experimental data
10:30		Coffee Break

Table 1: *Workshop Agenda*
Agenda of the workshop of Subgroup 19, held on 13 and 14 January 2003 in Geel, Belgium.

time	Speaker	Title/Activity
10:45	E. Bauge	A new model based evaluation of Europium isotopes
11:15	A. Koning	Predicting activation cross-sections with TALYS
11:45	S. Goriely	Microscopic models for practical applications
12:15		Lunch Break
14 January		
Afternoon Session		
14:00	S. Hilaire	Developments and prospects in level density modelling for nuclear applications
14:30	M. Avrigeanu	Semi-microscopic optical potentials for applications
15:00	J. Csikai	Proton activation cross-sections measured at Tohoku University
15:30	A. Plompen	Summary of activities at JAERI and Tohoku University
15:45		Coffee Break
16:00		Discussion on Achievements
16:30		Discussion on Future
17:15		Closure

The European Activation File project

R. Forrest, J. Kopecky and J.C. Sublet presented the European Activation File (EAF) project. A comprehensive European Activation SYstem (EASY) has been developed that consists of a Developer and a User component and includes both software tools and data libraries. The European Activation File contains a cross-sections file, a decay data file and a file containing safety related information derived from hazard, clearance and transport regulations. The Developers improve their libraries with a software tool called SAFEPAQ-II that is tailored to compare evaluated data from EAF with measured data, other evaluations and a set of TALYS default calculations. SAFEPAQ-II allows easy modification of the evaluated curves. Underlying SAFEPAQ-II are several other libraries, maintained in the form of a Microsoft Access database, such as a selected subset of the EXFOR database, a database of integral benchmark experiments, evaluated files from the various projects (ENDF, JENDL, JEFF, BROND, ...), a set of TALYS default calculations. A user interface provides access to the EAF libraries and includes an

inventory code called FISPACT that allows to calculate the radioactive inventory of materials irradiated in a given neutron spectrum as a function of time. R. Forrest demonstrated the use of differential experimental data for the development of the EAF library and showed several examples where work of the subgroup was already included in the EAF version of the EXFOR database. He also demonstrated the flexibility of SAFEPAQ-II. J. Kopecky reviewed the results of a systematic comparison with integral benchmarks and J.C. Sublet reviewed the status with regard to decay power benchmarks. The work presented the status current in January 2003 which was marked by the transition from EAF-2001 to EAF-2003 and a gradual extension of the upper limit of the evaluations from 20 to 55 MeV. The project has a policy of publishing new releases of the library in two year cycles. Finally, A. Filatenkov presented a large number of 14 MeV activation cross-section measurements carried out at the neutron generator of Khlopin Radium Institute (KRI) in St. Petersburg, Russia. A large number of these studies were carried out with support from the EURATOM fusion programme and in particular the EAF project. The data measured at KRI are well recognised and often provide a valuable point of reference for the measurements carried out at IRMM. A joint paper about reactions on Mo isotopes studied both at KRI and at IRMM was recently accepted for publication in Phys.Rev. C.

Documentation about the EAF project may be found in Ref. [2].

Cross-section measurements

Measurements of cross-sections were presented by P. Reimer, V. Semkova, R. Dóczi, F. Cserpák, A. Filatenkov (see above), A. Fessler, J. Csikai and A. Plompen. A. Fessler reviewed the measurements on Cr isotopes that had been carried out previous to the activities of the subgroup. P. Reimer and V. Semkova reviewed the measurements of cross-sections obtained at IRMM and in part at FZ Jülich of selected reactions on isotopes of V, Ni, Co, Cu, Zr, Mo, Tc, and Pb. This work is amply documented and details may be found through the references in Tab. 2.1 of Part A of this report. F. Cserpák reported measurements on ^{127}I and ^{129}I [1]. R. Dóczi reported on measurements at 14 MeV performed at U.Debrecen, in the region from threshold to 12 MeV at the Atomki Cyclotron and on the capture reaction on ^{115}In [1]. These measurements complement work carried out earlier at IRMM and FZ Jülich [7]. J. Csikai provided insight in recent measurements with the activation technique for proton-induced reactions carried out at the CYRIX laboratory of Tohoku University, Sendai, Japan together with M. Baba. In absence of M. Baba, A. Plompen shortly presented the neutron-induced reactions studied at the same laboratory by M. Baba and coworkers in the energy range from 20 to 65 MeV. These measurements, which are important

for development of the fusion related IFMIF facility, are of an exploratory nature and definitive results will be presented at a later occasion after completion of the measurement facility and data analysis tools. D.L. Smith *et al.* finally presented an elaborate account of the method of corrections for low energy neutrons that is followed for the IRMM measurements. This correction is of particular importance for low-threshold reactions studied with the ^{3}H$(d,n)^{4}$He neutron source reaction at 3 and 4 MeV incident deuteron energy [1].

Model calculations

Results of model calculations and model code development were presented by M. and V. Avrigeanu, S. Sudár, A. Fessler, S. Goriely, E. Bauge, S. Hilaire and A. Koning.

V. Avrigeanu [1] and S. Sudár reported on detailed calculations in a local approach for reactions on isotopes of V, Ni, Co and Mo with an enhanced version of the STAPRE-h code and for Tc, I and Pb with the STAPRE code. Results of these calculations are discussed in Part A and presented in Part C of the present report (See references therein). These model calculations frequently lead to excitation curves that improve on existing evaluations.

A. Fessler and S. Sudár presented results of sensitivity calculations for isotopes of Cr, Tc and Pb. It was shown how these sensitivity coefficients serve to identify the parameters to which a cross-section is most sensitive. They also quantify the required uncertainty for a model parameter given a prescribed target uncertainty of a cross-section. They may finally serve to provide uncertainty bands for cross-sections given a prescribed relative covariance matrix for the underlying parameters. The work presented by Fessler was published. See the discussion in Part A of the summary report for further details.

S. Goriely [1] reviewed the status of (semi-) microscopic nuclear model calculations. Such calculations are important for nuclei for which no or very little experimental information is available. They also serve to develop nuclear physics insight to guide more empirically oriented developments of parameter systematics. He demonstrated that the known nuclear masses can be reproduced by Hartree-Fock Bardeen-Cooper-Schriefer (HF-BCS) or Hartree-Fock-Bogoliubov (HFB) calculations with accuracies similar to the most refined variant of the liquid drop model (Finite Range Liquid Drop Model, FRLDM). He also showed how one may obtain nuclear level densities in the HF-BCS approach and how well these compare with known level spacings at the binding energy. The Quasi-particle Random Phase Approximation (QRPA) is invoked for the determination of gamma-ray strength functions with good results in the giant resonance region and interesting predictions for the isotopic dependence of the so-called pygmy resonance.

S. Goriely, E. Bauge and M. Avrigeanu showed different approaches to obtain the (real part of the) optical model in the double folding approach. M. Avrigeanu [1] performed this study for alpha-particles in the mass 100 region using carefully selected densities for the nuclei and the alpha-particle, a carefully selected effective interaction and taking care of the Pauli principle and the dispersion relation. The real part of the potential is obtained in this semi-microscopic approach while a judicious parameterisation of the imaginary part is included. No normalisation factors are needed to obtain a very good agreement of the data at the lowest energies available (15-25 MeV).

E. Bauge [1] showed calculations for the optical model with the double folding approach applied in first instance to neutron and proton scattering with an exploration of the case of deuterons. Nuclear densities are obtained in the constrained HFB approach while the nuclear interaction is the effective nucleon-nucleon interaction of Jeukenne-Lejeune-Mahaux for nuclear matter applied to nuclei in the local density approach with modifications to ensure Lane-consistency. These semi-microscopic optical models were included in the TALYS code and applied to the evaluation of neutron-induced reactions on Europium isotopes with good results.

S. Hilaire presented an analysis of various aspects of level density modelling using the combinatorial approach. The impact of collective enhancement factors for vibrational and rotational motion on level density parameters was studied as well as the impact of different assumptions for the spin cut-off parameter. The energy dependence of the latter was studied for four cases from mass 80 to mass 200 showing that deviations from the rigid body value can be both substantial and energy dependent. A study of the energy dependence of the level density parameter in this approach indicated that a generalised Ignatyuk formula would be needed to explain the results.

Finally A. Koning reviewed the status of the development of the TALYS code. Comments about TALYS may be found in Part A. The code is now used for many estimates performed at Bruyeres and in Petten. Results of the code's default calculations are employed by the EAF project and are shown in Part C of this report.

[1] These proceedings.

[2] R.A. Forrest, The European Activation System, EASY-2001 overview, UKAEA Report FUS449(2001); http://www.fusion.org.uk/EASY2001

[3] A. Fessler, A.J.M Plompen, D.L. Smith, J.W. Meadows, and Y. Ikeda, Nuclear Science and Engineering 134, 171 (2000).

Semi-microscopic optical potentials for applications

Marilena Avrigeanu

[1] *Association EURATOM-NASTI, "Horia Hulubei" National Institute for Physics and Nuclear Engineering (IFIN-HH), P.O.Box MG-6, 76900 Bucharest, Romania*

Abstract:
Progress on the use of the double-folding method for calculations of microscopic real potentials for complex particles is reported. Moreover, since a phenomenological imaginary part has to be considered together with the corresponding dispersion contributions to the real part, a global parameterisation of the Wood-Saxon potential was established taking into account the strong energy dependence and nuclear structure effects of the imaginary part. The new parameterisation satisfactorily describes the elastic scattering of α-particles on $A \sim 100$ target nuclei at incident energies from 14 to 32 MeV. The effective nucleon-nucleon interaction involved within optical potential calculation and analysis has been used also in multi-step direct calculations.

Introduction

The α-nucleus phenomenological optical potential (OP) is still extensively used in calculations for many applications due to the radiation damage effects within structural materials following $(n, x\alpha)$ reactions. However, it is not unique and the uncertainties of the parameter sets critically depend on the particular α-nucleus system, the incident energy as well as on the precision of the analyzed data. Moreover, unlike the nucleon case, there are no global potentials for α-particles that fit to good accuracy the scattering from many nuclei over a wide range of energies, as illustrated by the limited number of phenomenological OPs of the recent IAEA Reference Input Parameter Library (RIPL) [16]. Thus much work needs to be done in order to provide suitable α-particle OP calculations for applications like Accelerator Driven Systems (ADS).

On the other hand, the effective nucleon-nucleon (NN) interaction involved within OP calculation and analysis can be used in multi-step direct (MSD)

calculations. The main point could be the description of experimental double-differential cross-sections without use of any free parameter. Among the high-priority elements for the ADS and fusion-reactor projects there are Zr and Mo, and corresponding reference nuclear data for n-, H- and He-interactions are of actual interest for radiation damage estimates and radioactive waste transmutation projects.

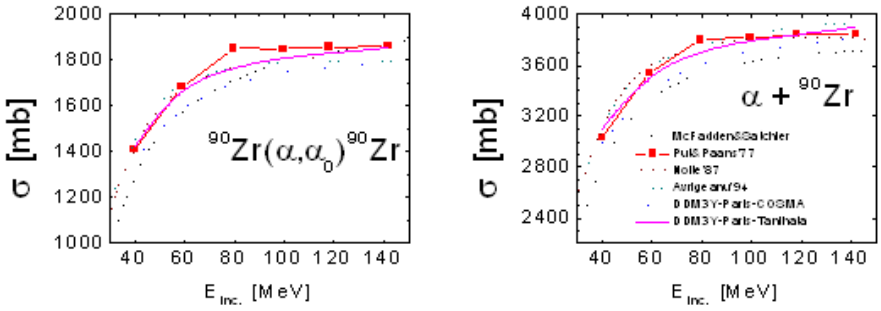

Figure 1: *Comparison of calculated elastic scattering and total cross-sections for* α+^{90}*Zr.*

Double-folding method calculation of nuclear potential for complex particles

Since the IFMIF project requests nuclear data evaluation for D incident on^{6,7}Li for D-energies up to 50 MeV, we have analyzed and proved [3,4,11,21] the possibility of using the double-folding (DF) method for calculation of the nuclear potential for complex particles (e.g. ^{2,3}H, ^{3,4}He) emitted in neutron induced reactions on medium nuclei. This is also of interest [6] for evaluation of nuclear data for D on ^{6,7}Li.

The basic input for the calculations of the double-folded OP are the nuclear densities of the colliding nuclei and the effective nucleon-nucleon (NN) interaction. Several of the most recent densities associated to the α-particle have been used in addition to the best-known expression of Satchler and Love; the experimental Tanihata densities [7], the realistic densities derived from the cluster-orbital shell model approximation (COSMA) [9], and the microscopic Baye density. The energy- and density-dependent (DDM3Y and BDM3Y) effective Paris and Reid NN potentials have been considered with an explicit treatment of the exchange potential [3, 9, 21].

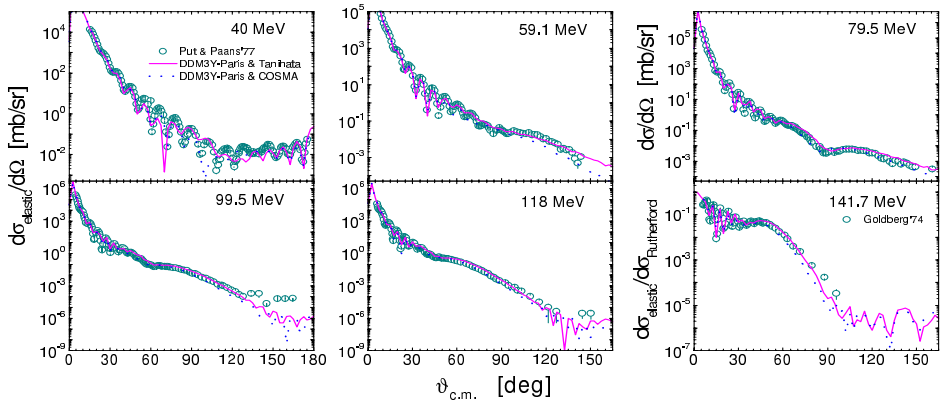

Figure 2: *Comparison of experimental and microscopic elastic-scattering angular distributions for* α+^{90}*Zr.*

Microscopic optical potential for α*-particles interacting with* ^{90}*Zr*

The microscopic real OPs have been validated through comparison with phenomenological OPs and the description of systematics of the experimental α-particle elastic-scattering angular distributions. It is important to underline that no adjustable parameter or normalisation constant are involved in the microscopic calculations. The volume integrals of the real phenomenological [10] and of the microscopic potentials for α+^{90}Zr based on the Tanihata density and DDM3Y-Paris effective interaction have been found to agree best.

Calculated differential elastic scattering cross-sections of α+^{90}Zr at incident energies of 40, 59.1, 79.5, 99.5, 118, and 141.7 MeV using the DDM3Y-Paris effective NN interactions with both Tanihata and COSMA densities are presented in comparison with the experimental data [10, 11] in Fig. 1. It can be seen that the microscopic OPs calculated in this work are able to describe the experimental angular distributions of elastically scattered α-particle over a large incident energy range.

Since no experimental data concerning the elastic-scattering and total reaction cross-sections for α+^{90}Zr have been reported so far, in Fig. 2 are shown comparatively the calculated cross-sections by means of either the phenomenological OPs or the microscopic ones corresponding to DDM3Y-Paris effective NN interaction and Tanihata/COSMA densities for $40 < E_\alpha < 142$ MeV. This comparative analysis shows that the microscopic elastic-scattering and total reaction cross-sections are in good agreement with those predicted by the phenomenological OPs along the whole energy range analyzed. This final comparison validates the

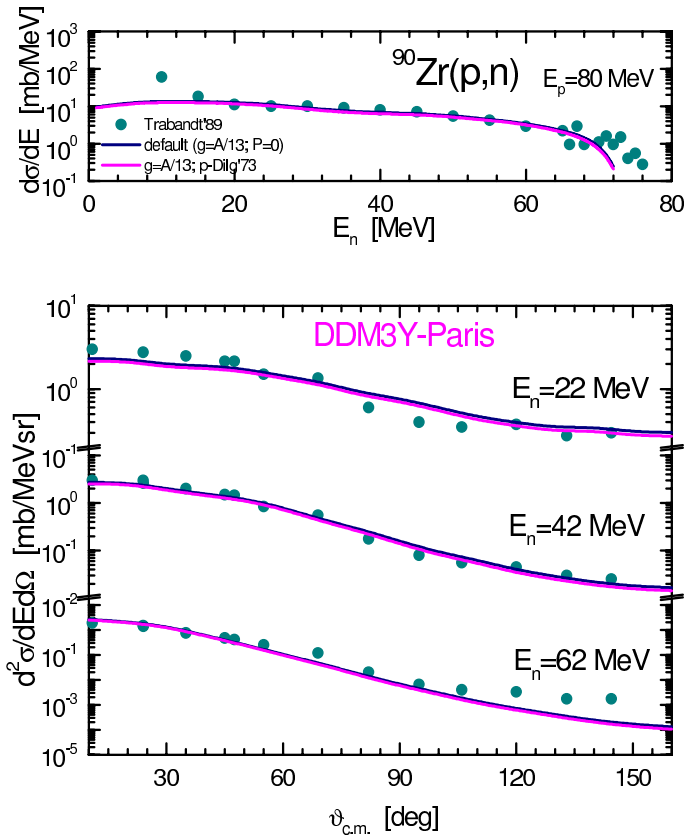

Figure 3: *Comparison of experimental and MSD cross-sections for the* (p, xn) *reactions on* ^{90}*Zr.*

procedure of calculating microscopic OPs and its use in applications.

Quantum-statistical MSD processes at low and intermediate energies on ^{90}*Zr and* ^{100}*Mo*

The quantum mechanical formalism developed by Feshbach, Kerman and Koonin [12] (FKK) for the multi-step processes has been extensively used to describe a large amount of experimental data covering a broad energy range. The assumptions and simplifying approximations considered in the application of the FKK theory have been analyzed and important refinements of calculations have been made (e.g. Ref. [13] and references therein). One of the important assumptions concerns the effective NN interaction, which is taken as a single Yukawa term with 1 fm range,

its strength V_0 being considered as the only free parameter of the FKK theory. However, it should be noted that, even when a consistent standard parameter set has been used as well as several other effects have been taken into account, the systematics of the phenomenological V_0 values still show discrepancies. Such uncertainties of the phenomenological effective NN-interaction strengths may reflect the eventual scaling of V_0 compensating for some effects which have been neglected and should be added to the theory. Thus, the use a more realistic effective NN interaction, which should be consistent with the corresponding OP real part [14] of the OM, has been stated as one of the open problems in the theoretical description of the MSD nuclear reactions [13]. The aim of one-month scientific

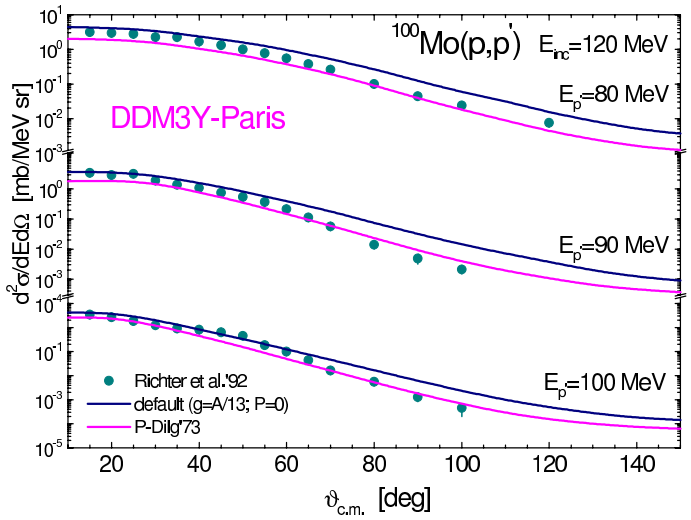

Figure 4: *Comparison of experimental and MSD cross-sections for the* (p, xn) *reactions on* ^{100}*Mo.*

visit at IRMM has been the provision of a reliable strength to be used within the FKK theory instead of the free parameter V_0. In this way we expect to overcome the uncertainties in fitting an effective interaction directly to MSD processes data. Thus an 1Y-equivalent NN interaction strength $V_0^{\rm eq}$ obtained from the DDM3Y-Paris effective interaction has been used within MSD calculations which (a) describes without any free parameter the experimental double-differential cross-sections, the nucleon emission spectra from the (p, n) and (p, p') on ^{90}Zr (Fig. 3) and ^{100}Mo (Fig. 4) isotopes at the incident energies of 80, 100 and 120 MeV, and (b) makes possible predictions of MSD double-differential cross-sections and nucleon emission spectra corresponding to (n, n') and (n, p) reactions on ^{90}Zr

and ^{100}Mo isotopes at the incident energies of 80, 100 and 120 MeV, where no experimental data exist.

The practical FKK calculations become independent by any free parameter, whose phenomenological values may compensate for the questionable handling of other quantities involved in the FKK formalism, e.g. the particle-hole state density, the optical potential for distorted waves, the DWBA matrix elements, the coupling between MSD and MSC emission chains [13]. Therefore further improvements concerning the pairing and shell corrections [7], which are important at low residual excitation energies but for high energetically emitted particles, are foreseen at this stage. These improvements are already included in the semi-classical Geometry Dependent Hybrid (GDH) subroutine of the STAPRE-H code [1] (updated version) at IFIN-HH in Bucharest.

(α, α') *analysis at incident energies around Coulomb barrier on* $A \sim 100$ *nuclei*

Two main questions are yet open in any search for a global parameter set, namely (i) the OMP parameter sets obtained from α-particle elastic scattering at high energies ($\geq$ 80 MeV) do not describe the low-energy ($\leq$ 40 MeV) elastic scattering or complete fusion data, and (ii) the statistical-model α-particle emission is much underestimated by OMPs which account for elastic scattering on the cold ground-state nuclei (e.g. Ref. [17]). The α-particle emission nuclear data for the isotopes of Zr and Mo are among the high-priority requests for ADS, the α-particle energy range involved being obviously mainly around the Coulomb barrier. The same and even lower energy range is the most important for many nuclear astrophysics applications while the mass region $70 < A < 100$ is generally underestimated in the nucleosynthesis calculations (e.g. Refs. [18–20] and references therein).

Moreover, especially the low-energy elastic-scattering data suffer from discrete and continuous ambiguities in the OMP parameters, whose uncertainties are also quite different for various target nuclei, incident energies as well as precision of data analyzed. Therefore, in order to avoid too much phenomenology in the description of these data, many attempts have been made to replace the phenomenological potential of Woods-Saxon (WS) type by a more microscopic α-nucleus potential using an effective interaction for the real potential. However, the situation is considered less optimistic regarding the α-nucleus OMP at low energies, where the imaginary-potential strong energy dependence and nuclear structure effects should be taken into account [19] while the data are sensitive to the potential only at the surface.

Recently the DF formalism for the α-nucleus optical potential has been revised at α-particle energies above 80 MeV, in order to study the exchange effects and

effective NN-interaction density dependence [8]. On the other hand, a review of the elastic α-nucleus scattering and three improved global α-particle OMPs at low sub-Coulomb energies have been just published [20] with the aim to determine a global potential over the whole mass region that is able to reproduce all the existing experimental data for α-particle elastic scattering as well as α-induced and (n,α) reactions. The three global semi-microscopic OMPs finally derived in this comprehensive study have the real part obtained by using the DDM3Y interaction within the DF procedure, and WS imaginary parts which have considered either a purely volume imaginary term (I), or a volume plus surface imaginary potential (II), as well as a damped surface potential together with the dispersive contribution to the real DF potential (III). However, in spite of the quite distinct assumptions, it was found that overall these three OMPs lead to cross-sections which do not exhibit any substantial differences apart from some at backward angles. Therefore, it has been concluded [20] that they can be regarded as providing the uncertainty level up to which it is possible today to predict globally α-induced reaction cross-sections, within a factor of even 10.

A recent measurement [18] of the α-particle elastic scattering on ^{92}Mo between 13 and 19 MeV, with almost the same high accuracy over five orders of magnitude, pointed out also ambiguities which do not allow determination of the shape of the OMP imaginary part unless an wider energy range will be involved.

Therefore, a fit of α-particle elastic scattering data at energies below 35 MeV has been restricted in the first phase of this work to the mass range $A \sim 100$ since Atzrott *et al.* [21] shown that the α-nucleus OMP real part becomes rather independent of the target mass for nuclei with masses $A \geq 90$. The α-induced or (n,α) reaction cross-sections have not yet been taken into account in this respect, in order to avoid the question marks due to the rest of the statistical-model parameters (e.g. the shaded areas in Figs. 4-9 of Ref. [20]).

A two-step analysis of the (α,α_0) angular distributions on ^{89}Y, ^{90,91}Zr, ^{92,94,96,98,100}Mo, ^{107}Ag, and ^{116,122,124}Sn has been carried out [20] by

(i) fit of an energy-dependent phenomenological imaginary part while the DF real potential is used (e.g. Figs. 5,6), and

(ii) determination of real phenomenological OMP parameters by fits of the same data keeping the imaginary part fixed (e.g. Figs. 7,8).

Finally, a method validation has concerned the application of these potentials to the ^{90}Zr data of Put and Paans [10] at 40 MeV.

The following points are either similar or different with respect to studies mentioned previously or hereafter:

- we have been looking for only one global α-particle real DF potential at low energies, with aim of understanding why the three OMPs of Ref. [20] lead overall to cross-sections which do not exhibit any substantial differences in spite of the quite distinct assumptions;

- we have used an explicit treatment of the exchange component [9] and no adjustable parameter or normalisation constant;

- we have not fitted α-induced or (n, α) reaction cross-sections, in order to avoid question marks due to the rest of the statistical model parameters [20], but we shall involve them within the final phase of independent validation;

- our analysis has concerned in the first phase only the mass range $A \sim 100$ but taking into account all available data as well as a complete phenomenological OMP;

- we have used the complete formulas [24] for the dispersive correction due to OMP phenomenological imaginary part (used only occasionally [25] for α-particles) whose effect will be distinctly shown in comparison with alternative formula [26] adopted in Ref. [20];

- apart from using [20] the DDM3Y effective NN interaction parameters of Kobos *et al.* [27] at different energies, we have checked the more suitable interaction M3Y-Reid and α-particle density distribution by means of the α-α elastic scattering analysis;

- we have looked for the energy dependence of the phenomenological imaginary OMP, at variance with Ref. [18], in order to consider properly the dispersive correction to the calculated DF real potential;

- apart from Ref. [28] we have not used volume integral systematics but directly the analysis of all available angular distributions of the α-particle elastic scattering.

Furthermore, the extension of this analysis to both lower and higher mass target nuclei is planned. The analysis of the few experimental α-particle total reaction cross-sections [29] will also be performed in the mass range $A \sim 50$, in order to understand on this basis why their description has been provided only by the OMP obtained by study of the α-particle elastic scattering by McFadden and Satchler [10]. At the same time the possibility to involve the same semi-microscopic optical potential above 40 or even 80 MeV will be analyzed. Next, we expect to use the same optical potential, obtained by analyzing the α-particle elastic scattering alone, in the Hauser-Feshbach statistical model analysis of the

(n,α) reaction cross-sections within the first MeVs of the excitation functions. Since in this case the discrete low-lying levels of the residual nuclei are more important besides the α-particle transmission coefficients, while only level density of the target nucleus may play a minor role, accurate validation of the α-particle OMP could be obtained. Moreover, there are cases such as the (n,α) reactions on ^{58,60}Ni where the level density of the target nucleus is also less important in this energy range while some structure found in their first measurement and comprehensive study [14] seems to be not explained yet [11]. Actually, even the latest analyses [15] still consider the large uncertainties in the (n,α) cross-sections as a general problem, in conjunction with nuclear level density approaches. This is the reason why we will do this kind of analysis as the last step of the α-particle OMP study, and will take into account especially the dispersive contribution of the OMP phenomenological imaginary part to the real DF potential in order to understand the particular behaviour at the lowest energies.

[1] RIPL, Report IAEA-TECDOC-1034, IAEA, Vienna, 1998; http://www-nds.iaea.or.at/ripl/ .

[2] M. Avrigeanu, G.S. Anagnostatos, A.N. Antonov, and J. Giapitzakis, Phys. Rev. C 62, 017001 (2000).

[3] M. Avrigeanu, A.N. Antonov, H. Lenske, and I. Stetcu, Nucl. Phys. A693, 616 (2001).

[4] I.V. Krouglov, M. Avrigeanu, and W. von Oertzen, Eur. Phys. J. A 12, 399 (2001).

[5] M. Avrigeanu, G.S. Anagnostatos, A.N. Antonov, and V. Avrigeanu, J.Nucl. Sci. Technol. S2, 595 (2002); Int. J. Modern Phys. E 11, 249 (2002).

[6] A.Yu. Konobeyev, Yu.A. Korovin, P.E. Pereslavtsev, U. Fisher, and U. von Mollendorff, Nucl. Sci. Eng. 139, 1 (2001).

[7] I. Tanihata *et al.*, Phys. Lett. B 289, 261 (1992).

[8] M.V. Zhukov *et al.*, Phys. Rep. 231, 151 (1993).

[9] Dao T. Khoa, Phys. Rev. C 63, 034007 (2001).

[10] L.W. Put and A.M.J. Paans, Nucl. Phys. A291, 93 (1977); L. McFadden and G.R. Satchler, Nucl. Phys. A84, 177 (1966); M. Nolte, H. Machner, and J. Bojowald, Phys. Rev. C 36, 1312 (1987); V. Avrigeanu, P.E. Hodgson, and M. Avrigeanu, Phys. Rev. C 49, 2136 (1994).

[11] D.A. Goldberg *et al.*, Phys. Rev. C 10, 1362 (1974).

[12] H. Feshbach, A. Kerman, and S. Koonin, Ann. Phys. (NY) 125, 429 (1980).

[13] M.B. Chadwick *et al.*, Acta Phys. Slovaca 49, 365 (1999).

[14] M. Avrigeanu, A. Harangozo, V. Avrigeanu, and A.N. Antonov, Phys. Rev. C 54, 2538 (1996); 56, 1633 (1997).

[15] M. Avrigeanu and V. Avrigeanu, J. Phys. G 20, 613 (1994); A. Harangozo, I. Stetcu, M. Avrigeanu, and V. Avrigeanu, Phys. Rev. C 58, 295 (1998).

[16] M. Avrigeanu and V. Avrigeanu, STAPRE-H95 Computer Code, IPNE Report NP-86-1995, Bucharest, 1995; News NEA Data Bank 17 (1995) 22, 25.

[17] P.P. Singh and P. Schwandt, Nukleonika 21, 451 (1976); J.M. Alexander, M.T. Magda, and S. Landowne, Phys. Rev. C 42, 1092 (1990).

[18] Zs. Fulop, G. Gyurky, Z. Mate, E. Somorjai, L. Zolnai, D. Galaviz, M. Babilon, P. Mohr, A. Zilges, T. Rauscher *et al.*, Phys.Rev.C 64, 065805 (2001).

[19] S. Goriely, J. Nucl. Sci. Technol., Suppl. 2, 536 (2002)

[20] P. Demetriou, C. Grama, and S. Goriely, Nucl. Phys. A707, 253 (2002).

[21] U. Atzrott, P. Mohr, H. Abele, C. Hillenmayer, and G. Staudt, Phys. Rev. C 53, 1336 (1996).

[22] M. Wit *et al.*, Phys. Rev. C 12, 1447 (1975).

[23] M. Avrigeanu, W. von Oertzen, A.J.M. Plompen, and V. Avrigeanu, Nucl. Phys. A 723, 104 (2003).

[24] C. Mahaux, H. Ngo, and G.R. Satchler, Nucl. Phys. A449, 354 (1986); A456, 134 (1986).

[25] H. Kitazawa, Y. Harima, and N. Mukai, Nucl. Phys. A510, 429 (1990).

[26] J.M. VanderKam *et al.*, J. Phys. G. 26, 1787 (2000); R. Capote *et al.*, J. Phys. G 27, B15 (2001).

[27] A.M. Kobos, B.A. Brown, P.E. Hodgson, G.R. Satchler, and A. Budzanowski, Nucl. Phys. A384, 65 (1982); A.M. Kobos, B.A. Brown, R. Lindsay, and G.R. Satchler, Nucl. Phys. A425, 205 (1984).

[28] A. Kumar and S. Kailas, Nuclear Model Parameter Testing for Nuclear Data Evaluation, Report INDC(NDS)-431, M. Herman (Ed.), IAEA, Vienna, 2002, p. 77.

[29] H. Vonach, R.C. Haight, and G. Winkler, Phys. Rev. C 28, 2278 (1983).

[30] S.M. Grimes *et al.*, Nucl. Sci. Eng. 124, 271 (1996); R.C. Haight *et al.*, Proc. of NDST97, Trieste, May 1997, vol. 1, p. 603.

[31] V. Avrigeanu, M. Avrigeanu, and T. Glodariu, Int. Workshop Fast Neutron Physics, Dresden, Germany, September 5-7, 2002.

[32] T. Kawano, T. Sanami, M. Baba, and H. Nakashima, J. Nucl. Sci. Tech. 36, 256 (1999); A.J. Koning, Nuclear Model Parameter Testing for Nuclear Data Evaluation, Report INDC(NDS)-431, M. Herman (Ed.), IAEA, Vienna, 2002, p. 117.

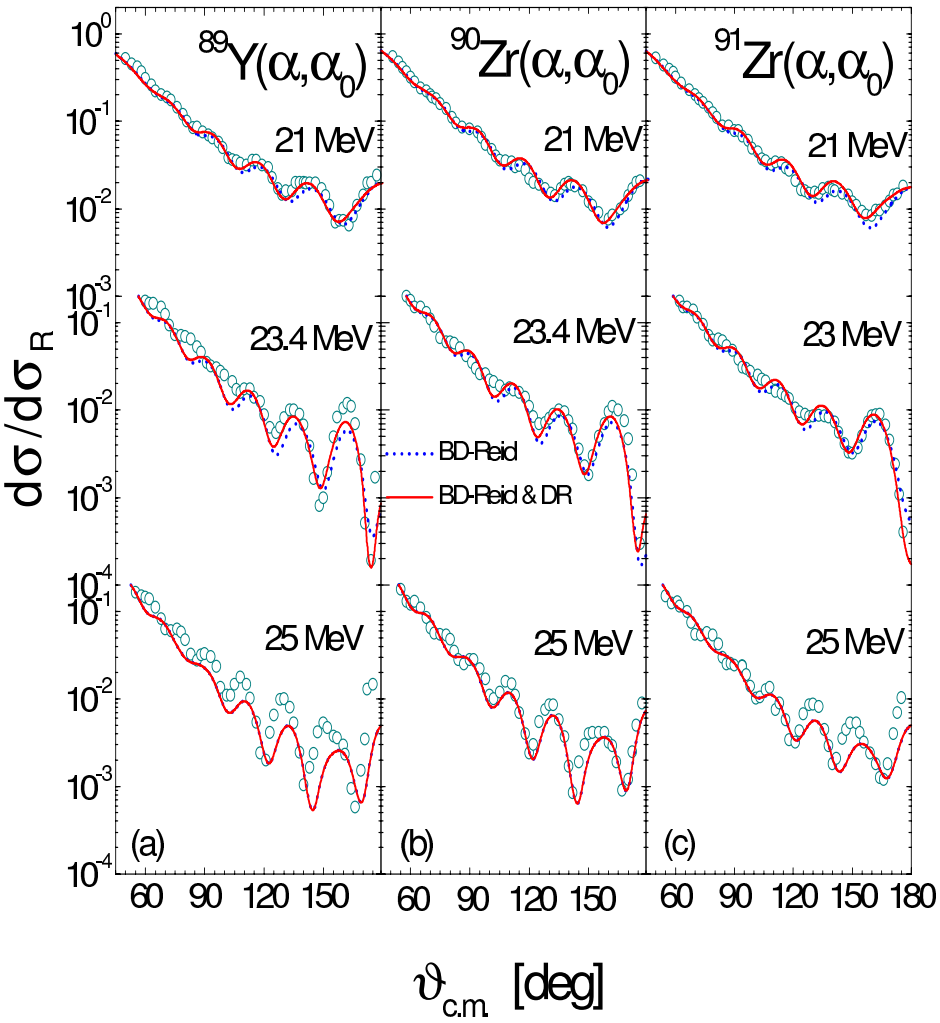

Figure 5: *Semi-microscopic analysis of α-particle elastic scattering on $A \sim 100$ nuclei [22] at energies below 25 MeV by using only DF method for OMP real part and also including the dispersion (DR) correction.*

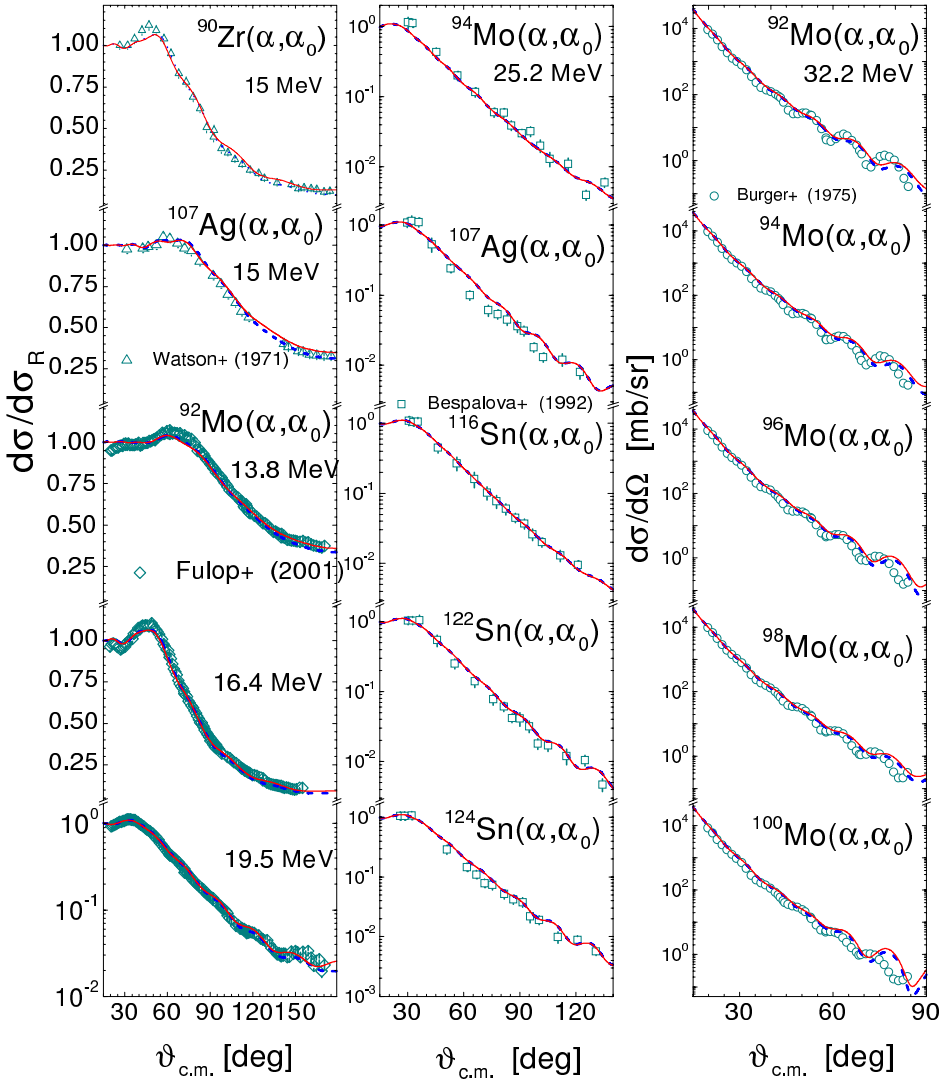

Figure 6: *Semi microscopic analysis of α-particle elastic scattering on $A \sim 100$ nuclei at energies below 32 MeV by using only DF method for OMP real part and also including the dispersion (DR) correction.*

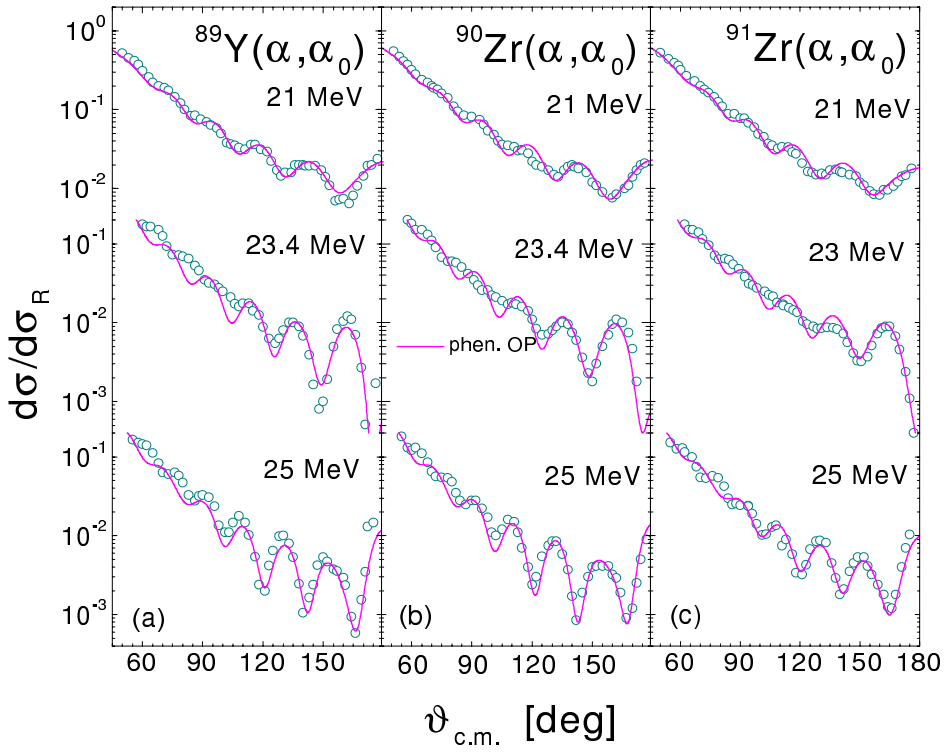

Figure 7: *Phenomenological analysis of α-particle elastic scattering on $A \sim 100$ nuclei [20] below 25 MeV.*

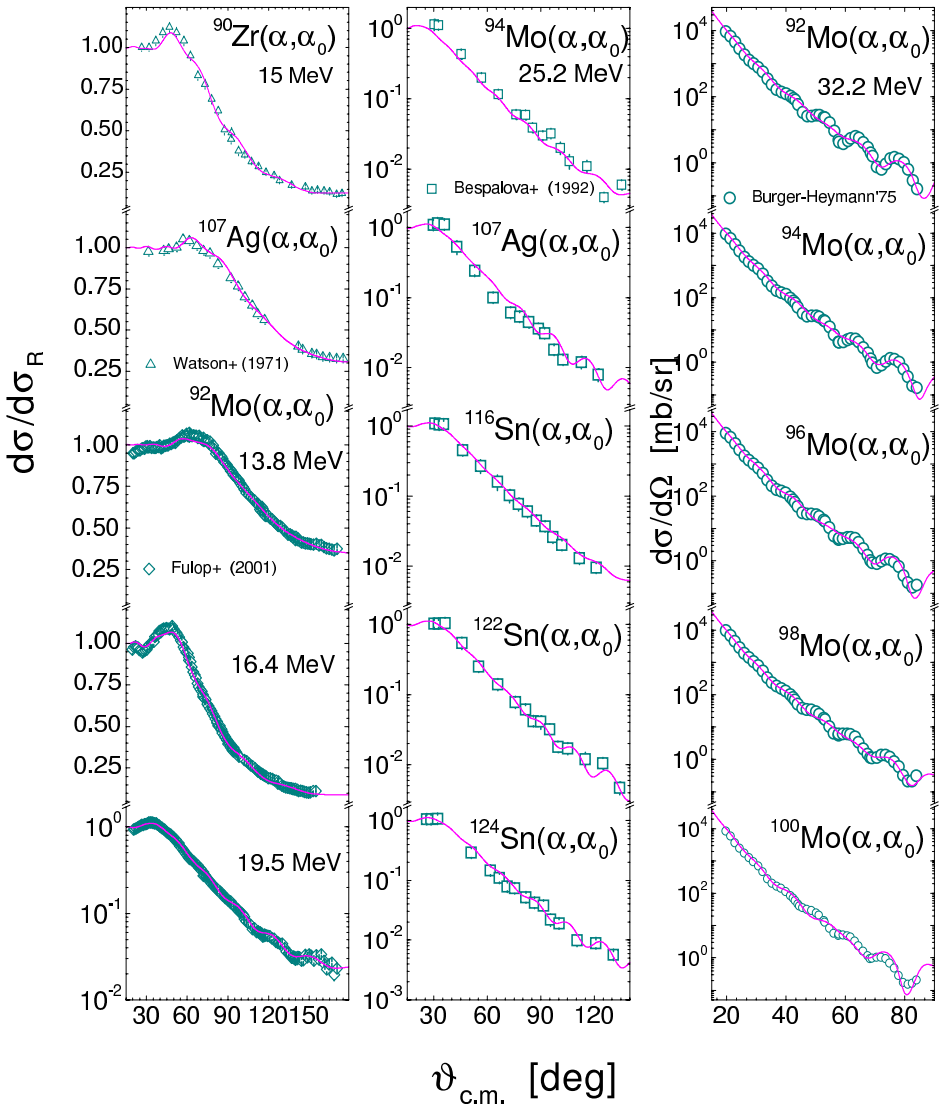

Figure 8: *Phenomenological analysis of α-particle elastic scattering on $A \sim 100$ nuclei below 32 MeV.*

Report on European activation file related tools

V. Avrigeanu

[1] *Association EURATOM-NASTI, "Horia Hulubei" National Institute for Physics and Nuclear Engineering (IFIN-HH), P.O.Box MG-6, 76900 Bucharest, Romania*

Abstract:
Progress of work on improved methods of nuclear model calculations for nuclear activation data carried out at IFIN-HH since the start of the activity of the OECD-NEA WPEC subgroup 19 is reported. In order to provide accurate predictions of further interest for EAF-2003, no use of normalisation or free parameters are involved. Model calculations have been validated by analysis of activation cross-sections of the all V, Co, Ni and Mo stable isotopes.

Introduction

Improved nuclear model calculation methods for nuclear activation data have been carried out by using the exciton and the Geometry-Dependent Hybrid (GDH) semi-classical models for pre-equilibrium emission (PE) and the Hauser-Feshbach statistical model (SM) within an updated version of the computer code STAPRE-H95 [1]. Basic points of our work have been:

(i) consideration of partial-wave PE effects able to provide suitable description of (n, p) and (n, α) reaction excitation functions above 15 MeV, at variance with usual PE models [2];

(ii) angular-momentum distribution of the nuclear-level density given, e.g. within the back-shifted Fermi gas (BSFG) model [4], by the nuclear moment of inertia I (found recently [4] to be only half of the rigid-body value I_r while the value $I = I_r$ is still widely used, e.g. [5]);

(iii) optical model potential (OMP) providing the α-particle transmission coefficients, which is still an open question especially if a microscopic approach is not involved [6].

The progress on the above item (i) was favoured by development in the meantime at IFIN-HH of a novel partial level-density (PLD) formalism [7], e.g. the recent IAEA Reference Input Parameter Library (RIPL [8]), and improved version of corresponding computer code PLD [9]. The first results were obtained in the case of the ^{51}V activation cross-section analysis [10, 11]. Work concerning the item (ii) has been done in connection with the main tasks of the former Subgroup 1 of the WPEC of OECD/NEANSC, concerning the (n, α) reaction and the nuclear level density which were underlined as generic problems. Since possible reasons for the well-known differences among the evaluated (n, α) cross-sections have been considered [12]

(1) competition of other channels,

(2) alpha-particle optical model potential,

(3) level density, and

(4) pre-formation factors in the pre-equilibrium emission (PE) model,

the actual model calculations have been validated by analysis of activation cross-sections of the isotopes ^{51}V, ^{59}Co, ^{58,60,61,62,64}Ni and ^{92,94,95,96,97,98,100}Mo by using

(a) unitary use of the common model parameters for different concerned mechanisms,

(b) consistent sets of input parameters determined by various independent data analysis,

(c) unitary account of a whole body of related experimental data for the above-mentioned isotope chains or neighbouring elements.

Compensation of opposite effects due to various less accurate parameter values has been thus avoided. This is particularly important since the first measurement at LANL-Los Alamos and comprehensive study [13, 14] of the alpha-production by neutrons on ^{58,60}Ni as well as ^{59}Co from threshold to 50 MeV have not supported any of the previous evaluations while latest analyses still consider the large uncertainties in the (n, α) cross-sections as a general problem, in conjunction also with LD approaches [15, 16]. Thus LD was the first subject of our major interest [17, 18], while for the above item (iii) we have firstly used or adjusted the phenomenological OMP proved able to describe alpha emission [7], and also considered [20] the semi-microscopic calculation using the double-folding method for the real potential (e.g. Ref. [21]) as the only proper treatment [6] of this matter.

Actually recent measurements [22, 23] at IRMM-Geel and FZ-Jülich of cross-sections for other channels in competition with (n, α) reactions, especially at incident energies between 14 and 21 MeV, have made possible enlarged analysis [23–25] of the calculated fast-neutron activation of ^{59}Co and ^{58,60,61,62,64}Ni isotopes. The same approaches have been involved in the case of ^{92,94,95,96,97,98,100}Mo activation, and comparison of calculated and available experimental excitation functions of (n, p), (n, α), $(n, 2n)$, and $(n, np + d)$ reactions proves a good agreement [11] in the limit of experimental errors. On the other hand, new measurements of activation cross-sections of also Mo isotopes were performed at the same time [26] at IRMM-Geel for neutron energies from 16 to 20.5 MeV. The comparison with them of the calculated values could be considered a blind exercise, while in this report is given a revision of the Mo calculated data by taking into account also the latest IRMM data. However, firstly are briefly mentioned various independent data analyses used for fixing a consistent sets of input parameters, other than the LD and γ-ray strength functions $f_{E1}(E_\gamma)$ described previously [18] also for the A in the range from 90 to 100.

Optical Model Potentials

The calculation of the neutron transmission coefficients was carried out through the analysis of the OMP for the interaction of neutrons with the target nuclei $^{92,94-98,100}$Mo, for energies up to 20 MeV, by using the SPRT method [27]. This detailed analysis is necessary since the neutron OMP used in Hauser-Feshbach calculations should provide realistic total reaction cross-sections over a wide incident energy range, as well as a reasonable description of the emission of low-energy neutrons in statistical processes. On the other hand, additional questions have concerned the molybdenum isotopes which show a rapidly changing character from that of the essentially spherical ^{92}Mo (with a filled $1g_{9/2}$ neutron shell) to nuclei making a transition from collective vibrators to the deformed rotors. Consequently, as the isotopic mass and collectivity of the Mo isotopes increase, discrepancies appear for description of the nucleon scattering by means of the spherical optical-statistical and even direct-reaction models.

For the OMP analysis of the neutron total cross-sections available at BNL we have firstly derived broad energy-averages over 200 keV of the data for the representative isotopes ^{92}Mo and ^{98}Mo. They were compared with several optical model predictions [28–31], of which the OMP obtained earlier [28, 29] at ANL was based on the data measured up to 5.5 MeV and involved with good results [32] in the analysis of data of neutron inelastic scattering from molybdenum isotopes obtained recently [33] at IRMM. Our comparison of the corresponding calculated and available experimental [34] neutron s- and p-wave strength functions and

the potential scattering radius RŠ led to the conclusion that the spherical OMP of Lagrange [31] provides similar results to the more complex vibrational and dispersive models, recently developed by Smith [30]. On the other hand, this potential was involved previously [35] (Figs. 3-4) in IFIN-HH analysis of differential elastic scattering cross-sections for ^{92,100}Mo at neutron energies of 7, 9 and 11 MeV, and inelastic scattering on low-lying excited levels of ^{92,96,98,100}Mo. However, since the total neutron cross-sections are overestimated at energies below 1 MeV (Fig. 1), the OMP of Smith [30] for natural molybdenum was used within this range. The calculation of the proton transmission coefficients was based on the analysis of the interaction of protons with the target nucleus ^{93}Nb, taking firstly into account the proton reaction data [36] for energies up to 5.5 MeV. In addition there have been calculated and compared with the experimental data the cross-sections for the reaction ^{93}Nb$(p,n)^{93}$Mo in the incident energy range of 2-6 MeV. Thus, we have used the OMP of Johnson *et al.* [36] with the energy dependence suggested by Lagrange [37] and the values of the depth W_D for the imaginary part of the OMP given by the smooth curve of the anomalous dependence $W_D(A)$ found by Flynn *et al.* [38]. On the other hand, we have taken the advantage of new ^{93}Nb$(p,\gamma)^{94}$Moreaction cross-section measurements below 5 MeV reported in the meantime [39] and used them for additional validation of the proton OMP involved in our calculation. Our presents results (Fig. 2) solved the discrepancies reported [39] for the model description of the (p,γ) data above 3.5 MeV, at the same time with a good agreement obtained with the (p,n) reaction data.

The OMP for calculation of α-particle transmission coefficients was established previously19 by analysis of experimental (n,α) reaction cross-sections just above the effective Coulomb barrier.

The γ-ray Strength Functions

The γ-ray strength functions $f_{E1}(E_\gamma)$ which are used for the calculation of the γ-ray transmission coefficients, have been obtained by means of a modified energy-dependent Breit-Wigner (EDBW) model [40, 41]. Systematic EDBW correction factors F_{SR} were established [18] for $A = 41 - 105$ by analyzing the experimental average radiative widths $\Gamma_{\gamma 0}^{\rm exp}$ of the s-wave neutron resonances, and assuming that $F_{SR} = \Gamma_{\gamma 0}^{\rm exp}/\Gamma_{\gamma 0}^{\rm EDBW}$. The $f_{E1}(E_\gamma)$ thus obtained were finally checked by calculation of capture cross-sections of ^{93}Nb and $^{92,94-98,100}$Mo nuclei (Fig. 3).

The Distorted Wave Born Approximation (DWBA) method

The collective enhancement of the direct scattering cross-section due to the low-energy surface vibrations of quadrupole and octupole multipolarity, included

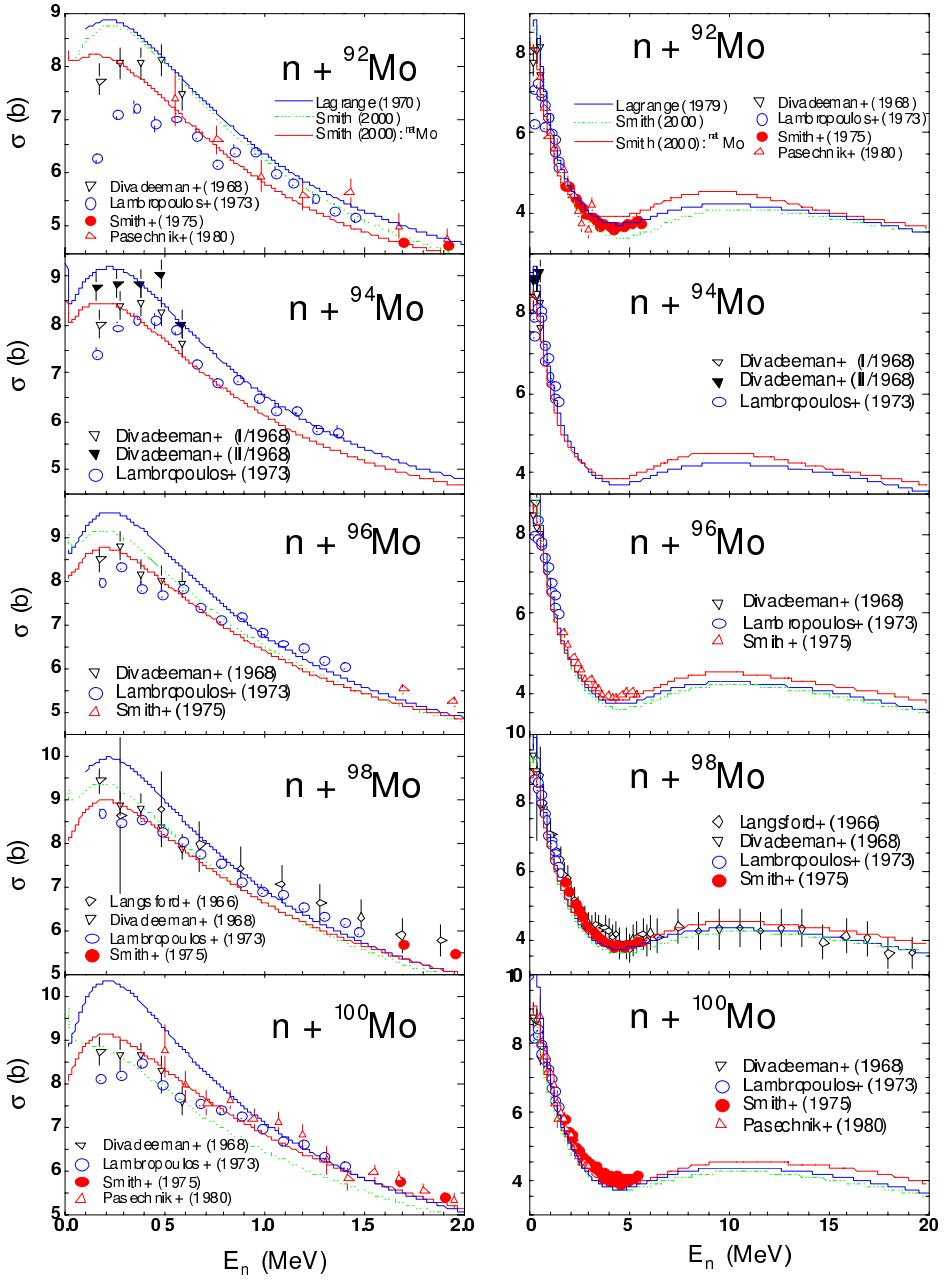

Figure 1: *Comparison of calculated and experimental neutron total cross-sections for* ^{92,94,96,98,100}*Mo*

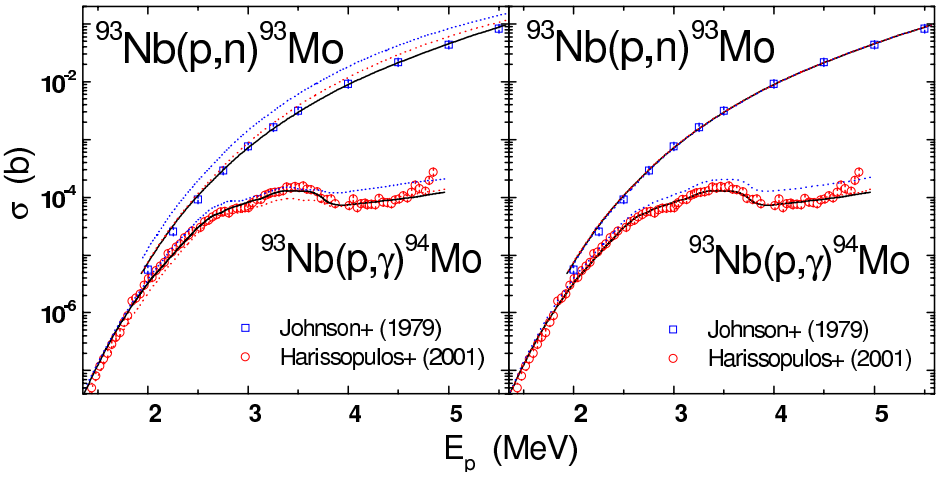

Figure 2: *Comparison of experimental [36, 39] and calculated* (p, γ) *and* (p, n) *and reaction cross-sections.*

by means of the DWBA method and deformations parameters are generally considered. However, anomalous enhancement of DWBA cross-sections near the threshold of inelastic scattering was reported around $A \sim 100$ when global OMP parameters were used [32]. Moreover, since it was often claimed that DWBA is inappropriate for evaluation of fission-product data, recent measurements [33] as well as DWBA and coupled-channels (CC) analyses [32] were performed for ^{98,100}Mo. Thus Kawano *et al.* [32] found that the problem comes from the optical potential used, i.e. when an adopted OMP to DWBA calculation is physically reasonable, differences between the calculated cross-sections with the DWBA and those with the CC theory are small. Finally, it was concluded that the DWBA is an appropriate method to evaluate cross-sections of inelastic scattering from the Mo isotopes, by using the ANL "regional" parameter set [29]. This achievement should be even more correct in the case of Lagrange [31] OMP based on SPRT analysis.

Following also Kawano *et al.*, we have calculated the direct inelastic scattering only for the one-phonon states (2^+ and 3^-) of the Mo isotopes, while cross-sections for two-phonon triplet (0^+, 2^+, and 4^+) are expected to be small. The deformation parameters β_2 and β_3 for the even-even target nuclei were taken from latest tabulations [42]. For the odd-A isotopes we have adopted, as values for excitation energies and deformation parameters of collective states, the average between corresponding values for the neighbouring even-even Mo isotopes [43]. Finally, total direct inelastic scattering cross-sections (Fig. 4) were obtained by

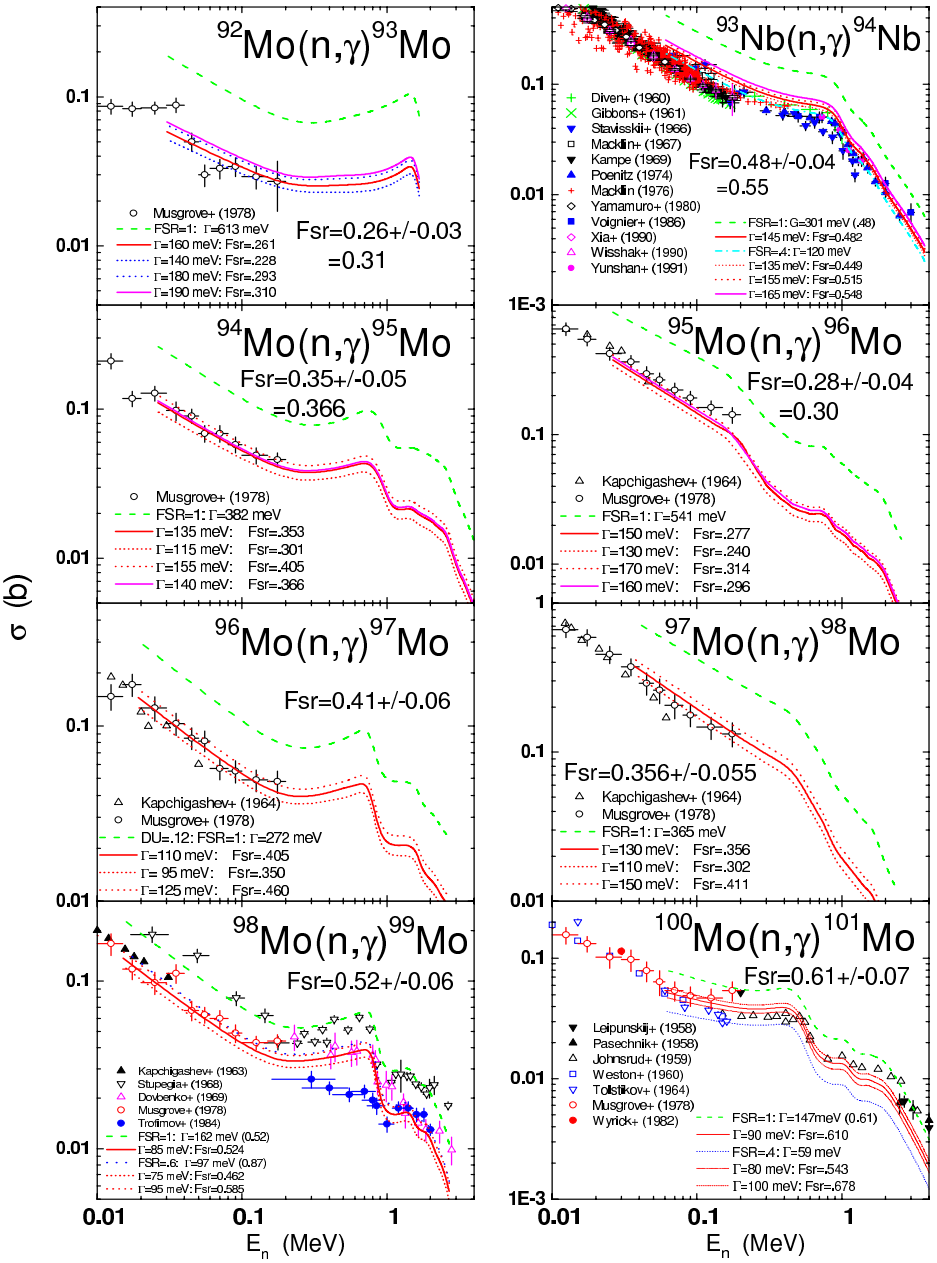

Figure 3: *Comparison of calculated and experimental neutron capture cross-sections of* ^{93}*Nb and* $^{92,94-98,100}$*Mo isotopes.*

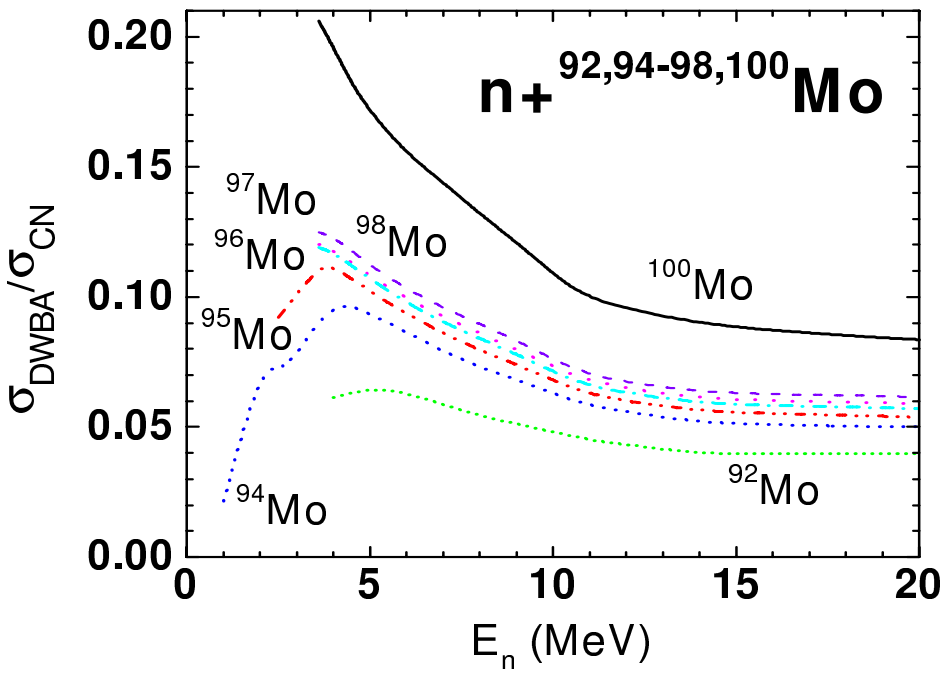

Figure 4: *Ratios of direct inelastic scattering cross-section to neutron reaction cross-section for* $^{92,94-98,100}$*Mo.*

using the DWUCK4 code [44].

Fast neutron activation analysis of the $^{92,94-98,100}$***Mo isotopes***

Completion of the previous analysis [11] has taken into account also the activation measurements performed at the same time at IRMM for incident energies from 16 to 20.5 MeV. On the other hand, the main change with respect to previous analysis concerned the PLD formalism [7, 9] including surface effects, and a value of 40 MeV for the Fermi energy. A slight change concerned also the pre-formation probability considered for the deuteron PE emission, described by using the Milano-group method for the α-particle PE emission (e.g. Refs. in [1]). The corresponding single-particle state density at the Fermi level has been assumed twice that of the α-particles [6] while a deuteron pre-formation probability of 0.5-0.6 has been found now to describe the experimental deuteron-emission spectra at 14.8 MeV [45]. It can be compared with the value 0.18 used for the pre-formation probability considered in this work for the α-particles PE emission.

The first step of this work has been the study of activation cross-sections for

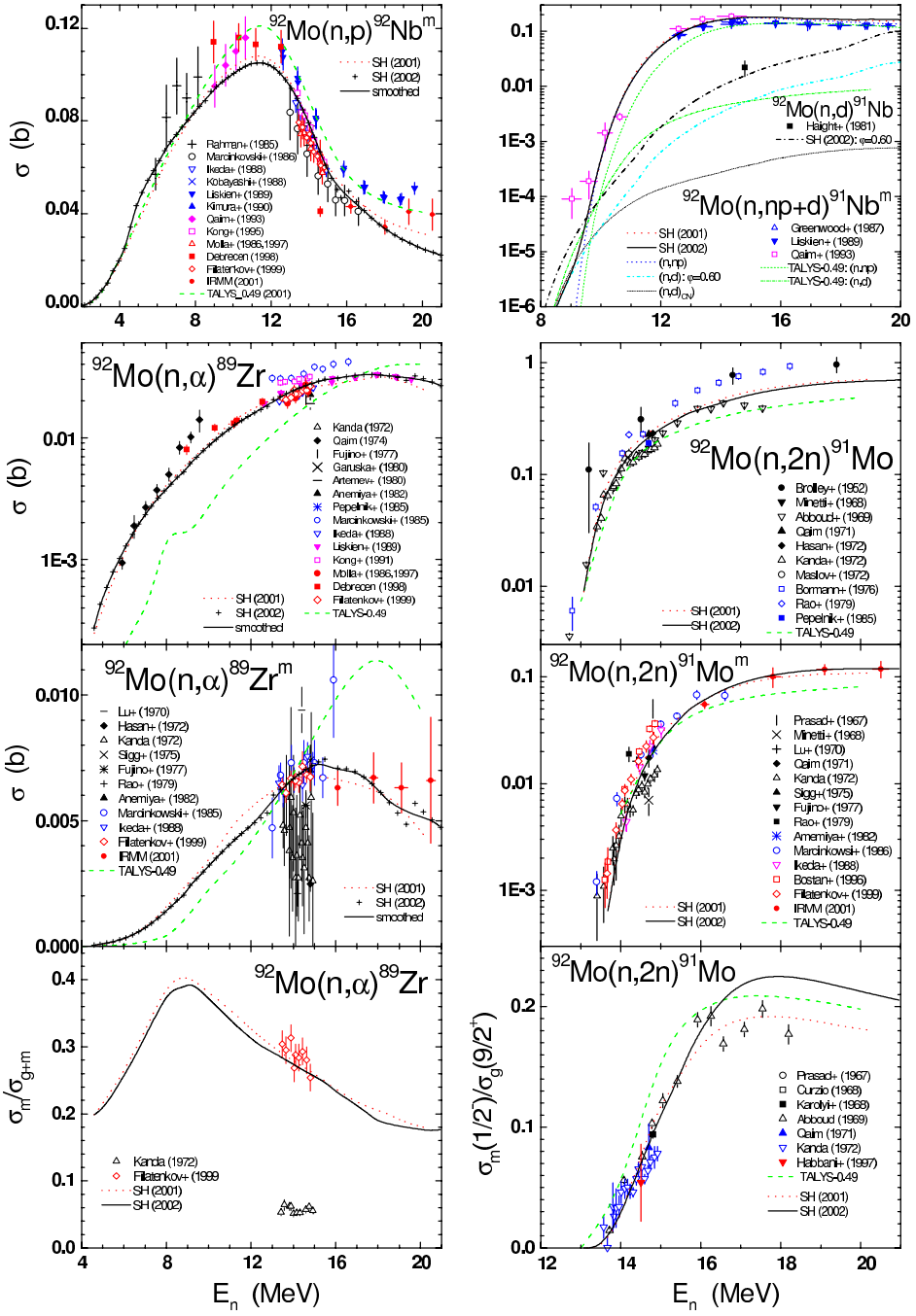

Figure 5: *Comparison of experimental and calculated fast-neutron cross-sections for* ^{92}*Mo.*

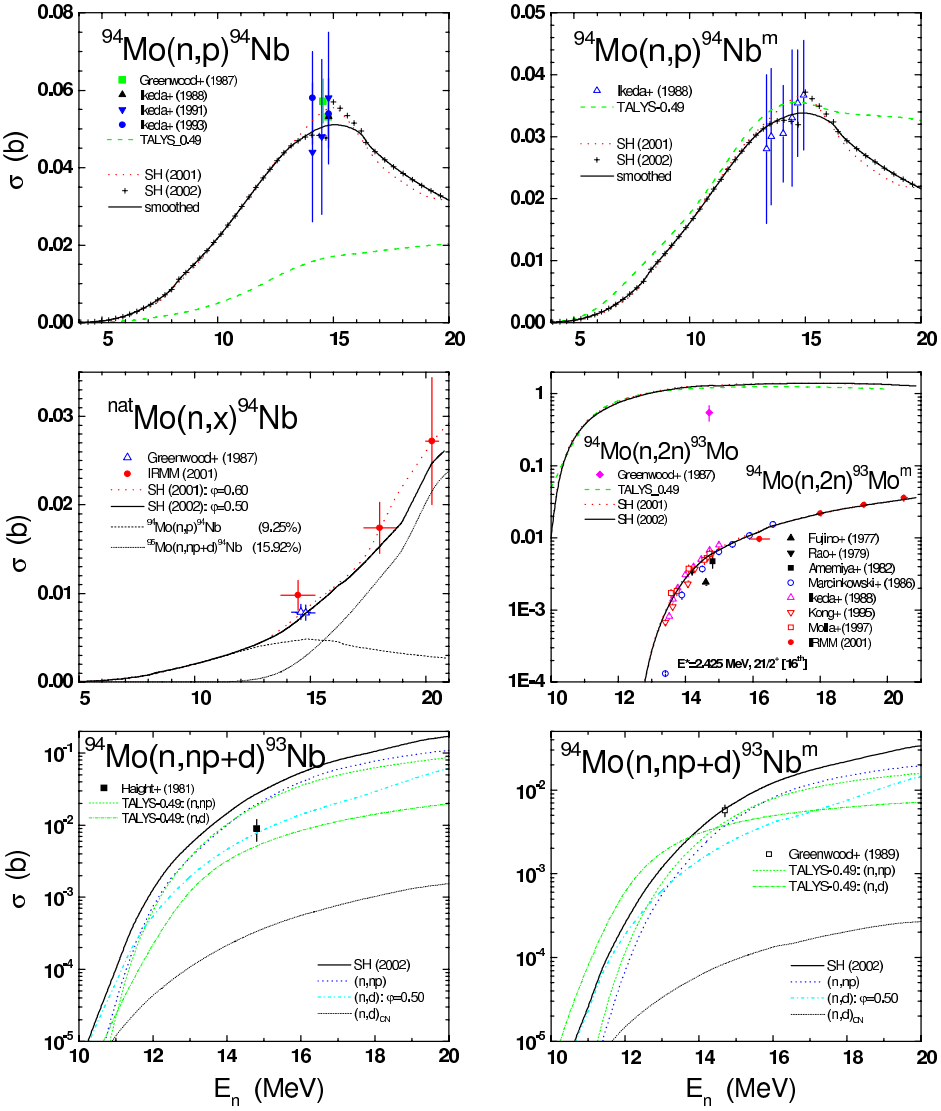

Figure 6: *Comparison of experimental and calculated neutron-activation cross-sections for* ^{94}*Mo.*

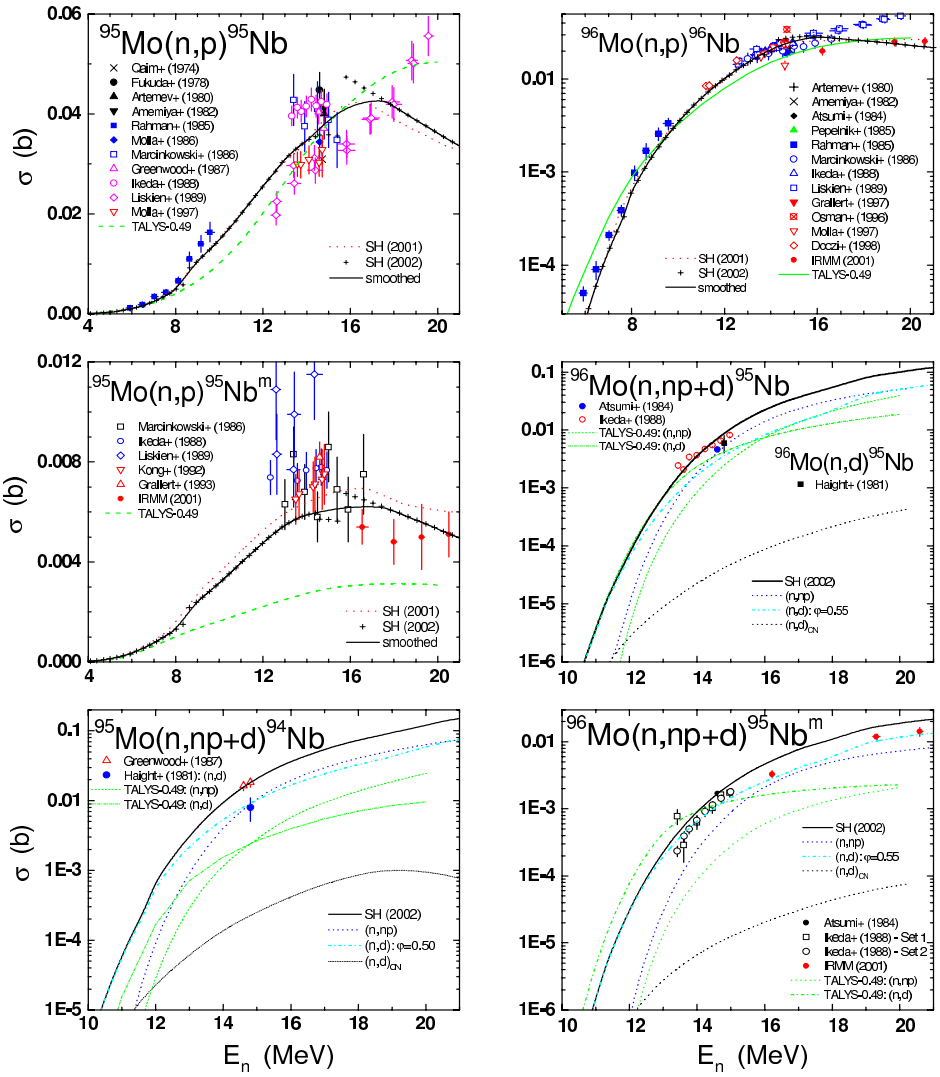

Figure 7: *Comparison of experimental and calculated neutron-activation cross-sections for* ^{95,96}*Mo.*

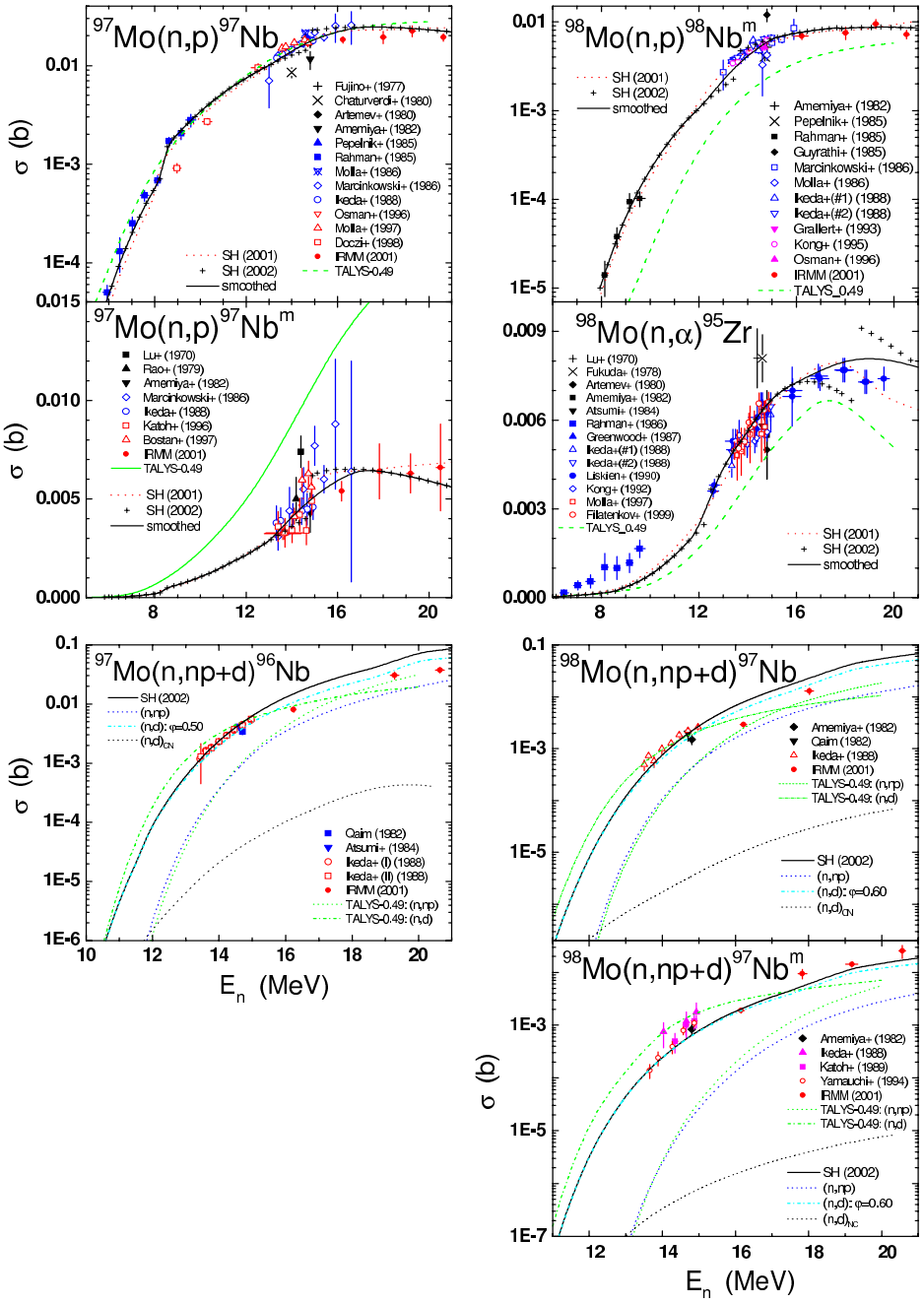

Figure 8: *Comparison of experimental and calculated neutron-activation cross-sections for* ^{97,98}*Mo.*

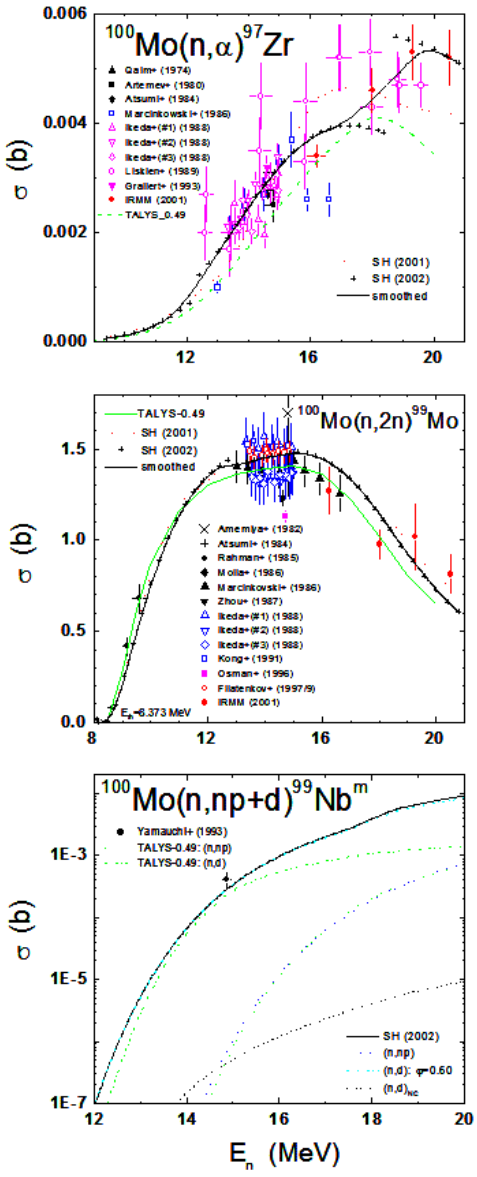

Figure 9: *Comparison of experimental and calculated neutron-activation cross-sections for* ^{100}*Mo.*

reactions induced on ^{92}Mo, i.e. ^{92}Mo$(n,p)^{92m}$Nb, ^{92}Mo$(n,\alpha)^{89g,m}$Zr, ^{92}Mo$(n,2n)^{91g,m}$Mo and ^{92}Mo$(n,np)^{91m}$Nb (Fig. 5), for which there is also a large amount of measured data but yet many discrepancies between even recent data sets, while three basic evaluations performed in the last decade at well-known laboratories show wide differences, e.g. up to $\sim$ 50% for the (n,p) reaction [46,47] and $\sim$65% for the (n,α) reaction [47,48]. The agreement between calculated and the available experimental data could be considered good in the limit of experimental errors.

However, the PE effects are also lowest in the case of the lightest stable isotope ^{92}Mo. For the validation of this mechanism they are more important the isotopes ^{98,100}Mo (Figs. 8-9) and especially the $(n,2n)$ reaction on the heaviest isotope. The correct description of the recent experimental data around the maximum of this reaction excitation function (Fig. 9) can be considered positive in this respect.

Furthermore, the comparison of the calculated and available experimental excitation functions of (n,p), (n,α), $(n,2n)$and $(n,np+d)$ reactions on the target nuclei $^{94,96-98}$Mo (Figs. 6-8) proves a good agreement in the limit of the experimental errors. It is supported thus the PE approach involved firstly in the case of ^{51}V, namely the effect of the thresholds for various partial waves contributions to the PE processes [11] which are shown by the calculated cross-sections (small crosses in Figs. 5-9) before applying a smoothing procedure (thick solid curves). They are compared with the results of the previous analysis [11], where it was shown the same structure, as well as with the predictions [2] of TALYS.

The quite schematic model adopted for the deuteron PE emission could be the reason of some discrepancies between the calculated and experimental $(n,np+d)$ reaction cross-sections. The assumption of the d-particle state density closely related to the phenomenological α-particle state density [50] $g_\alpha = A/10.36$ MeV^{-1} could be questionable especially concerning the energy dependence. Unfortunately the present analysis shows similar numbers of favourable and doubtful cases in this respect, and further work would be useful.

Finally one may consider that actual revision of these calculations by taking into account also the new IRMM data proved both

(i) the usefulness of the activation cross-sections at neutron energies just above the common value of 15 MeV, and

(ii) the prediction power as well as the accuracy limits of the present calculations, mainly related to the decay schemes in the case of the isomer ratio calculations.

The latter point concerns the low-lying discrete levels where missing experimental branching ratios or even any γ-decay data for some levels may hardly affect the

isomeric cross-section calculated values. The γ-ray strength functions $f_{E1}(E_\gamma)$ description has received an additional validation in the case of the analysis of the ^{94}Mo$(n,2n)^{93m}$Mo reaction, where the 16$^{\rm th}$ excited state is the isomeric one and there is no feeding of it from the higher discrete levels. Unfortunately only in such limit cases one may avoid the use of the low-lying level decay schemes, while they remain critical in the general case. The magnitude of this effect could be the subject of further analysis.

[1] M. Avrigeanu and V. Avrigeanu, *STAPRE-H95 Computer Code*, IPNE Report NP-86-1995, Bucharest, 1995; News NEA Data Bank 17 (1995) 22, 25.

[2] A. Fessler, E. Wattecamps, D.L. Smith, and S.M. Qaim, Phys. Rev. C 58, 996 (1998).

[3] W. Dilg, W. Schantl, H. Vonach and M. Uhl, Nucl. Phys. A217, 269 (1973).

[4] S.F. Mughabghab and C. Dunford, Phys. Rev. Lett. 82,4083 (1998)

[5] S.M. Qaim, Proc. NDST-1994, Gatlingurg, May, 1994, v. 1, p. 186.

[6] The Model Code Meeting, May 21-22, 2002, EC/JRC/IRMM, Geel, Belgium.

[7] A. Harangozo, I. Stetcu, M. Avrigeanu, and V. Avrigeanu, Phys. Rev. C 58, 295 (1998).

[8] P. Oblozinsky, Development of Reference Input Parameter Library for Nuclear Model Calculations of Nuclear Data, Report IAEA-TECDOC-1034, IAEA, Vienna, 1998; http://www-nds.iaea.or.at/ripl/ .

[9] M. Avrigeanu and V. Avrigeanu, Comp. Phys. Comm. 112, 191 (1998).

[10] P. Reimer, V. Avrigeanu, A.J.M. Plompen, and S.M. Qaim, Phys. Rev. C 65, 014604 (2001).

[11] M. Avrigeanu, V. Avrigeanu, and A.J.M. Plompen, J. Nucl. Sci. Technol. Suppl. 2, 803 (2002).

[12] C.Y. Fu and D.C. Larson, Comparison of Evaluated Data for Chromium-52, Iron-56 and Nickel-58, Report NEA/WPEC-1, OECD, Paris, 1996.

[13] R.C. Haight *et al.*, Proc. of NDST97, Trieste, May 1997, vol. 1, p. 603.

[14] S.M. Grimes *et al.*, Nucl. Sci. Eng. 124, 271 (1996).

[15] T. Kawano, T. Sanami, M. Baba, and H. Nakashima, J. Nucl. Sci. Tech. 36, 256 (1999).

[16] A.J. Koning, in Nuclear Model Parameter Testing for Nuclear Data Evaluation, M. Herman (Ed.), Report INDC(NDS)-431, IAEA, Vienna, 2002, p. 117.

[17] V. Avrigeanu, T. Glodariu, A.J.M. Plompen, and H. Weigmann, J. Nucl. Sci. Technol. S. 2, 746 (2002);

[18] M. Avrigeanu, V. Avrigeanu, and T. Glodariu, Workshop on Activation Data Ű EAF 2003, Prague, June 24-26, 2002.

[19] V. Avrigeanu, P.E. Hodgson, and V. Avrigeanu, Phys. Rev. C 49, 2137 (1994).

[20] M. Avrigeanu, this workshop.

[21] M. Avrigeanu *et al.*, Phys. Rev. C 62, 017001 (2000); Nucl. Phys. A693, 616 (2001); I.V. Krouglov, M. Avrigeanu, and W. von Oertzen, Eur. Phys. J. A 12, 399 (2001).

[22] A. Fessler and S.M. Qaim, Radiochim. Acta 84, 1 (1999).

[23] A.J.M. Plompen *et al.*, Proc. PHYSOR 2002, Oct. 7-10, 2002, Seoul, Korea (in press).

[24] V. Avrigeanu, M. Avrigeanu, and T. Glodariu, Fast Neutron Physics Int. Workshop, Dresden, Sept. 5-7, 2002.

[25] V. Avrigeanu, M. Avrigeanu, and T. Glodariu, Report EFF-Doc-835, Dec. 2002.

[26] A.J.M. Plompen, D.L. Smith, P. Reimer, S.M. Qaim, V. Semkova, F. Cserpak, V.‘Avrigeanu, and S. Sudar, ND2001 and J. Nucl. Sci. Technol. (in press).

[27] J.P. Delaroche, Ch. Lagrange, and J. Salvy, IAEA-190 (IAEA, Vienna, 1976), vol. 1, p. 251.

[28] A.B. Smith, P.T. Guenther, and J. Whalen, Nucl. Phys. A244, 213 (1975).

[29] A.B. Smith, P.T. Guenther, and J. Whalen, Nucl. Phys. A415, 1 (1984).

[30] A.B. Smith, J. Phys. G 26, 1467 (2000).

[31] Ch. Lagrange, in Neutron Data for Structural Materials for Fast Reactors, edited by K.H. Bockhoff (Pergamon Press, Oxford, 1979), p. 756.

[32] T. Kawano, Y. Watanabe, and M. Kawai,, J. Nucl. Sci. Tech. (Japan), 35, 519 (1998).

[33] I.-G. Birn, A. Meister, E. Wattecamps, and H. Weigmann, Nuclear Data for Science and Technology, edited by G. Reffo *et al.* (SIF, Bologna, 1997), p. 526.

[34] S.F. Mughabghab, M. Divadeenam, N.E. Holden, Neutron cross-sections (AP, New York, 1981), v. 1.

[35] M. Ivascu, M. Avrigeanu, and V. Avrigeanu, IFIN Report NP-28-1983, Bucharest, 1983.

[36] C.H. Johnson, A. Galonsky, and R.L. Kernell, Phys. Rev. C 20, 2052 (1979).

[37] Ch. Lagrange, Phys. Rev. C 22, 896 (1980).

[38] D.S. Flynn, R.L. Hershberger, and F. Gabbard, Phys. Rev. C 20, 1706 (1979).

[39] S. Harissopulos *et al.*, Phys. Rev. C 64, 055804 (2001).

[40] D.G. Gardner and F.S. Dietrich, Report UCRL-82998, LLNL-Livermore, 1979.

[41] M. Avrigeanu, V. Avrigeanu, G. Cata, and M. Ivascu, Rev. Roum. Phys. 32, 837 (1987).

[42] S. Raman *et al.*, At. Data Nucl. Data Tables, 36, 1 (1987); R.H. Spear, ibid., 42, 55 (1989).

[43] C. Kalbach, Phys. Rev. C 62, 044608 (2000).

[44] P.D. Kunz, DWUCK4 user manual, OECD/NEA Data Bank, 1984 (IFIN-HH version at NEA-DB).

[45] R.C. Haight, S.M. Grimes, R.G. Johnson and H.H. Barschall, Phys. Rev. C 23, 700 (1981).

[46] S.M. Qaim, R. Wolfle, and B. Strohmaier, Phys. Rev. C 40, 1993 (1989).

[47] P.E. Garret, L.A. Bernstein, J.A. Baker, K. Hauschild, C.A. McGrath, D.P. McNabb, W. Younes, M.B. Chadwick et al, Phys. Rev. C 62, 054608 (2000).

[48] N. Yamamuro, Nucl. Sci. Eng. 109, 128 (1991).

[49] A.J. Koning, S. Hilaire and M.C. Duijvestijn, Proc. Int. Conf. on Nuclear Data for Science and Technology – ND2004, Sep. 26 – Oct. 1, 2004, Santa Fe, USA, in print.

[50] E. Gadioli and E. Gadioli-Erba, Z. Phys. A 299, 1 (1981).

Microscopic evaluation of Eu isotopes

Eric Bauge

CEA DIF, Département de Physique Théorique et Appliquée, Service de Physique Nucléaire, BP 12, 91680 Bruyères-le-Châtel, France

Abstract:
Complete evaluations of the n+$^{146-154}$Eu reactions have been performed using only nuclear reaction models for incident neutron energies between 1 keV and 30 MeV. In this work, a strong emphasis has been put on using the most microscopic ingredients possible for models to ensure a graceful degradation of the predictive power of the model when going to Eu isotopes with no experimental information. Comparisons with experimental data and other evaluations are performed, showing that the methodology used in this work is a viable way of evaluating nuclear data.

Evaluating reaction cross-sections for europium isotopes constitutes a difficult challenge for the evaluator. The difficulty lies in the very limited amount of available experimental data for all but the stable ^{151}Eu and ^{153}Eu isotopes, especially for the observables related to the optical model. This lack of experimental data is one reason motivating our use of Semi Microscopic Optical Model Potentials (SMOMP) [1] using nuclear structure results as input. These SMOMPs have been shown to produce reliable predictions with no parameter adjustment. The other reason for using the SMOMP is the proximity of the $N = 82$ shell closure, which induces shape changes when one gets farther away from this closure. This shape change also induce changes in the direct reaction models, from the spherical optical model for low deformations ($\beta < 0.1$), up to the rotational optical model for large deformations ($\beta > 0.2$), and vibrational model for intermediate deformations. These changes are propagated into the statistical model by use of different specific transmission coefficients for each step of the sequential evaporation process, since the first evaporated neutron is emitted from a nucleus that is significantly more deformed than the nucleus that emits the n$^{\text{th}}$ neutron. This treatment is made possible by both the use of the TALYS code [2] that allows for such a change of transmission coefficient along a sequential evaporation chain, and the use of the SMOMP that can generate all the needed transmission coefficients when linked with the right nuclear structure information. This type

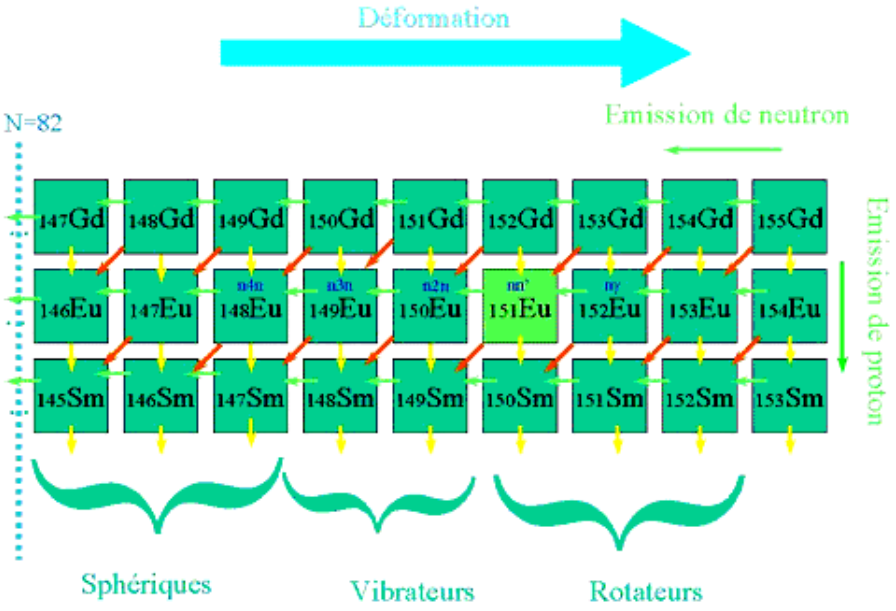

Figure 1: *Influence of nuclear structure on modelling of reactions.*

of modelling implies that a considerable effort must be done for studying nuclear structure for all the possible residual nuclei. Fig. 1 illustrates the above discussion in the case of the n+^{151}Eu reaction.

The nuclear structure of even-even residual nuclei was studied using collective Hamiltonian calculations [3] with a potential energy surface obtained by Hartree-Fock-Bogoliubov calculations using the Gogny D1S interaction [4]. Fig. 2 shows the results of such calculations for ^{144}Sm, ^{148}Sm and ^{152}Sm. In this figure, one observes the evolution from a spherical shape for ^{144}Sm, to an axially deformed shape for ^{152}Sm, through a triaxial dynamically deformed shape for ^{148}Sm.

For odd and odd-odd nuclei, densities are calculated using the constrained axial HFB/D1S method at deformations interpolated between those calculated for the even-even neighbour nuclei. The radial densities given by those calculations are then folded with the Lane-consistent nuclear matter optical model potential as explained in Refs. [1,5] to produce optical model potentials for neutron and proton incident on all the needed residual nuclei. The folding is performed according to

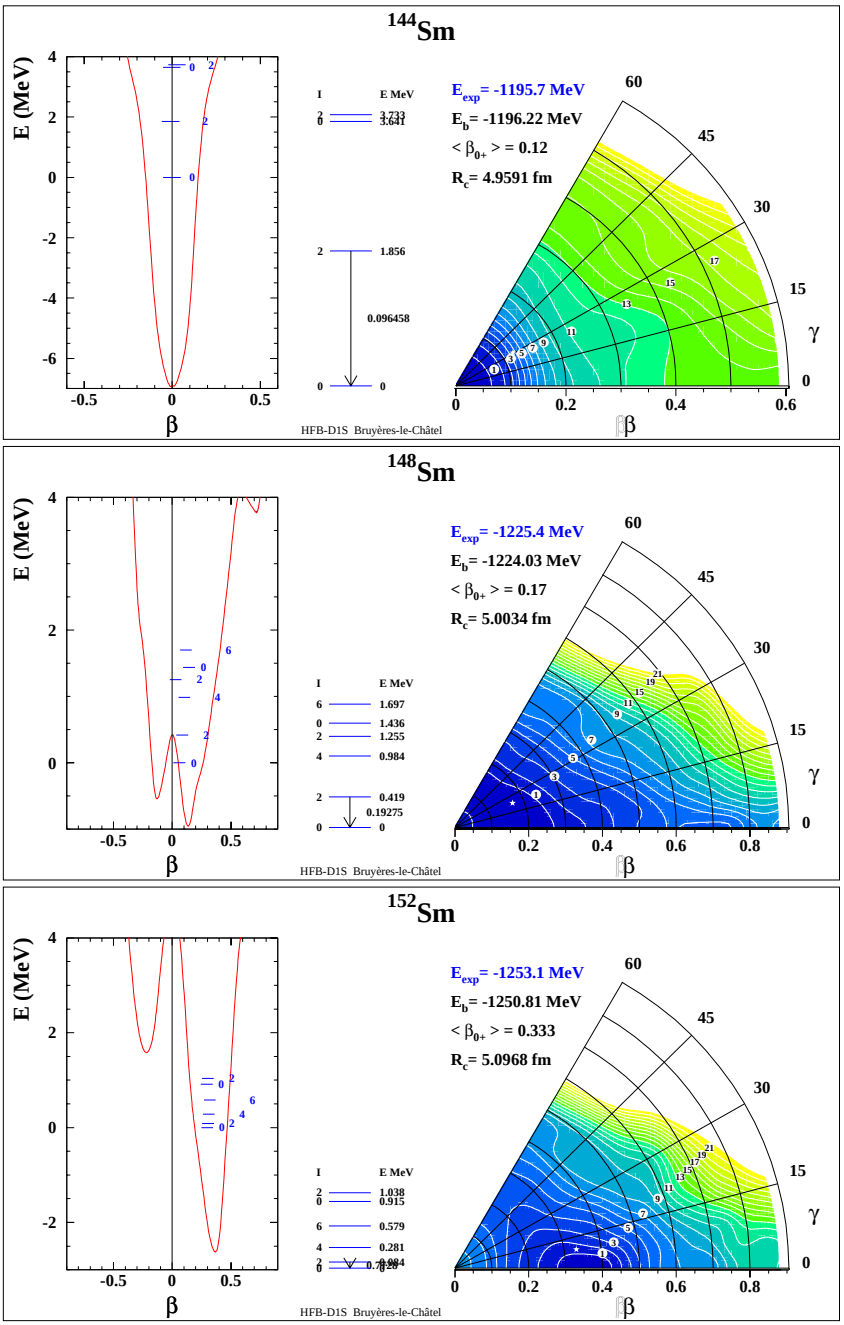

Figure 2: *Evolution of the shape of Sm isotopes. Collective Hamiltonian calculations for three Sm isotopes.*

the following equation

$$U(\vec{r},E) = \frac{1}{(t\sqrt{\pi})^3}\int \rho(\vec{r'})\frac{u(\rho(\vec{r'}),E)}{\rho(\vec{r'})}e^{-\frac{(\vec{r}-\vec{r'})^2}{t^2}}d\vec{r'}$$

In this equation $U(\vec{r},E)$ is the OMP for the target nucleus, $\rho(\vec{r})$ is the density of the target nucleus, $u(\rho,E)$ is the OMP in nuclear matter, and t the range of the Gaussian widening form factor. This potential is included in the Schrödinger Equation that is appropriate for the reaction mechanism implied by the deformation (spherical OMP, vibrational OMP, or rotational OMP), and solved by ECIS [6], giving observables such as total cross-section, reaction cross-section, direct elastic and inelastic cross-section, as well as transmission coefficients. These observables can be compared to experimental data like in Figs. 3 and 4. In Fig. 3 we compare the elastic and inelastic scattering differential cross-sections for the reaction p+^{153}Eu at 12 MeV. The good agreement between calculations and data shows that the collectivity of the target nucleus as well as its radial density distribution is well described by the nuclear structure model. Similar agreement is found for the p+$^{151-154}$Eu reactions.

The left panel of Fig. 4 shows the calculated total cross-sections for n+^{148,150,152,154}Sm reactions between 1 and 15 MeV incident neutron energy compared with the experimental cross-section for n+^{148}Sm. This figure highlights the good agreement between the predicted and measured n+^{148}Sm total cross-sections, moreover it displays the evolution of the n+Sm total cross-sections with the neutron number N. The right panel of Fig. 4 shows the calculated relative total cross-sections difference between ^{154}Sm and ^{148}Sm compared to its experimental counterpart. The calculated cross-section differences exhibit a very good agreement (typically less than 2 percent, and at most 5 percent of the ^{148}Sm cross-section) with the data, showing that the N-variations of the OMP are well accounted for by the nuclear structure calculations as well as the isovector term of the OMP, like in Ref. [7].

The transmission coefficients and reaction cross-sections calculated using the above OMP for all possible residual nuclei are then fed to the TALYS [2] program which calculates cross-sections for all the open channels with the exciton pre-equilibrium model, and the Hauser-Feshbach statistical evaporation model. TALYS performs these calculations using a database of default parameters for discrete levels, level density parameters, γ-decay widths, etc... that comes from the RIPL-2 parameter library [8]. No adjustments were performed on the parameters relevant to the Hauser-Feshbach model and only small variations of the pre-equilibrium parameters were allowed. The resulting evaluated data is then compared to experimental data. Fig. 5 shows comparisons between evaluated and

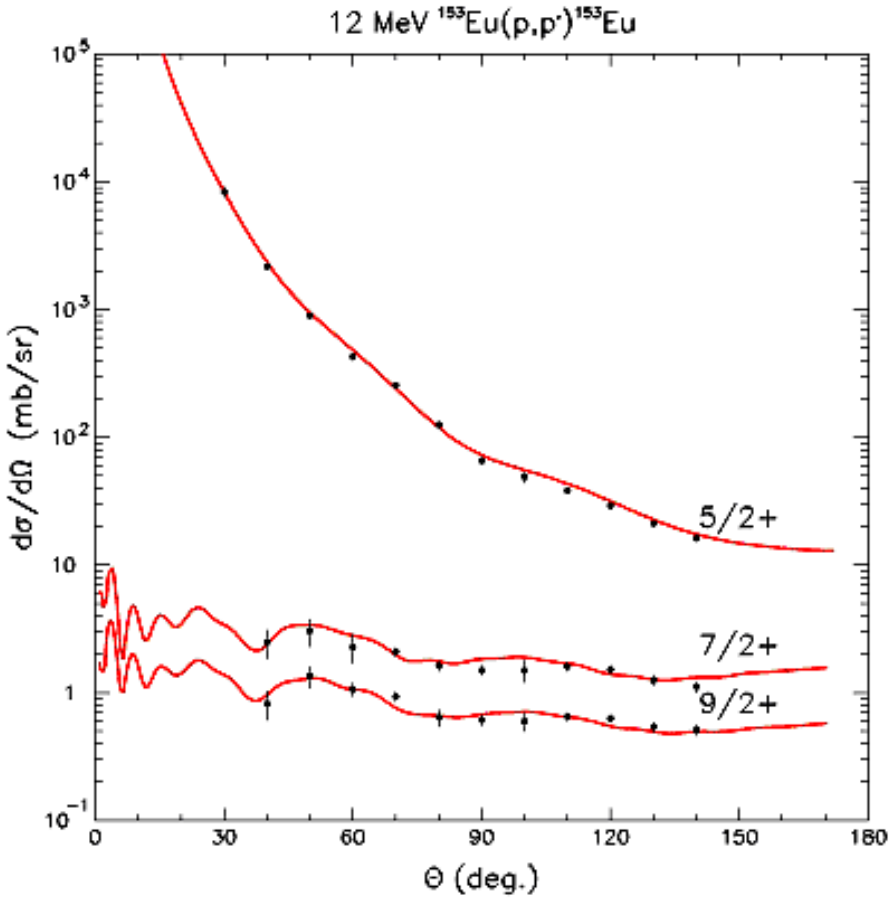

Figure 3: *Elastic and inelastic scattering differential cross-sections for the 12 MeV* $p+^{153}$*Eu reaction.*

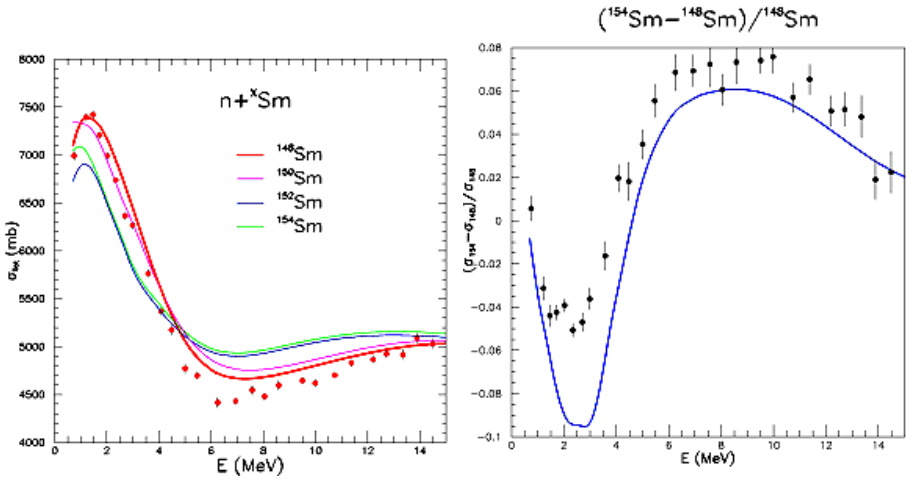

Figure 4: *Total cross-sections and cross-sections differences for Sm isotopes.*

measured data for the n+^{151}Eu entrance channel between 1 keV and 30 MeV. The agreement between the evaluation and the data is very good for the (n,γ), $(n,3n)$, and $(n,4n)$ channels. However, for the $(n,2n)$ channels the comparison is not so easy since experimental data sets are inconsistent with each other. One can nevertheless conclude that given the inconsistencies between experimental values, our evaluation produces a reasonable description of the data. Fig. 5 shows a similar comparison for the n+^{153}Eu entrance channel with similar conclusions except for the absence of experimental data inconsistency in the $(n,2n)$ channel. All these good agreements for ^{151}Eu and ^{153}Eu are remarkable, given that they are obtained using only the unadjusted microscopic OMP and the unadjusted RIPL-2 parameter library in TALYS. Moreover, given the microscopic nature of the OMPs, the evaluations for other isotopes are likely to be good representations of reality, provided that the RIPL-2 parameters (especially Γ_γ and capture related parameters) for those isotopes are reasonably good.

Finally, in Fig. 7, our evaluations (BRC6) were compared to other evaluations (ENDF/BVI.7, JENDL-3.3, JEFF-3.0) for the n+^{151}Eu entrance channel. Comparisons for the (n,γ) channel exhibit very few differences, especially at low neutron energies, but at energies near 1 MeV sizeable differences appear. However, if one is to believe the experimental data (Fig. 5), our evaluation which matches the experimental available data up to 1 MeV is to be preferred. For the $(n,2n)$ channel, the picture is very different: due to the inconsistencies between data sets the cross-section are spread over a large interval reflecting the experimental data sets chosen

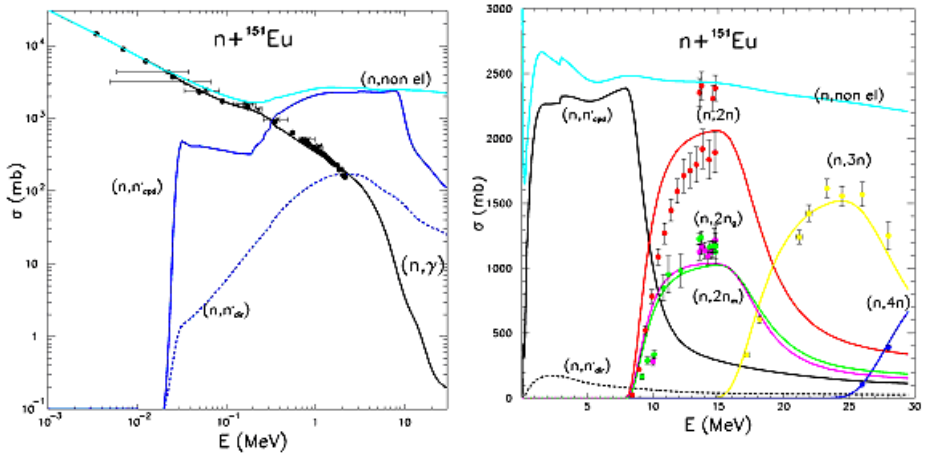

Figure 5: *Comparisons between evaluated n+151Eu cross-sections and experimental data.*

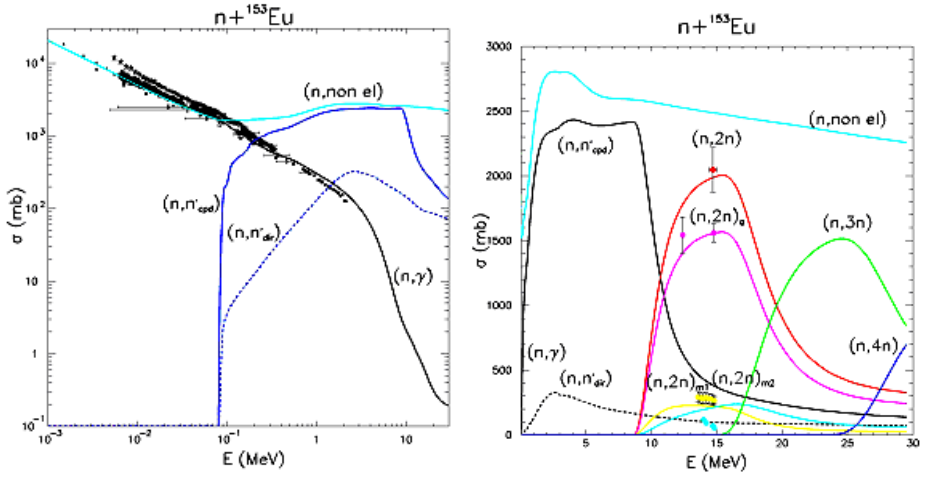

Figure 6: *Comparisons between evaluated n+153Eu cross-sections and experimental data.*

by evaluators for adjusting model parameters. Our assessment of the different evaluations is that the "truth" must be somewhere between ENDF/B-VI.7 and our BRC6. For inelastic scattering evaluations are similar in the 5-10 MeV range, but the high energy behaviour of the JENDL and JEFF evaluations are suspect. Finally, for the $(n, 3n)$ channel, there is a strong agreement between the ENDF/B-VI.7 and BRC6, evaluations and to a lesser extent JENDL, while JEFF-3.0 clearly underestimates this channel.

Similar comparisons were also performed for the n+^{153}Eu entrance channel, with similar results, the only difference being that all the disagreement between evaluations on the $(n, 2n)$ channel is smaller. The general impression left after this comparison between evaluations, is that BRC6 and ENDF/B-VI.7 are in reasonable agreement with each other and with the data whereas both JENDL-3.3 and JEFF-3.0 exhibit some severe problems. Our recommendation is to use BRC6 as the basis for the future release of the JEFF-3.1 Eu evaluated data files after matching with the existing low energy (< 1 keV) data.

[1] E. Bauge, J.P. Delaroche, M. Girod, Phys. Rev. C 63, 024607 (2001).

[2] A.J. Koning, S. Hilaire, M. Duijvestijn, Proc.Int.Conf. on Nuclear Data for Science and Technol., 26 Sep.-1 Oct., Santa Fe, USA (2004)

[3] J. Libert, M. Girod, J.P. Delaroche, Phys. Rev. C 60, 054301 (1999).

[4] J.F. Berger, M. Girod, D. Gogny, Comp. Phys. Comm. 63, 365 (1990).

[5] E. Bauge, J.P. Delaroche, M. Girod, G. Haouat, J. Lashkar, Y. Patin, J. Sigaud, J. Chardine, Phys. Rev. C 61, 034306 024607 (2000).

[6] J. Raynal, Rapport CEA No. CEA-R-2772 (1994).

[7] F.S. Dietrich, J.D. Anderson, R.W. Bauer, S.M. Grimes, R.W. Finlay, W.P. Abfalterer, F.B. Bateman, R.C. Haight, G.L. Morgan, E. Bauge, J.P. Delaroche, P. Romain, Phys. Rev. C 67, 044606 (2003).

[8] RIPL-2 database, http://iaeand.iaea.or.at/ripl

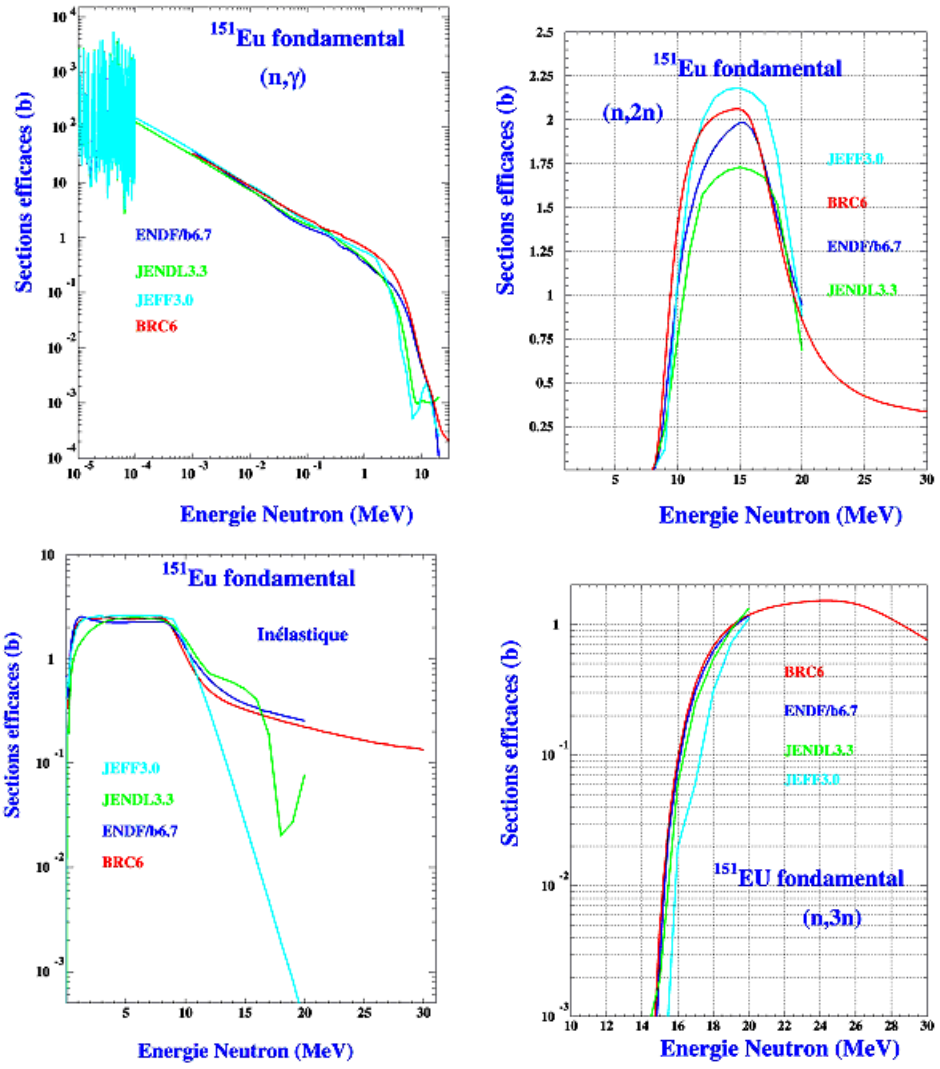

Figure 7: *Comparisons between different evaluated n+^{153}Eu cross-section for MT= 102, 16,17 and 4.*

Measurements and nuclear model calculations for neutron induced reactions on ^{127}I, ^{129}I isotopes up to 21 MeV

F. Cserpák[1], S. Sudár[1], A.J.M. Plompen[2]

[1] *Institute of Experimental Physics, University of Debrecen, H-4001 Debrecen 10, P.O.B. 105, Hungary*
[2] *European Commission, DG-Joint Research Centre, Institute for Reference Materials and Measurements, B-2440 Geel*

Abstract:
Excitation functions were measured by the activation technique for the ^{127}I$(n,2n)^{126}$I, ^{129}I$(n,2n)^{128}$I, ^{129}I$(n,p)^{129}$Te and ^{129}I$(n,\alpha)^{126}$Sb reactions from 16 MeV to 21 MeV neutron energy. Isomeric cross-section ratios for the ^{129}I$(n,p)^{129m,g}$Te, ^{129}I$(n,\alpha)^{126m,g}$Sb reactions were also determined. The irradiations were performed at the Geel Van de Graaff accelerator. Quasi mono-energetic neutrons were produced via ^{3}H$(d,n)^{4}$He reaction. The radioactivity of the activation products was determined by high resolution γ-ray spectrometry. For most of the reactions on the radioactive ^{129}I isotope, the present measurement provides the first consistent set of data. Statistical model calculations taking into account the pre-compound effects were performed for all reactions, and acceptable agreement was found with the measured data.

Introduction

The measurement of cross-sections with the activation technique is an efficient method to survey the status of our knowledge with regard to (n,xn), (n,xp) and $(n,x\alpha)$ reactions and of course for reactions leading to activation product.
The special interest of this measurement is that the ^{129}I isotope is a long-lived radioactive fission product. This is the reason why only a few experimental data exist for neutron induced reactions on this isotope.

Experimental techniques

Cross-sections were measured by the activation technique, commonly used at Geel (For references see Tab. 2.1 in part A of this report).

Samples

Iodine samples were prepared from nuclear waste in the form of the PbI_2 compound, encapsulated in Al or plexi-glass cylinders. The inner diameter of one sample was 14 mm, thickness of the wall was 0.5 mm and the thickness of the sample was about 2.5 mm. The total mass of the encapsulated powder in one sample is about 2 g including PbI_2 and a certain amount of other compounds. From the origin of the sample material, it is evident that the samples contain both iodine isotopes, ^{127}I and ^{129}I. Therefore, in addition to the cross-section measurement, detailed investigations were performed to determine the ^{127}I, ^{129}I and Pb content of the samples. The gamma attenuation method and the comparative neutron activation technique were used to determine the ^{127}I and Pb content of the sample, while the m(^{129}I)/m(^{127}I) ratio was determined by mass spectrometry at IRMM.

Irradiation

All samples were irradiated at the Geel 7 MV Van-de-Graaff accelerator. Neutrons from 16 to 20.7 MeV were obtained by use of the $^{3}\mathrm{H}(d,n)^{4}\mathrm{He}$ reaction with deuteron energies of 1, 2, 3, and 4 MeV and a titanium-tritide target of 2 mg/cm^2. The used irradiation setup is a light weight holder that allows samples to be placed from 1 to 5 cm from the neutron producing target with angles varying from 0° to 135° with respect to the incident deuteron beam. In this setup the influence of multiple scattering is less then 2 % for the investigated reactions. For the cross-section measurements the samples were placed at 0° to the beam and about 2 cm distance from the target. Depending on the half life of the reaction product, the irradiation time varied from 1 hour to 3 days. In all cases the beam intensity variation is measured and corrected for by the use of a BF_3 proportional counter, the count rates of which are stored in multichannel scaling mode. For the determination of neutron fluences the $^{27}\mathrm{Al}(n,p)^{27}\mathrm{Mg}$, $^{27}\mathrm{Al}(n,\alpha)^{24}\mathrm{Na}$ and $^{93}\mathrm{Nb}(n,2n)^{92m}\mathrm{Nb}$ standard cross-sections were used. Monitor foils were attached to the front and the back of the samples. The mean fluences for the samples were calculated integration over the volume of the sample.

Activity determination

Activities of all irradiated samples and monitors were determined by γ-ray counting. For all measurements the same HPGe detector was used which was calibrated with point sources obtained from PTB and DAMRI. Corrections were made for summing coincidence, self absorption and sample size.

Nuclear model calculations

Calculation with STAPRE code

Nuclear reaction model calculations were performed using the computer code STAPRE [1]. The pre-equilibrium emission was taken into account by the exciton model while the width-fluctuation corrected Hauser-Feshbach formula was used for first chance emission from the equilibrated system. Direct interactions were taken into account by using Multi Step Direct reaction cross-section calculated by the EMPIRE-II code [2]. The absorption cross-section was reduced by the according to the MSD and the (n, n') reaction were corrected by the MSD contribution. The particle transmission coefficients were generated via the spherical optical model using the computer code SCAT 2 [3]. For the energy and mass dependence of the effective matrix element of the internal transition, the $|M|^2$ = FM/(A^3E) formula was used. The FM value was dependent on the level density formalism. For the preformation factor of the α-particles, a value of 0.25 was used in the formulation of the emission rates. The excited states of the product nuclei were described by the available information on the discrete levels using the ENSDF data files of Brookhaven National Laboratory, USA. At higher energies the levels were treated as a continuum, described by the back-shifted Fermi gas model [4]. The selection method of the level density parameters is described below. The transmission coefficients of photons have considerable significance in calculations on isomeric cross-sections. They were derived from the gamma-ray strength functions. For the E1 radiation, the Brink-Axel model (1952) with global parameters was applied, while for the M1, E2, M2, E3 and M3 radiation the Weisskopf model was used. The unknown branching ratios for the discrete levels were calculated using the gamma transmission coefficients calculated in a way similar to that implemented in the STAPRE for the continuum.

Calculation with EMPIRE-II code

The version 2.16 of the EMPIRE (Montenotte) code was used for the calculation. The standard library of input parameters was used which includes the nuclear masses, optical model parameters, ground state deformations, discrete levels, decay branches, level densities, moments of inertia (MOMFIT), and strength functions. The particle transmission coefficients were generated via the spherical optical model using the computer code (SCAT2) using the default set of global parameters: Wilmore-Hodgson [5] for neutrons, Bechetti Greenlees [6], and for α-particles, Avrigeanu's [7] potential. In the calculation the Multi Step Direct, Multi Step Compound and Hauser-Feshbach model with width fluctuation correction (HRTW) were used. The code conserves particle flux by dividing

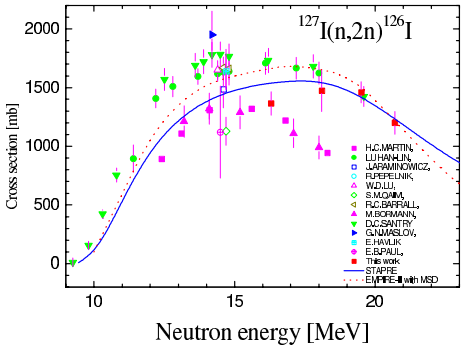

Figure 1: *Measured and calculated excitation functions for the* $^{127}I(n,2n)^{126}I$ *reaction*

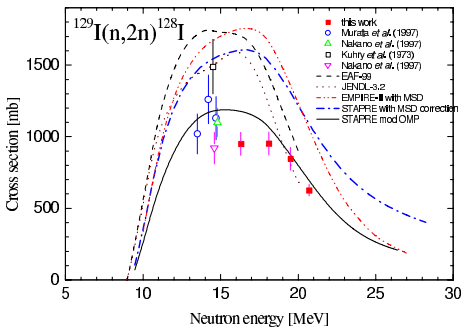

Figure 2: *Measured and calculated excitation functions for the* $^{129}I(n,2n)^{128}I$ *reaction*

the absorption cross-section of the optical model between the different types of reaction mechanism. For the level densities, the dynamic approach of the EMPIRE-II was used. In this case the formalism of the super-fluid model (BCS) is applied below the critical excitation energies and the Fermi gas model above the critical energy. Selection of the optical model parameters (OMP) for model calculation on ^{127,129}I target nuclei were based on the measured total cross-section data of ^{127}I and ^{129}I which were collected from the EXFOR database. Detailed studies were available only for the ^{127}I isotope. The transmission coefficients were calculated by the SCAT-2 optical model (OM) code. Global and local OM parameters were tested for the calculation by comparing the experimental data with the model calculation. The best average deviation between the calculated and measured total cross-sections was obtained with the global Wilmore-Hodgson [5] parameters or Koning's [8] local and global OM parameters for both silver and iodine. The level density parameters a for the calculation were selected by interpolating the data of the neighbouring isotopes, taking into account the odd-even systematic from the Plyaskin data [9]. The back shift parameter (Δ) was determined individually for all nuclei used in the model calculation. The cumulative plot of the known discrete levels, collected from the ENSDF database, was fitted by the BSFG formula while the level spacing at the neutron binding energy were kept on the experimental value.

Results

The $^{127}I(n,2n)^{126}I$ reaction

The measured and calculated excitation functions of ^{127}I$(n,2n)^{126}$I reaction are shown on Fig. 1. Besides the 14 MeV data more cross-sections were measured in wider energy range (Santry *et al.*, Lu Han Lin *et al.*, Martin *et al.*, Bormann *et al.*). The data of Santry *et al.* and Lu Han Lin *et al.* seem to agree within the error limit. The Martin *et al.* and Bormann *et al.* data are significantly lower. The present measurements at IRMM are in agreement with those by Santry *et al.* and Lu Han Lin *et al.* The model calculations with both the STAPRE and the EMPIRE codes are near to the experimental data, especially above 16 MeV. Below this energy, the calculations are lower than the data by Santry *et al.* and Lu Han Lin *et al.* and the agreement with the calculations with EMPIRE is better.

The $^{129}I(n,2n)^{128}I$ reaction

Cross-sections for radioactive target nuclei, like ^{129}I, are poorly studied. For ^{129}I, only the ^{129}I$(n,2n)^{128}$I reaction was studied previously in the 14 MeV region. The measured cross-section and the calculations are shown on Fig. 2. The latest measured data agree with our measurements. The measured data show lower values than expected from systematics and a model calculation using global OM parameters. The calculations with both the STAPRE and the EMPIRE code overestimate the measured data using these parameter sets. To improve the description of the experimental data, the parameters of the optical model were modified. The calculation with these parameters is shown by the continuous line in Fig. 2. The absorption cross-section was decreased by the new parameters and therefore both the calculated (n,p) and (n,α) cross-sections decreased achieving better overall agreement between the model calculations and the experimental data (see below).

The $^{129}I(n,p)^{129m,g}Te$ reactions

The final nucleus of the ^{129}I$(n,p)^{129}$Te reaction has an isomeric state allowing the study of isomer and ground states production cross-sections. Figs. 3 and 4 depict the measured and calculated excitation functions of the ^{129}I$(n,p)^{129g}$Te and ^{129}I$(n,p)^{129m}$Te reactions. The results with EMPIRE show quite low cross-section compared with experiment, even if the OMP leads to overestimation of the (n,2n) excitation function. The STAPRE calculations with modified OM parameters in the neutron channel describe the magnitude of the cross-section quite well, but the shape of the excitation function is not fully in agreement

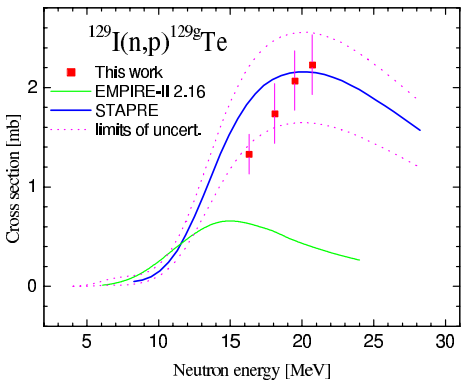

Figure 3: *Measured and calculated excitation functions for the* $^{129}I(n,p)^{129g}Te$ *reaction*

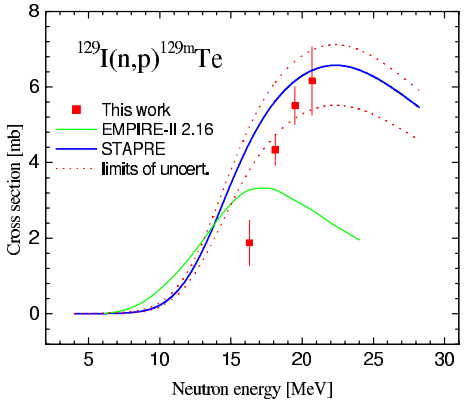

Figure 4: *Measured and calculated excitation functions for the* $^{129}I(n,p)^{129m}Te$ *reaction*

with experiment. The STAPRE calculations without pre-compound emission gives values similar to those obtained with EMPIRE, indicating that the main contribution arises from pre-compound emission. The dotted lines show the uncertainties of the calculation based on the estimated uncertainties of the model parameters. This uncertainty does not include the uncertainty connected to the absorption cross-section reduction caused by the change of the OMP parameters, which would be quite high.

The $^{129}I(n,\alpha)^{126m,g}Sb$ *reactions*

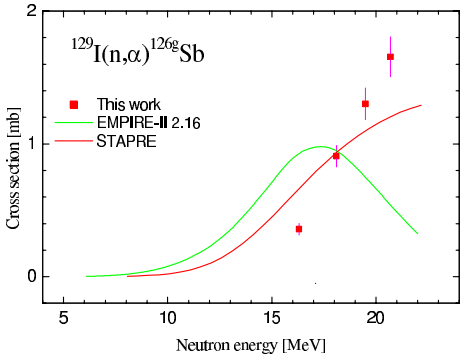

Figure 5: *Measured and calculated excitation functions for the* $^{129}I(n,\alpha)^{126g}Sb$ *reaction*

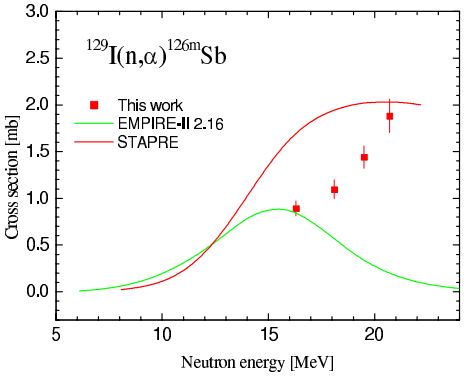

Figure 6: *Measured and calculated excitation functions for the* $^{129}I(n,\alpha)^{126m}Sb$ *reaction*

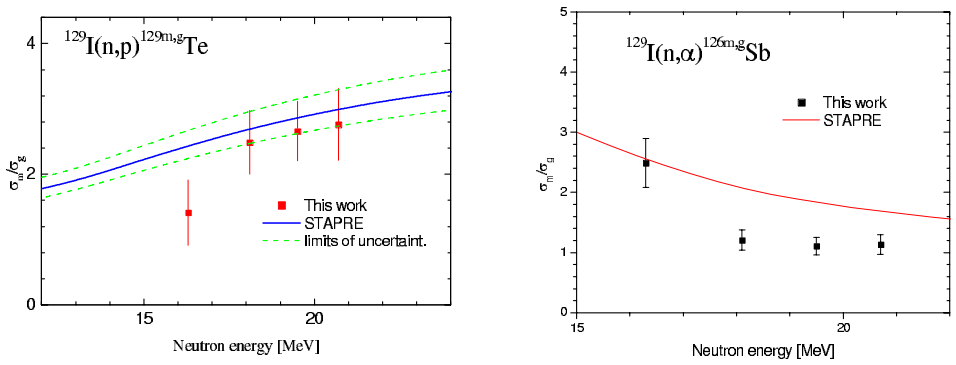

Figure 7: *Measured and calculated isomeric cross-section ratios for the* $^{129}I(n,p)^{129m,g}Te$ *and* $^{129}I(n,\alpha)^{126m,g}Sb$ *reactions*

Figs. 5 and 6 present the measured and calculated excitation function for the ^{129}I$(n,\alpha)^{126g}$Sb and ^{129}I$(n,\alpha)^{126m}$Sb reactions. The EMPIRE code gives quite low cross-section compared with the experiment, similar to the case of the (n,p) excitation functions presented above. The STAPRE calculations with the modified OM parameters for the neutron channel describe the magnitude of the cross-section quite well, but the shape of the excitation function does not fully agree with experiment.

The isomeric cross-section ratios do not depend as strongly on the model parameters as the cross-section. This can be seen in the left part of Fig. 7, which depicts the isomeric cross-section ratio for the ^{129}I$(n,p)^{129m,g}$Te reaction. The uncertainties caused by the uncertainty of the same model parameters as shown in Figs. 3 and 4 have less effect on the isomeric cross-section ratio than is the case for the excitation functions. Comparing the experimental data and the model calculation, in the case of the ^{129}I$(n,p)^{129m,g}$Te reaction only one experimental data point is a bit far from the model calculation. For the ^{129}I$(n,\alpha)^{126m,g}$Sb reaction the isomeric cross-section ratios from the model and the experiment are in agreement at only one energy. This suggests some inconsistency in the measurements.

Summary

New experimental cross-sections were determined for neutron induced reaction on the iodine isotopes, especially for the radioactive target of ^{129}I. The model calculations with the STAPRE and EMPIRE II show some discrepancy in the

high-energy region. The present measurements are in better agreement with the STAPRE. The isomeric cross-section ratios are less sensitive for the model parameters than the excitation functions; therefore they give better indication between the inconsistencies of the experimental data.

[1] M. Uhl and B. Strohmaier, *Computer code for particle induced activation cross-section and related quantities*, Institut für Radiumforschung und Kernphysik, Vienna, Report 76/01 and Addenda to this report.
See also Strohmaier B. and Uhl M., International Energy Agency Report IAEA-SMR-43 (1980) 313

[2] M. Herman, R. Capote Noy, P. Oblozinsk, A. Trkov and V. Zerki, *Recent Development and Validation of the Nuclear Reaction Code EMPIRE*, Int. Conf. Nuclear Data for Science and Technology, Tsukuba 2001

[3] O. Bersillon, *SCAT 2: Un programme de modele optique spherique*, Centre dt'Etudes de Bruyéres-le-Châtel Report, CEA-N-2227 (1981)

[4] W. Dilg, W. Schantl, H. Vonach and M. Uhl, *Level density parameters for the back-shifted Fermi gas model in the mass range 40<A<250*, Nucl. Phys. A217 (1973) 26

[5] D. Wilmore and P.E. Hodgson, *The calculation of neutron cross-sections from optical potentials* Nucl. Phys. 55 (1964) 673

[6] F. Becchetti, W. Greenless, *Polarisation Phenomena in Nuclear Reactions*, H.H. Barschall, W. Haeberli (Eds.) 682

[7] V. Avrigeanu, P.E. Hodgson, M. Avrigeanu, Report OUNP-94-02(1994) and Phys. Rev. C49 (1994) 2136

[8] A.J. Koning, private communication

[9] V.I. Plyaskin and R.A. Kosilov, INDC(CCP)-424, p.27

Validation of neutron reference activation libraries

R. Dóczi[1], S. Sudár[1], A. Fenyvesi[2], S. Szegedi[1], M. Fayez-Hassan[3], S.M. Qaim[4] and J. Csikai[1,2]

[1] *Institute of Experimental Physics, University of Debrecen, H-4010 Debrecen 10, P.O.B. 105, Hungary*
[2] *Institute of Nuclear Research of the Hungarian Academy of Sciences (ATOMKI), H-4001 Debrecen, P.O.B. 51, Hungary*
[3] *Atomic Energy Authority, Nuclear Research Centre, Experimental Nuclear Physics Department, P.O.B. 13759, Cairo, Egypt*
[4] *Institut für Nuclearchemie, Forschungszentrum Jülich GmbH, D-52425 Jülich, Germany*

Abstract:
Some new activation cross-sections were measured and calculated in order to validate the neutron reference activation libraries and to provide data from threshold to 20 MeV for different applications [1, 2]. Special attention was paid to the ^{27}Al$(n,p)^{27}$Mg reaction in order to complete the fluence monitors for short-lived isotopes. Neutron sources and measuring methods used in these investigations are discussed in detail [3, 4].

Investigations of cross-sections around 14 MeV neutron energy

Starting from the fact that the cross-sections for the production of short-lived isotopes are scanty and discrepant new precise data around 14 MeV were determined in a collaboration with the IRMM Geel for the following reactions: ^{19}F$(n,p)^{19}$O, ^{31}P$(n,\alpha)^{28}$Al ^{50}Ti$(n,p)^{50}$Sc ^{54}Cr$(n,p)^{54}$V ^{62}Ni$(n,p)^{62m}$Co and ^{208}Pb$(n,p)^{208}$Tl. Samples were irradiated at the DT neutron generator of the Institute of Experimental Physics, University of Debrecen using 180 keV analyzed D^+-beam. A fast pneumatic rabbit system was used for the transportation of the samples between the irradiation and measuring positions with the selection of different irradiation, cooling and measuring times. Activities of the samples were measured by a HPGe of 100 cm^3 sensitive volume. Evaluation of the gamma spectra was based on the Gamma Acquisition and Analysis program. The ^{27}Al$(n,p)^{27}$Mg reaction has been applied as a fluence monitor placed together with the sample at 45° emission angle which assured an incident neutron energy

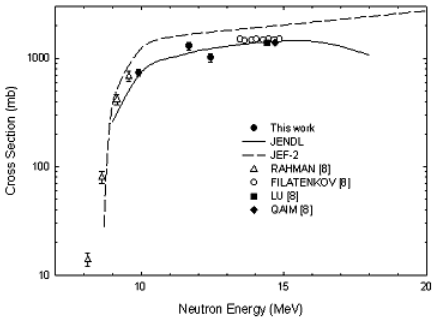

Figure 1: *Excitation function of the* ^{100}*Mo*$(n, 2n)^{99}$*Mo reaction*

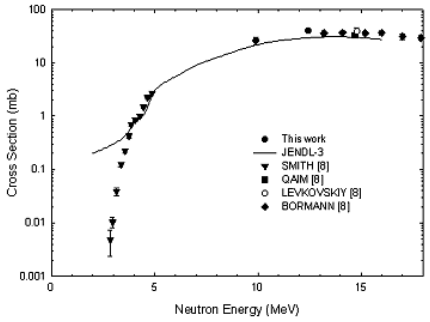

Figure 2: *Excitation function of the* ^{51}*V*$(n, p)^{51}$*Ti reaction*

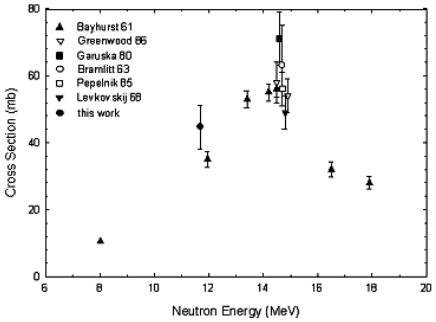

Figure 3: *Excitation function of the* ^{45}*Sc*$(n, \alpha)^{42}$*K reaction*

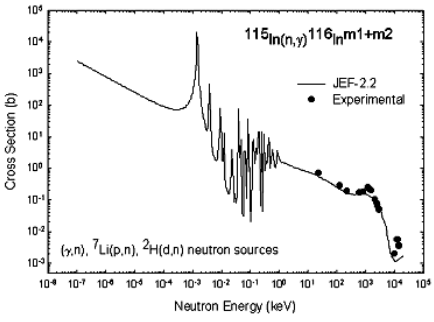

Figure 4: *Excitation function of the* ^{115}*In*$(n, \gamma)^{116m1+m2}$*In reaction*

of 14.60 $\pm$ 0.15 MeV. Results are summarised in Table 1 and compared with the literature data. These data are recommended for the normalisation of the excitation functions. It should be noted that except for the ^{31}P$(n, \alpha)^{28}$Al reaction no evaluated excitation functions are available in the Reference Neutron Activation Library [5] for the other reactions studied in this experiment.

Investigations of cross-section curves in the problem range

For the determination of the cross-sections in the 8-13 MeV problem range neutrons were produced by the variable energy MGC-20 cyclotron of ATOMKI using a D_2 gas target. Details of the properties of such a neutron source have been described elsewhere [3]. High-purity (Goodfellow) natural-metal disk-shaped samples were irradiated for 5 to 6 h. Samples were placed in the 0° direction relative to the deuteron beam of $\sim$1.5 μA intensity. The ^{27}Al$(n, \alpha)^{24}$Na reaction was used as a neutron flux monitor while the variation of the flux in time was

recorded by a BF_3 counter. The absolute activity of samples was determined by a HPGe detector and the peak area analyses was based on the programs Nucleus and the FGM spectrum fitting code. The reactions and the decay data [6] of the measured residual radionuclides are summarised in Tab. 2. On the basis of the results summarised in Tab. 3 and Figs. 1-3 the following conclusions could be drawn:

1. The excitation function of the ^{100}Mo$(n,2n)^{99}$Mo reaction agrees well with the JENDL-3.2 evaluation.
2. In the case of the ^{51}V$(n,p)^{51}$Ti and ^{45}Sc$(n,\alpha)^{42}$K reactions our data agree with recent [7, 7, 8] measurements. New precise data around 14 MeV are required for the normalisation of the excitation functions.
3. The excitation function of the ^{28}Si$(n,p)^{28}$Al reaction was measured in the 7.6-14.7 MeV range [10]. Data points measured in our experiment agree well with those measured by Mannhart and Schmidt [11] with higher accuracy. It should be noted, however, that the ENDF/B-VI and the JENDL-Act96 [5] evaluations overestimate the excitation function with about 15% in the problem range.

Investigations of dosimetry reactions

The improvement of the activation unfolding method used for the determination of flux density spectra requires more precise cross-section curves for the relevant dosimetry reactions. Energy monitors especially for DD and DT neutrons must be completed, too. For this reason the ^{115}In$(n,n'\gamma)^{115m}$In, ^{115}In$(n,\gamma)^{116}$In and the ^{27}Al$(n,p)^{27}$Mg reactions were investigated. The excitation function of the ^{115}In$(n,n'\gamma)^{115m}$In reaction has been determined from threshold to 3 MeV using the ^{7}Li(p,n) and DD reactions as neutron sources. The ^{7}Li(p,n) reaction has been produced by the 5MV Van de Graaff Generator of the ATOMKI, Debrecen. As shown in Table 4 there is only a slight change in the cross-section curve in the 2-3 MeV energy range, therefore, a value of 325 $\pm$ 25 mb obtained at 2.49 MeV can be recommended for D-D plasma neutron dosimetry.

The excitation function of the ^{115}In$(n,\gamma)^{116m1+m2}$In reaction ($T_{1/2}$=2.18 s and 54.3 min) has been measured in the 25 keV and 3 MeV energy range using (γ,n), ^{7}Li(p,n) and ^{2}H$(d,n)^{3}$He reactions as neutron sources. Previous data measured by different (γ,n) sources were re-evaluated using contemporary decay schemes and more precise energy-efficiency curves of the NaI(Tl) and the Ge(Li) detectors. Results summarised in Tab. 4 and shown in Fig. 4 agree well with the JEF-2.2 evaluation. The same (γ,n) sources were used as for the measurements of energy dependence of isomeric cross-section ratios [12].

The excitation function of the ^{27}Al$(n,p)^{27}$Mg reaction in the energy region from 13.0 to 23.0 MeV was evaluated by means of statistical analysis of the experimental data and the values from STAPRE calculations. Group cross-sections, their uncertainties and the correlation matrix are tabulated for the 12.5-20 MeV energy range [13]. The ^{27}Al$(n,p)^{27}$Mg reaction in the 12-15 MeV range can be used as an energy monitor. It should be noted that the measured and the calculated data beyond 16 MeV are discrepant. In order to complete the data in the problem range, cross-sections for 12 energy points were measured in Debrecen and in cooperation with INC (Jülich) in the range from 7.6 to 14.8 MeV. Results suggest a maximum in the excitation functions with a value of about 110 mb around 11 MeV. A possible structure in the excitation function around the maximum is questionable.

Table 1: *Results obtained at 14.60 $\pm$ 0.15 MeV neutron energy*

Reaction	cross-section (mb)	Literature data [2] (mb)
^{19}F$(n,p)^{19}$O	21.5 $\pm$ 1.1	15.30 (14.6 MeV)
		21.00 (14.9 MeV)
		17.70 (14.6 MeV)
		22.2 (14.7 MeV)
		21.00 (14.7 MeV)
		16.4 (14.7 MeV)
		23.3 (14.8 MeV)
		51.00 (14.8 MeV)
		109 (14.7 MeV)
		14.3 (14.7 MeV)
		135 (14.5 MeV)
^{31}P$(n,\alpha)^{28}$Al	135.8 $\pm$ 7.0	104 (14.9 MeV)
		110 (14.9 MeV)
		132 (14.7 MeV)
		104 (14.6 MeV)
		102 (14.6 MeV)
		96.8 (14.7 MeV)
		142 (14.5 MeV)
		124 (14.7 MeV)
		129 (14.8 MeV)
		153 (14.7 MeV)
		146 (14.5 MeV)

Table 1: *Results obtained at 14.60 ± 0.15 MeV neutron energy*

Reaction	cross-section (mb)	Literature data [2] (mb)
^{50}Ti$(n,p)^{50}$Sc	13.28 ± 0.82	17.00 (14.8 MeV)
		14.1 (14.7 MeV)
		20.00 (14.8 MeV)
		15.4 (14.8 MeV)
		14.3 (14.4 MeV)
		9.900 (14.6 MeV)
		25.00 (14.8 MeV)
		27.00 (14.7 MeV)
		9.00 (14.7 MeV)
		28 (14.7 MeV)
		17.00 (14.5 MeV)
		27 (14.8 MeV)
^{54}Cr$(n,p)^{54}$V	18.0 ± 3.3	14.00 (14.8 MeV)
		15.3 (14.6 MeV)
		16.4 (14.7 MeV)
		15.0 (14.8 MeV)
		18.0 (14.7 MeV)
		13.5 (14.8 MeV)
^{62}Ni$(n,p)^{62m}$Co	21.92 ± 2.5	14.60 (14.70 MeV)
		11.70 (14.8 MeV)
		21.00 (14.7 MeV)
		106 (14.7 MeV)
		22.00 (14.1 MeV)
^{208}Pb$(n,p)^{208}$Tl	0.9 ± 0.15	0.500 (14.2 MeV)
		0.500 (14.5 MeV)
		1.2 (14.6 MeV)
		0.4 (14.4 MeV)
		0.96 (14.5 MeV)

Table 2: *Reactions and decay data for the investigations of the problem range*

Reaction	$T_{1/2}$	E_γ(keV)	I_γ(%)
^{51}V$(n,p)^{51}$Ti	5.76 min	320.084	93
^{100}Mo$(n,2n)^{99}$Mo	2.7277 d	140.474	90.7
		739.508	12.14
^{45}Sc$(n,\alpha)^{42}$K	12.3 h	1524.58	18.8
^{28}Si$(n,p)^{28}$Al	2.2406 min	1778.988	100
^{27}Al$(n,p)^{27}$Mg	9.462 min	843.757	73
^{27}Al$(n,\alpha)^{24}$Na	15.02 h	1368.598	100

Table 3: *Measured cross-sections in the problem range*

Reaction	En (MeV)	cross-section (mb)
^{100}Mo$(n,2n)^{99}$Mo	9.92 ± 0.20	735 ± 53
	11.68 ± 0.20	1010 ± 93
	12.44 ± 0.22	1293 ± 112
^{51}V$(n,p)^{51}$Ti	9.92 ± 0.20	25.7 ± 4.4
^{45}Sc$(n,\alpha)^{42}$K	11.68 ± 0.20	44.7 ± 5.6
^{28}Si$(n,p)^{28}$Al	7.6±0.2	202±28
	9.3±0.2	213±30
	10.3±0.2	244±31
	11.2±0.2	260±33
	12.5±0.2	253±35
	14.7±0.2	239±30

Table 4: *Cross-sections measured for the* ^{115}*In*$(n, n'\gamma)^{115m}$*In and* ^{115}*In*$(n, \gamma)^{116}$*In reactions.*

E_n (MeV)	^{115}In$(n, n'\gamma)^{115m}$In	^{115}In$(n, \gamma)^{116}$In
	σ (mb)	σ (mb)
0.024		710
0.13		275
0.22		190
0.62		165
0.83		175
1.2		250
1.3		242.2
1.4		215.6
1.5		200.9
2.14	299.0	99.9
2.24	312.0	85.5
2.35	321.7	78.8
2.49	325.0	68.6
2.52	328.2	63.3
2.72	344.5	54.4
2.85	328.2	49.2
2.96	354.2	44.5
10.2	211.0	2.0
12.4	174.0	5.6

Acknowledgements

The authors are grateful to E. Nagy, J. Szegedi for their technical assistance. Thanks are due to the crew of the MGC-20 cyclotron (ATOMKI). This work was supported in part by the Hungarian Research Fund Hungarian Research Fund (OTKA D35480, T037190) and the János Bolyai scholarship.

[1] CINDA 2000, The Index to Literature and Computer Files on Microscopic Neutron data (IAEA, Vienna, 2000)

[2] V. McLane , C.L. Dunford, and P.F. Rose, Neutron cross-sections Academic, New York, (1988), Vol. 2

[3] Á. Grallert, J. Csikai, and S.M. Qaim, Nucl. Instrum. Methods A, 337, 615 (1994)

[4] IAEA-TECDOC-913, (IAEA, Vienna) November 1996

[5] IAEA-TECDOC-1285, (IAEA, Vienna) 2002

[6] E. Browne and R.B. Firestone, Table of Radioactive Isotopes, V. S. Shirley, Ed. John Wiley and Sons, New York (1987)

[7] W. Mannhart, D. Schmidt, D.L. Smith, Proc. Int. Conf. Nuclear Data for Science and Technology, Trieste, Italy, May 19-24,1997, p. 505, G. Reffo, A. Ventura, C. Grandi, Eds., Bologna, Italy, 1997

[8] M. Bostan, and S.M. Qaim, Phys. Rev. C, 49, 266, 1994.

[9] A. Fessler, *et al*., Nucl. Sci. Eng., 134, 171, 2000.

[10] J. Csikai, IAEA Final Report, 1998. Contract No. 7687-RO

[11] W. Mannhart and D. Schmidt, J. Nucl. Sci. and Technology, Vol 1, Supplement 2, August 2002, pp. 218-221

[12] J. Bacsó, J. Csikai, B. Kardos, D. Kiss, Nucl. Phys. 67. (1965) 443-448.

[13] K.I. Zolotarev, A.B. Pashchenko, J. Csikai, IAEA Final Report, 1998. Contract No. 7687-RO; K.I. Zolotarev, INDC(NDS)-448, IAEA Vienna (2003), p. 25

Microscopic nuclear models for practical applications

S. Goriely

Institut d'Astronomie et d'Astrophysique, Université Libre de Bruxelles, Bvd. du Triomphe, Campus de la Plaine, CP 226, 1050-Brussels, Belgium

Abstract:
Although important effort has been devoted in the last decades to measure reaction cross-sections, in many different nuclear applications only theoretical predictions can fill the gaps. This holds true also for the various nuclear ingredients to the reaction models. Most of the nuclear ingredients in cross-section calculations need to be extrapolated in an energy and mass domain out of reach of laboratory measurements, where parameterised systematics based on experimental data can fail drastically. It is now feasible to extract data from microscopic or semi-microscopic global predictions based on sound and reliable nuclear models which, in turn, can compete with more phenomenological highly-parameterised models in the reproduction of experimental data.
Many global microscopic approaches have been developed for the last decades and are now more or less well understood. However, they are almost never used for practical applications, because of their lack of accuracy in reproducing experimental data, especially when considered globally on a large data set. This low accuracy mainly originates from computational complications making the determination of free parameters by fits to experimental data time-consuming. This reliability vs. accuracy character of nuclear theories are detailed for most of the relevant quantities needed to estimate reaction cross-sections, namely nuclear masses, nuclear level densities, optical potentials and γ-ray strengths. Phenomenological, as well as microscopic models are available for each of these ingredients. Nowadays, microscopic models can be tuned at the same level of accuracy as the phenomenological models, re-normalised on experimental data, and therefore could replace the phenomenological inputs little by little in practical applications. The latest developments as well as the needs for further theoretical investigations in each of these subfields are stressed.

Introduction

Strong, weak and electromagnetic interaction processes play an essential role in many different applications of nuclear physics, such as accelerator driven waste incineration, production of radioisotopes for therapy and diagnostics, charged-particle beam therapy, material analysis as well as nuclear astrophysics. Although important effort has been devoted in the last decades to measure reaction cross-sections, experimental data only cover a minute fraction of the whole set of data required for such nuclear physics applications. Required reactions often concern unstable or even exotic (neutron-rich, neutron-deficient, superheavy) species for which no experimental data exist. Given applications (e.g nuclear astrophysics, accelerator-driven systems) involve a large number (thousands) of unstable nuclei for which many different properties have to be determined (including ground and excited state properties, strong, weak and electromagnetic interaction properties). Finally, the energy range for which experimental data is available is restricted to the small range reachable by present experimental setups. To fill the gaps, only theoretical predictions can be used.

For specific applications such as nuclear astrophysics or accelerator-driven systems, a large number of data need to be extrapolated far away from the experimentally known region. In this case, two major features of the nuclear theory must be contemplated, namely its *reliability* and *accuracy*. A microscopic description by a physically sound model based on first principles ensures a reliable extrapolation away from the experimentally known region. For these reasons, when the nuclear ingredients to the reaction models (e.g. Hauser-Feshbach) cannot be determined from experimental data, use is made preferentially of microscopic or semi-microscopic global predictions based on sound and reliable nuclear models which, in turn, can compete with more phenomenological highly-parameterised models in the reproduction of experimental data. The selection criterion of the adopted model is fundamental, since most of the nuclear ingredients in rate calculations need to be extrapolated in an energy and mass domain out of reach of laboratory measurements, where parameterised systematics based on experimental data can fail drastically. Global microscopic approaches have been developed for the last decades and are now more or less well understood. However, they are almost never used for practical applications, because of their lack of accuracy in reproducing experimental data, especially when considered globally on a large data set. Different classes of nuclear models can be contemplated according to their reliability, starting from local macroscopic approaches up to global microscopic approaches. We find in between these two extremes, approaches like the classical (e.g liquid drop, droplet), semi-classical (e.g Thomas-Fermi), macroscopic-microscopic (e.g classical with microscopic corrections),

semi-microscopic (e.g microscopic with phenomenological corrections) and fully microscopic (e.g mean field, shell model, QRPA) approaches. In a very schematic way, the higher the degree of reliability, the less accurate the model used to reproduce the bulk set of experimental data. The classical or phenomenological approaches are highly parameterised and therefore often successful in reproducing experimental data, or at least much more accurate than microscopic calculations. The low accuracy obtained with microscopic models mainly originates from computational complications making the determination of free parameters by fits to experimental data time-consuming. This reliability vs accuracy character of nuclear theories are detailed below for most of the relevant quantities needed to estimate reaction rates, namely nuclear masses, nuclear level densities, optical potentials, and γ-ray strength functions. Nowadays, microscopic models can be tuned at the same level of accuracy as the phenomenological models, and therefore could replace the phenomenological inputs little by little in practical applications. The needs for further theoretical investigations in each of these fields are also stressed in the following sections.

Global microscopic models for reaction cross-section calculations

Reaction models

As far as reactions on heavier nuclei are concerned, most of the low-energy cross-section calculations for practical applications are based on the statistical model of Hauser-Feshbach [1, 2]. Such a model makes the fundamental assumption that the capture process takes place with the intermediary formation of a compound nucleus in thermodynamic equilibrium. The energy of the incident particle is then shared more or less uniformly by all the nucleons before releasing the energy by particle emission or γ-de-excitation. The formation of a compound nucleus is usually justified by assuming that the level density in the compound nucleus at the projectile incident energy is large enough to ensure an average statistical continuum superposition of available resonances. The statistical model has proven its ability to predict cross-sections accurately. However, this model suffers from uncertainties stemming essentially from the predicted nuclear ingredients describing the nuclear structure properties of the ground and excited states, and the strong and electromagnetic interaction properties. Clearly, the knowledge of the ground state properties (masses, deformations, matter densities) of the target and residual nuclei is indispensable. When not available experimentally, this information has to be obtained from nuclear mass models. The excited state properties have also to be known. Experimental data may be scarce above some excitation energy, and especially so for nuclei located far from the valley

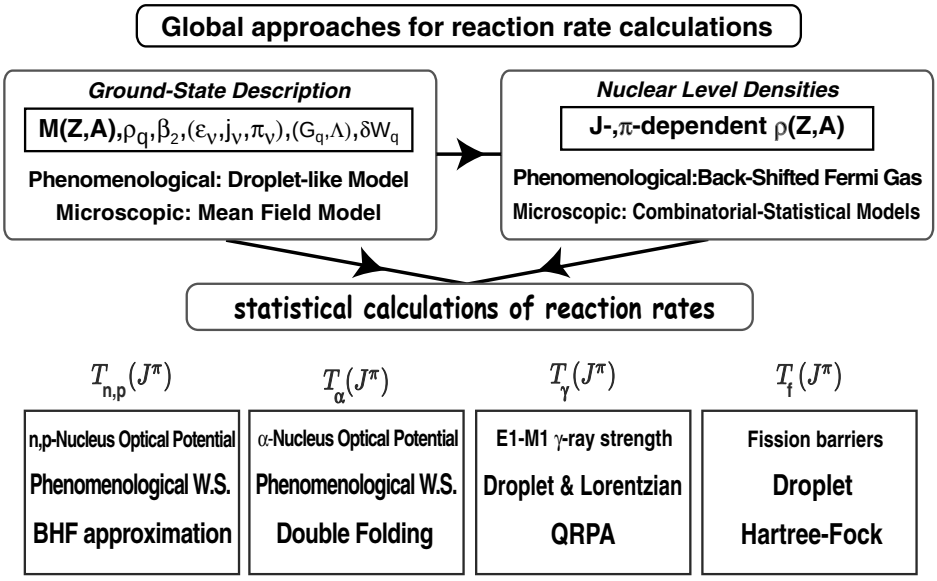

Figure 1: *Global phenomenological and microscopic theories used to estimate the ground- and excited state properties, as well as transmission coefficients T of relevance in the Hauser-Feshbach model. Details are given in the text.*

of nuclear stability. This is why frequent resort to a level density prescription is mandatory. In the Hauser-Feshbach formalism, the probability for particle emission are calculated by solving the Schrödinger equation with the appropriate optical potential for the particle-nucleus interaction. Finally, the electromagnetic de-excitation of the compound nucleus is calculated assuming the dominance of dipole E1 transitions (the M1 transitions are usually included as well, but do not contribute significantly. They will not be discussed further here). As schematised in Fig. 1, phenomenological, as well as microscopic models are available for each of these ingredients. Nowadays, microscopic models can be tuned at the same level of accuracy as the phenomenological models, re-normalised on experimental data if needed, The nuclear models available today to estimate all these nuclear ingredients are described below.

Prediction of ground state properties

Among the ground state properties, the atomic mass $M(Z, A)$ is obviously the most fundamental quantity. Although masses for more than about 2000 nuclei are known experimentally [3, 4], important nuclear applications, like the accelerator-driven systems or nuclear astrophysics, involve exotic neutron-rich and neutron-deficient nuclei for which no experimental data exist. The calculation of the reaction cross-section also requires the knowledge of other ground state properties, such as the deformation, density distribution, single-particle level scheme, pairing force, shell correction energies, ... for which nuclear structure theory must provide predictions.

Attempts to develop formulas estimating the nuclear masses of nuclei go back to the 1935 "semi-empirical mass formula" of von Weizsäcker [5]. Being inspired by the liquid-drop model of the nucleus, this is the macroscopic mass formula *par excellence*. Improvements have been brought little by little to the original mass formula, leading to the development of macroscopic-microscopic mass formulas [6], where microscopic corrections to the liquid drop part are introduced in a phenomenological way. In this framework, the macroscopic and microscopic features are treated independently, both parts being connected exclusively by a parameter fit to experimental masses. Later developments included in the macroscopic part properties of infinite and semi-infinite nuclear matter and the finite range character of nuclear forces. Until recently the atomic masses were calculated on the basis of one form or another of the liquid-drop model, the most sophisticated version of which is the “finite-range droplet model" (FRDM) [7]. Despite the great empirical success of this formula (it fits the 1888 $Z \geq 8$ masses with an rms error of 0.689 MeV), it suffers from major shortcomings, such as the incoherent link between the macroscopic part and the microscopic

correction, the instability of the mass prediction to different parameter sets, or the instability of the shell correction. There is an obvious need to develop a mass formula that is more closely connected to the basic nuclear interactions. Two such approaches can reasonably be contemplated at the present time, one being the non-relativistic Hartree-Fock (HF) method, and the other the relativistic Hartree method, also known as the relativistic mean-field (RMF) method. Progress in the HF and RMF mass models has been slow, presumably because of the computer-time limitations that arose in the past with deformed nuclei. Nuclear forces are traditionally determined by fitting to the masses (and some other properties) of less than ten or so nuclei. The resulting forces give rise to rms deviations from the 1888 experimental masses [3] well in excess of 2 MeV. This is far from reaching the level of precision found by droplet-like models (around 0.7 MeV).

The result is that the most microscopically founded mass formulas of practical use were till recently those based on the so-called ETFSI (extended Thomas-Fermi plus Strutinsky integral) method [8]. The ETFSI method is a high-speed approximation to the HF method based on Skyrme forces, with pairing correlations generated by a δ-function force that is treated in the usual BCS approach. In the latest version of the ETFSI mass model (ETFSI2), eleven parameters are found to reproduce the 1719 experimental masses of the $A \geq 36$ nuclei with an rms deviation of 0.709 MeV [9] comparable with the one obtained with the droplet-like formula. The ETFSI model remains an approach of the macroscopic-microscopic type, although it provides a high degree of coherence between the macroscopic and microscopic terms through the unifying Skyrme force underlying both parts. A logical step towards improvements obviously consists in considering now the HF method as such. It was demonstrated very recently [10, 11] that HF calculations in which a Skyrme force is fitted to essentially all the mass data are not only feasible, but can also compete with the most accurate droplet-like formulas available nowadays. Such HF calculations are based on the conventional Skyrme force of the form

$$\begin{aligned} v_{ij} &= t_0(1+x_0P_\sigma)\delta(\mathbf{r}_{ij}) + t_1(1+x_1P_\sigma)\frac{1}{2\hbar^2}\{p_{ij}^2\delta(\mathbf{r}_{ij}) + h.c.\} \\ &\quad + t_2(1+x_2P_\sigma)\frac{1}{\hbar^2}\mathbf{p}_{ij}.\delta(\mathbf{r}_{ij})\mathbf{p}_{ij} + \frac{1}{6}t_3(1+x_3P_\sigma)\rho^\gamma\delta(\mathbf{r}_{ij}) \\ &\quad + \frac{i}{\hbar^2}W_0(\boldsymbol{\sigma_i}+\boldsymbol{\sigma_j}).\mathbf{p}_{ij}\times\delta(\mathbf{r}_{ij})\mathbf{p}_{ij} \quad , \end{aligned} \tag{1}$$

and a δ-function pairing force acting between like nucleons,

$$v_{pair}(\boldsymbol{r}_{ij}) = V_{\pi q}\,\delta(\boldsymbol{r}_{ij}) \quad , \tag{2}$$

in which the density independent zero range pairing force is characterised by a strength parameter $V_{\pi q}$ allowed to be different for neutrons and protons, and also to

be slightly stronger for an odd number of nucleons ($V^{-}_{\pi q}$) than for an even number ($V^{+}_{\pi q}$), i.e., the pairing force between neutrons, for example, depends on whether N is even or odd. Both mass formulas add to the energy corresponding to the above force the Coulomb energy and a phenomenological Wigner term of the form

$$E_W = V_W \exp\left\{ -\lambda \left(\frac{N-Z}{A} \right)^2 \right\} + V'_W |N-Z| \exp\left\{ -\left(\frac{A}{A_0} \right)^2 \right\} . \quad (3)$$

The first competing HFBCS mass table (in which the pairing interaction is treated in the BCS approximation) was obtained with the MSk7 Skyrme and pairing parameters which were determined by fitting to the full data set of 1719 $A \geq 36$ masses [3] with a final rms error of 0.702 MeV.

In the case of the highly neutron-rich nuclei, the validity of the BCS approach to pairing is questionable. The BCS procedure neglects the fact that the scattering of nucleon pairs between different single-particle states under the influence of the pairing interaction will actually modify the single-particle states, a difficulty that becomes particularly serious close to the neutron-drip line, where nucleon pairs will be scattered into the continuum. For such nuclei, this problem is avoided in the HF-Bogoliubov (HFB) method, which puts the pairing correlations into the variational function, so that the single-particle and pairing aspects are treated simultaneously and on the same footing. Lately [12, 13], a new Skyrme force has been derived on the basis of HF calculations with pairing correlations taken into account in the Bogoliubov approach, using a δ-function pairing force. The rms error with respect to the masses of all the 2135 measured nuclei of the 2001 Audi & Wapstra compilation [4] with $Z, N \geq 8$ is 0.674 MeV (see Fig. 2). The quality of the new predictions is similar to the one obtained with HFBCS. The complete mass table, HFB-2, has been constructed, giving all nuclei lying between the two drip lines over the range $Z, N \geq 8$ and $Z \leq 120$. A comparison between HFB and HFBCS masses shows that the HFBCS model is a very good approximation to the HFB theory, in particular for masses. The extrapolated masses never differing by more than 2 MeV below $Z \leq 110$. The reliability of the predictions far away from the experimentally known region, and in particular towards the neutron drip line, is however increased thanks to the improved treatment of the pairing correlations. Figure 3 provides a comparison between the HFB and FRDM predictions. It demonstrates vividly that two mass models which reproduce measured masses with comparable rms deviations can diverge more or less markedly in their predictions for nuclei far from stability. It should also be noted that, even if the HFB and FRDM mass parabolas present more or less the same slope, they sometimes differ noticeably in their predicted deformations or shell structures.

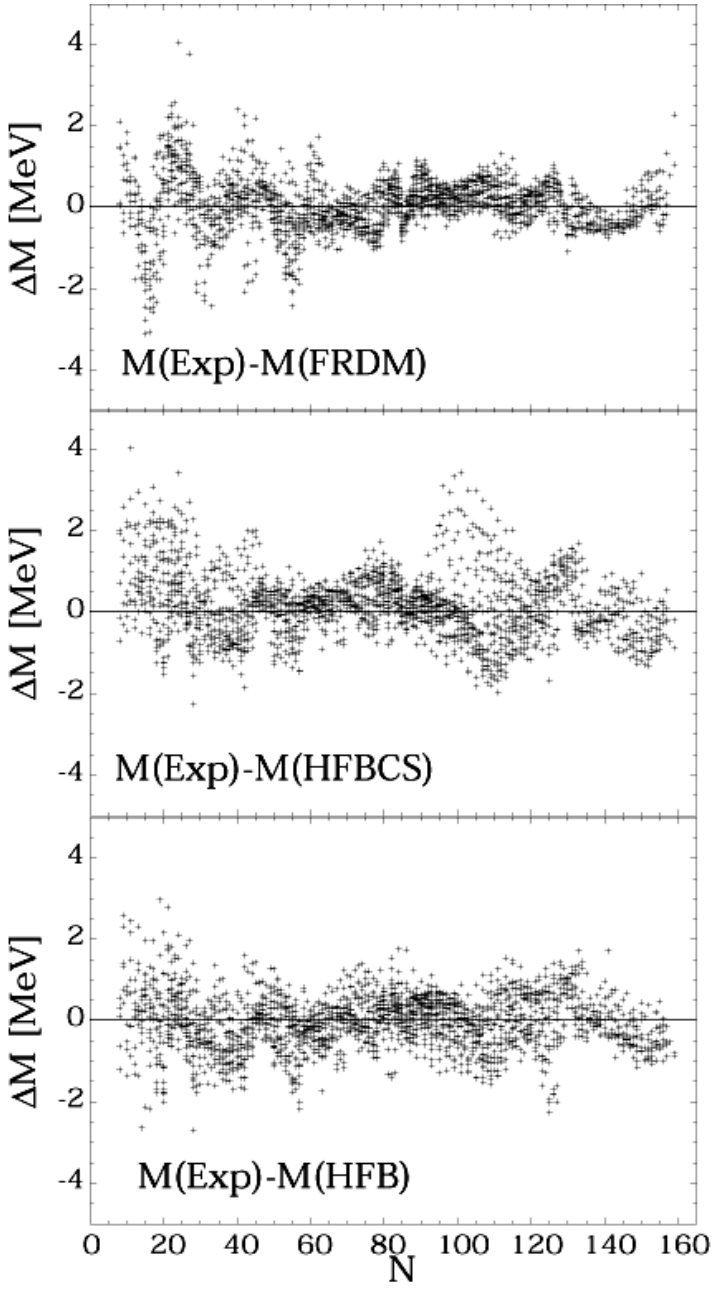

Figure 2: *Comparison between measured masses [4] and the predictions of three mass models: FRDM [7] (upper panel), HFBCS [11] (middle), and HFB [13] (lower).*

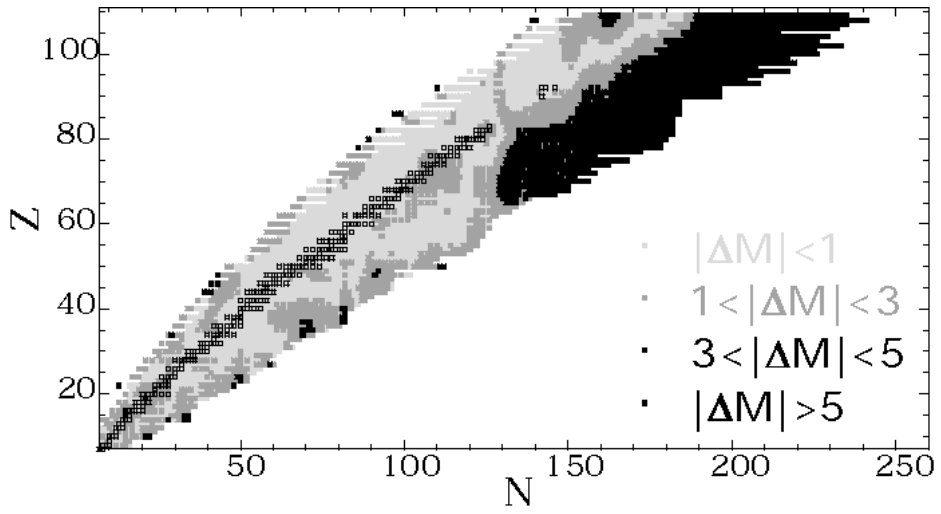

Figure 3: *Mapping of the chart of the nuclides in the ranges* N *and* $Z \geq 8$ *and* $Z \leq 110$ *with the differences* $\Delta M = M_{\rm HFB} - M_{\rm FRDM}$ *between the HFB and FRDM theoretical predictions. The differences are coded as indicated in the figure.*

Although complete mass tables have now been derived within the HFB approach, further developments that could have an impact on mass extrapolations towards the neutron drip line are still needed. The most likely changes will be those associated with making the pairing force density-dependent within the Lipkin Nogami prescription. More fundamentally, mean field models need to be improved, so that all possible observables (such as giant dipole, Gamow-Teller excitations, nuclear matter properties) can be estimated coherently on the basis of one unique effective force. For example, empirical values of the nucleonic effective mass or the Landau-Migdal parameters can be in contradiction with the values deduced from the existing forces. In particular, adding a t_4 term to the Skyrme force (with a density and momentum dependent term) is likely to reconcile the large nucleonic mass required to fit masses with nuclear matter calculations [14]. These various nuclear aspects are extremely complicate to reconcile within one unique framework and this quest towards universality will most certainly be the focus of fundamental nuclear physics research for the coming decade.

Concomitantly, future shell model calculations (e.g in the quantum Monte-Carlo approach) will certainly provide further fundamental insight on the nuclear properties of exotic nuclei. In particular, shell model calculations have shown that the spin-iso-spin dependent part of the nucleon–nucleon interaction in nuclei

could lead to a change of the magic numbers $N = 8, 20$ in the exotic neutron-rich region [15]. These effects are probably underestimated in Skyrme Hartree-Fock calculations because the interaction is truncated to be of the δ-function type. Future global shell-model calculations will certainly reveal interesting properties of heavier exotic neutron-rich nuclei.

Nuclear level densities

As for the determination of the nuclear ground state properties, until recently, only classical approaches were used to estimate nuclear level densities (NLD) for practical applications. Although reliable microscopic models (in the statistical and combinatorial approaches) have been developed for the last four decades, the back-shifted Fermi gas model (BSFG) approximation–or some variant of it– remains the most popular approach to estimate the spin-dependent NLD, particularly in view of its ability to provide a simple analytical formula(e.g [16, 17]). Although numerous parameterisations of the BSFG formula are available today, only few propose a global formula applicable to the whole nuclear chart. One such efficient parameterisation is given here as an example (see [18] for more details). It corresponds to the classical BSFG approximation of the state density $\rho(U)$ and level density $\rho(U, J)$ of a nucleus (Z, A) with a given angular momentum J and excitation energy U, i.e

$$\rho(U) = \frac{\sqrt{\pi}}{12a^{1/4}(U-\delta)^{5/4}} \mathrm{e}^{2\sqrt{a(U-\delta)}} \tag{4}$$

$$\rho(U, J) = \frac{2J+1}{2\sqrt{2\pi}\sigma^3}\, \rho(U)\, \mathrm{e}^{-(J+1/2)^2/2\sigma^2} \tag{5}$$

where microscopic (shell, pairing and deformation) corrections to the binding energy are introduced in the U-dependent NLD parameter a by the approximation [17]

$$a(U) = \tilde{a}[1 + 2\,\gamma\, E_{mic}\, \mathrm{e}^{-\gamma(U-\delta)}] \quad . \tag{6}$$

The microscopic energy $E_{mic} = E_{tot}(Z, A) - E_{LD}$ is derived from the experimental (or theoretical) binding energy $E_{tot}(Z, A)$ and the simple spherical liquid drop formula

$$E_{LD} = a_v A + a_s A^{\frac{2}{3}} + (a_{sym} + a_{ss} A^{-\frac{1}{3}}) A I^2 + a_c \frac{Z^2}{A^{\frac{1}{3}}} \tag{7}$$

where $I = (N - Z)/A$. A fit to the 1888 $N, Z \geq 8$ experimental masses [3] (with a final rms deviation of only 3 MeV) leads to the liquid drop parameters (in

MeV) $a_v = -15.6428$, $a_s = 17.5418$, $a_{sym} = 27.9418$, $a_{ss} = -25.3440$ and $a_c = 0.70$. Concerning the NLD parameters, a fit to the experimental s-neutron resonance spacings [16] gives $\tilde{a} = 0.101A + 0.036A^{2/3}$ [MeV^{-1}], $\gamma = 0.03$, $\sigma^2 = 0.0194A^{5/3}\sqrt{U/a}$ and $\delta = 0.5$, 0, -0.5 MeV for even-even, odd-mass and odd-odd nuclei, respectively. As shown in Fig. 4, this global parameterisation predicts experimental resonance spacings with a high degree of accuracy [18].

However, it is often forgotten that the BSFG model essentially introduces phenomenological improvements to the original analytical formulation of Bethe, and consequently none of the important shell, pairing and deformation effects are properly accounted for in such a description. Drastic approximations are usually made in deriving analytical formulae and often their shortcomings in matching experimental data are overcome by empirical parameter adjustments. It is well accepted that the shell correction to the NLD cannot be introduced by neither an energy shift, nor a simple energy-dependent level density parameter, and that the complex BCS pairing effect cannot be reduced to an odd-even energy back-shift (e.g [17]). This shortcoming is cured to some extent by adjustments of a more or less large number of free parameters. Such a procedure introduces, however, a substantial unreliability if predictions have to be made when experimental data are scarce or non-existent, as it is very often the case in certain, sometimes extended, ranges of excitation energies, or for nuclei far from stability of importance for the modelling of the p-process and for a large variety of other applications. The lack of measured level densities still constitutes the main problem faced by the NLD models and the parameter fitting procedures they require, even if the number of analyses of slow neutron resonances and of cumulative numbers of low energy levels grows steadily. This concerns in particular the s-wave neutron resonance spacings D at the neutron separation energy S_n. For a nucleus $(Z, A+1)$ resulting from the capture of a low-energy neutron by a target (Z, A) with spin J_0, D is given by

$$\begin{aligned} D &= \frac{2}{\rho(S_n, J_0 + 1/2) + \rho(S_n, J_0 - 1/2)} && \text{for } J_0 > 0 \\ &= \frac{2}{\rho(S_n, 1/2)} && \text{for } J_0 = 0, \end{aligned} \qquad (8)$$

the factor of 2 in the numerator relating to the classical assumption of equal probabilities of both parities π at all energies.

Several approximations used to obtain the NLD expressions in an analytical form can be avoided by quantitatively taking into account the discrete structure of the single-particle spectra associated with realistic average potentials [19]. In this

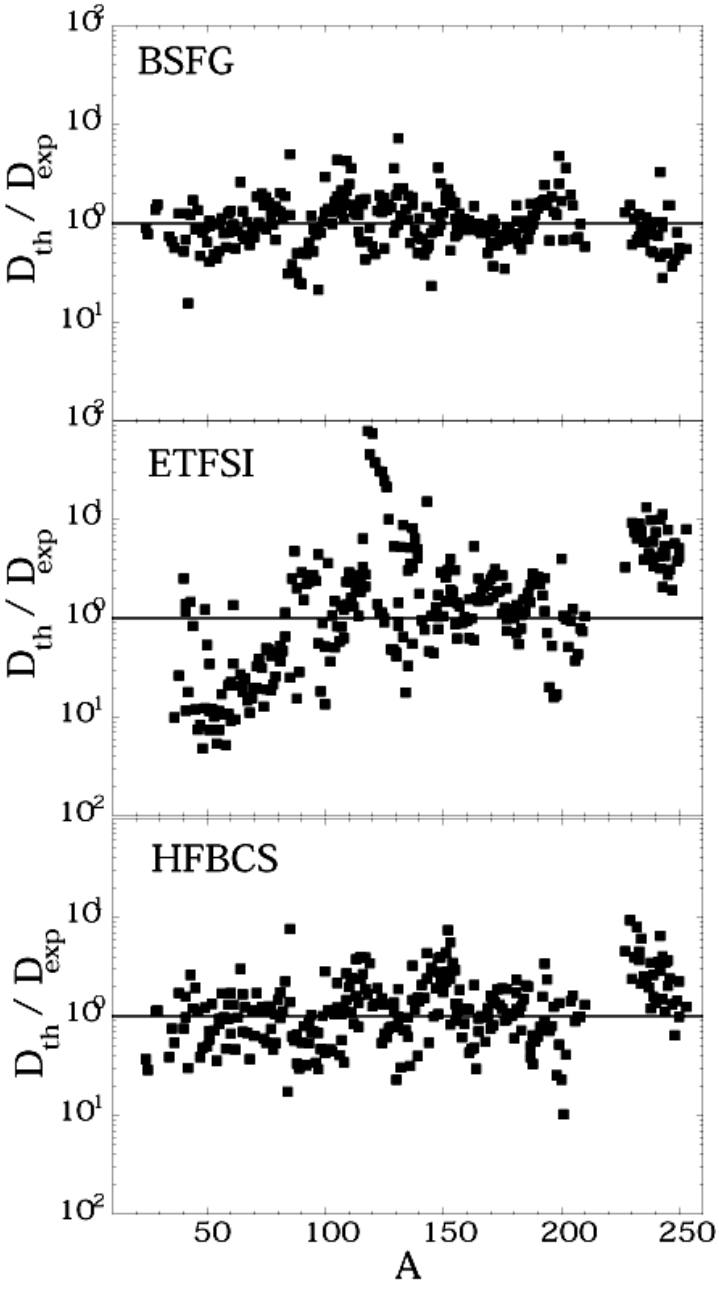

Figure 4: *Comparison between experimental s-wave neutron resonance spacings $D_{\rm exp}$ at the neutron separation energy S_n and predicted values $D_{\rm th}$ derived from the use of the ETFSI [17] (middle panel) or of a HFBCS [21] (lower panel) model. The results from the global BSFG approximation of [18] are also shown (upper panel).*

approach, the intrinsic J-independent level density is expressed as

$$\omega(U) = \frac{\mathrm{e}^{S(U)}}{(2\pi)^{3/2}\sqrt{D(U)}} \tag{9}$$

and the T-dependent entropy S and excitation energy U are derived from the summation on the doubly degenerate single-particle levels ε_q^k (with blocking effect for odd nucleon systems)

$$S(T) = 2\sum_{q=n,p}\sum_{k}\ \ln\Big[1+\exp(-E_q^k/T)\Big] + \frac{E_q^k/T}{1+\exp(-E_q^k/T)} \tag{10}$$

$$U(T) = E(T) - E(T=0) \tag{11}$$

where the total energy is given by

$$E(T) = \sum_{q=n,p}\sum_{k}\ \varepsilon_q^k\ \Big[1 - \frac{\varepsilon_q^k - \lambda_q}{E_q^k}\tanh(\frac{E_q^k}{2T})\Big] - \frac{\Delta_q^2}{G} \tag{12}$$

and $E_q^k = \sqrt{(\varepsilon_q^k - \lambda_q)^2 + \Delta_q^2}$ is the quasi-particle energy.
The lengthy expression for the determinant $D(T)$ can be found in [20].

The usual T-dependent BCS equations determine the gap parameter Δ_q and the chemical potential λ_q as a function of the constant pairing strength G_q

$$N_q = \sum_k \Big[1 - \frac{\varepsilon_q^k - \lambda_q}{E_q^k}\tanh(\frac{E_q^k}{2T})\Big] \tag{13}$$

$$\frac{2}{G_q} = \sum_k\ \frac{1}{E_q^k}\tanh(\frac{E_q^k}{2T}) \tag{14}$$

The J-dependence is obtained in the usual Gaussian approximation (Eq. 5) with the spin cut-off parameter for axially-deformed nuclei derived from the summation on the projection on the symmetry axis of the single-particle angular momentum ω_q^k

$$\sigma^2(T) = \frac{1}{2}\sum_{q=n,p}\sum_{k}\ {\omega_q^k}^2\ \mathrm{sech}^2(\frac{E_q^k}{2T}) \tag{15}$$

This approach has the advantage of treating in a natural way shell, pairing and deformation effects on all the thermodynamic quantities. The computation of the NLD by this technique corresponds to the exact result that the analytical

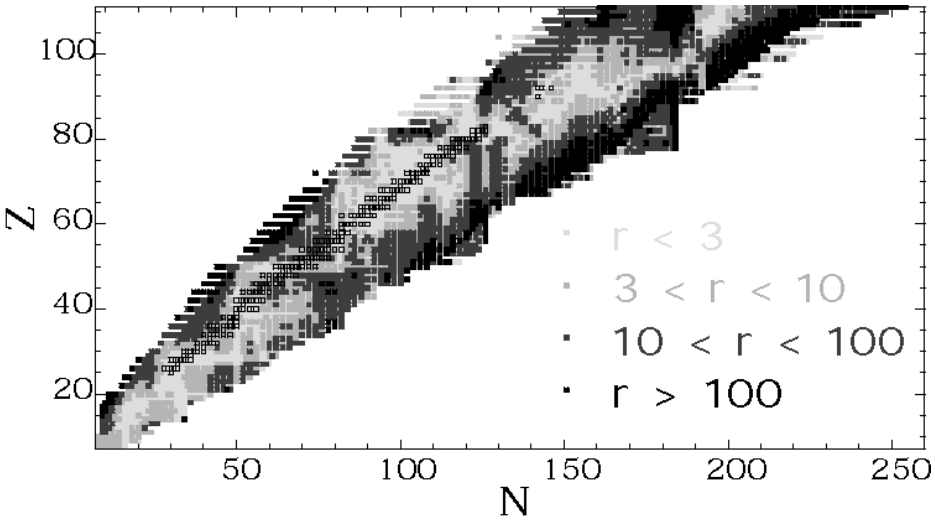

Figure 5: *Comparison between the state densities $\omega(U)$ (see Eq. 9) at the neutron separation energy $U = S_n$ calculated by the HFBCS and BSFG models already selected in Fig. 4. The values of r displayed for all nuclides in the ranges N and $Z \geq 8$ and $Z \leq 110$ located between the proton and neutron drip lines are defined as $r = 10^{|\log(\omega_{\rm HFBCS}/\omega_{\rm BSFG})|}$. Its values are coded as indicated in the figure.*

approximation tries to reproduce, and remains by far the fastest and most reliable method for estimating NLD (despite some inherent problems related to the choice of the single-particle configuration and pairing strength). A NLD formula based on the ETFSI ground state properties (single-particle level scheme and pairing strength) has been proposed in [17]. Though it represents the first global microscopic formula which could decently reproduce the experimental neutron resonance spacings, some large deviations, for example in the Sn region, are found (see Fig. 4). These deficiencies are cured in the new HFBCS-based model [21] which predicts all the experimental s-wave resonance spacings with an accuracy of typically a factor of about 2, which is comparable to the one obtained by the phenomenological BSFG formula (Fig. 4). The microscopic NLD formula also gives reliable extrapolation at low energies where experimental data on the cumulative number of levels is available. Furthermore, the microscopic model is re-normalised on experimental (neutron resonance spacings and low-lying levels) data to account for the available experimental information. The HF-BCS-based model can now be used in practical applications with a high degree of reliability. NLD's are provided in a tabular form in order to avoid the loss of precision with analytical fits.

In spite of the good aforementioned agreement between the BSFG and HFBCS-based level density predictions when experimental data are available, Fig. 5 shows that large differences may exist between them for nuclei located far from the line of nuclear stability. Important effort still has to be made to improve the microscopic description of collective (rotational and vibrational) effects, and the disappearance of these effects at increasing energies. Coherence in the pairing treatment of the ground- and excited-state properties also needs to be worked out more deeply. Global combinatorial calculations (e.g [22]) will also increase the reliability of the NLD predictions for exotic nuclei. Experimental information, as provided by the primary γ-ray spectra (e.g [23]) will strongly help in the near future to orientate microscopic models.

Optical potential

Due to the long-standing effort devoted to the microscopic description of nuclear matter, the phenomenological potentials of Woods-Saxon type have long been replaced by the nucleon-nucleus optical potential [24, 25] derived from a Reid's hard core nucleon–nucleon interaction by applying the Brückner–Hartree–Fock approximation. This so-called JLM potential has recently been updated by Bauge *et al.* [26] who empirically re-normalised the energy dependence of the potential depth to reproduce scattering and reaction observables for spherical and quasi-spherical nuclei between ^{40}Ca and ^{209}Bi in a large energy range from the keV

region up to 200 MeV. The resulting real (V) and imaginary (W) components of the JLMB nucleon (upper sign for neutrons and lower for protons) potential

$$V(E) = \lambda_V(E) \left[V_0(E) \pm \lambda_{V1} \frac{\rho_n - \rho_p}{\rho_n + \rho_p} V_1(E) \right] \quad (16)$$

$$W(E) = \lambda_W(E) \left[W_0(E) \pm \lambda_{W1} \frac{\rho_n - \rho_p}{\rho_n + \rho_p} W_1(E) \right] \quad (17)$$

are expressed as a function of the density distributions ρ, and the iso-scalar (V_0) and isovector (W_0) potentials to ensure the Lane consistency, i.e the iso-spin symmetry. The iso-scalar normalisation coefficients $\lambda_{V,V1}$ are determined mainly on elastic scattering differential cross-sections and the isovector coefficients $\lambda_{W,W1}$ on quasi-elastic (p, n) scattering observables. The resulting parameterisation is characterised in particular by an isovector component of the imaginary part which is about 50% larger than the original contribution of [24]. At large neutron excesses, this enhancement reduces the imaginary component, i.e the neutron absorption channel, and consequently the radiative neutron capture cross-section. The weakness of the present BHF approaches lies in the fact that the asymmetry component of the JLMB semi-microscopic model is obtained by differentiating a symmetric nuclear BHF matter calculation with respect to the asymmetry parameter. Future BHF calculations of the asymmetric nuclear matter, such as [27], would be most useful to test this crucial effect at large neutron excesses. This semi-microscopic potential gives satisfactory results, though some improvements might be required in the low-energy description of the potential and the treatment of deformed nuclei.

Regarding the α-nucleus optical potential, the situation is less optimistic, especially at the low sub-Coulomb barrier energies. This results from the lack of a large enough body of experimental data for sub-Coulomb cross-sections combined with the difficulties to construct global and reliable α-nucleus optical potential. These theoretical problems are magnified by the fact that, at sub-Coulomb energies, the reaction rate predictions are highly sensitive to these potentials through the corresponding α-particle transmission coefficients. Global potentials of the Woods-Saxon type (e.g [28]) mainly determined on the basis of elastic scattering data at energies above the Coulomb barrier have been found to give rise to poor predictions when extrapolated at low energies, as shown by the $^{144}\mathrm{Sm}(\alpha,\gamma)^{148}\mathrm{Gd}$ experiment [29].

An attempt to develop a global α-nucleus optical potential to describe scattering and reaction cross-sections in the low energy region ($E \lesssim 20$ MeV) has been developed in the Woods-Saxon [30] and double folding [31, 32] approaches. In the latter, the real part of the optical potential is obtained by the double-folding

procedure using the M3Y nucleon-nucleon interaction [33], i.e

$$V_{df}(\vec{R}, E) = \int\int \rho_p(r_p)\rho_T(r_T)v_{eff}\,(E, \rho, s)\,d^3r_p d^3r_T \tag{18}$$

where $\rho = \rho_p + \rho_T$, $s = |\vec{R} + \vec{r}_p - \vec{r}_T|$ and $\rho_p(\vec{r}_p)$ and $\rho_T(\vec{r}_T)$ are the density distributions of the projectile and target, respectively, $\vec{R}$ is the separation of the centers of mass of the target and the projectile, and v_{eff} is the effective nucleon-nucleon interaction, which depends on energy E and local densities ρ_p and ρ_T. As α is a spinless particle, only the iso-scalar $v_{eff}(S = 0, T = 0)$ component of the effective interaction is considered. The M3Y effective interaction is given

$$v_{eff}(E, \rho, s) = g(E, s) \cdot f(E, \rho) \tag{19}$$

with

$$g(E, s) = 7999\frac{\exp(-4s)}{4s} - 2134\frac{\exp(-2.5s)}{2.5s} + J_{00}(E)\delta(s), \tag{20}$$

where the single nucleon exchange term J_{00} is

$$J_{00}(E) = -276(1 - 0.005E_p/A_p) \tag{21}$$

and E_p/A_p is the energy per nucleon of the projectile. The density dependence is obtained by means of

$$f(\rho) = C\left[1 + \alpha e^{-\beta\rho}\right]. \tag{22}$$

where the energy-independent parameters C, α and β are determined by fitting the volume integral of $v_{eff}(E, \rho, s)$ to the strength of the real G-matrix effective interaction obtained from Brueckner-Hartree-Fock calculations for nuclear matter of various densities ρ and at various energies [24].

As far as the imaginary part is concerned, large uncertainties on the theoretical formulation still exists. In particular, the volume or surface character of the potential is still difficult to ascertain. The imaginary part is most of the time described by a Woods-Saxon form with energy-independent geometry parameters. Three types of imaginary potentials were constructed by [32] from the assumption of volume or surface absorption, or from the adoption of the so-called dispersion relations that link the real and imaginary parts of the optical potential. The diffuseness and radius of these potentials have been chosen to be constant or to depend on the mass number. The energy dependence of the depth of the volume and surface terms of the imaginary potential is given by a Fermi-type function

instead of the conventional Brown-Rho parameterisation, and the parameters are adjusted to reproduce the experimental scattering and reaction data.

The three resulting global α-nucleus optical potentials derived by [32] are able to reproduce the bulk of the existing experimental data at low sub-Coulomb energies. However, experimental data at low energies [scattering data, α-capture or (n,α) cross-sections] are scarce, particularly for masses $A > 100$, making the predictive power of the new parameterisations still uncertain. Cross-sections predicted with the different potentials can differ by more than one order of magnitude at low energies. The different potentials can be regarded as providing the uncertainty level up to which we are able today to predict globally α-induced reaction cross-sections. Additional experimental data, extending over a wide mass range (especially low-energy radiative captures in the specific mass range $A \simeq 100$ and $A \simeq 200$), are of paramount importance to further constrain the determination of a reliable global α-nucleus optical potential at low energies. Much theoretical and experimental work remains to be done in this area.

γ-ray strength function

The total photon transmission coefficient from a compound nucleus excited state is one of the key ingredients for statistical cross-section evaluation. It strongly depends on the low-energy tail of the giant dipole resonance (GDR), which generally dominates on the M1 transition. The photon transmission coefficient is most frequently described in the framework of the phenomenological generalised Lorentzian model [34–36]. In this approximation,

$$T_{E1}(\varepsilon_\gamma) = \frac{8}{3}\frac{NZ}{A}\frac{e^2}{\hbar c}\frac{1+\chi}{mc^2}\,\frac{\varepsilon_\gamma^4\,\Gamma_{GDR}(\varepsilon_\gamma)\varepsilon_\gamma^4}{(\varepsilon_\gamma^2 - E_{GDR}^2)^2 + \Gamma_{GDR}^2(\varepsilon_\gamma)\varepsilon_\gamma^2}, \tag{23}$$

where E_{GDR} and Γ_{GDR} are the energy and width of the GDR, m is the nucleon mass and $\chi \simeq 0.2$ is an exchange-force contribution to the dipole sum rule. This model is even the only one used for practical applications. The Lorentzian GDR approach suffers, however, from shortcomings of various sorts. On the one hand, it is unable to predict the enhancement of the E1 strength at energies below the neutron separation energy demonstrated by nuclear resonance fluorescence experiments [38]. This departure from a Lorentzian profile may manifest itself in various ways, and especially in the form of a so-called pygmy E1 resonance which is observed in fp-shell nuclei, as well as in heavy spherical nuclei near closed shells (Zr, Mo, Ba, Ce, Sn and Pb). On the other hand, even if a Lorentzian function provides a suitable representation of the E1 strength, the location of its maximum and its width remain to be predicted from some underlying model for each nucleus.

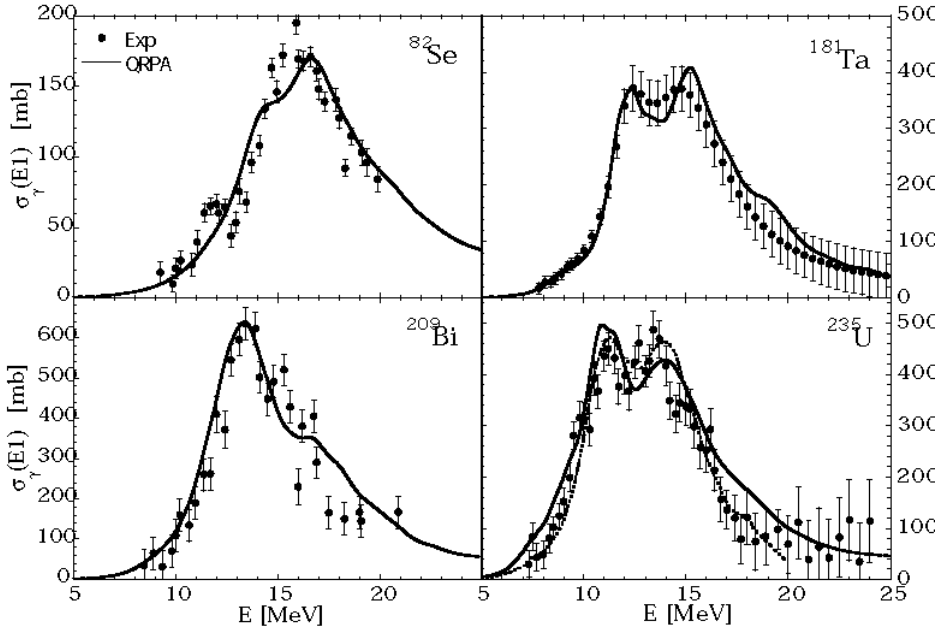

Figure 6: *Comparison of the QRPA predictions (solid line) with the experimental photo-absorption cross-sections [41] for* ^{82}Se, ^{181}Ta, ^{209}Bi *and* ^{235}U. *The QRPA peak energies were slightly re-normalised to reproduce the experimental GDR energy. The dash line shown for* ^{235}*U corresponds to the cross-section recommended by the Obninsk evaluated photo-nuclear library [41].*

These properties are usually obtained from a droplet-type of model [39]. This approach clearly lacks reliability when dealing with exotic nuclei.

In view of this situation, combined with the fact that the GDR properties and low-energy resonances may influence substantially the predictions of radiative capture cross-sections, it is clearly of substantial interest to develop models of the microscopic type which are hoped to provide a reasonable reliability and predictive power for the E1 strength function. Attempts in this direction have been conducted within models like the thermodynamic pole approach [16], the theory of finite Fermi systems or the QRPA approximation [37]. The spherical QRPA model making use of a realistic Skyrme interaction (the SLy4 Skyrme force) has even been used recently for *large-scale* derivations of the E1 strength function [40]. This global calculation predicts the location of the GDR energy in close agreement with experimental data, the rms deviation of the predictions from measurements for 84 nuclides amounting to about 300 keV only. The final E1

strength functions is obtained by folding the QRPA strengths with a Lorentzian function to take the deformation effects and the damping of the collective motion into account. The QRPA E1 strength functions reproduce satisfactorily the photo-absorption [16, 41] as well as the average resonance capture data at low energies [35]. We illustrate in Fig. 6 how the QRPA calculation reproduces the photo-absorption cross-sections of four (spherical and deformed) nuclei in the whole GDR region [41]. In particular, the GDR energy and width, as well as the double peak structure observed experimentally are rather well reproduced by the QRPA model.

The aforementioned QRPA calculations have been performed for all the $8 \leq Z \leq 110$ nuclei lying between the two drip lines. In the neutron-deficient region, as well as along the valley of β-stability, the QRPA distributions are very close to a Lorentzian profile. Significant departures from a Lorentzian are found for neutron-rich nuclei. In particular, QRPA calculations show that the neutron excess affects the spreading of the isovector dipole strength, as well as the centroid of the strength function. The energy shift is found to be larger than predicted by the usual $A^{-1/6}$ or $A^{-1/3}$ dependence given by the phenomenological liquid drop approximations [39]. In addition, some extra strength is predicted to be located at sub-GDR energies, and to increase with the neutron excess. The more exotic the nucleus, the stronger this low-energy component. This is illustrated in Fig. 7 for the E1-strength function in the Sn isotopic chain. Among the 8 distributions shown in Fig. 7, only the $A = 150$ one corresponds to a deformed configuration responsible for the double peak structure. For the $A \geq 140$ neutron-rich isotopes, an important part of the strength is concentrated at low energies ($E \lesssim 5 - 7$ MeV). Phenomenological models are unable to predict such low energy components, whatever their collectivity is. In particular for ^{150}Sn, all phenomenological systematics (as used for cross-section calculation) predict a γ-ray strength peaked around 15 MeV with a full width at half maximum of about 4.5 MeV [16] which is obviously very different from the microscopic estimate (Fig. 7). The above-described feature of the QRPA E1-strength function for nuclei with a large neutron excess is found to be qualitatively independent of the adopted effective interaction [40]. Even if the low-lying strength represents only about a few percent of the total E1 strength, it can produce an increase by more than an order of magnitude of the radiative capture cross-section by some exotic neutron-rich nuclei [36, 40]. Future HFB-QRPA calculations including deformation effects will hopefully increase the reliability of the present predictions.

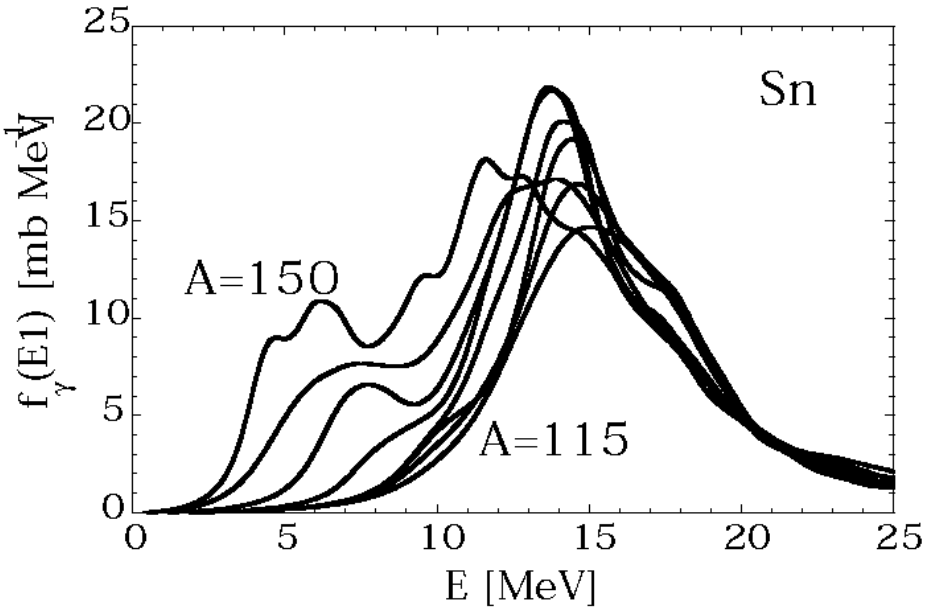

Figure 7: *E1-strength function for the Sn isotopic chain predicted by the QRPA with the SLy4 Skyrme force. Only isotopes ranging between A=115 and A=150 by steps of* ΔA*=5 are displayed.*

Reaction rates predictions

To illustrate the present status of our ability to predict reaction cross-sections, we show in Fig. 8 a comparison of the neutron capture reaction cross-section at 5 MeV estimated within the statistical model of Hauser-Feshbach making use of two different sets of nuclear ingredients, namely "macroscopic" and "microscopic" inputs as described in the previous subsections. More precisely, the first set based on the "microscopic" inputs includes the HFB ground state properties [13], HFBCS-based NLD [21], QRPA γ-ray strength [40] and the JLMB potential [26], while the "macroscopic" set is obtained with the FRDM masses [7], the BSFG NLD [18], the Lorentzian $E1$-strength [36] and the JLM potential [24]. The large deviations observed in Fig. 8 illustrate the uncertainties affecting the reaction cross-section estimate for stable as well as unstable neutron-deficient and neutron-rich nuclei. In particular, microscopic models give rise to very different predictions than the widely used macroscopic ones. Much work remains to be done, especially in the neutron-rich region to improve the reliability and accuracy of the present approaches, towards more microscopic and universal models.

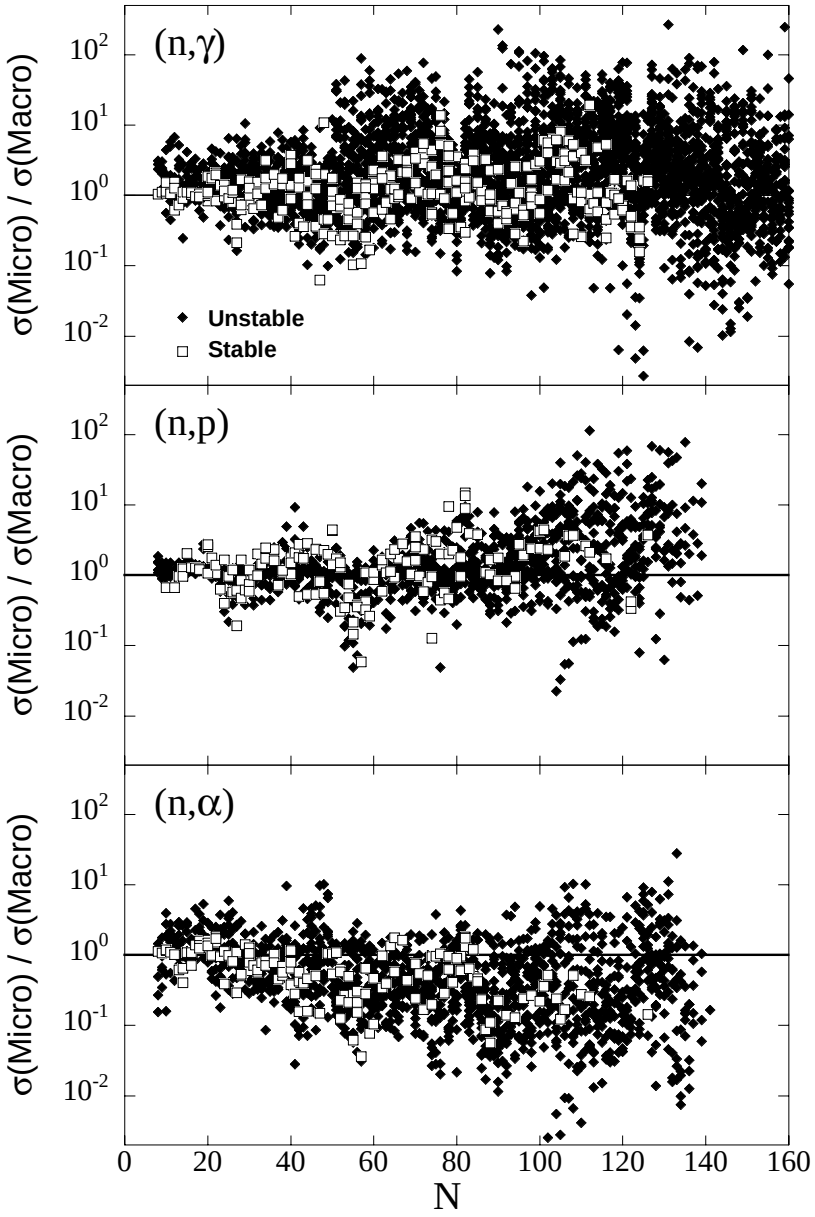

Figure 8: *Ratio of the "microscopic" to the "macroscopic" neutron capture cross-sections at an incident energy of 5 MeV predicted by the Hauser-Feshbach model for all nuclei with* $8 \leq Z \leq 94$ *and lying between the proton and neutron drip lines. Only cross-sections predicted to be larger than 1* μ*b are shown. The unstable nuclei correspond to black diamonds and the stable ones to open squares. See text for more details.*

Conclusions

An important effort has been devoted in the last decades to measure reaction cross-sections. However, major difficulties remain. In many applications, the nuclear data of need have to be predicted exclusively by theoretical modelling.

The extrapolation to exotic nuclei or energy ranges far away from experimentally known regions constrains the use of nuclear models to the most reliable ones, even if phenomenological approaches sometime present a better ability to reproduce experimental data. A subtle compromise between the reliability, accuracy and applicability of the different theories available has to be found according to the specific application considered. Microscopic models can now be adjusted to reach a level of accuracy similar to (or better than) the phenomenological models. Re-normalised on experimental data if needed, these microscopic models can replace the phenomenological approaches little by little in practical applications. In addition, further investigations should aim at describing reliably and accurately all nuclear properties within one unique framework. This universality aspect of the microscopic predictions corresponds to one of the major challenges of fundamental nuclear physics research for the coming decades.

A continued effort to improve our predictions of the reaction cross-sections is obviously required. Priority should be given to a better description of the ground-state properties (and most particularly an improved treatment of the nuclear pairing interaction), nuclear level density and the α-nucleus optical potential, as well as a better understanding of given nuclear effects affecting exotic neutron-rich nuclei, such as the soft dipole modes. This continued effort to improve the microscopic nuclear predictions is concomitant with new measurements of masses far away from stability, but also reaction cross-sections on stable and unstable targets.

Acknowledgments: S.G. is FNRS senior research assistant

[1] W. Hauser, H. Feshbach, (1952) *Phys. Rev.* **87**, 366

[2] J.A. Holmes, S.E. Woosley, W.A. Fowler, B.A. Zimmerman, Tables of thermonuclear-reaction-rate data for neutron-induced reactions on heavy nuclei (2000) *At. Nucl. Data Tables* **18**, 306–412

[3] G. Audi, A.H. Wapstra, The 1995 update to the atomic mass evaluation (1995) *Nucl. Phys.* **595**, 409–480

[4] G. Audi, A.H. Wapstra, 2002. private communication

[5] C.F. von Weizsäcker, (1935) *Zeit. Phys.* **99**, 431

[6] W.D. Myers, W.J. Swiatecki, Nuclear masses and deformations (1966) *Nucl. Phys.* **81**, 1–60

[7] P. Möller, J.R. Nix, W.D. Myers, W.J. Swiatecki, Nuclear ground-state masses and deformations (1995) *At. Nucl. Data Tables* **59**, 185–381

[8] Y. Aboussir, J.M. Pearson, A.K. Dutta, F. Tondeur, Nuclear masses via an approximation to the Hartree-Fock method (1995) *At. Nucl. Data Tables* **61**, 127–176

[9] S. Goriely, Capture Gamma-Ray Spectroscopy and Related Topics (AIP) ed. S. Wender (2000) p. 287

[10] F. Tondeur *et al.*, Towards a Hartree-Fock mass formula (2000) *Phys. Rev.* **C62**, 024308

[11] S. Goriely, F. Tondeur, J.M. Pearson, A Hartree-Fok nuclear mass table (2000) *At. Nucl. Data Tables* **77**, 311–381

[12] M. Samyn *et al.*, A HFB mass formula (2002) *Nucl. Phys.* **700**, 142

[13] S. Goriely *et al.*, Hartree-Fock mass formulas and extrapolation to new mass data (2002) *Phys. Rev.* **C66**, 024326

[14] M. Farine, J.M. Pearson, F. Tondeur, Skyrme force with surface-peaked effective mass, (2002) *Nucl. Phys.* **696**, 396

[15] T. Otsuka *et al.*, Magic numbers in exotic nuclei and spin-isospin properties of the NN interaction (2001) *Phys. Rev. Lett.* **87**, 082502

[16] Reference Input Parameter Library, IAEA-Tecdoc-1034 1998. (also available at *http://iaeand.iaea.or.at/ripl*)

[17] S. Goriely, A new nuclear level density formula including shell and pairing correction in the light of a microscopic model calculation (1996) *Nucl. Phys.* **605**, 28–60

[18] S. Goriely, Nuclear reaction data relevant to nuclear astrophysics *J. Nucl. Science and Technology* (ed. K. Shibata, 2002) No. 2. p. 536–541

[19] P. Decowski *et al.*, On superconductivity effects in nuclear level density (1968) *Nucl. Phys.* **110**, 129–141

[20] L.G. Moretto, Statistical description of a paired nucleus with the inclusion of angular momentum (1972) *Nucl. Phys.* **185**, 145–165

[21] P. Demetriou, S. Goriely, Microscopic nuclear level densities for practical applications, (2001) *Nucl. Phys.* **695**, 95–108

[22] S. Hilaire, J.P. Delaroche, A.J. Koning, Generalized particle-hole state densities within the equidistant spacing model, (1998) *Nucl. Phys.* **632**, 417–441

[23] S. Siem *et al.*, Level densities and gamma-strength functions in ^{148,149}Sm (2002) *Phys. Rev.* **C65**, 044318

[24] J.P. Jeukenne, A. Lejeune and C. Mahaux, Optical-model potential in finite nuclei from Reid's hard core interaction (1977) *Phys. Rev.* **C16**, 80–96

[25] E. Bauge, J.P. Delaroche, M. Girod, Semimicroscopic nucleon-nucleus spherical optical potential model for nuclei with $A \geq 40$ at energies up to 200 MeV (1998) *Phys. Rev.* **C58**, 1118

[26] E. Bauge, J.P. Delaroche, M. Girod, Lane-consistent, semimicroscopic nucleon–nucleus optical model (2001) *Phys. Rev.* **C63**, 024607

[27] W. Zuo, I. Bombaci, U. Lombardo, Asymmetric nuclear matter from an extended Brueckner-Hartree-Fock approach, (1999) *Phys. Rev.* **C60**, 024605

[28] L. McFadden, G.R. Satchler, (1966) *Nucl. Phys.* **84**, 177

[29] E. Somorjai *et al.*, Experimental cross-section of ^{144}Sm$(\alpha,\gamma)^{148}$Gd and implications for thep-process (1998) *Astron. Astrophys.* **333**, 1112–1116

[30] C. Grama, S. Goriely, Nuclei in the Cosmos (Editions Frontières) eds. N. Prantzos *et al.* (1998) p. 463

[31] P. Mohr, α-nucleus potentials for the neutron-deficient p nuclei (2000) *Phys. Rev.* **C61**, 045802

[32] P. Demetriou, C. Grama, S. Goriely, Improved global alpha-optical model potentials at low energies (2002) *Nucl. Phys.* **707**, 142–156

[33] A.M. Kobos *et al.*, Folding-model analysis of elastic and inelastic α-particle scattering using a density-dependent force (1984) *Nucl. Phys.* **425**, 205

[34] J. Kopecky, R.E. Chrien, Observation of the M1 giant resonance by resonance averaging in ^{106}Pd (1987) *Nucl. Phys.* **468**, 285–300

[35] J. Kopecky, M. Uhl, Test of gamma-ray strength functions in nuclear reaction model calculations (1990) *Phys. Rev.* **C41**, 1941–1955

[36] S. Goriely, Radiative neutron captures by neutron-rich nuclei and the r-process nucleosynthesis (1998) *Phys. Lett.* **B436**, 10–18

[37] S.G. Kadmenskii, V.P. Markushev, V.I. Furman, Radiative widths of neutron resonances. Giant dipole resonances (1983) Sov. J. Nucl. Phys. **37**, 165–168.

[38] K. Govaert *et al.*, Dipole excitations to bound states in ^{116}Sn and ^{124}Sn (1998) *Phys. Rev.* **C57**, 2229–2249

[39] W.D. Myers *et al.*, Droplet model of the giant dipole resonance (1977) *Phys. Rev.* **C15**, 2032–2043

[40] S. Goriely, E. Khan, Large-scale QRPA calculation of E1-strengths and its impact on the neutron capture cross-section (2002) *Nucl. Phys.* **706**, 217–232

[41] Photonuclear data for applications; cross-sections and spectra, IAEA-Tecdoc-1178 (2000)

Experimental study of activation cross-section for application purposes – Status Report

M. Hagiwara[1], M.S. Uddin[1], N. Kawata[1], T. Itoga[1], N. Hirabayashi[1], M. Baba[1], A. Hermanne[2], F. Tárkányi[3], F. Ditrói[3], S. Takács[3] and J. Csikai[4]

[1] *Cyclotron and Radioisotope Center, Tohoku University, Sendai, Japan*
[2] *Cyclotron Laboratory, Free University Brussels, Brussels, Belgium*
[3] *Institute of Nuclear Research of the Hungarian Acad. of Sci. (ATOMKI), Debrecen, Hungary*
[4] *Institute of Experimental Physics, University of Debrecen, Debrecen, Hungary and ATOMKI, Debrecen, Hungary*

Abstract:
Activation cross-section data play an important role in basic science and in many applications. Data are required for successful development of an accelerator based transmutation system, for production of medical radioisotopes, for determining beam parameters of accelerated particles, for thin layer activation technology, radiation safety, etc. The status of the published nuclear data is in some cases not up to the requirements. As the predictions of model calculations are not always reliable, experimental data are of vital importance. Only very few laboratories perform systematic experimental investigations for dedicated applications. Such investigations are very time consuming and are in many cases they not detailed enough for use in applications.

In the frame of the JSPS-HAS collaboration an experimental programme was started last year between the Tohoku University, the Debrecen University and the Institute of Nuclear Research in the following research fields:

- Experimental determination of activation cross-sections of medium energy proton and deuteron induced nuclear reactions (up to 200 MeV).
- Compilation, evaluation and preparation of a recommended database of experimental cross-sections of selected reactions.
- Data validation through integral data measurements.

Table 1: *Investigated reactions*

Target	Particle	Energy max	Data evaluation	Products
		(MeV)	(status)	
Ta	p	70	completed	^{175,176,177,180}Ta, ^{173,175}Hf, ^{178}W, ^{179}Lu
Pd	p	70	partly	
Zn	p	70	no	
Pt	p	70	partly	
Fe	p	70	no	
W	p	42	partly	
Pd	d	21	partly	
Pt	d	21	partly	
W	d	50	completed	^{181,182m,182g,183,184m}Re, ^{184g,186}Re,^{177}Ta,^{187}W

- Investigations of neutron spectra produced by medium energy protons and deuterons in reactor construction materials.

In the frame of a bilateral cooperation standing for several years between the Cyclotron Laboratory of the Free University Brussels and the Institute of Nuclear Research, Debrecen a large amount of new experimental and recommended data have already been produced up to 40 MeV mainly for medical and beam monitoring purposes.

As the characteristics of the accelerators available at the 3 institutes are quite different, covering irradiations over a wide energy range was distributed over the participating laboratories. High-energy irradiations (up to 90 MeV proton energy) were performed at the Tohoku University. The Brussels CGR 560 Cyclotron gives the possibility for irradiations up to E_p=42 MeV. Debrecen has a smaller cyclotron delivering protons up to 20 MeV. All laboratories also can provide accelerator based mono-energetic neutron sources to perform neutron cross-section measurements and well equipped radiochemistry laboratories for the necessary chemical separation.

In the Table 1 the irradiations already performed in the frame both collaborations are indicated together with the covered energy range and the status of the data evaluation:

The irradiations were done at the external beams of the different cyclotrons by using the stacked foil irradiation technique. The beam intensity was determined in a Faraday cup and/or with well known monitor reactions. The activity of the

irradiated samples was measured nondestructively by HPGe gamma spectroscopy. The specificity of our measurements and data evaluations lies in the following aspects:

- The monitor foils covered the whole energy range allowing measurements of activation cross-sections relative to monitor reactions
- Detailed compilation and critical evaluation of the literature data
- Validation of the data through thick target integral measurements
- Investigation of not only the long-lived products
- Investigation of applications in different fields
- Large experience of the participants in measurement, compilation, evaluation and application of cross-section data

It was very difficult to optimise the experiments and measurements due to the limitations of the available foil thicknesses, the available beam times and the number of available gamma detectors. In the future we would like to extend the beam energies towards higher energies and to include radioisotopes with shorter half lives than those we were able to measure in this programme. For more intensive use of the available capacity of the gamma spectra measurement we would like to solve the restrictions in transport of the irradiated samples between the collaborations to assure the detection of low activity, long-lived products.

The programme is partly supported by the Hungarian Research Fund OTKA (Contract no. T037190) and connected to different IAEA CRP programmes.

Compilation of measured activation cross-sections

D.L. Smith[1], A. Fessler[1,2], V. Semkova[3], P. Reimer[2], and A.J.M. Plompen[2]

[1] *Nuclear Engineering Division, Argonne National Laboratory, Argonne, IL 60439, USA*
[2] *EC-JRC-IRMM, Retieseweg 111, 2440 Geel, Belgium*
[3] *Institute for Nuclear Research and Nuclear Energy, Bulgarian Academy of Sciences, 1784 Sofia, Bulgaria*

Abstract:
Measured nuclear data are of little value until they are made conveniently available for evaluators and users. A record of research activity in a particular area is provided through the index CINDA. However, actual experimental results, along with descriptive material required to interpret and judge the quality of these results, must be obtained from archived ASCII experimental data files maintained at the various nuclear data centres. These results are compiled and documented using an internationally adopted standard format referred to as EXFOR (EXchange FORmat). We have prepared EXFOR files for a number of neutron activation reactions measured as part of the WPEC Subgroup 19 project. Among the materials considered were natural elements as well as various specific isotopes for F, Na, Mg, Al, Si, P, Cl, Ti, V, Cr, Mn, Fe, Co, Ni, Cu, Zr, Nb, Mo, Tc, Sn, Ba, and Pb. A list of the studied reactions and about 100 corresponding data sets acquired from measurements carried out mainly at IRMM and FZ-Jülich is provided. Since this experimental work was performed in Europe, the prepared files are transmitted to the NEA Data Bank, Paris, France, for review. There they are checked for formatting errors and corrections are made prior to including them in the archives. The role of CINDA and the characteristics of the EXFOR format are discussed briefly, and an example of a prepared EXFOR file is presented.

Introduction

Subgroup 19 of the OECD-Nuclear Energy Agency Working Party for Evaluation Cooperation (WPEC) was established with the mission of improving the available database of neutron activation cross-sections and related information required

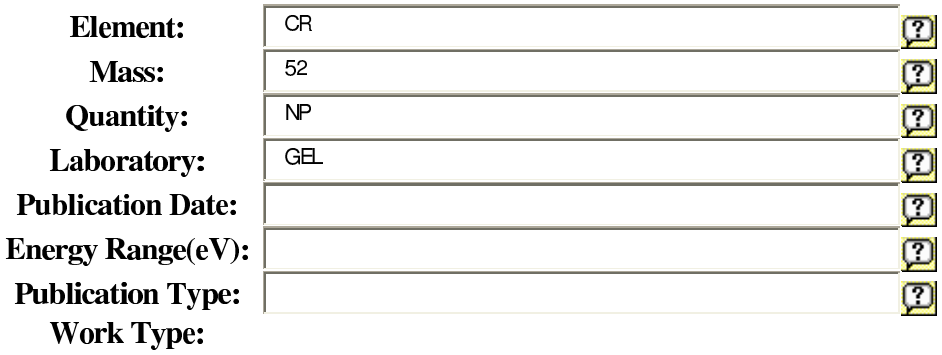

Figure 1: *Query block for CINDA retrieval from the NNDC*

for nuclear energy applications. This objective is being fulfilled by a combined effort of measurements, nuclear modelling and parameter sensitivity studies, experimental data compilation, and data evaluation. Although a major emphasis has been placed on the energy range $\approx$ 13-20 MeV that is of particular interest for nuclear waste transmutation applications, Subgroup 19 has also undertaken studies at both lower and higher energies. However, this project has avoided investigating reactions that involve strong contributions from the resonance region, e.g., (n, γ) activation processes, since the measurement and data analysis techniques required to acquire reliable data at these low energies differ considerably from what is normally needed for fast-neutron studies. This paper focuses on those aspects of Subgroup 19 work performed mainly at IRMM, Belgium, and FZ-Jülich, Germany.

No experimental measurement project is complete until the final results have been reported. While journal publication of results from measurements is an essential part of any comprehensive research activity, this medium is often inadequate for the reporting of useful but very detailed numerical information, mainly due to space constraints. This paper reports on data compilation and reporting activities of Subgroup 19 that supplement formal publication in journals or conference proceedings. The present work involves preparing detailed files in a standardised format of pertinent numerical experimental results obtained during the course of this project as well as of some closely related results generated by members of the Subgroup during the recent time period immediately preceding the formal convening of Subgroup 19 in the year 2000. In this paper we begin by describing briefly the two mechanisms available for cataloguing/compiling experimental neutron reaction information at the core nuclear data centres. A list

of reactions that have been studied experimentally under present auspices, and for which data sets have been or are being prepared for submission to the data centres is currently included in Part A of this report. The current status of these data sets is also reviewed. A specific example of archived information will be provided. Finally, future plans for the ongoing compilation work within the framework of Subgroup 19 will be discussed.

CINDA

The international core data centres maintain a shared catalogue (index) of available neutron nuclear data that is appropriately entitled "Computer INdex of Neutron DAta" (CINDA). There are four core data centres as follows:

- The USA National Nuclear Data Center at Brookhaven National Laboratory, USA
- The NEA Data Bank at Paris, France
- The IAEA Nuclear Data Section at Vienna, Austria
- The Russian Nuclear Data Center at the Fiziko-Energeticheskij Institut, Obninsk, Russia

Access to these core data centres as well as to other specialised nuclear data centres can be found, e.g., by selecting the underlined hypertext block entitled "Nuclear Reaction Data Centers Network" on the NNDC Internet Homepage located at http://www.nndc.bnl.gov. CINDA is accessible from the Internet sites maintained by each of the core nuclear data centres. All classes of neutron data information are indexed, including experimental differential and integral data, nuclear modelling information, etc. Archived nuclear data information is readily retrieved using database search engines. This is done according to criteria defined by one or more key parameters. For example, Fig. 1 reproduces the query block that can be found when using the search engine available at the NNDC Internet site. This particularly query asks for retrieval of all data originating from IRMM (code symbol "GEL") on the ^{52}Cr$(n,p)^{52}$V reaction, without any explicit conditions concerning data energy range, publication type, or work type.

Interactive "Help" files are provided for the user at each of the data-center Internet sites to assist in narrowing the search to the specific information that is desired. A CINDA reference manual also exists for guidance purposes [1]. As an example, consider a CINDA retrieval of available information on the ^{52}Cr$(n,p)^{52}$V reaction from IRMM according to the query parameters specified

National Nuclear Data Center
CINDA Retrieval

29-NOV-2002

Element	: CR
Mass	: 52
Quantity	: NP
Laboratory	: GEL
Publication Date	:
Energy Range(eV)	:
Publication Type	: ALL
Work Type	: ALL

CR-52

Quant.	Energy range	Lab	Reference		Comments
(n,p)	9.3+6 2.1+7	GEL Expt Rept	JUEL-3502	9800	Fessler+.VDG,ACTIV: TBL
	9.3+6 2.1+7	GEL Expt Conf	97TRIEST 399	9705	Fessler+.VDG,ACTIV: NDG
	9.3+6 2.1+7	GEL Expt Data	EXFOR22406.003	9809	.22 PTS SIG NP

Generated at by CINONL 29-NOV-2002

Figure 2: *CINDA retrieval of all information on* $^{52}Cr(n,p)^{52}V$ *from IRMM*

in Fig 1. The results retrieved on 29 November 2002, provided in HTML format, appear in Fig. 2.

It is found that the only available data set from IRMM compiled in EXFOR that satisfies the selected criteria is the one by Fessler. These data have appeared in a report (Fessler's thesis), at a conference (Trieste, 1997), and they have been published. Also, they are available in an EXFOR file to which a direct Internet hyperlink is provided within the indicated CINDA HTML page. The information provided in CINDA includes energy range, date, laboratory, type of information (in this case "Expt" for experimental), formal reference(s), and limited descriptive material about the experiment.

EXFOR

Mention was made about EXFOR files in the preceding section. EXFOR stands for EXchange FORmat. It is an internationally adopted standard ASCII data formatting system for representing certain types of compiled experimental nuclear data, e.g., cross-sections, in shared archival files. An EXFOR on-line "Help" file can be found at the above-mentioned data-center Internet sites [2]. In the US, these files are frequently referred to by the label CSISRS. For the most part the

EXFOR formats are quite transparent to the casual reader, but individuals who prepare EXFOR files must be very careful to follow the formatting rules precisely otherwise checking codes and search engines designed to retrieve information, to manipulate these data files, to prepare data lists and plots, etc., will not function properly. These files consist of information blocs with beginning and ending records. The information included can be either textual descriptive and bibliographic material or numerical data. Standardised code words and headings are used to advise the reader as to the precise content of each information bloc. Fig. 3 is an example of such a file. In fact it is the very same ^{52}Cr$(n,p)^{52}$V data file by Fessler from IRMM to which a hyperlink is indicated in Fig. 2. The printout of this file appears exactly as it was generated by the NNDC computer system using its EXFOR retrieval software. Note that there is also an Internet hyperlink within this file to the journal where the compiled work was published, in this case in Physical Review. Before a prepared EXFOR file can be posted in the system by the receiving data center, and ultimately made available to all the other data centres through an on-going exchange agreement, this file must be checked for format and content errors. Since the experimental work was carried out in Europe, the NEA Data Bank, Paris, France, is the appropriate center for transmittal and processing of the prepared EXFOR files from this project. Once a file is accepted for archiving in the EXFOR system, it is assigned a unique Ascension Number that can be used for identification and retrieval purposes. For example, the Ascension Number 22406.003 uniquely identifies the ^{52}Cr$(n,p)^{52}$V numerical cross-section data set illustrated in Fig. 3. The number to the left of the decimal point identifies the complete file (called an "Entry") while the number to the right of the decimal point refers to the particular segment of the file that contains the pertinent numerical data (called a "Subentry").

```
REQUEST        7428001   20021129          5                          0  0    0
ENTRY            22406   20000114                                  22406000    1
SUBENT         22406001   20000114                                  22406001    1
BIB                15         63                                    22406001    2
INSTITUTE  (2ZZZGEL,2GERJUL)                                        22406001    3
REFERENCE  (J,PR/C,58,996,1998)                                     22406001    4
AUTHOR     (A.FESSLER,E.WATTECAMPS,D.L.SMITH,S.M.QAIM)              22406001    5
TITLE      Excitation Functions of (N,2N), (N,P), (N,NP+PN+D), and  22406001    6
            (N,ALPHA) Reactions on Isotopes of Chromium             22406001    7
FACILITY   (VDG,2ZZZGEL) CN-Type HVEC 7 MV Van De Graaff            22406001    8
           (CYCLO,2GERJUL) Compact Cyclotron CV28                   22406001    9
INC-SOURCE (D-T)(2ZZZGEL),Deuterium on 2.047 Mg/Cm2 Thick Ti-T      22406001   10
            Target.                                                 22406001   11
           (D-D)(2GERJUL),Deuterium Through a 5.3 Micro-M Nb-       22406001   12
            Window on a Small Gas Cell (3.7 CM LONG, 4 CM           22406001   13
            DIAM.), Filled with D2 at 1.8 Bar.                      22406001   14
METHOD     (ACTIV) Samples were Activated at 1 Cm Distance to the   22406001   15
            Target and at 0 Deg with Respect to the Beam Direction  22406001   16
            At Geel, Some Samples were Activated at Angles of 0,    22406001   17
            30, 60, 105, and 110 Deg. In this Way the Neutron       22406001   18
            Energy Variation with Angle from the Source Reaction    22406001   19
            Could be Used For the Excitation Function Measurement.  22406001   20
           Flux Monitored with Al, Fe, and Nb Foils Sandwiched      22406001   21
            Between Samples.                                        22406001   22
```

```
           (TOF) Determination of N Spectrum                        22406001   23
           (GSPEC)                                                  22406001   24
DETECTOR   (HPGE)                                                   22406001   25
           (BF3) Directional Long Counter at Geel For Monitoring    22406001   26
                 Of Neutron Flux During Irradiation                 22406001   27
           (SCIN) Ne-213 Liquid Scintillator at Geel For N          22406001   28
                 Spectrum Determination                             22406001   29
MONITOR    (13-AL-27(N,P)12-MG-27,,SIG)                             22406001   30
           (13-AL-27(N,A)11-NA-24,,SIG)                             22406001   31
           (26-FE-56(N,P)25-MN-56,,SIG)                             22406001   32
           (41-NB-93(N,2N)41-NB-92-M,,SIG)                          22406001   33
MONIT-REF  (,N.P.KOCHEROV+,R,IAEA-NDS-141,,1993)                    22406001   34
           Data Extracted from the Irdf-90.2 Evaluation from the    22406001   35
            Iaea Worldwideweb Site                                  22406001   36
DECAY-MON  (12-MG-27,9.46MIN,DG,843.8,0.718,DG,1014.4,0.28)         22406001   37
           (11-NA-24,14.96HR,DG,1368.6,1.0)                         22406001   38
           (25-MN-56,2.58HR,DG,846.8,0.989,DG,1810.7,0.272)         22406001   39
           (41-NB-92-M,10.15D,DG,934.4,0.991)                       22406001   40
CORRECTION Data Corrected For Contribution of Background Neutrons,  22406001   41
            Neutron Flux Fluctuations During Irradiations,          22406001   42
            Coincidence Losses, Gamma-Ray Abundance, Gamma-Ray      22406001   43
            Self-Absorption, Detector Efficiency, Geometry.         22406001   44
ERR-ANALYS (ERR-T   ) Total Data Uncertainty Given Includes        22406001   45
                 Errors Due to:                                     22406001   46
           (ERR-1) - Max Sample Weight Error  0.1-1.0%              22406001   47
           (ERR-S)- Max Counting Statistics Error error             22406001   48
                   (1.5-17.0%)                                      22406001   49
           (ERR-2)- Max Sample Geometry error  (1.0-1.5%),          22406001   50
           (ERR-3)- Irradiation Geometry  error (0.5%),             22406001   51
           (ERR-4)- Self-Absorption  error (0.5%),                  22406001   52
           (ERR-5)- Max Correction For Background Neutrons          22406001   53
                    error    0.6-2.0%                              22406001   54
           (ERR-6)- Max Coincidence Summing Correction error        22406001   55
           (ERR-7)- Max Emission Probability error  0.4-3.5%        22406001   56
           (ERR-8)- Max Half Life of Activity error    0.2-4.0%     22406001   57
           (ERR-9)- Max Detector Efficiency error  (1.5-3.0%)       22406001   58
           (MONIT-ERR)-Max Reference cross-section error            22406001   59
                      (1.5-3.5%)                                    22406001   60
           Total Error (5.0-22.0%)                                  22406001   61
STATUS     (TABLE) Data Taken from Main Reference, Tables 3 & 4.    22406001   62
           (APRVD)   Data Compiled by the Author                    22406001   63
HISTORY    (19991118C)   Compiled by A.Fessler at ANL               22406001   64
           (20000114U) Last checking has been done by SM            22406001   65
ENDBIB               63                                            22406001   66
COMMON               11          6                                 22406001   67
ERR-S      ERR-1      ERR-2      ERR-3      ERR-4      ERR-5        22406001   68
ERR-6      ERR-7      ERR-8      ERR-9      MONIT-ERR               22406001   69
PER-CENT   PER-CENT   PER-CENT   PER-CENT   PER-CENT   PER-CENT     22406001   70
PER-CENT   PER-CENT   PER-CENT   PER-CENT   PER-CENT                22406001   71
  17.0       1.0        1.5        0.5        0.5        2.0       22406001   72
        0.3        3.5        4.         3.        3.5             22406001   73
ENDCOMMON            11          6                                 22406001   74
ENDSUBENT            11                                            2240600199999
SUBENT        22406003   20000114                                  22406003    1
BIB                   3          5                                 22406003    2
REACTION   (24-CR-52(N,P)23-V-52,,SIG)                             22406003    3
SAMPLE     .High Purity Metallic Chromium Samples (99.9%) Of        22406003    4
            1.3 Cm Diameter and 0.1 Cm Thickness and Rectangular  22406003    5
            Samples (1 CM X 1 CM) Of 50 Mg of Enriched 52Cr-Oxid. 22406003    6
DECAY-DATA (23-V-52,3.75MIN,DG,1434.1,1.0)                          22406003    7
ENDBIB                5                                             22406003    8
NOCOMMON              0          0                                  22406003    9
DATA                  4         22                                  22406003   10
EN         EN-ERR     DATA       ERR-T                             22406003   11
MEV        MEV        MB         MB                                22406003   12
       9.31     2.E-01   5.08E+01        3.5                       22406003   13
  1.033E+01    2.2E-01   5.51E+01        3.6                       22406003   14
  1.157E+01    2.4E-01   6.53E+01        3.9                       22406003   15
  1.227E+01    2.6E-01   7.07E+01        4.4                       22406003   16
  1.371E+01    2.5E-01   8.82E+01        5.6                       22406003   17
  1.501E+01    2.5E-01   8.29E+01        4.1                       22406003   18
  1.595E+01    2.5E-01   7.47E+01        3.6                       22406003   19
  1.602E+01    2.5E-01   7.96E+01        3.9                       22406003   20
  1.602E+01    2.5E-01    7.6E+01        3.8                       22406003   21
  1.699E+01     2.E-01   6.58E+01        4.3                       22406003   22
  1.699E+01     2.E-01   6.17E+01        4.1                       22406003   23
  1.754E+01     3.E-01   5.93E+01        3.7                       22406003   24
```

```
  1.773E+01    2.5E-01   5.83E+01        4.1                    22406003   25
  1.773E+01    2.5E-01   5.74E+01        3.2                    22406003   26
   1.78E+01     3.E-01   5.89E+01        3.2                    22406003   27
  1.873E+01    3.5E-01   4.55E+01        2.7                    22406003   28
  1.904E+01    2.5E-01   4.66E+01        3.1                    22406003   29
  1.904E+01    2.5E-01   4.05E+01        2.7                    22406003   30
   1.97E+01     4.E-01   3.42E+01        1.7                    22406003   31
  2.024E+01    2.5E-01   2.88E+01        2.1                    22406003   32
  2.024E+01    2.5E-01   2.83E+01        2.6                    22406003   33
   2.17E+01     5.E-01   2.71E+01        2.6                    22406003   34
ENDDATA             24                                          22406003   35
ENDSUBENT            4                                          2240600399999
ENDENTRY             2                                          2240699999999
ENDREQUEST           1                                          Z999999999999
```

Figure 3: *EXFOR file for the $^{52}Cr(n,p)^{52}V$ data set from Fessler at IRMM*

Data Compiled in the Subgroup 19 Project

We are concerned here with reviewing the status of a particular data compilation activity within the context of the Subgroup 19 project. The status information is summarised in Table 2.1 of Part A of this report. All but the reactions on Zr, Mo and some recent Ni reactions were compiled by the authors (DLS, corrections AP). Those reactions that have been studied are listed and progress made in archiving these acquired data in the EXFOR system is indicated. There are 112 data sets included here. Instances of publication are also mentioned. Note that closely related experimental work carried out during the time period immediately preceding the official start of Subgroup 19 in 2000 are also mentioned in the Table for completeness.

Future Plans

For each reaction studied experimentally and listed in Table 2.1 of Part A, the analyses of raw data is completed, results were presented in reports and conference contributions and it is intended to prepare journal articles, and generate the missing EXFOR files dealing with the experimental results for submission to the NEA Data Bank, Paris, France.

Summary

The experimental work of Subgroup 19 on neutron-activation cross-sections encompasses measurements, analysis of the experimental data, publication of the experimental results, preparation of EXFOR files, and submission of these files to the NEA Data Bank for archiving and exchange with other nuclear data centres worldwide. These separate tasks have already been completed for a large number

of reactions, but some further work remains to be done, as indicated in the status review presented in Table 2.1 of Part A of this report. The effort needed to complete these unfinished tasks is a minor one so that the Subgroup 19 can be brought to a successful end in the spring of 2005.

Acknowledgements. We are indebted to the European Commission and to the US Department of Energy, Science Programmes, for the support and encouragement that made it possible to carry out this work.

[1] CINDA Manual: On-line at http://www.nea.fr/cinda/manual/manual.html.

[2] EXFOR "Help": On-line at: http://www.nndc.bnl.gov/nndc/exfor/exhelp.htm.

Correction for low energy neutrons by spectral indexing

D.L. Smith[1], A.J.M. Plompen[2], V. Semkova[3]

[1] *Nuclear Engineering Division, Argonne National Laboratory, Argonne, IL 60439, USA*
[2] *EC-JRC-IRMM, Retieseweg 111, 2440 Geel, Belgium*
[3] *Institute for Nuclear Research and Nuclear Energy, Bulgarian Academy of Sciences, 1784 Sofia, Bulgaria*

Abstract:
An important component of the WPEC Subgroup 19 project on neutron activation cross-sections is the measurement of cross-sections for several reactions at specific energies. However, neutron sources produced in the laboratory by accelerators are rarely purely mono-energetic. In particular, low energy neutrons are present in almost all cases, due not only to the basic properties of neutron source reactions such as ^{2}H$(d,n)^{3}$He, ^{3}H$(p,n)^{3}$He, ^{3}H$(d,n)^{4}$He, etc., but also to neutron production and scattering near the experimental area as well as to room-return effects. In some cases, the response to these spurious neutrons exceeds that from primary-energy neutrons. Consequently, in order to derive quasi-mono-energetic results from measurements in real laboratory environments it is necessary to correct for those neutrons having energies other than the primary energy, particular those with lower energies. We have applied the method of "spectral indexing" for this purpose. Measurements of laboratory neutron spectra have been made at IRMM by the time-of-flight method. A collection of well-characterised standard neutron activation reactions were then employed as monitors to provide spectral sensitivity. These monitor materials were included in sample packets along with the studied materials having "unknown" reaction properties. Few-group spectral representations at the sample position were defined and the parameters of these representations were adjusted by the method of generalised least squares using the known response characteristics of the spectral-index reactions. The method is described in general terms and its practical application in this research project — illustrated with some numerical results — is discussed.

1. Introduction

In order to obtain accurate differential cross-section results from experimentally measured reaction rates it is necessary to correct the raw data for a variety of experimental effects. Among these are corrections for the specific nature of the neutron source used in the experiment. Mono-energetic neutron cross-sections, i.e., cross-section values at a single well-defined energy, are most often sought in nuclear experiments because these data can be compared directly with theoretical results and they can also be used as input for a wide variety of analytical exercises. Such measurements are an important component of the WPEC Subgroup 19 project. However, Nature is uncooperative in the sense that sources of strictly mono-energetic neutrons are rare, and then they are usually limited to narrow neutron-energy ranges [1]. In this context, we are not talking about the natural variation of neutron energy that comes about due to target-thickness and kinematic effects of the source. This type of energy spread generally can be calculated quite well from a model of the experimental process, and reliable corrections then can be applied in most instances of interest for present purposes [2]. Rather, we are concerned here with the diversity of neutron energies due to two specific origins: i) fundamental characteristics of the source reaction, i.e., the excitation of multiple levels in the reaction product nucleus, several distinct open reaction channels, etc., and ii) perturbations of the source neutrons by the environment due to neutron scattering and secondary reactions that occur in the laboratory.

While neutrons can be generated by a variety of other means such as natural radioactivity, nuclear reactors, and photo-nuclear processes, we are interested here in neutrons produced by charged-particle (CP) reactions of the general form A(CP;y,xn)B, where "xn" indicates one or more neutrons and "y" accounts for any additional emitted light-particles or photons. The most common charged particles employed for neutron production are protons, deuterons, and α-particles, and beams of these particles are routinely produced for this purpose at accelerator facilities. As a rule, the higher the incident CP energy, the greater the complexity of the generated neutron spectrum. In order to qualify as a useful neutron source for "mono-energetic" measurements, especially in experiments such as neutron activation where timing conditions cannot be imposed to sort out the influence of neutrons with various energies, it is necessary that the neutron spectrum be dominated by a single primary group "P" with energies close to a mean value with a modest spread introduced only by kinematics and other straightforward experimental perturbations. The remaining neutrons will usually have lower energies so we choose to label them as "LE". They may consist of one or more isolated peaks or groups, or they may form an effective continuum due to the influence of many closely spaced nuclear levels.

In this paper we discuss a method for correcting experimentally measured neutron activation reaction rate data for the effects of neutrons extraneous to the primary peak of a quasi-mono-energetic source. This is a pragmatic approach that relies on determinations of effective neutron spectra by the use of direct spectrum measurement information as well as reaction rates measured using reactions that are sufficiently well known that they can be treated as either primary or secondary standards for practical purposes. In Section 2 of this paper we discuss the basic formalism in considerable detail. In Section 3, we discuss the time-of-flight measurements used to obtain trial neutron spectra for the adjustment process. In Section 4, we indicate what needs to be considered so that the formalism can be implemented in practical situations. Section 5 discusses briefly our experience in applying this method to the analysis of experimental data acquired during the WPEC Subgroup 19 project. Finally, Section 6 summarises the present work and points out some strengths and weaknesses of the spectral index method.

2. Description of the Formalism

For convenience we can represent a typical differential neutron source spectrum for a quasi-monoenergetic reaction by the expression

$$\phi(E) = \phi_P(E) + \phi_{LE}(E) \tag{1}$$

where E signifies emitted source neutron energy. A neutron activation experiment will measure indirectly, by the detection of emitted decay radiations from the product nucleus, a total peak molar reaction rate F_t which can be expressed in simplest terms by the formula

$$F_t = N_A\eta \int_0^\infty \sigma(E)\phi(E)dE = N_A\eta \left[\int_0^\infty \sigma(E)\phi_P(E)dE + \int_0^\infty \sigma(E)\phi_{LE}(E)dE \right] \tag{2}$$

where N_A is Avogadro's number, $\sigma(E)$ is the energy differential reaction cross-section, $\phi(E)$ is absolute differential neutron flux, and η symbolically accounts for any other factors required to insure that the measured and calculated reaction rates are entirely comparable. Integration over the neutron spectrum is shown to be from zero to infinity without loss of generality. In practice, however, the integration is actually over an energy range (E_{min}, E_{max}) such that few if any neutrons in the considered spectrum have energies either above or below this specified range. The first term of the reaction rate accounts for the effect of neutrons in the primary

peak while the second term is due to the low energy neutrons. We can rewrite Eq. (2) in the form

$$F_t = N_A \eta \left[C_P \sigma(E_n) \int_0^\infty \phi_P(E) dE + \int_0^\infty \sigma(E) \phi_{LE}(E) dE \right] \tag{3}$$

where E_n is the effective mean energy of the primary neutron group that is given by the expression

$$E_n = \frac{\int_0^\infty E \phi_P(E) dE}{\int_0^\infty \phi_P(E) dE} \tag{4}$$

and C_P is a correction factor that can be calculated with good accuracy using knowledge of charged particle energy loss in the target, kinematics, and the neutron emission angular distribution [2]. Generally, the factor C_P does not differ very much from unity although this correction factor should be determined routinely in the analysis of neutron activation data. It accounts for the effects of a modest spread of the effective neutron energy from an essentially monoenergetic source due to kinematic effects, etc., as mentioned above. If the total neutron flux in the primary group is denoted by Φ_P, where

$$\Phi_P = \int_0^\infty \phi_P(E) dE, \tag{5}$$

Eq. (3) can then be rewritten in the form

$$F_t = N_A \eta C_P \sigma(E_n) \Phi_P \left\{ 1 + \frac{\int_0^\infty \sigma(E) \phi_{LE}(E) dE}{C_P \sigma(\langle E \rangle) \Phi_P} \right\} \tag{6}$$

The second term inside the braces {...} is the correction for non-primary (i.e., low-energy) neutrons. For convenience, we can replace the quantity in braces by the factor $1/C_{LE}$. Then we have

$$\sigma(E_n) = \frac{C_{LE} F_t}{N_A \eta C_P \Phi_P} \tag{7}$$

The factor C_{LE} will have values in the range (0,1). The correction for low energy neutrons is near unity when there is effectively no correction at all and it is considerably smaller than unity when there is a substantial correction to be considered. One way to look at this is that the measured reaction rate must be reduced to account for the low energy neutron component before a determination

of the "mono-energetic" cross-section can be made from the measured data. In practice, the effect of this correction factor may be very modest or even negligible if the total number of low energy neutrons is small compared to those in the primary group and/or if the differential cross-section $\sigma(E)$ has a high threshold energy that lies above the energies of most of these low energy secondary neutrons. However, the correction for low energy neutrons can be very large if the cross-sections are large at low energies compared to those at high energies and there are many low energy neutrons. When C_{LE} is very small, the reliability of the derived cross-section $\sigma(E_n)$ tends to be poor because the uncertainty in the correction factor C_{LE} will be substantial. In any event, in order to derive accurate cross-sections it is usually necessary to calculate this correction, and to do so requires quantitative knowledge of the shape of the neutron spectrum $\phi(E)$ as well as that of the cross-section excitation function $\sigma(E)$.

In this paper we demonstrate how the combination of knowledge of the neutron spectrum derived from time of flight, supplemented where needed by information derived from reaction rates for well-known reactions also measured in this spectrum, can be used to estimate the required low energy neutron correction factor C_{LE} through what amounts to a "bootstrap" approach. Cross-section information for well understood standard reactions, which we have chosen to call "spectral index reactions", are obtained from existing evaluated cross-section data files such as ENDF/B, JEFF, JENDL, etc. Nuclear modelling may be used to generate cross-section excitation functions when the available experimental information alone is insufficient to generate reliable evaluated differential cross-section results.

In order to develop a procedure for correcting reaction rate data for low energy neutrons it is necessary first to represent the smooth neutron spectrum function $\phi(E)$ by a discrete set of group flux parameters Φ_k such that the total neutron flux in the spectrum is given by

$$\Phi = \int_0^\infty \phi(E)dE = \sum_{k=1}^{m} \Phi_k \tag{8}$$

where

$$\Phi_k = \int_{E_{l,k}}^{E_{h,k}} \phi(E)dE \tag{9}$$

and $E_{l,k}$ and $E_{h,k}$ are the selected low and high energy limits of the k^{th} group. One of these groups should encompass the primary neutron peak while the remaining

groups span the low energy range of secondary neutrons. A corresponding group representation of the cross-section is also required. This can be accomplished in various ways. One approach is to define a group cross-section σ_k for the k^{th} group by the formula

$$\sigma_k = \sigma(\epsilon_k) \tag{10}$$

where

$$\epsilon_k = (E_{l,k} + E_{h,k})/2 \tag{11}$$

The group cross-section defined this way is the differential cross-section at the mean energy of the group. A second approach is to define the group cross-section by the formula

$$\sigma_k = [\sigma(E_{l,k}) + \sigma(E_{h,k})]/2 \tag{12}$$

The group cross-section defined this way is the average of the differential cross-section values at the two limits of the energy group interval. Finally, one can define the group cross-section by the formula

$$\sigma_k = \frac{\int_{E_{l,k}}^{E_{h,k}} \sigma(E)\phi(E)dE}{\int_{E_{l,k}}^{E_{h,k}} \phi(E)dE} \tag{13}$$

In this approach, the cross-section is obtained as the weighted average of the differential cross-section values across the group with the spectral shape used as the weighting function. These distinct methods will produce somewhat different values. If the cross-section and spectrum vary smoothly and gradually, these differences will be relatively modest. However, if the group limits are broad and the cross-section and spectra vary considerably with energy then the differences will be significant. From a practical point of view, the number of groups, group limits, and method of determining the group cross-section should be customised for each situation, and the selections should be made so that the following approximation is as good as possible:

$$\int_0^\infty \sigma(E)\phi(E)dE \approx \sum_{k=1}^{m} \sigma_k \Phi_k \tag{14}$$

The approach taken by the PTB Group [3], as well as by Fessler from IRMM [Fessler 1997], has been to use unadjusted neutron spectrum representations

determined solely by measured time-of-flight (TOF) data to correct the experimental reaction rates F_t for low energy neutrons in the determination of monoenergetic cross-sections. The PTB group measures the neutron spectrum with each activation irradiation since their accelerator based neutron source employs a cyclotron that is inherently pulsed. Fessler relied on spectral representations measured at IRMM at an earlier time [2]. Basically, there are three problems associated with this approach. First, the neutron spectra generated from accelerator bombardment of various individual targets have been shown to be quite different. Furthermore, the characteristics of the neutron spectra, particularly in the low energy regime, have been demonstrated at IRMM to vary noticeably with time and extent of target usage. This comes about due to depletion of the primary target material (e.g., deuterium or tritium) as well as from the build-up of certain neutron producing contaminants in the target. This factor is not a serious problem for the PTB experiments since spectra were measured frequently, but it certainly was a concern in FesslerŠs work at IRMM. The second problem is difficult to avoid, even in the case of repeated TOF spectrum measurements as performed at PTB. It derives from the fact that the spectrum measured at a significant distance from the source (by TOF) will differ from the spectrum actually seen by the sample located at a relatively close distance from the target. These differences result from neutron in-scattering effects and other perturbations existing in the laboratory that cannot be easily modelled. The third problem arises due to the fact that, unless rather long flight paths and detectors that are sensitive to very low energy neutrons are employed, the measured spectra will suffer from relatively poor resolution and/or inadequate representation of the neutron spectrum below several hundred keV. Nevertheless, spectral information obtained by TOF does provide an important starting point for determining low energy neutron corrections in neutron activation experiments.

Recognising these problems, we have developed a method of data correction based on spectrum adjustment that we refer to here as “spectral indexing”. Indeed, we use the group fluxes Φ_k derived judiciously from separate TOF measurements as the starting point. Since the spectra vary from target to target, and with individual targets after the passage of time, we rely on using prior spectrum representations for each incident charged-particle energy that correspond to averages of these experimental results. We then introduce a set of multiplicative group-flux parameters g_k so that the measured total reaction rate F_t can be approximated in the following manner:

$$F_t = N_A \eta \int_0^\infty \sigma(E)\phi(E)dE \approx N_A \eta \sum_{k=1}^{m} g_k \sigma_k \Phi_k \tag{15}$$

The procedure is to adjust the parameters g_k by the method of least squares [4, 5] to yield the best possible agreement between the calculated and measured reaction rates for a collection of standard "spectral index" reactions. Ideally, one would expect that parameters g_k to be fairly close to unity if the neutron spectrum were well represented and the standard cross-section values were well known. Departures of the g_k values from unity serve to reflect the imperfect state of our knowledge of these various physical parameters. Using these adjusted factors we can compensate for this imperfection and obtain reasonable values for the unknown cross-sections. Measurements that involve several standard reactions are required to obtain enough information to adjust the spectra effectively. These various reactions should have distinct thresholds and excitation-function shapes in order to play useful roles in the adjustment process.

Thus, we are confronted with the following set of equations to solve:

$$F_{t,i} \approx N_A \eta \sum_{k=1}^{m} g_k \sigma_{i,k} \Phi_k \quad (i = 1...n) \tag{16}$$

For convenience we drop the subscript t and denote the reaction rates for the various spectral index reactions simply by F_i. Furthermore, we define a set of quantities $G_{i,k}$ by the formula

$$G_{i,k} = N_A \eta \sigma_{i,k} \Phi_k \tag{17}$$

Then, Eq. (16) can be expressed as a matrix equation:

$$\mathbf{F} = \mathbf{G}\mathbf{g} \tag{18}$$

where $\mathbf{F}$ is the n-dimension vector with experimental reaction rates F_i, $\mathbf{g}$ is the m-dimension vector consisting of the adjustment parameters g_k, and $\mathbf{G}$ is the n x m matrix that contains the elements $G_{i,k}$. In the simple least squares method (SLSM), the least squares condition requires satisfying the condition

$$(\mathbf{F} - \mathbf{G}\mathbf{g})^T \mathbf{V}_F^{-1} (\mathbf{F} - \mathbf{G}\mathbf{g}) = minimum, \tag{19}$$

where $\mathbf{V}_F$ is the covariance matrix which expresses the uncertainties in the measured reaction rates, including possible correlations between the various reactions; superscript T indicates matrix transposition while superscript -1 indicates matrix inversion. Note that in this paper we use bold letters throughout to signify vectors and matrices.

A serious limitation of the simple least-squares formalism in the present context is the requirement that n exceed m, i.e., that measurements be made with more distinct spectral index reactions than the number of considered energy groups

used to represent the entire spectrum. This is may not always be feasible, so we have resorted to an application of the generalised least squares method (GLSM) [4, 5] in developing our method of spectral indexing. This mathematical technique is somewhat more complex than SLSM and requires additional information as input. To avoid confusion we summarise below the totality of information that is required to apply GLSM in the context of the present application:

(i) a set of n measured total reaction rates F_i represented by an n-dimensional vector $\mathbf{F}$;

(ii) an n x n covariance matrix $\mathbf{V}_F$ that characterises the uncertainties in $\mathbf{F}$;

(iii) a collection of group fluxes Φ_k generated from TOF measurements of the neutron spectrum;

(iv) prior estimates of the m group-flux adjustment parameters $g_{0,k}$ represented by an m-dimensional vector $\mathbf{g}_0$ (prior values $g_{0,k}$ are normally set equal to unity);

(v) an m x m covariance matrix $\mathbf{V}_0$ that characterises the estimated uncertainties in $\mathbf{g}_0$ (relatively large uncertainties are assumed, usually of the order of 30% or larger);

(vi) a collection of m group cross-section values for each of the n different spectral index reactions, namely, $\sigma_{i,k}$.

GLSM then seeks to satisfy the condition

$$[\mathbf{F}-\mathbf{F}_0-\mathbf{G}(\mathbf{g}-\mathbf{g}_0)]^T\,\mathbf{V}_F^{-1}\,[\mathbf{F}-\mathbf{F}_0-\mathbf{G}(\mathbf{g}-\mathbf{g}_0)]+ \\ \big(\mathbf{g}-\mathbf{g}_0\big)^T\mathbf{V}_0^{-1}(\mathbf{g}-\mathbf{g}_0\big) = \text{minimum}, \tag{20}$$

where the vector $\mathbf{F}_0$ consists of the n elements

$$F_{0,i}=\sum_{k=1}^{m} G_{i,k}g_{0,k}. \tag{21}$$

The quantities $F_{0,i}$ are to be interpreted as reaction rates calculated (not measured) using the prior parameters $g_{0,k}$.

The formal GLSM solution to this problem can be found in the literature [4, 5]. It is given in terms of four matrix equations, namely,

$$\mathbf{g}=\mathbf{g}_0+\mathbf{V}_0\mathbf{G}^T(\mathbf{Q}+\mathbf{V}_F)^{-1}(\mathbf{F}-\mathbf{F}_0), \tag{22}$$

$$\mathbf{Q}=\mathbf{G}\mathbf{V}_0\mathbf{G}^T \tag{23}$$

$$\mathbf{V}_g=\mathbf{V}_0-\mathbf{V}_0\mathbf{G}^T(\mathbf{Q}+\mathbf{V}_F)^{-1}\mathbf{G}\mathbf{V}_0, \tag{24}$$

$$(\chi^2)_{min}=(\mathbf{F}-\mathbf{F}_0)^T(\mathbf{Q}+\mathbf{V}_F)^{-1}(\mathbf{F}-\mathbf{F}_0). \tag{25}$$

The scalar quantity $(\chi^2)_{min}$ provides a test of "goodness of fit" for the adjusted solution vector $\mathbf{g}$. A consistent solution, i.e., one for which calculated reaction rates agree with measured ones within uncertainties, is indicated if $(\chi^2)_{min}/f < 1$. The degrees of freedom parameter is $f = n$, i.e., it equals the number of data points used for adjustment purposes.

3. Neutron Spectrum Measurements

Spectra of low energy neutrons produced by 1-, 2-, 3- and 4-MeV deuterons incident on two distinct tritiated-titanium targets having deposits of 2 mg/cm^2 Ti were measured by the time-of-flight method using a liquid scintillator detector which was positioned at 3 m from the target. The first target, GEEL-9, had experienced considerable prior deuteron bombardment while the second target, GEEL-20, was relatively new. The 7-MV IRMM Van de Graaff accelerator was operated in pulse mode with a 2.5 MHz repetition rate and a full width at half maximum of 1.5 ns, as determined from the width of the prompt gamma peak. The centroid of the prompt gamma peak seen by the detector was used to determine the arrival time of the deuteron burst at the target. The NE-213 liquid scintillator detector (Detector #4) that was used in these measurements has the following dimensions: 4-inch diameter x 1-inch thick. It had been characterised previously by C. Goddio [6] for measurements of ^{238}U(n, n'). The light-output function of this detector was determined for the critical incident neutron-energy region from 0 to 3.5 MeV, and it was smoothly joined to a measured function of a nominally identical detector to extrapolate the curve to energies up to 20 MeV. Determination of the light output function was performed experimentally by using mono-energetic neutrons and relying on the known angular distribution of the primary T(p, n)-source neutrons. The neutron response functions were analyzed using the code NRESP7 while the equivalent electron energy scale was determined by measurements with single energy gamma sources. These data were analyzed with code GRESP7. Finally, the neutron detector efficiency was determined as a function of the equivalent electron threshold energy with the code NEFF7.

Time-of-flight is measured as a difference between the deuteron arrival time at a capacitive pick-off positioned about 40 cm upstream from the target and neutron arrival at the NE-213 detector. The pick-off loop signal passes a fast Ortec VT20 pre-amplifier and an ORTEC 934 constant fraction discriminator (CFD) with a 3 ns delay. An Ortec 934 CFD is also used for the anode signal from Detector #4 with a 5 ns delay. The intrinsic time resolution of Detector #4 is 0.5 ns. This was measured using a ^{60}Co source relative to a thin plastic scintillator of 0.18 ns intrinsic time resolution. Time was measured using an Ortec 567 time-to-pulse-height converter. The ADC used was a Canberra 8015 with a fixed dead-time

(0.8 μs), and spectra were recorded with 0.35061 ns/channel. For the present work, the threshold was determined with gamma sources as 0.15(2) MeV-electron equivalent. This was determined from the pulse-height (PH) spectrum gated by the discriminator signal. The PH spectrum was derived from the dynode signal of Detector #4 using a Canberra 2020 spectroscopy amplifier with 0.5 μs shaping. In the present work, pulse-shape (PS) analysis was used to reduce gamma-ray background and to unambiguously identify the prompt gamma-peak. This was accomplished using a Canberra 2160 PS analysis module. For ease of analysis, a gate was set in the 1-d pulse shape spectrum, unlike the more sophisticated 2-d approach that uses PH versus PS matrices, as described by C. Goddio [6]. The present approach is less efficient due to the inherent mixing of neutron and gamma events in the PS signal for low-pulse-height events and the need to keep $> 95\%$ of all neutron events. Due to the difficulty of achieving good neutron-gamma pulse discrimination, and in order to investigate the contributions of in-scattered neutrons, it was decided to use a collimated detector [6] and to measure each spectrum both with and without a plug (1 m PE). The collimator did not shield the detector, contrary to the arrangement encountered in the work of [6]. The spectra were normalised using the integrated beam charge on target. The plug-subtracted spectra were compared to measurements without a collimator (bare detector measurements). To within a few percent, the measured TOF spectra were identical. The plug measurements showed that in-scatter from the collimator is important for energies just below the nominal energy. The time resolution function that was applicable to the time-of-flight measurements at Geel was defined by a combination of the pick-up loop (< 0.2 ns), the detector (0.5 ns), and the distribution of deuteron arrival times. In the present experiment, the latter component has a FWHM of 1.5 ns; however, there is also considerable tailing, typically several tens of ns. Normally, deuteron arrival times are measured periodically by time-of-flight between a silicon surface barrier detector (SBD) and the pick-up loop. The SBD detects forward-scattered deuterons that are deflected by a thin gold foil. The overall time resolution of this system is 0.2 ns. The specific angle is assured by employing a pinhole collimator in front of the SBD. The present measurements were hindered by the absence of Au foils. Therefore, the time-resolution function was deduced by subtracting the gamma-suppressed spectra from the unsuppressed TOF spectra. This enabled the prompt gamma distribution to be obtained. As demonstrated in Ref. [6] this provides an excellent measure of the beam arrival time distribution.

By comparing the (shifted and normalised) prompt-gamma distribution with the neutron peak contribution it was determined that there were no neutrons to be found with energies between 8-10 MeV and the primary neutron peak. Fourier unfolding of the spectra was used to confirm this result in a qualitative fashion.

However, an inadequate setting of the ADC time resolution (0.35 ns/ch) prevented achieving a convincing verification by this technique. This resolution was too coarse for a system with 0.6 ns resolution. Thus, oscillatory behaviour was encountered which required digital filtering and corresponding distortion of the results.

Figures 1-4 show neutron-energy spectra obtained from deuteron bombardment of metal tritide targets by the above procedures. Differences between the low energy components arising from a heavily used target (GEEL-9) and a fresh target (GEEL-20) are clearly evident. Differences in the low-energy neutron yields as a function of the deuteron energy are also evident in these plots. Averages of two spectra — one from a heavily used ("old") target and one from a relatively unused ("fresh") target — are shown in both Figs. 1 and 3. These average spectra were used to generate values for the matrix $\mathbf{G}$, as discussed above.

Fig. 5 shows the variations in the neutron spectra obtained from the heavily used target (GEEL-9) for three different incident deuteron energies. The growing importance of the low energy neutrons relative to the primary peak as a function of increased deuteron energy is apparent. This results not only from the rapidly increasing production of secondary neutrons with increasing deuteron energy but also from the declining yield of primary neutrons with increasing deuteron energy.

4. Implementation of the Formalism

Several issues have to be addressed in order to implement the formalism described in this paper in a practical manner. These are discussed in considerable detail below.

First, the group energy limits must be selected. From a mathematical point of view, the GLSM approach tends to work best if a minimal number of group intervals are established, i.e., if a limited number of free parameters are involved. One of these groups should include all the neutrons in the primary neutron peak while the remaining groups are used to describe the low energy neutron spectrum. Relegating the primary neutron peak to a single group generally presents few problems since any corrections arising from the energy spread of that peak due to typical physical effects in the experiments are normally taken care of in determining the correction factor CP mentioned above. The difficulty arises in selecting a minimal number of groups to adequately represent the low energy neutron spectrum. If the variations with energy of the spectrum and the cross-section are relatively smooth across most of the energy region encompassed by the low energy neutrons, then a good representation can be obtained by utilising relatively few groups. However, if there is considerable structure, either in the

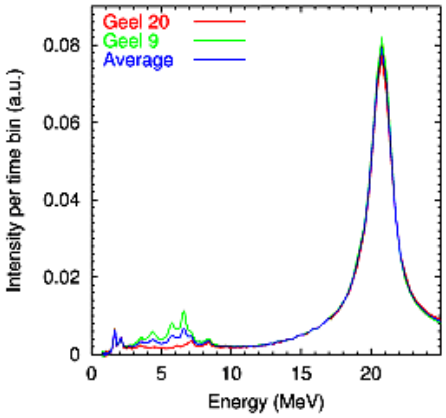

Figure 1: *Neutron spectra from GEEL-9 and GEEL-20 for 4-MeV deuterons*

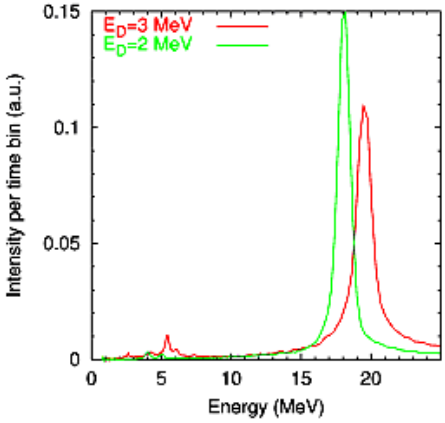

Figure 2: *Neutron spectra for 2- and 3-MeV neutrons for GEEL-9*

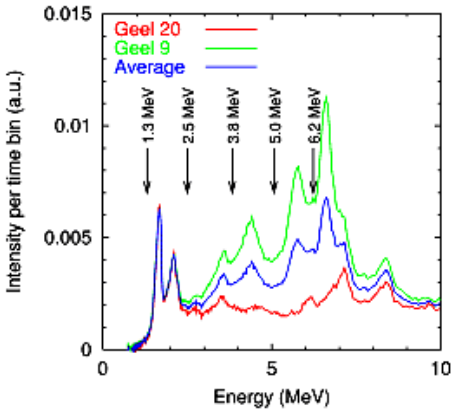

Figure 3: *Same as Fig. 1 except only the low-energy portion of spectrum is shown*

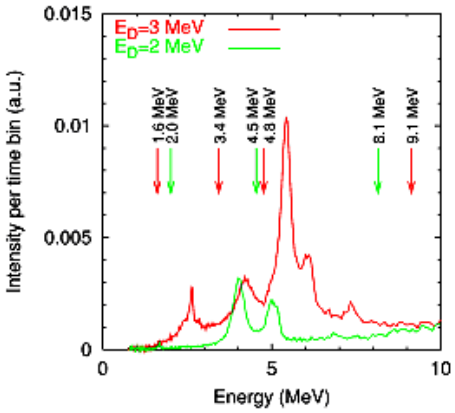

Figure 4: *Same as Fig. 2 except only the low-energy portion of spectrum is shown*

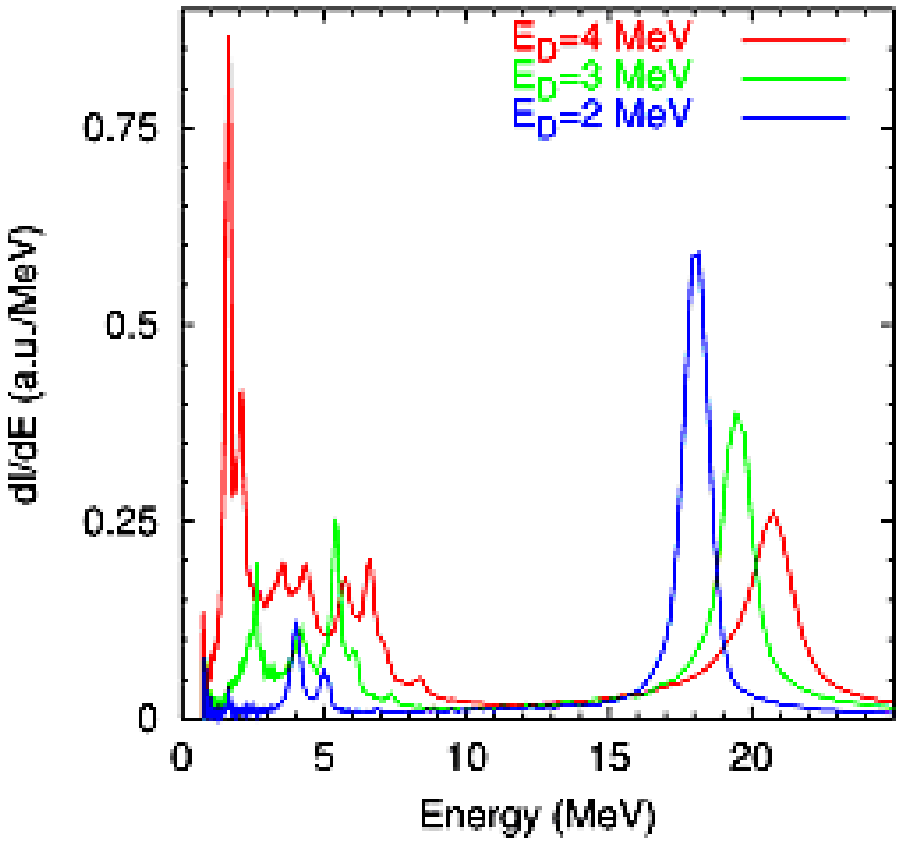

Figure 5: *Neutron spectra for GEEL-9 at three deuteron energies.*

spectrum itself or in the standard cross-sections utilised for spectral indexing, or in both, then it may be difficult to model the physical situation with just a few groups without encountering discrepancies. A considerable number of groups may be required and their limits will have to be selected carefully to enable the approximation indicated in Eq. (15) to be well satisfied by performing a least-squares determination of the spectral adjustment parameters $\mathbf{g}$. In our work, a trial and error approach was required to find compromise choices of group numbers and energy group limits that gave reasonable results in the various situations we encountered. In spite of this, we found that the quality of results obtained from this process fell somewhat short of our initial expectations, probably due to the limitations of the spectral information obtained by TOF and the spectral sensitivity properties of the selected standard reactions employed for spectral indexing. In the present application, we have utilised a maximum of 6 groups altogether so that at most 5 groups were available to represent the low-energy neutron spectra. For analytical convenience we chose to assign Group 1 to the highest-energy, primary neutrons and the remaining groups to the low-energy neutrons. Thus, the group energies decrease with increasing group number (reverse order) in this investigation. Table 1 lists the chosen energy limit for each of groups corresponding to three incident deuteron energies. These energies were selected for experiments involving accelerator production of neutrons at IRMM by means of the $^3\mathrm{H}(d,n)^4\mathrm{He}$ reaction since this neutron-source reaction was the one used for neutron activation measurements in the range 13-20 MeV. The limits are clearly tailored to the individual deuteron energies.

Second, the issue of neutron flux normalisation must be addressed. In principle, the determination of absolute neutron cross-sections requires knowledge of the absolute neutron flux. The present adjustment procedure cannot be expected to yield normalised group fluxes directly. That is the sum of these fluxes cannot be expected to add up to the total absolute neutron flux, a quantity that should be independent of the spectrum shape. We have avoided this concern, as do most experimental investigators in this field, by performing reaction rate ratio measurements relative to primary or secondary standards or to calibrated neutron fluence monitors. If the mono-energetic reaction rate, corrected for low energy neutrons (C_{LE}) and primary peak perturbations (C_P), is denoted by F_P, and the unknown and standard cross-sections at energy E_n are denoted by σ_x and σ_s, respectively, then

$$\sigma_x(E_n) = (F_{P_x}/F_{P_s})\sigma_s(E_n), \tag{26}$$

where E_n is obtained as indicated in Eq. (4). This technique is described in more detail in [7]. Briefly, we note that once a set of group neutron fluxes adjustment parameters g has been determined by GLSM, this set should be used consistently

Table 1: *Neutron-group energy definitions for three incident deuteron energies*

Group	$E_D = 4$ MeV	$E_D = 3$ MeV	$E_D = 2$ MeV
	Range (MeV)	Range (MeV)	Range (MeV)
1	>10.16	>9.13	>8.14
2	6.23 – 10.16	4.76 – 9.13	4.54 – 8.14
3	5.07 – 6.23	3.43 – 4.76	2.01 – 4.54
4	3.83 – 5.07	1.61 – 3.43	
5	2.50 – 3.83		
6	1.31 – 2.50		

for all reaction rate calculations thereby avoiding the need for knowledge of absolute neutron fluxes. Third, the present formalism requires that we provide a covariance matrix $\mathbf{V}_F$ for the measured reaction rates as well as one for the prior estimates of group flux adjustment parameters $\mathbf{g}_0$, namely, $\mathbf{V}_0$. To simplify the implementation of the present method, without much apparent sacrifice of its effectiveness, we assume that both of these matrices are diagonal. This leaves us only with the task of estimating the uncertainties in $\mathbf{F}$ and $\mathbf{g}_0$. It would appear at first glance that the uncertainties due to the reaction rates could be determined solely from the experimentally determined raw reaction rate data. Then, the diagonal elements of the covariance matrix $\mathbf{V}_F$ should be given by

$$(\mathbf{V}_F)_{i,i} = f_{i,exp}^2 F_i^2, \tag{27}$$

where $f_{i,exp}$ is the fractional experimental error associated with measuring the i^{th} reaction rate. However, there are other uncertainties that should be considered in generating $\mathbf{V}_F$. Those uncertainties associated with the spectral index cross-sections that form the elements of matrix $\mathbf{G}$ are relatively modest. Nevertheless, it is important that they be included in some fashion in the GLSM analysis. Furthermore, uncertainties in the group flux parameters Φ_k estimated from TOF experiments should be considered since they also influence the determination of the elements of $\mathbf{G}$. Inclusion of the additional uncertainties from these two sources can be accomplished by applying a trick that, while not completely rigourous, usually yields adequate results. This trick involves adding additional terms to the variances of the matrix $\mathbf{V}_F$. The procedure for doing this depends on assumptions related to correlations between the various flux and cross-section parameters. In the present investigation, fluxes and cross-sections have been assumed in all cases to be uncorrelated. If, in addition, we assume that all the group cross-sections for the i^{th} reaction have a fixed and fully correlated fractional error $f_{\sigma,i}$, and that the

Table 2: *Prior values used for the group parameters and their errors in this work*

Group	4 MeV		3 MeV		2 MeV	
	g_0	$\Delta g_0/g_0$	g_0	$\Delta g_0/g_0$	g_0	$\Delta g_0/g_0$
1	1	0	1	0	1	0
2	1	0.33	0.752	0.25	0.75	0.25
3	1	0.44	0.646	0.36	0.649	0.36
4	1	0.55	0.695	0.31		
5	1	0.24				
6	1	0.13				

groups fluxes also have equal fractional errors f_Φ that are fully correlated, we are led to the following simple extension of Eq. (27)

$$(\mathbf{V}_F)_{i,i} \approx (f_{i,exp}^2 + f_{\sigma,i}^2 + f_\Phi^2)F_i^2. \tag{28}$$

However, if the cross-section and group flux errors are assumed to be uncorrelated, then from Eq. (16) we are led to the expression

$$(\mathbf{V}_F)_{i,i} \approx f_{i,exp}^2 F_i^2 + N_A^2\eta^2 \sum_{k=1}^{m} (f_{\Phi_k}^2 + f_{\sigma_{i,k}}^2) g_{0,k}^2 \sigma_{i,k}^2 \Phi_k^2 \tag{29}$$

for the variances, where f_{Φ_k} is the fractional error in Φ_k and $f_{\sigma_{i,k}}$ is the fractional error in $\sigma_{i,k}$. Note that elements of the prior parameter vector $\mathbf{g}_0$ are used in this estimation process since the final values that will emerge for elements of the solution vector $\mathbf{g}$ are unknown initially. As indicated above, we generally assume that all the elements of $\mathbf{g}_0$ are unity. This is equivalent to assuming that the best initial guess for the spectrum group values are those generated directly from the spectrum data derived via TOF measurements, averaged over various target conditions (new vs. old). Since the adjustments to certain group spectral parameters g_k required to achieve consistent results for the standard spectral index reactions may be substantial, it is important that the assumed prior errors represented by the matrix $\mathbf{V}_0$ be sufficiently large to allow adequate freedom in the adjustment process. As mentioned above, we have determined that one should normally assume errors on the order of the order of 30% for $\mathbf{g}_0$ in order to insure that included spectral-index data have a meaningful impact on the GLSM determination of $\mathbf{g}$. Table 2 gives the fractional errors actually used in the present investigation. Fourth, a set of standard reactions must be selected for use in the spectral index adjustment process. The choice of reactions inevitably will be a

Table 3: *Reactions used for spectral index purposes. E_T is the reaction threshold energy, E_γ the gamma-ray energy of the product activity and σ the cross-section.*

Reaction	E_T[a] (MeV)	$T^b_{1/2}$	E_γ (MeV)	σ Origin
^{59}Co$(n,2n)^{58}$Co	10.63	70.86 D	0.811	ENDF/B-6
^{93}Nb$(n,2n)^{92m}$Nb	9.86	10.15 D	0.934	Wagner+
^{27}Al$(n,\alpha)^{24}$Na	3.25	14.96 H	1.369, 2.754	Wagner+
^{56}Fe$(n,p)^{56}$Mn	2.97	2.58 H	0.847	ENDF/B-6
^{27}Al$(n,p)^{27}$Mg	1.90	9.46 M	0.843, 1.014	ENDF/B-6
^{58}Ni$(n,p)^{58}$Co	0	70.86 D	0.811	ENDF/B-6
^{115}In$(n,n'\gamma)^{115m}$In	0.34	4.49 H	0.336	ENDF/B-6

[a] Qtool module LANL-T2 website [10]
[b] Evaluated Nuclear Structure Data [11].

compromise that takes into consideration the following factors: reaction thresholds (various); reaction excitation function shapes (various); reaction product half-lives; convenient materials (foils and powders from which samples can be made easily); isotopic abundance (high for more effective use of the material); decay products (conveniently measured); availability of material (e.g., cost); well characterised cross-section excitation functions. For practical reasons, we need to limit the number of spectral index reactions utilised in order to prevent the irradiated dosimeter packets from becoming too thick. Otherwise, the corrections for geometric effects and neutron absorption would become excessive leading to a new set of concerns. For the present work, we have chosen the seven standard reactions listed in Table 3 for spectral index purposes. These reactions all involve the use of metallic foils that can be made quite thin. Furthermore, these materials are relatively inexpensive even for chemically pure samples. Table 3 also lists threshold energies, half lives, decay gamma rays, and origin of evaluated standard cross-sections for the spectral index reactions [8, 9]. These cross-sections are plotted in Fig. 6. To be useful for spectrum adjustment purposes, the excitation function data illustrated in Fig. 6 must be converted to group cross-sections according to the procedures discussed above. The results of this exercise appear in Tables 4-6 and Figs. 7-9. The figures are particularly useful because they provide the reader with a visual sense of the relative importance of the various reactions in the adjustment of individual spectrum group parameters g_k.

For present purposes, it is assumed that a particular cross-section is uncertain by a fixed amount across all the groups for a given incident deuteron energy. That

Table 4: *Group cross-sections (in mb) for incident deuterons of 4 MeV*

Reaction	Group 1	Group 2	Group 3	Group 4
^{59}Co$(n,2n)^{58}$Co	825.55			
^{93}Nb$(n,2n)^{92m}$Nb	292.75	1.107		
^{27}Al$(n,\alpha)^{24}$Na	32.01	5.742	0.072	
^{56}Fe$(n,p)^{56}$Mn	42.60	6.472	0.774	0.030
^{27}Al$(n,p)^{27}$Mg	26.76	11.828	4.099	1.603
^{58}Ni$(n,p)^{58}$Co	71.41	112.873	53.560	50.792
^{115}In$(n,n'\gamma)^{115m}$In	54.93	58.579	34.433	41.645
	Group 4	Group 5		
^{27}Al$(n,p)^{27}$Mg	0.575			
^{58}Ni$(n,p)^{58}$Co	38.364	14.997		
^{115}In$(n,n'\gamma)^{115m}$In	59.508	97.140		

Table 5: *Group cross-sections (in mb) for incident deuterons of 3 MeV*

Reaction	Group 1	Group 2	Group 3	Group 4
^{59}Co$(n,2n)^{58}$Co	876.23			
^{93}Nb$(n,2n)^{92m}$Nb	344.16			
^{27}Al$(n,\alpha)^{24}$Na	43.15	1.717		
^{56}Fe$(n,p)^{56}$Mn	50.97	2.972	0.007	
^{27}Al$(n,p)^{27}$Mg	30.69	9.938	1.007	0.088
^{58}Ni$(n,p)^{58}$Co	82.39	123.57	37.12	16.55
^{115}In$(n,n'\gamma)^{115m}$In	54.69	76.92	33.13	42.66

Table 6: *Group cross-sections (in mb) for incident deuterons of 2 MeV*

Reaction	Group 1	Group 2	Group
^{59}Co$(n,2n)^{58}$Co	843.47		
^{93}Nb$(n,2n)^{92m}$Nb	397.64		
^{27}Al$(n,\alpha)^{24}$Na	62.075	0.338	
^{56}Fe$(n,p)^{56}$Mn	61.296	0.607	0.001
^{27}Al$(n,p)^{27}$Mg	40.455	2.020	0.493
^{58}Ni$(n,p)^{58}$Co	111.420	28.646	24.090
^{115}In$(n,n'\gamma)^{115m}$In	54.400	18.550	24.892

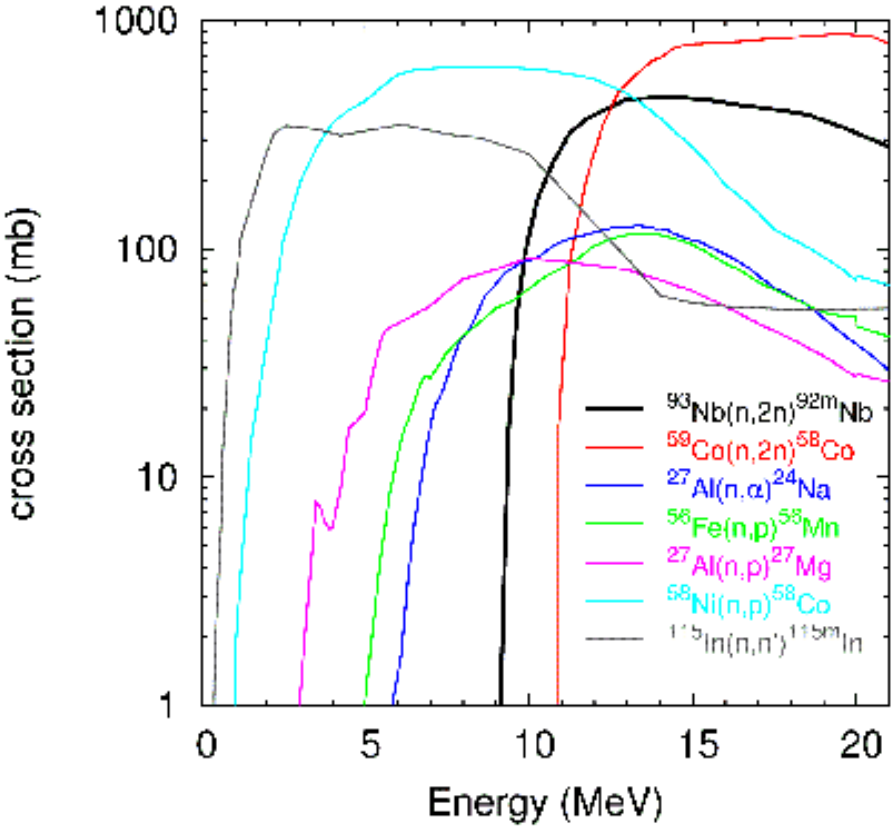

Figure 6: *Plots of selected spectral index cross-section excitation functions*

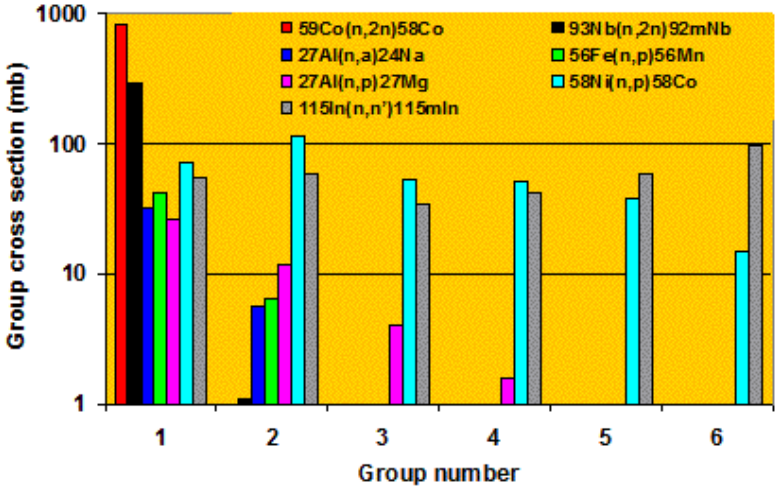

Figure 7: *Group cross-sections for incident deuterons of 4 MeV*

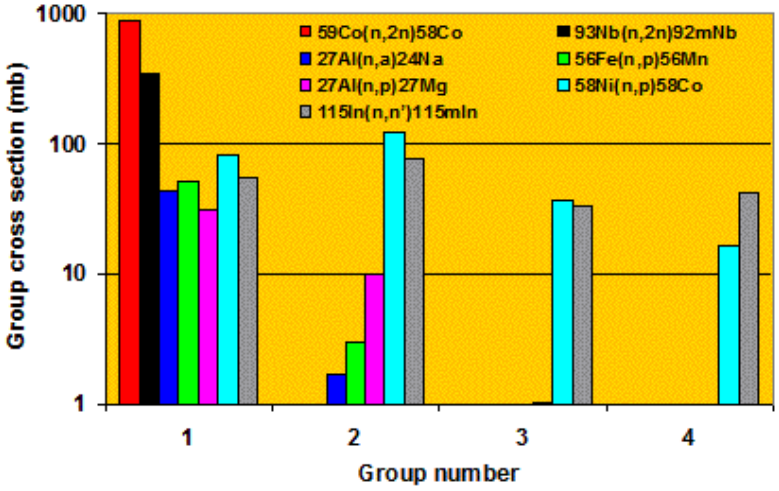

Figure 8: *Group cross-sections for incident deuterons of 3 MeV*

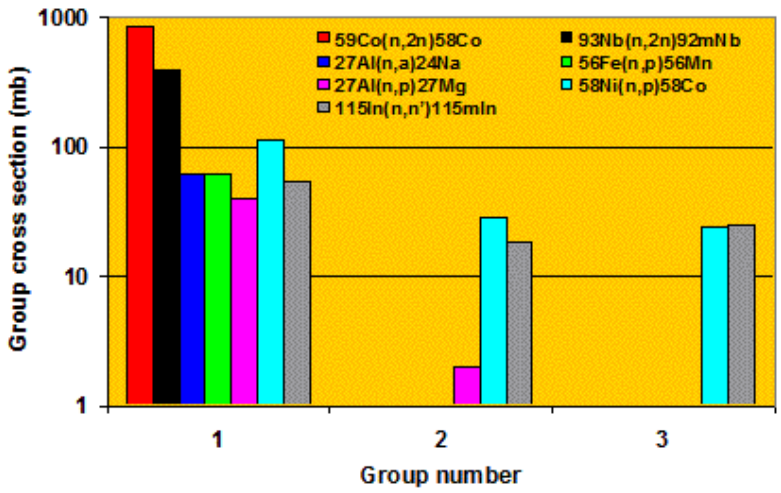

Figure 9: *Group cross-sections for incident deuterons of 2 MeV*

uncertainty is a compromise value that best represents the estimated uncertainty in the region where the cross-section strength contributes most to the observed reaction rate. Thus, we have assumed that the uncertainties are those given in Table 7.

5. Results from GLSM Analysis

The procedure for correcting data for low energy neutrons described in this paper has been applied to the analysis of neutron activation data acquired from measurements at IRMM for the WPEC Subgroup 19 project. There are various ways to assess the viability of the method. Perhaps the best of these is to compare values of the correction factor C_{LE} obtained for the spectral index reactions corresponding to various reactions, targets, and experimental conditions. Figs. 10 and 11 are samples of these results. It is evident that for the higher threshold reactions where the values of C_{LE} are near to unity that the variations in determined values of the corrections are modest on a percentage basis. However, when the corrections are large, i.e., for small C_{LE}, then the scatter in correction values on a percentage basis are quite substantial, thus leading to the need for a relatively large error assignment to the derived cross-sections to account for this effect.

We have established that the correction method described and illustrated in this

Table 7: *Assumed uncertainties (in %) for spectral-index group cross-sections*

Reaction	$E_D = 4$ (MeV)	$E_D = 3$ (MeV)	$E_D = 2$ (MeV)
^{59}Co$(n, 2n)^{58}$Co	5.6	3.4	2.6
^{93}Nb$(n, 2n)^{92m}$Nb	5	3	2
^{27}Al$(n, \alpha)^{24}$Na	5.1	3	2.4
^{56}Fe$(n, p)^{56}$Mn	6	6	6
^{27}Al$(n, p)^{27}$Mg	10	10	8
^{58}Ni$(n, p)^{58}$Co	10	10	10
^{115}In$(n, n'\gamma)^{115m}$In	6	5	6

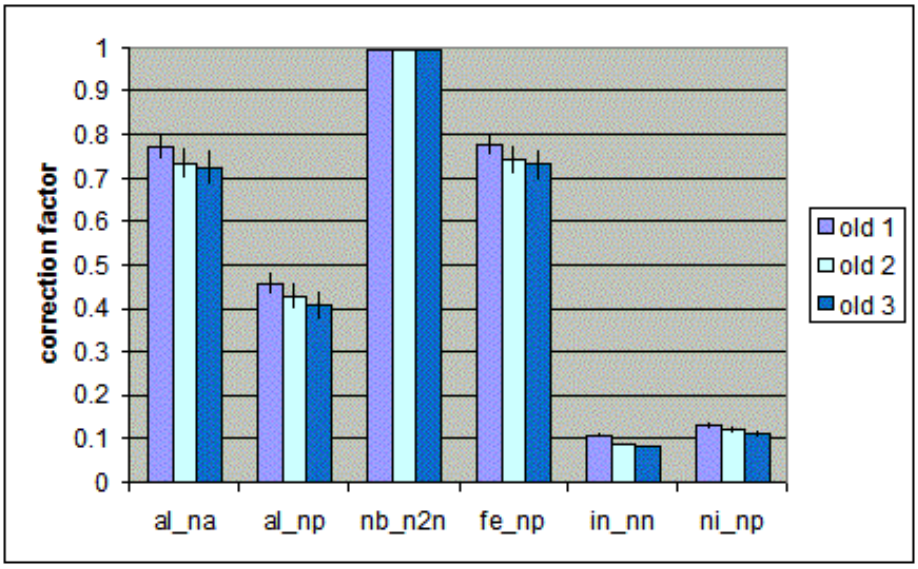

Figure 10: *Comparison of correction factors C_{LE} for well-used ("old") target*

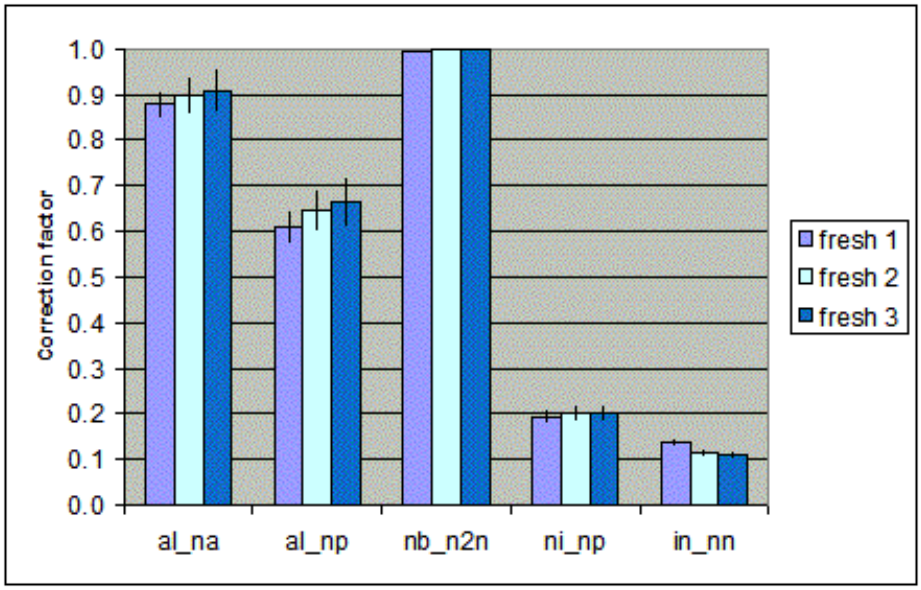

Figure 11: *Comparison of correction factors CLE for new ("fresh") target*

paper is fundamentally sound. It appears that what is required to permit even more reliable quantitative results to be obtained by the procedure is to begin with more accurate representations of the neutron spectra involved in these measurements, both in energy and angular detail. These measurements need to be made with a long flight path and thus with resolutions superior to the existing data set. Better knowledge of the spectra below 2-3 MeV would be especially helpful. In fact, such a spectrum measurement programme has already been initiated in collaboration with a group at the Ohio University Edwards Accelerator Laboratory, utilising the beam-swinger TOF system at this laboratory. Completion of this measurement and data analysis programme is pending. Spectral adjustments to the group cross-sections would still be required even with these new data in order to compensate for persistent differences between the spectra measured by TOF and the effective spectra experienced by the sample packets during irradiations performed close to the accelerator target. However, it is anticipated that these adjustments would not have to be as large as those encountered in the initial attempts mentioned in the present work, thus leading to greater reliability of the GLSM analysis procedure. Better knowledge of the neutron spectra and their intrinsic details would also enable refinements in selecting group limits compared to the current choices. Furthermore, it would be useful to add a few additional spectral index reactions

that could offer improved sensitivity to the low energy neutrons in certain specific groups than is provided by the set indicated in Table 3. In particular, it would be useful to incorporate additional reactions with thresholds in the energy region from 3-6 MeV.

6. Summary

In order to obtain reliable mono-energetic neutron cross-sections, particularly at energies above 10 MeV, and in instances where the reactions studied have relatively low thresholds, it is very important to correct the raw experimental reaction rate data for the influence of low energy neutrons. In the present investigation this has been accomplished in two stages. First, neutron spectra from the charged-particle-induced source reactions were measured by neutron TOF. Second, these prior spectra were adjusted, following conversion to group representations, by the method of spectral indexing with the aid of GLSM analysis. Reaction rate data for several well-known reactions with various threshold energies were employed in this process. It was demonstrated that even though these corrections can be quite large, it is still possible to obtain fairly reliable qualitative results provided that the correction process is carried out in a rigourous manner using reasonable prior spectrum estimates and accurate spectral index cross-section values. In general, however, the method currently gives the most reliable quantitative results in situations where there are relatively low numbers of low energy neutrons and the reactions in question have sufficiently high thresholds. Given our contemporary limited knowledge of the detailed structure of the neutron spectra, we have found that it is very important to assign large uncertainties to the prior values of the adjustment parameters so that the spectral index data can have an impact on their adjustment. Finally, applications of this method would benefit greatly from more accurate determinations, by direct methods such as time-of-flight with improved resolution, of low energy secondary neutron spectra and from the inclusion of some additional standard spectral index reactions, particular those with thresholds in the 3-6 MeV range.

Acknowledgements We are indebted to the European Commission, Joint Research Centre, and to the US Department of Energy, Science Programmes, for the financial support and encouragement that made it possible to carry out this work.

[1] M. Drosg, Nuclear Science and Engineering 106, 279 (1990).

[2] A. Fessler, Activation cross-sections and Isomeric cross-section Ratios in Neutron Induced Reactions on Cr-, Fe-, and Ni-Isotopes in the Energy

Range 9 to 21 MeV, Thesis, Department of Mathematics and Natural Science Studies, University of Cologne, Cologne, Germany (1997).

[3] S. Cabral, G. Boerker, H. Klein, and W. Mannhart, Nuclear Science and Engineering 106, 308 (1990).

[4] D.L. Smith, Probability, Statistics, and Data Uncertainties in Nuclear Science and Technology, American Nuclear Society, LaGrange Park, IL, USA (1991).

[5] D.L. Smith, "A Least-squares Computational Tool Kit", Report ANL/NDM-128, Argonne National Laboratory (1993).

[6] C. Goddio, Inelastic scattering of ^{238}U with the (n,n') technique, Thesis, U.Gent, Belgium, unpublished (1999).

[7] A. Fessler, A.J.M Plompen, D.L. Smith, J.W. Meadows, and Y. Ikeda, Nuclear Science and Engineering 134, 171 (2000).

[8] Evaluated Nuclear Data File, ENDF/B-6, National Nuclear Data Center, Brookhaven National Laboratory, NY, USA (2001).

[9] M. Wagner, H. Vonach, A. Pavlik, B. Strohmaier, S. Tagesen, and J. Martinez-Rico, Physics Data 13-5, 34 (1990).

[10] Internet Utility Program "Qtool" for on-line computation of reaction Q-values and thresholds, T-16 Division, Los Alamos National Laboratory, Los Alamos, NM, USA. Internet: http://t2.lanl.gov (2003).

[11] Evaluated Nuclear Structure Data File, ENSDF, National Nuclear Data Center, Brookhaven National Laboratory, NY, USA (2001).

Part C

Numerical Data and Graphical Comparison of Measured Data with Recent Evaluations and Model Calculations*

*Tables and graphs have been prepared by V. Semkova under EC-JRC-IRMM Service Contract Nr. 10174.

1. Measured data in tabular form

All numerical data for cross-sections measured by the participants are presented in tabular form. The reports and publications where these numerical results have appeared before can be found in Tab. 2.1 of the summary report (Part A).

Table 1.1: *Results obtained at 14.60 ± 0.15 MeV neutron energy*

^{19}F$(n,p)^{19}$O			
E_n(MeV)	σ(mb)	E_n(MeV)	σ(mb)
16.064±0.062	14.55±0.78	17.026±0.040	12.27±0.72
17.777±0.032	9.85±0.56	19.101±0.012	8.37±0.50
20.310±0.010	7.43±0.67		
14.60±0.15	21.5±1.1		
^{23}Na$(n,p)^{23}$Ne			
E_n(MeV)	σ(mb)	E_n(MeV)	σ(mb)
16.127±0.062	35.8±1.67	17.119±0.041	31.16±2.1
17.887±0.032	26.17±1.67	19.174±0.011	24.62±1.98
20.463±0.010	17.27±1.59		
^{23}Na$(n,\alpha)^{20}$F			
E_n(MeV)	σ(mb)	E_n(MeV)	σ(mb)
16.127±0.062	102.11±4.81	17.119±0.041	88.79±6.32
17.887±0.032	65.91±3.87	19.174±0.011	41.24±3.44
20.463±0.010	27.37±2.28		
^{25}Mg$(n,p)^{25}$Na			
E_n(MeV)	σ(mb)	E_n(MeV)	σ(mb)
16.083±0.062	60.95±5.00	17.053±0.040	58.19±5.33
17.810±0.032	43.95±3.93	19.142±0.011	36.13±3.41
20.353±0.010	28.16±3.24		
^{27}Al$(n,p)^{27}$Mg			
E_n(MeV)	σ(mb)	E_n(MeV)	σ(mb)
16.010±0.061	56.27±1.92	16.947±0.041	48.08±1.65
17.680±0.032	41.17±1.43	18.978±0.011	37.60±1.82
20.171±0.010	31.56±2.10		

Table 1.1: *Results obtained at 14.60 ± 0.15 MeV neutron energy*

^{28}Si$(n,p)^{28}$Al			
E_n(MeV)	σ(mb)	E_n(MeV)	σ(mb)
7.6±0.2	202±28	9.3±0.2	213±30
10.3±0.2	244±31	11.2±0.2	260±33
12.5±0.2	253±35	14.7±0.2	239±30
17.025±0.040	176.71±9.41	17.776±0.032	149.97±8.76
19.097±0.011	105.32±6.87	20.303±0.010	93.92±9.68
^{29}Si$(n,p)^{29}$Al			
E_n(MeV)	σ(mb)	E_n(MeV)	σ(mb)
16.047±0.062	133.22±5.57	17.004±0.041	117.99±5.95
17.749±0.032	96.41±5.17	19.066±0.011	87.49±5.99
20.272±0.010	62.81±6.31		
^{29}Si$(n,x)^{28}$Al			
E_n(MeV)	σ(mb)	E_n(MeV)	σ(mb)
16.047±0.062	59.3±7.14	17.004±0.041	105.72±7.02
17.749±0.032	151.63±8.41	19.066±0.011	208.58±13.53
20.272±0.010	228.58±17.94		
^{31}P$(n,\alpha)^{28}$Al			
E_n(MeV)	σ(mb)	E_n(MeV)	σ(mb)
16.044±0.062	107.07±5.46	16.998±0.041	95.73±5.53
17.744±0.032	72.5±3.98	19.058±0.011	51.52±3.51
20.261±0.010	34.29±3.10		
14.60±0.15	135.8±7.0		
^{35}Cl$(n,2n)^{34m}$Cl			
E_n(MeV)	σ(mb)	E_n(MeV)	σ(mb)
16.124±0.062	18.22±1.55	17.112±0.040	24.57±1.81
17.879±0.032	30.42±2.23	19.226±0.011	33.56±2.7
20.450±0.010	32.81±3.31		
^{37}Cl$(n,p)^{37}$S			
E_n(MeV)	σ(mb)	E_n(MeV)	σ(mb)
16.124±0.062	25.5±1.98	17.112±0.040	21.05±2.02
17.879±0.032	19.88±1.47	19.226±0.011	14.89±1.26
20.450±0.010	11.11±1.14		

Table 1.1: *Results obtained at 14.60 ± 0.15 MeV neutron energy*

^{45}Sc$(n,\alpha)^{42}$K			
E_n(MeV)	σ(mb)	E_n(MeV)	σ(mb)
11.68±0.20	44.7±5.6		
^{46}Ti$(n,p)^{46m}$Sc			
E_n(MeV)	σ(mb)	E_n(MeV)	σ(mb)
16.089±0.062	44.11±2.74	17.065±0.040	36.94±3.04
17.823±0.032	33.92±3.07	19.154±0.011	32.95±3.22
20.369±0.010	29.21±2.87		
^{50}Ti$(n,p)^{50}$Sc			
E_n(MeV)	σ(mb)	E_n(MeV)	σ(mb)
16.089±0.062	15.96±1.19	17.065±0.040	18.14±1.43
17.823±0.032	18.83±1.42	19.154±0.011	16.97±1.36
20.369±0.010	14.03±1.31		
14.60±0.15	13.28±0.82		
^{51}V$(n,p)^{51}$Ti			
E_n(MeV)	σ(mb)	E_n(MeV)	σ(mb)
9.92±0.20	25.7±4.4		
15.0±0.2	26±2	16.1±0.2	25±2
17.028±0.04	26.22±1.35	17.777±0.032	23.63±1.07
19.101±0.011	17.90±1.09	20.313±0.010	13.55±1.02
^{51}V$(n,\alpha)^{48}$Sc			
E_n(MeV)	σ(mb)	E_n(MeV)	σ(mb)
11.7±0.2	8.3±0.8	13.4±0.1	14.1±1.2
13.9±0.2	15.4±1.1	14.3±0.2	14.2±1.2
15.0±0.2	18.2±1.7	16.2±0.2	19.8±1.8
18.0±0.1	21.1±1.8	19.3±0.1	19.8±1.8
20.5±0.1	14.6±1.6		
^{nat}V$(n,x\alpha)^{47}$Sc			
E_n(MeV)	σ(mb)	E_n(MeV)	σ(mb)
11.7±0.2	0.055±0.005	13.4±0.1	0.094±0.010
13.9±0.2	0.086±0.005	14.3±0.2	0.089±0.006
15.0±0.2	0.14±0.01	16.2±0.2	0.40±0.02
18.0±0.1	4.0±0.2	19.3±0.1	10.8±0.6
20.5±0.1	17.3±1.3		

Table 1.1: *Results obtained at 14.60 ± 0.15 MeV neutron energy*

^{50}Cr$(n,x)^{49}$V			
E_n(MeV)	σ(mb)	E_n(MeV)	σ(mb)
14.25±0.20	350.5±62.1	17.20±0.25	626.1±78.9
18.80±0.30	699.2±77.0	19.00±0.32	680±92.1
^{52}Cr$(n,2n)^{51}$Cr			
E_n(MeV)	σ(mb)	E_n(MeV)	σ(mb)
14.25±0.20	330.3±17.0	17.20±0.25	591.0±29.1
18.80±0.30	621.9±31.1	19.40±40.3	637.4±33.2
^{52}Cr$(n,p)^{52}$V			
E_n(MeV)	σ(mb)	E_n(MeV)	σ(mb)
9.31±0.20	50.8±3.5	10.33±0.22	55.1±3.6
11.57±0.24	65.3±3.9	12.27±0.26	70.7±4.4
13.71±0.25	88.2±5.6	15.01±0.25	82.9±4.1
15.95±0.25	74.7±3.6	16.02±0.25	79.6±3.9
16.99±0.20	65.8±4.3	17.54±0.30	59.3±3.7
17.73±0.25	58.3±4.1	17.80±0.30	58.9±3.2
18.73±0.35	45.5±2.7	19.04±0.25	46.6±3.1
19.70±0.40	34.2±1.7	20.24±0.25	28.8±2.1
21.70±0.50	27.1±2.6		
16.02±0.25	76.0±3.8	16.99±0.20	61.7±4.1
17.73±0.25	57.4±3.2	19.04±0.25	40.5±2.7
20.24±0.25	28.3±2.6		
^{53}Cr$(n,p)^{53}$V			
E_n(MeV)	σ(mb)	E_n(MeV)	σ(mb)
11.57±0.24	28.3±6.0	12.27±0.26	36.4±5.7
13.71±0.25	48.9±6.0	15.01±0.25	46.4±4.3
15.95±0.25	42.3±3.5	16.02±0.25	48.4±2.9
16.99±0.20	45.8±4.3	17.73±025	45.7±3.4
17.80±0.30	40.5±5.2	18.73±0.35	30.5±2.8
19.04±0.25	35.2±2.8	19.70±0.40	19.7±2.2
20.24±0.25	16.8±1.3	21.70±0.50	15.4±2.3
16.02±0.25	49.2±3.6	16.99±0.20	43.9±5.6
17.73±0.25	41.2±5.0	19.04±0.25	28.0±3.1
20.24±0.25	20.0±2.1		

Table 1.1: *Results obtained at 14.60 ± 0.15 MeV neutron energy*

^{53}Cr$(n,x)^{52}$V			
E_n(MeV)	σ(mb)	E_n(MeV)	σ(mb)
16.02±0.25	26.1±2.1	16.99±0.20	55.3±4.2
17.73±0.25	70.9±5.0	19.04±0.25	77.7±5.5
20.24±0.25	78.1±5.8		
^{54}Cr$(n,p)^{54}$V			
E_n(MeV)	σ(mb)	E_n(MeV)	σ(mb)
16.02±0.25	22.4±1.7	16.99±0.20	26.3±2.0
17.73±0.25	27.1±2.1	19.04±0.25	21.1±1.8
20.24±0.25	14.3±1.5		
14.60±0.15	18.0±3.3		
^{54}Cr$(n,\alpha)^{51}$Ti			
E_n(MeV)	σ(mb)	E_n(MeV)	σ(mb)
16.02±0.25	14.1±1.2	16.99±0.20	14.3±1.4
17.73±0.25	14.3±1.3	19.04±0.25	10.3±0.9
20.24±0.25	6.1±0.7		
^{54}Cr$(n,x)^{53}$V			
E_n(MeV)	σ(mb)	E_n(MeV)	σ(mb)
16.02±0.25	6.5±0.6	16.99±0.20	15.0±1.6
17.73±0.25	22.5±2.3	19.04±0.25	35.3±2.5
20.24±0.25	32.5±3.0		
^{55}Mn$(n,\alpha)^{52}$V			
E_n(MeV)	σ(mb)	E_n(MeV)	σ(mb)
16.065±0.062	22.22±1.38	17.028±0.040	19.64±1.21
17.777±0.032	17.64±1.09	19.101±0.011	13.33±0.94
20.313±0.010	8.44±0.73		
^{54}Fe$(n,x)^{52}$Mn			
E_n(MeV)	σ(mb)	E_n(MeV)	σ(mb)
16.05±0.25	0.02±0.01	16.89±0.30	0.05±0.01
17.82±0.30	0.19±0.02	19.14±0.35	0.26±0.03
20.35±0.40	0.34±0.03		
^{54}Fe$(n,x)^{52m,g}$Mn			
E_n(MeV)	σ(mb)	E_n(MeV)	σ(mb)
16.05±0.30	0.00±0.65	19.15±0.40	0.43±0.16
20.36±0.50	0.46±0.11		

Table 1.1: *Results obtained at 14.60 ± 0.15 MeV neutron energy*

^{54}Fe$(n,2n)^{53}$Fe			
E_n(MeV)	σ(mb)	E_n(MeV)	σ(mb)
15.22±0.22	22.6±2.0	15.64±0.27	26.6±2.0
16.07±0.20	39.1±3.0	16.51±0.30	48.2±3.7
17.06±0.22	61.1±4.6	17.54±0.29	63.1±5.2
17.82±0.25	71.4±6.2	17.91±0.30	69.4±6.9
18.21±0.40	72.6±4.8	18.30±0.32	75.6±4.9
19.15±0.30	81.4±7.7	20.36±0.35	88.2±7.2
^{54}Fe$(n,2n)^{53m,g}$Fe			
E_n(MeV)	σ(mb)	E_n(MeV)	σ(mb)
18.87±0.37	0.004±0.001	19.15±0.40	0.006±0.002
20.08±0.40	0.013±0.003	20.36±0.50	0.011±0.003
20.90±0.50	0.016±0.004		
^{56}Fe$(n,p)^{56}$Mn			
E_n(MeV)	σ(mb)	E_n(MeV)	σ(mb)
16.044±0.062	89.55±3.77	17.744±0.032	65.23±2.87
19.058±0.011	49.26±3.21	20.261±0.010	44.42±3.26
^{57}Fe$(n,x)^{56}$Mn			
E_n(MeV)	σ(mb)	E_n(MeV)	σ(mb)
16.044±0.062	29.09±2.79	17.744±0.032	65.97±3.5
19.058±0.011	93.22±5.32	20.261±0.010	98.17±7.56
^{57}Fe$(n,p)^{57}$Mn			
E_n(MeV)	σ(mb)	E_n(MeV)	σ(mb)
16.067±0.062	41.12±17.76	17.032±0.040	41.64±18.12
17.778±0.032	35.80±15.57	19.107±0.011	26.82±11.69
20.317±0.010	20.53± 9.00		
^{59}Co$(n,2n)^{58}$Co			
E_n(MeV)	σ(mb)	E_n(MeV)	σ(mb)
13.32±0.25	614±36	14.81±0.17	770±26
15.27±0.16	787±44	15.56±0.19	841±30
15.68±0.18	800±28	16.26±0.20	808±31
17.03±0.17	853±33	17.98±0.06	869±45
18.36±0.15	889±70	19.28±0.09	910±47
19.94±0.09	915±45	20.35±0.08	900±50

Table 1.1: *Results obtained at 14.60 ± 0.15 MeV neutron energy*

^{59}Co$(n,2n)^{58m,g}$Co			
E_n(MeV)	Isomerratio	E_n(MeV)	Isomerratio
15.27±0.16	0.68±0.06	15.56±0.19	0.66±0.05
17.03±0.17	0.68±0.06	17.98±0.06	0.65±0.06
19.28±0.09	0.69±0.05		
^{59}Co$(n,2n)^{58m}$Co			
E_n(MeV)	σ(mb)	E_n(MeV)	σ(mb)
15.27±0.16	535±56	15.56±0.19	555±50
17.03±0.17	580±61	17.98±0.06	564±64
19.28±0.09	628±60		
^{59}Co$(n,p)^{59}$Fe			
E_n(MeV)	σ(mb)	E_n(MeV)	σ(mb)
14.81±0.16	46.8±2.8	15.27±0.16	45.0±3.1
17.03±0.17	37.3±2.5	20.56±0.07	31.5±2.8
^{58}Ni$(n,\alpha)^{55}$Fe			
E_n(MeV)	σ(mb)	E_n(MeV)	σ(mb)
7.48±0.20	81.7±7.6	8.47±0.23	91.4±8.2
9.53±0.25	95.0±8.3	10.61±0.30	92.9±8.4
11.55±0.33	102.2±8.9	12.30±0.35	104.9±8.9
12.97±0.20	98.5±8.0	14.25±0.20	101.6±8.9
17.20±0.25	66.2±5.8	18.80±0.30	55.7±5.0
19.40±0.32	50.4±4.5		
^{58}Ni$(n,x\alpha)^{54}$Mn			
E_n(MeV)	σ(mb)	E_n(MeV)	σ(mb)
14.25±0.20	0.3±0.1	17.20±0.25	12.4±1.1
18.80±0.30	22.2±1.9	19.40±0.32	26.8±2.3
^{58}Ni$(n,t)^{56}$Co			
E_n(MeV)	σ(mb)	E_n(MeV)	σ(mb)
17.78±0.18	0.35±0.05	19.26±0.09	0.26±0.07

Table 1.1: *Results obtained at 14.60 ± 0.15 MeV neutron energy*

^{58}Ni$(n,p)^{58}$Co			
E_n(MeV)	σ(mb)	E_n(MeV)	σ(mb)
1.29±0.08	8±0.6	1.99±0.05	47±3
2.41±0.04	116±10	14.81±0.17	291±20
15.27±0.16	260±20	15.68±0.18	228±0
16.26±0.20	181±15	17.03±0.17	135±10
17.19±0.18	120±12	18.82±0.18	92±15
19.28±0.09	78±14	20.34±0.08	71±14
^{58}Ni$(n,p)^{58m,g}$Co			
E_n(MeV)	Isomerratio	E_n(MeV)	Isomerratio
0.97±0.04	0.30±0.05	1.29±0.08	0.30±0.05
1.40±0.04	0.29±0.04	1.99±0.05	0.31±0.05
2.41±0.04	0.24±0.02	3.41±0.04	0.29±0.02
15.27±0.16	0.55±0.06	16.26±0.20	0.55±0.04
17.03±0.17	0.54±0.04	19.28±0.09	0.56±0.05
^{58}Ni$(n,p)^{58m}$Co			
E_n(MeV)	σ(mb)	E_n(MeV)	σ(mb)
1.29±0.08	2.4±0.4	1.99±0.05	15±1.7
2.41±0.04	26±2	15.27±0.16	143±10
16.26±0.20	99±7	17.03±0.17	73±6
19.28±0.09	44±4		
^{58}Ni$(n,2n)^{57}$Ni			
E_n(MeV)	σ(mb)	E_n(MeV)	σ(mb)
14.81±0.17	38±2	15.27±0.16	45±3
15.8±0.25	51±3	16.14±0.28	55±4
17.19±0.18	65±4	17.72±0.18	65±4
18.04±0.12	71±7	18.82±0.18	75±4
20.34±0.08	82±6		
^{58}Ni$(n,x)^{57}$Co			
E_n(MeV)	σ(mb)	E_n(MeV)	σ(mb)
14.81±0.17	658±27	15.27±0.16	704±28
15.68±0.18	729±28	16.05±0.19	749±35
16.26±0.20	774±35	17.03±0.17	794±35
17.19±0.18	797±30	17.58±0.17	815±31
18.36±0.15	831±33	18.82±0.18	849±37
19.28±0.09	850±37	20.35±0.08	875±40

Table 1.1: *Results obtained at 14.60 ± 0.15 MeV neutron energy*

^{60}Ni$(n,p)^{60}$Co			
E_n(MeV)	σ(mb)	E_n(MeV)	σ(mb)
13.32±0.25	161±7	14.81±0.17	136±10
15.27±0.16	119±7	16.05±0.19	102±4
17.73±0.12	69±6	19.29±0.09	55±3
19.94±0.08	50±5		
^{60}Ni$(n,p)^{60m,g}$Co			
E_n(MeV)	Isomerratio	E_n(MeV)	Isomerratio
15.27±0.16	0.54±0.07		
^{60}Ni$(n,p)^{60m}$Co			
E_n(MeV)	σ(mb)	E_n(MeV)	σ(mb)
15.27±0.16	64±7	16.26±0.20	46±4
17.98±0.06	27±3	19.29±0.09	20±3
^{61}Ni$(n,p)^{61}$Co			
E_n(MeV)	σ(mb)	E_n(MeV)	σ(mb)
14.81±0.17	74±7	15.27±0.16	65±6
16.26±0.20	56±5	18.04±0.12	47±3
19.04±0.07	39±4		
^{61}Ni$(n,x)^{60m}$Co			
E_n(MeV)	σ(mb)	E_n(MeV)	σ(mb)
19.29±0.09	65±6		
^{62}Ni$(n,\alpha)^{59}$Fe			
E_n(MeV)	σ(mb)	E_n(MeV)	σ(mb)
12.97±0.20	13.0±1.2	14.25±0.20	19.7±1.5
17.20±0.25	16.0±1.4	18.80±0.30	15.8±1.4
19.40±0.32	15.1±1.5		
^{62}Ni$(n,x)^{61}$Co			
E_n(MeV)	σ(mb)	E_n(MeV)	σ(mb)
15.27±0.16	4.6±3	16.26±0.20	9.2±3
18.04±0.12	48±7	19.04±0.07	67±9
^{62}Ni$(n,p)^{62m}$Co			
E_n(MeV)	σ(mb)	E_n(MeV)	σ(mb)
14.60±0.15	21.92±2.5		

Table 1.1: *Results obtained at 14.60 ± 0.15 MeV neutron energy*

^{63}Cu$(n,\alpha)^{60}$Co			
E_n(MeV)	σ(mb)	E_n(MeV)	σ(mb)
13.32±0.25	45±2	14.81±0.17	42±3
15.99±0.20	32±2	16.26±0.20	30±2
17.19±0.18	28±2	17.58±0.17	22±1
18.18±0.10	18±1	19.04±0.07	14±1
19.94±0.09	12±1		
^{90}Zr$(n,p)^{90m}$Y			
E_n(MeV)	σ(mb)	E_n(MeV)	σ(mb)
14.81±0.17	12.3±0.7	15.27±0.16	12.4±0.1
16.34±0.20	12.0±0.8	17.03±0.17	10.9±0.9
18.04±0.12	11.0±0.7	19.05±0.07	10.0±0.8
20.56±0.07	8.8±0.7		
^{90}Zr$(n,\alpha)^{87m}$Sr			
E_n(MeV)	σ(mb)	E_n(MeV)	σ(mb)
14.81±0.17	3.91±0.32	15.27±0.16	4.33±0.38
16.34±0.20	4.69±0.41	17.03±0.17	4.81±0.39
18.04±0.12	4.82±0.37	19.05±0.07	4.63±0.39
20.56±0.07	4.31±0.40		
^{91}Zr$(n,p)^{91m}$Y			
E_n(MeV)	σ(mb)	E_n(MeV)	σ(mb)
14.81±0.17	20.0±1.0	15.27±0.16	22.0±2.0
16.34±0.20	22.5±2.5	18.04±0.12	21.5±2.5
19.05±0.07	19.0±2.0	20.56±0.07	18.0±1.6
^{91}Zr$(n,x)^{90m}$Y			
E_n(MeV)	σ(mb)	E_n(MeV)	σ(mb)
14.81±0.17	2.58±0.21	15.27±0.16	4.58±0.51
17.03±0.17	10.8±0.78	18.04±0.12	15.6±1.2
19.05±0.07	24.5±2.4	20.56±0.07	28.0±2.5
^{92}Zr$(n,x)^{91m}$Y			
E_n(MeV)	σ(mb)	E_n(MeV)	σ(mb)
14.81±0.17	1.32±0.11	15.27±0.16	2.21±0.17
16.34±0.20	7.09±0.80	17.03±0.17	9.79±0.90
18.04±0.12	13.3±0.88	19.05±0.07	22.0±1.5
20.56±0.07	27.0±2.7		

Table 1.1: *Results obtained at 14.60 ± 0.15 MeV neutron energy*

^{92}Zr$(n,p)^{92}$Y			
E_n(MeV)	σ(mb)	E_n(MeV)	σ(mb)
14.81±0.17	21.9±2.4	15.27±0.16	23.5±2.5
16.34±0.20	26.5±2.7	17.03±0.17	26.6±2.8
18.04±0.12	26.0±3.4	19.05±0.07	25.2±3.5
19.38±0.08	25.0±2.5	20.56±0.07	23.0±3.4
^{94}Zr$(n,\alpha)^{91}$Sr			
E_n(MeV)	σ(mb)	E_n(MeV)	σ(mb)
14.81±0.17	5.29±0.41	16.34±0.20	6.74±0.61
19.34±0.09	6.80±0.54		
^{94}Zr$(n,p)^{94}$Y			
E_n(MeV)	σ(mb)	E_n(MeV)	σ(mb)
14.81±0.17	9.00±0.78	16.34±0.20	13.23±1.37
19.34±0.09	14.87±1.17		
^{93}Nb$(n,2n)^{92m}$Nb			
E_n(MeV)	σ(mb)	E_n(MeV)	σ(mb)
16.033±0.062	441.85±23.58	16.981±0.040	433.75±23.83
17.723±0.032	422.44±22.68	19.030±0.011	376.11±22.27
20.229±0.010	305.72±19.84		
^{93}Nb$(n,\alpha)^{90m}$Y			
E_n(MeV)	σ(mb)	E_n(MeV)	σ(mb)
16.033±0.062	5.22±0.31	16.981±0.04	4.96±0.31
17.723±0.032	5.22±0.31	19.03±0.011	5.08±0.35
20.229±0.01	4.79±0.34		
^{92}Mo$(n,2n)^{91m}$Mo			
E_n(MeV)	σ(mb)	E_n(MeV)	σ(mb)
16.1±0.1	55± 5	17.8±0.2	100±21
19.1±0.2	117±13	20.5±0.2	118±21
^{92}Mo$(n,p)^{92m}$Nb			
E_n(MeV)	σ(mb)	E_n(MeV)	σ(mb)
16.22±0.26	43.1±2.9	18.00±0.13	34.3±3.1
19.27±0.12	40.9±5.5	20.51±0.13	39.7±6.7

Table 1.1: *Results obtained at 14.60 ± 0.15 MeV neutron energy*

^{92}Mo$(n,\alpha)^{89m}$Zr			
E_n(MeV)	σ(mb)	E_n(MeV)	σ(mb)
16.1±0.1	6.3±0.7	17.8±0.2	6.7±1.0
19.1±0.3	6.3±1.0	20.5±0.2	6.6±2.5
^{94}Mo$(n,2n)^{93m}$Mo			
E_n(MeV)	σ(mb)	E_n(MeV)	σ(mb)
16.2±0.3	9.6±0.8	18.0±0.1	22.0±1.8
19.3±0.1	28.7±2.4	20.5±0.1	35.9±3.7
^{95}Mo$(n,p)^{95m}$Nb			
E_n(MeV)	σ(mb)	E_n(MeV)	σ(mb)
16.6±0.3	5.4±0.7	18.0±0.1	4.8±0.9
19.3±0.1	5.0±1.3	20.5±0.1	5.1±0.9
^{96}Mo$(n,p)^{96}$Nb			
E_n(MeV)	σ(mb)	E_n(MeV)	σ(mb)
16.22±0.05	19.9±1.8	19.33±0.07	25.1±2.5
20.63±0.08	25.3±2.7		
^{96}Mo$(n,x)^{95m}$Nb			
E_n(MeV)	σ(mb)	E_n(MeV)	σ(mb)
16.2±0.5	3.3±0.4	19.3±0.1	12.0±1.0
20.6±0.1	14.2±2.1		
^{97}Mo$(n,p)^{97}$Nb			
E_n(MeV)	σ(mb)	E_n(MeV)	σ(mb)
16.23±0.04	18.2±1.3	18.01±0.13	19.4±2.7
19.27±0.13	22.4±2.9	20.64±0.07	19.3±1.7
^{97}Mo$(n,p)^{97m}$Nb			
E_n(MeV)	σ(mb)	E_n(MeV)	σ(mb)
16.2±0.1	5.4±0.5	17.8±0.1	6.4±1.4
19.2±0.2	6.3±1.0	20.5±0.2	6.6±2.2
^{97}Mo$(n,x)^{96}$Nb			
E_n(MeV)	σ(mb)	E_n(MeV)	σ(mb)
16.23±0.04	8.1±0.7	19.33±0.07	30.6±4.2
20.63±0.08	37.6±4.1		

Table 1.1: *Results obtained at 14.60 ± 0.15 MeV neutron energy*

^{98}Mo$(n,p)^{98m}$Nb			
E_n(MeV)	σ(mb)	E_n(MeV)	σ(mb)
16.22±0.26	6.9±0.6	18.01±0.13	7.5±1.2
19.25±0.13	9.5±1.1	20.51±0.12	7.2±0.8
^{98}Mo$(n,x)^{97}$Nb			
E_n(MeV)	σ(mb)	E_n(MeV)	σ(mb)
16.22±0.09	2.9±0.2	18.02±0.12	12.8±1.7
^{98}Mo$(n,x)^{97m}$Nb			
E_n(MeV)	σ(mb)	E_n(MeV)	σ(mb)
16.15±0.09	1.9±0.2	17.83±0.13	9.4±1.9
19.18±0.17	14.2±1.5	20.56±0.09	25.5±7.1
^{100}Mo$(n,\alpha)^{97}$Zr			
E_n(MeV)	σ(mb)	E_n(MeV)	σ(mb)
16.2±0.3	3.4±0.2	18.0±0.1	4.6±0.4
19.3±0.1	5.3±0.5	20.5±0.1	5.2±0.5
^{100}Mo$(n,2n)^{99}$Mo			
E_n(MeV)	σ(mb)	E_n(MeV)	σ(mb)
16.2±0.1	1272±127	18.0±0.2	980±78
19.3±0.2	1018±180	20.5±0.2	814±105
9.92±0.20	735±53	11.68±0.20	1010±93
12.44±0.22	1293±112		
^{nat}Mo$(n,x)^{94}$Nb			
E_n(MeV)	σ(mb)	E_n(MeV)	σ(mb)
14.5±0.7	9.9±1.6	18.0±0.7	17.6±1.4
20.3±0.3	28.3±7.3		

Table 1.1: *Results obtained at 14.60 ± 0.15 MeV neutron energy*

^{99}Tc$(n, n'\gamma)^{99m}$Tc			
E_n(MeV)	σ(mb)	E_n(MeV)	σ(mb)
0.48±0.08	6.3±3.9	0.98±0.06	78.5±11.8
2.02±0.04	211.0±17.0	2.98±0.03	222.8±19.0
3.97±0.03	239.0±20.1	4.93±0.03	323.0±30.4
5.43±0.02	318.0±39.0	5.91±0.01	310.0±41.0
7.47±0.20	309.1±19.2	8.62±0.22	297.4±16.2
9.56±0.23	269.0±21.7	10.72±0.24	204.8±22.6
12.42±0.29	110.1±19.9	13.88±0.15	77.4±4.8
14.36±0.20	77.1±6.8	14.81±0.19	64.8±4.0
16.26±0.26	60.8±5.4	17.99±0.13	56.2±6.2
19.34±0.10	63.8±10.2	20.59±0.10	71.2±22.5
^{99}Tc$(n, p)^{99}$Mo			
E_n(MeV)	σ(mb)	E_n(MeV)	σ(mb)
8.62±0.22	1.1±0.2	9.75±0.23	2.5±0.1
10.55±0.24	4.2±0.3	11.62±0.27	5.9±0.5
12.42±0.28	9.0±0.8	13.88±0.16	11.3±0.6
14.36±0.20	13.6±1.2	14.81±0.18	14.6±1.1
16.16±0.26	14.3±0.9	17.82±0.19	15.0±0.8
19.14±0.21	14.3±0.9	20.43±0.18	16.1±1.3
^{99}Tc$(n, \alpha)^{96}$Nb			
E_n(MeV)	σ(mb)	E_n(MeV)	σ(mb)
8.62±0.22	0.6±0.1	9.75±0.23	1.1±0.1
10.55±0.24	1.7±0.1	11.62±0.27	2.5±0.2
12.42±0.28	3.4±0.3	13.88±0.16	4.5±0.3
14.36±0.20	5.7±0.5	14.81±0.18	6.1±0.6
16.16±0.26	6.3±0.3	17.82±0.19	6.3±0.3
19.14±0.21	5.8±0.4	20.43±0.18	5.3±0.4
^{115}In$(n, n'\gamma)^{115m}$In			
E_n(MeV)	σ(mb)	E_n(MeV)	σ(mb)
2.14	299	2.24	312
2.35	321.7	2.49	325
2.52	328.2	2.72	344.5
2.85	328.2	2.96	354.2
10.2	211	12.4	174

Table 1.1: *Results obtained at 14.60 ± 0.15 MeV neutron energy*

$^{115}\mathrm{In}(n,\gamma)^{116}\mathrm{In}$			
E_n(MeV)	σ(mb)	E_n(MeV)	σ(mb)
0.024	710	0.13	275
0.22	190	0.62	165
0.83	175	1.2	250
1.3	242.2	1.4	215.6
1.5	200.9	2.14	99.9
2.24	85.5	2.35	78.8
2.49	68.6	2.52	63.3
2.72	54.4	2.85	49.2
2.96	44.5	10.2	2
12.4	5.6		
$^{119}\mathrm{Sn}(n,p)^{119m}\mathrm{In}$			
E_n(MeV)	σ(mb)	E_n(MeV)	σ(mb)
16.099±0.062	7.30±0.64	17.079±0.040	10.29±0.81
17.839±0.032	12.42±0.86	19.176±0.011	12.79±1.03
20.393±0.010	12.00±1.12		
$^{127}\mathrm{I}(n,2n)^{126}\mathrm{I}$			
E_n(MeV)	σ(mb)	E_n(MeV)	σ(mb)
16.3	1365±100	18.1	1474±179
19.5	1460± 90	20.7	1200± 96
$^{129}\mathrm{I}(n,2n)^{128}\mathrm{I}$			
E_n(MeV)	σ(mb)	E_n(MeV)	σ(mb)
16.3	951±80	18.1	953±80
19.5	846±80	20.7	625±40
$^{129}\mathrm{I}(n,p)^{129g}\mathrm{Te}$			
E_n(MeV)	σ(mb)	E_n(MeV)	σ(mb)
16.3	1.41±0.49	18.1	2.48±0.48
19.5	2.66±0.45	20.7	2.70±0.54
$^{129}\mathrm{I}(n,p)^{129m}\mathrm{Te}$			
E_n(MeV)	σ(mb)	E_n(MeV)	σ(mb)
16.3	1.88±0.6	18.1	4.33±0.4
19.5	5.51±0.5	20.7	6.16±0.90

Table 1.1: *Results obtained at 14.60 ± 0.15 MeV neutron energy*

$^{129}\mathrm{I}(n,\alpha)^{126g}\mathrm{Sb}$			
E_n(MeV)	σ(mb)	E_n(MeV)	σ(mb)
16.3	0.35±0.044	18.1	0.9±0.12
19.5	1.3±0.12	20.7	1.65±0.15
$^{129}\mathrm{I}(n,\alpha)^{126m}\mathrm{Sb}$			
E_n(MeV)	σ(mb)	E_n(MeV)	σ(mb)
16.3	0.89±0.08	18.1	1.09±0.10
19.5	1.44±0.12	20.7	1.88±0.18
$^{138}\mathrm{Ba}(n,2n)^{137m}\mathrm{Ba}$			
E_n(MeV)	σ(mb)	E_n(MeV)	σ(mb)
16.075±0.062	993.3±53.8	17.036±0.040	1060.5±56.1
17.791±0.032	1110.4±63.3	19.115±0.011	941.2±60.0
20.325±0.010	671.4±50.7		
$^{204}\mathrm{Pb}(n,n'\gamma)^{204m}\mathrm{Pb}$			
E_n(MeV)	σ(mb)	E_n(MeV)	σ(mb)
3.45±0.03	43±3	14.81±0.17	62±4
16.26±0.20	51±3	17.95±0.12	42±5
19.39±0.09	36±3	20.53±0.08	26±4
$^{204}\mathrm{Pb}(n,2n)^{203}\mathrm{Pb}$			
E_n(MeV)	σ(mb)	E_n(MeV)	σ(mb)
18.0±0.1	2007±185	18.7±0.2	1923±147
19.2±0.2	1852±132	19.4±0.1	1827±138
20.5±0.1	1461±140	20.5±0.1	1544±108
$^{204}\mathrm{Pb}(n,2n)^{203m}\mathrm{Pb}$			
E_n(MeV)	σ(mb)	E_n(MeV)	σ(mb)
16.26±0.20	1039±72	17.95±0.12	1030±70
19.11±0.09	1032±82	20.31±0.08	828±73
$^{204}\mathrm{Pb}(n,3n)^{202m}\mathrm{Pb}$			
E_n(MeV)	σ(mb)	E_n(MeV)	σ(mb)
18.0±0.1	0.17±0.07	18.7±0.2	3.8±0.54
19.2±0.2	13.4±2.15	19.4±0.1	18.3±2.2
20.5±0.1	82.2±12.58		

Table 1.1: *Results obtained at 14.60 ± 0.15 MeV neutron energy*

^{206}Pb$(n,3n)^{204m}$Pb			
E_n(MeV)	σ(mb)	E_n(MeV)	σ(mb)
18.1±0.1	4.2±0.3	19.4±0.1	92.1±6.4
20.7±0.1	292±31		
^{206}Pb$(n,\alpha)^{203}$Hg			
E_n(MeV)	σ(mb)	E_n(MeV)	σ(mb)
16.1±0.2	0.86±0.09	17.2±0.1	1.9±0.2
18.7±0.2	2.6±0.2	19.2±0.2	3.3±0.3
20.0±0.1	3.9±0.4	20.5±0.1	3.7±0.4
^{208}Pb$(n,p)^{208}$Tl			
E_n(MeV)	σ(mb)	E_n(MeV)	σ(mb)
14.60±0.15	0.9 ±0.15	14.81±0.17	0.96±0.22
16.26±0.20	2.1±0.3	17.95±0.12	4.2±0.5
19.05±0.09	6.1±0.6	19.30±0.09	6.1±0.7
20.50±0.08	8.1±0.8		
^{nat}Pb$(n,x)^{204}$Tl			
E_n(MeV)	σ(mb)	E_n(MeV)	σ(mb)
18.0±0.1	5.1±1.1	18.7±0.1	4.5±0.6
20.0±0.1	8.7±1.1	20.5±0.1	13.2±1.8

2. Comparison of measured data with earlier work, evaluations, TALYS and selected EMPIRE-II calculations

Below the measured data are presented in graphs together with other experimental data that were found in the EXFOR database, and with the recent ENDF/B-VI.8, JENDL-3.3, JEFF-3.0, EAF-2003 and ADL evaluations, as well as with Talys-0.57 model calculations and selected EMPIRE-II model calculations. Comparison with dedicated model calculations carried out by the subgroup members can be found in the reports and publications listed in Tab. 2.1.

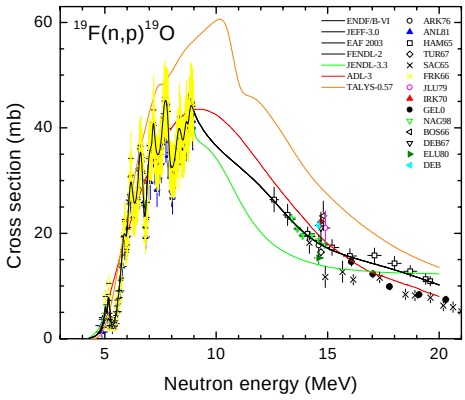

Figure 2.1: $^{19}F(n,p)^{19}O$ *reaction.*

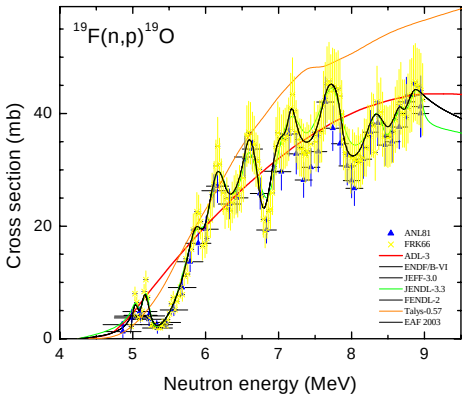

Figure 2.2: $^{19}F(n,p)^{19}O$ *reaction (4-10 MeV).*

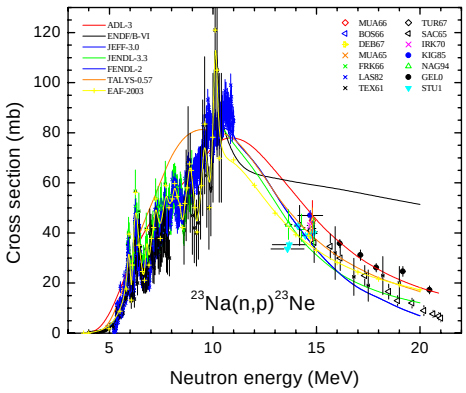

Figure 2.3: $^{23}Na(n,p)^{23}Ne$ *reaction.*

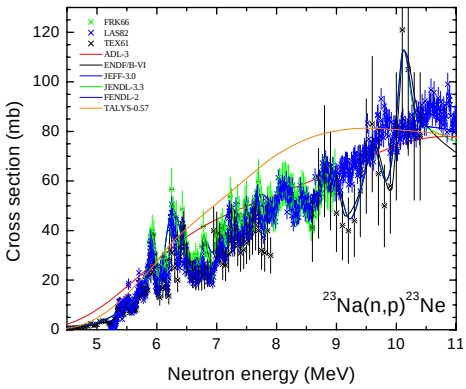

Figure 2.4: $^{23}Na(n,p)^{23}Ne$ *reaction (4-12 MeV).*

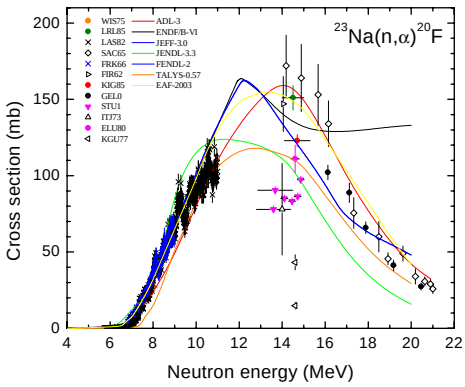

Figure 2.5: $^{23}Na(n,\alpha)^{20}F$ *reaction.*

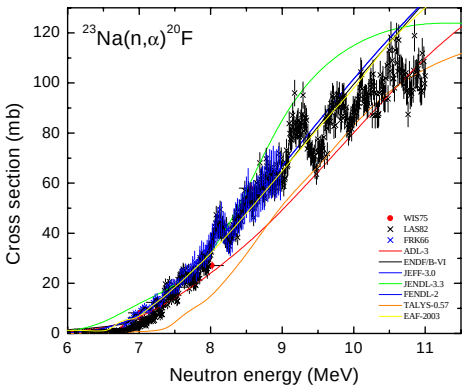

Figure 2.6: $^{23}Na(n,\alpha)^{20}F$ *reaction (4-12 MeV).*

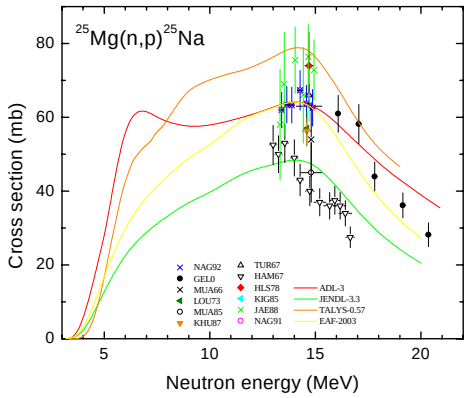

Figure 2.7: $^{25}Mg(n,p)^{25}Na$ *reaction.*

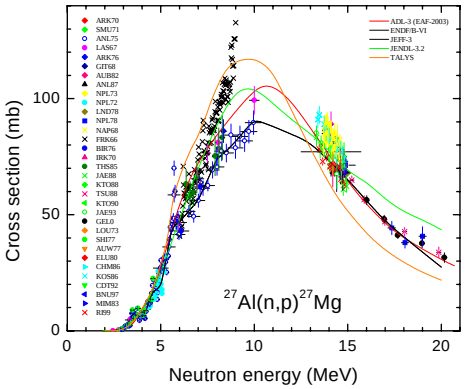

Figure 2.8: $^{27}Al(n,p)^{27}Mg$ *reaction.*

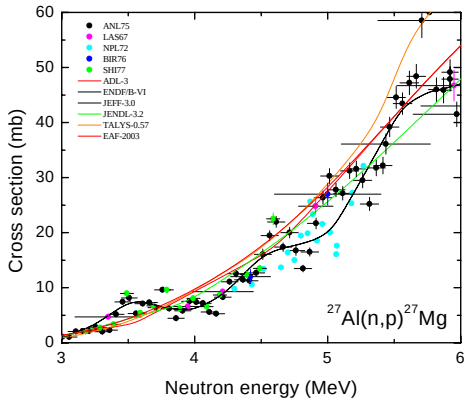

Figure 2.9: $^{27}Al(n,p)^{27}Mg$ *reaction (3-6 MeV).*

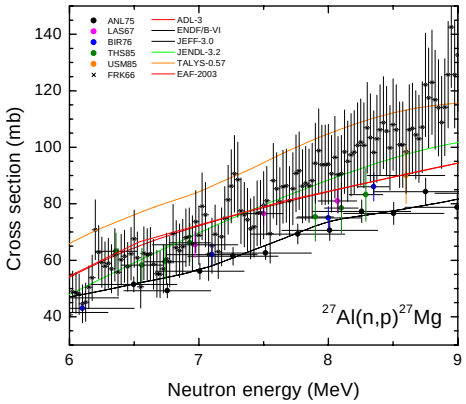

Figure 2.10: $^{27}Al(n,p)^{27}Mg$ *reaction (6-9 MeV).*

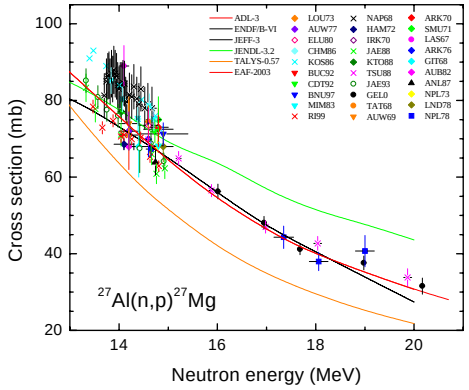

Figure 2.11: $^{27}Al(n,p)^{27}Mg$ *reaction (13-22 MeV).*

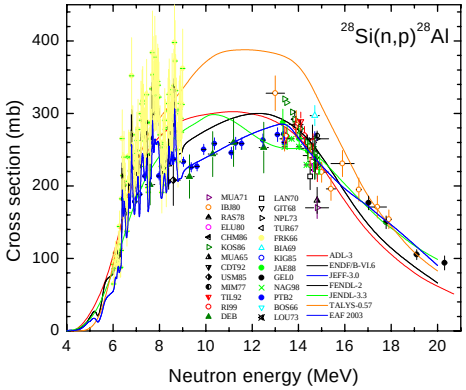

Figure 2.12: $^{28}Si(n,p)^{28}Al$ *reaction.*

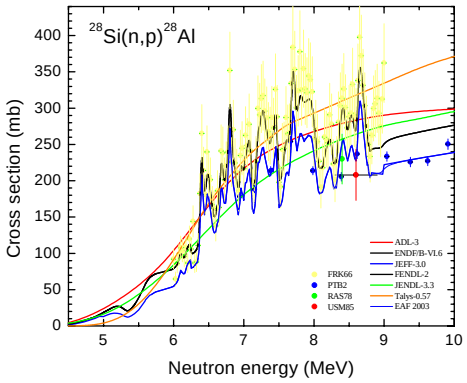

Figure 2.13: $^{28}Si(n,p)^{28}Al$ *reaction (4-10 MeV).*

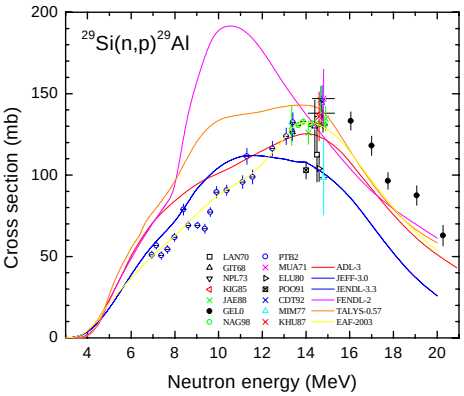

Figure 2.14: $^{29}Si(n,p)^{29}Al$ *reaction.*

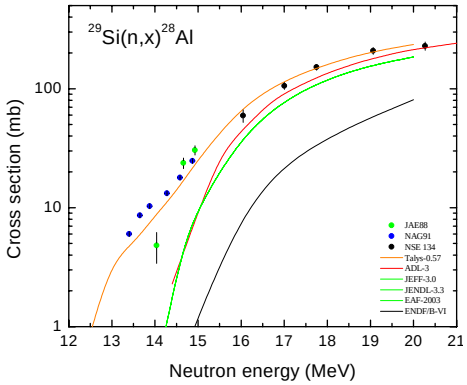

Figure 2.15: $^{29}Si(n,x)^{28}Al$ *reaction.*

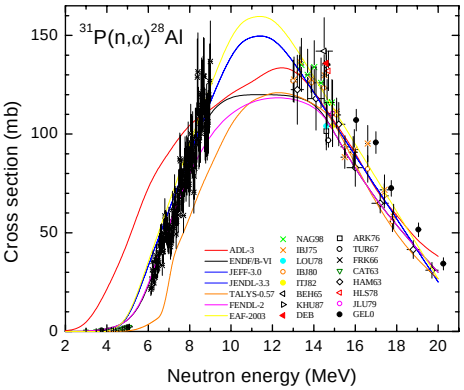

Figure 2.16: $^{31}P(n,\alpha)^{28}Al$ *reaction.*

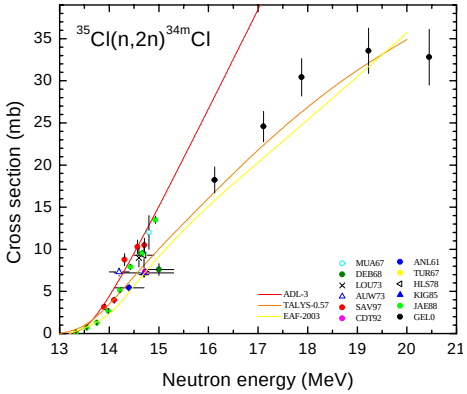

Figure 2.17: $^{35}Cl(n,2n)^{34m}Cl$ *reaction.*

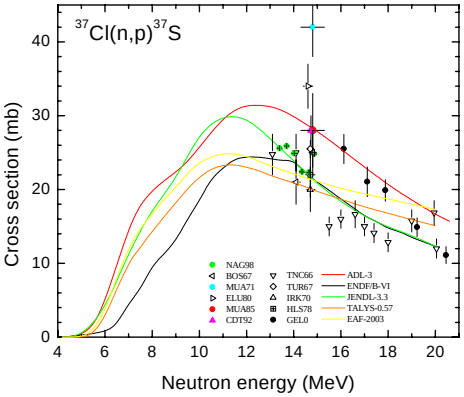

Figure 2.18: $^{37}Cl(n,p)^{37}S$ *reaction.*

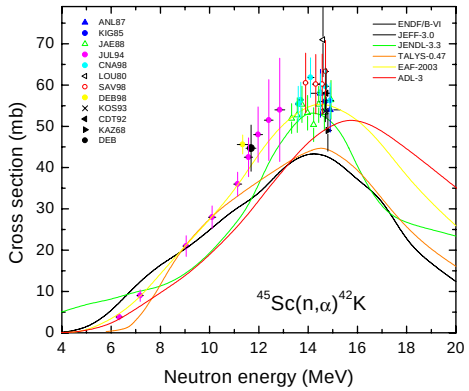

Figure 2.19: $^{45}Sc(n,\alpha)^{42}K$ *reaction.*

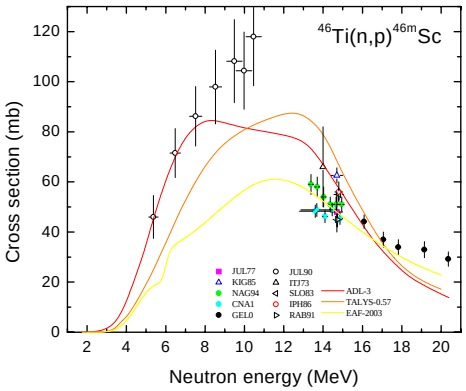

Figure 2.20: $^{46}Ti(n,p)^{46m}Sc$ *reaction.*

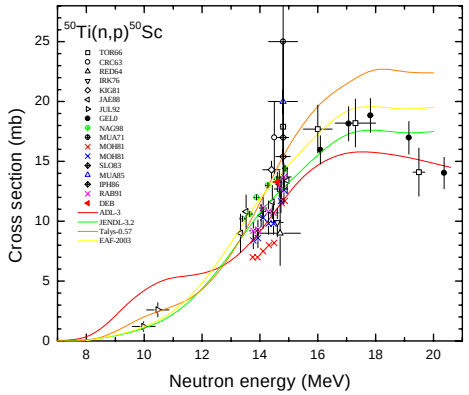

Figure 2.21: $^{50}Ti(n,p)^{50}Sc$ *reaction.*

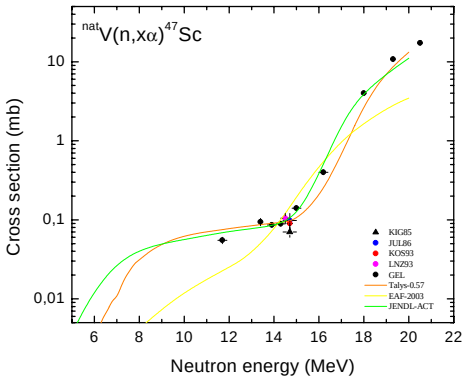

Figure 2.22: $^{nat}V(n,x\alpha)^{47}Sc$ *reaction.*

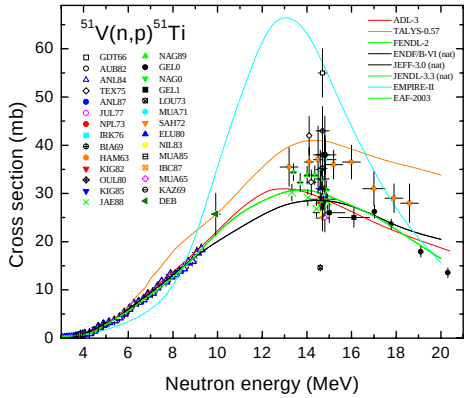

Figure 2.23: $^{51}V(n,p)^{51}Ti$ *reaction.*

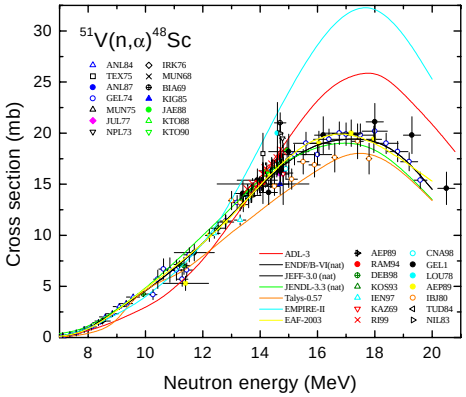

Figure 2.24: $T^{51}V(n,\alpha)^{48}Sc$ *reaction.*

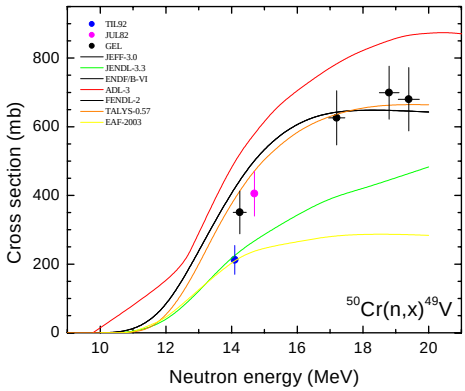

Figure 2.25: $^{50}Cr(n,x)^{49}V$ *reaction.*

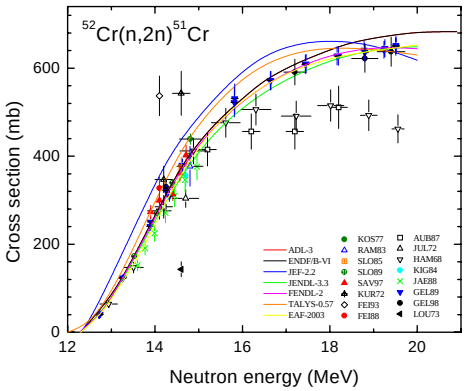

Figure 2.26: $^{52}Cr(n,2n)^{51}Cr$ *reaction.*

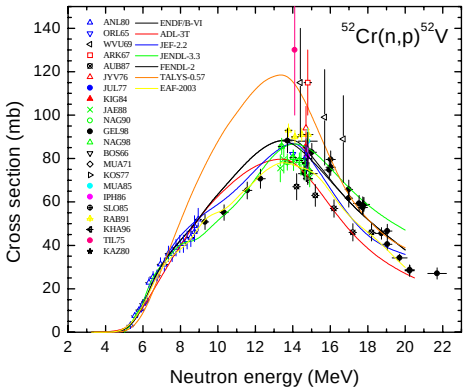

Figure 2.27: $^{52}Cr(n,p)^{52}V$ *reaction.*

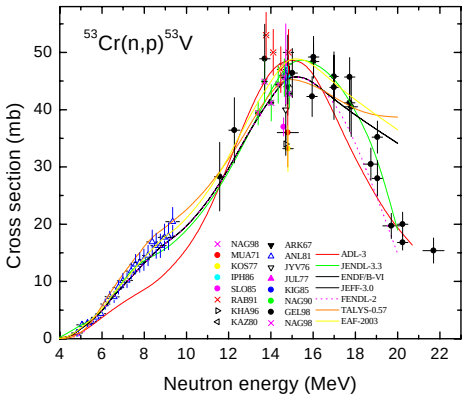

Figure 2.28: $^{53}Cr(n,p)^{53}V$ *reaction.*

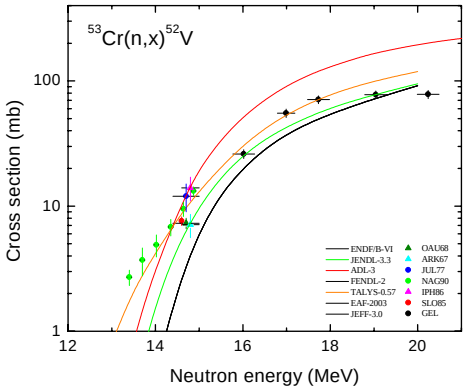

Figure 2.29: $^{53}Cr(n,x)^{52}V$ *reaction.*

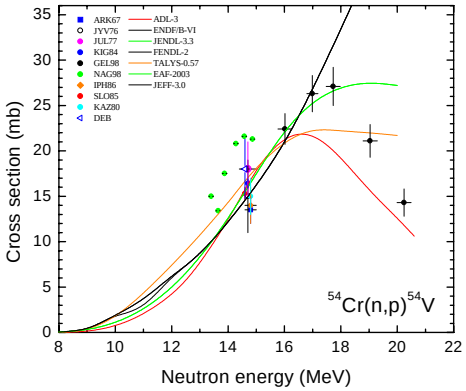

Figure 2.30: $^{54}Cr(n,p)^{54}V$ *reaction.*

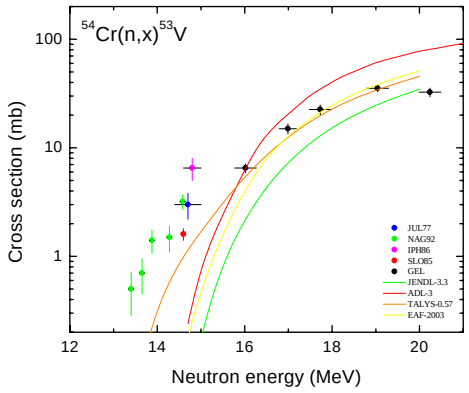

Figure 2.31: $^{54}Cr(n,x)^{53}V$ *reaction.*

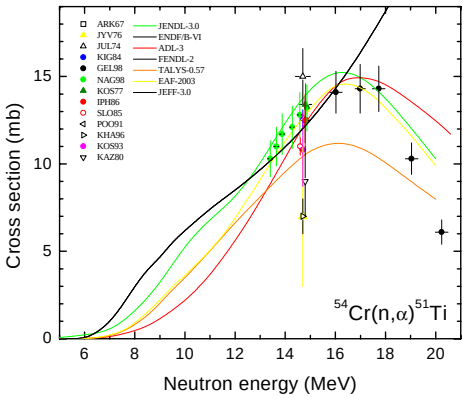

Figure 2.32: $^{54}Cr(n,\alpha)^{51}Ti$ *reaction.*

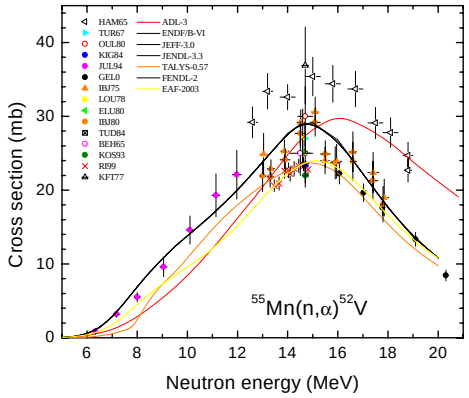

Figure 2.33: $^{55}Mn(n,\alpha)^{52}V$ *reaction.*

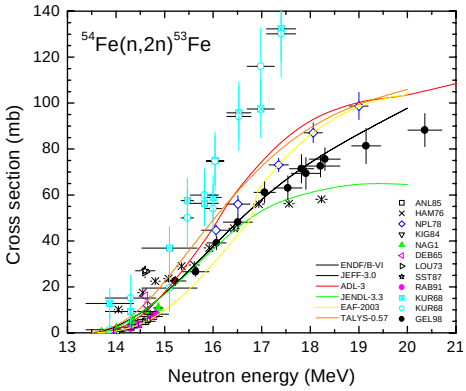

Figure 2.34: $^{54}Fe(n,2n)^{53}Fe$ *reaction.*

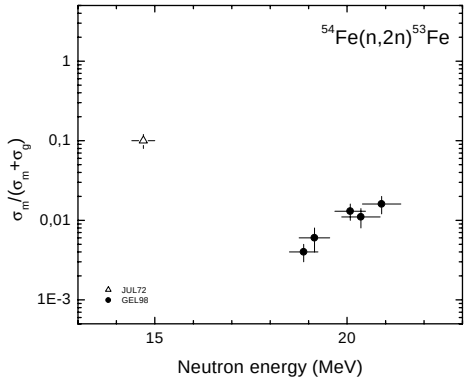

Figure 2.35: $^{54}Fe(n,2n)^{53m,g}Fe$ *reaction.*

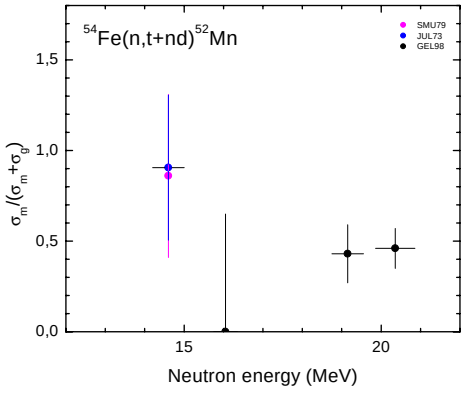

Figure 2.36: $^{54}Fe(n,x)^{52m,g}Mn$ *reaction.*

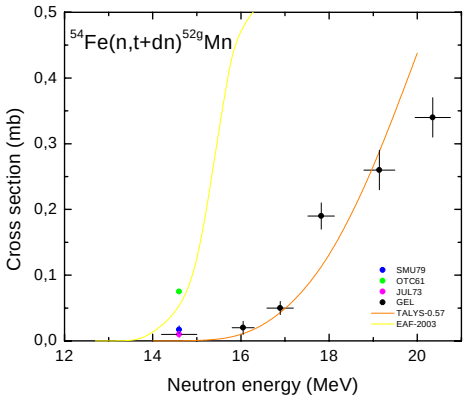

Figure 2.37: $^{54}Fe(n,x)^{52}Mn$ *reaction.*

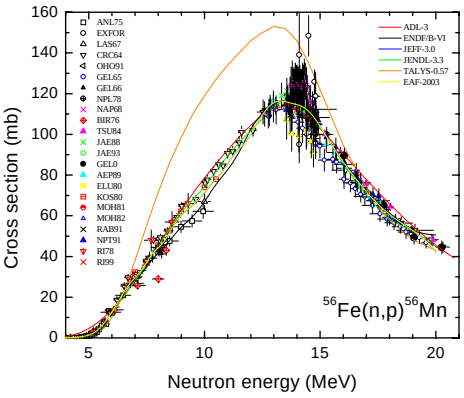

Figure 2.38: $^{56}Fe(n,p)^{56}Mn$ *reaction.*

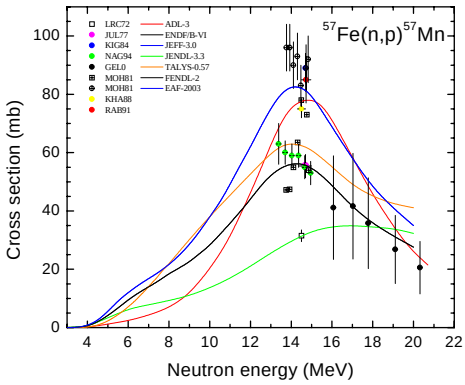

Figure 2.39: $^{57}Fe(n,p)^{57}Mn$ *reaction.*

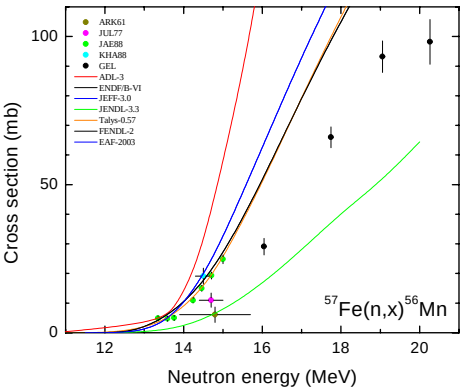

Figure 2.40: $^{57}Fe(n,x)^{56}Mn$ *reaction.*

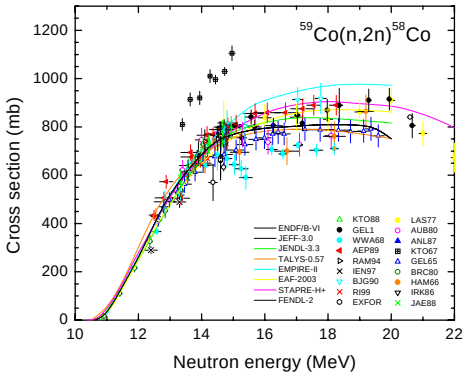

Figure 2.41: $^{59}Co(n,2n)^{58}Co$ *reaction.*

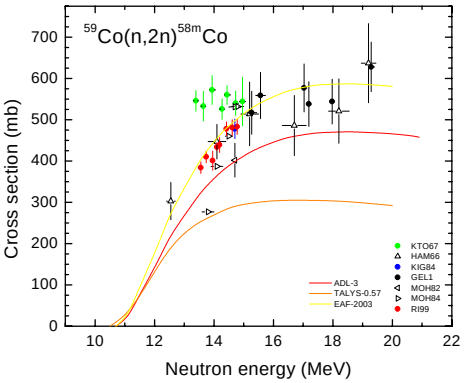

Figure 2.42: $^{59}Co(n,2n)^{58m}Co$ *reaction.*

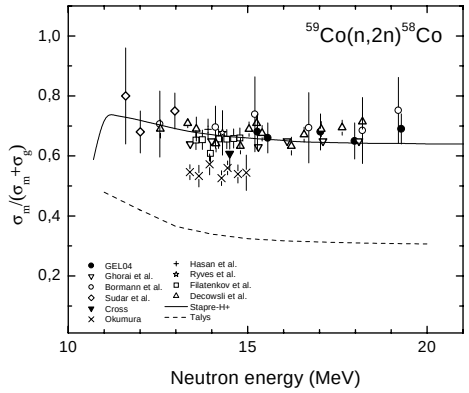

Figure 2.43: $^{59}Co(n,2n)^{58m,g}Co$ *reaction.*

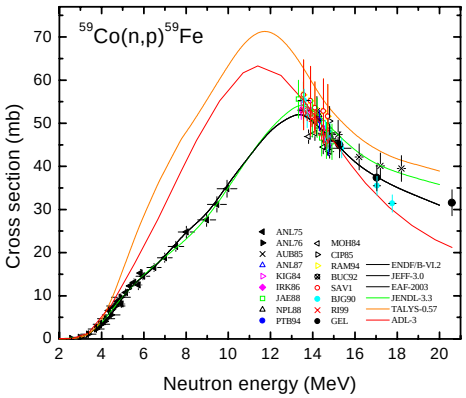

Figure 2.44: $^{59}Co(n,p)^{59}Fe$ *reaction.*

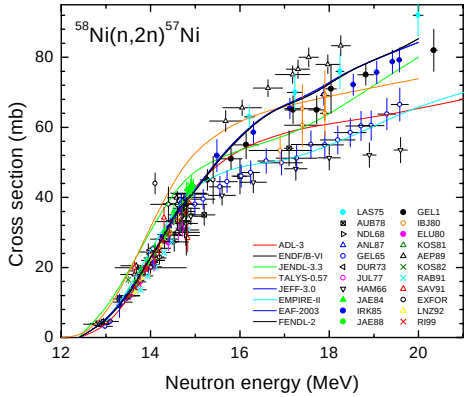

Figure 2.45: $^{58}Ni(n,2n)^{57}Ni$ *reaction.*

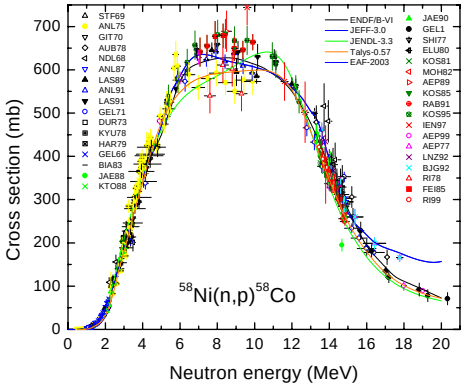

Figure 2.46: $^{58}Ni(n,p)^{58}Co$ *reaction.*

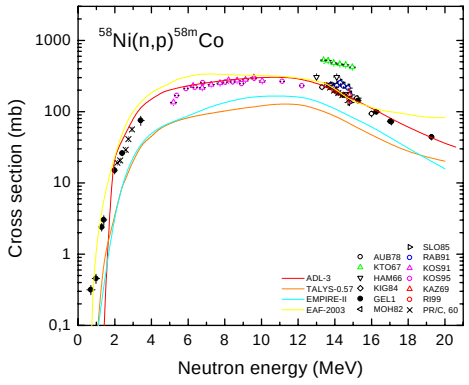

Figure 2.47: $^{58}Ni(n,p)^{58m}Co$ *reaction.*

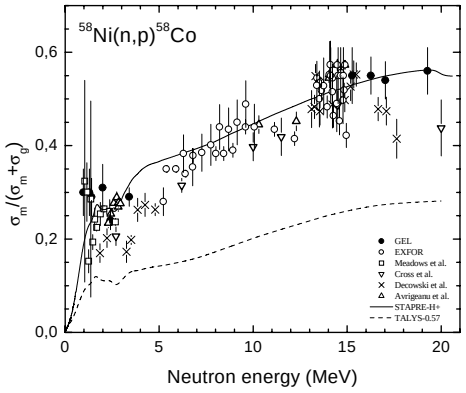

Figure 2.48: $^{58}Ni(n,p)^{58m,g}Co$ *reaction.*

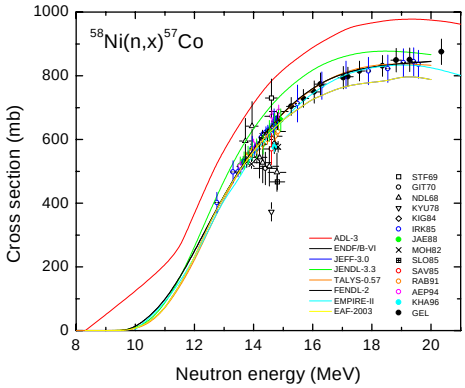

Figure 2.49: $^{58}Ni(n,x)^{57}Co$ *reaction.*

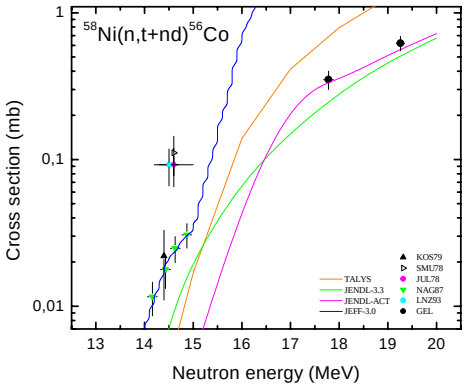

Figure 2.50: $^{58}Ni(n,t)^{56}Co$ *reaction.*

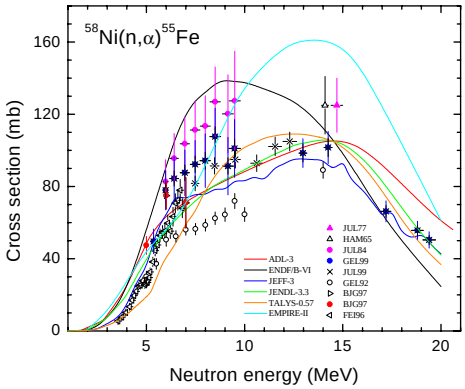

Figure 2.51: $^{58}Ni(n,\alpha)^{55}Fe$ *reaction.*

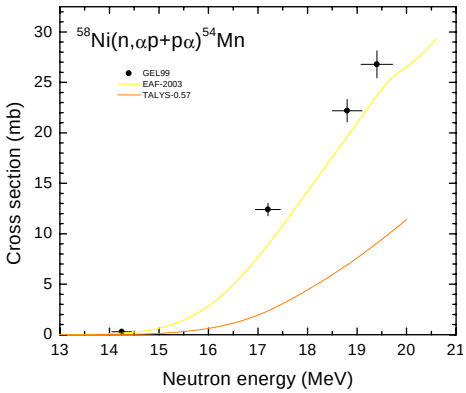

Figure 2.52: $^{58}Ni(n,x\alpha)^{54}Mn$ *reaction.*

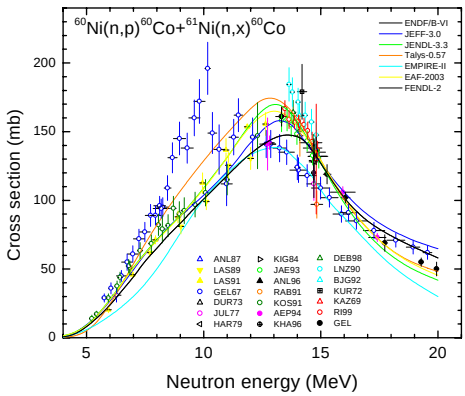

Figure 2.53: $^{60}Ni(n,p)^{60}Co$+$^{61}Ni(n,x)^{60}Co$ *reaction.*

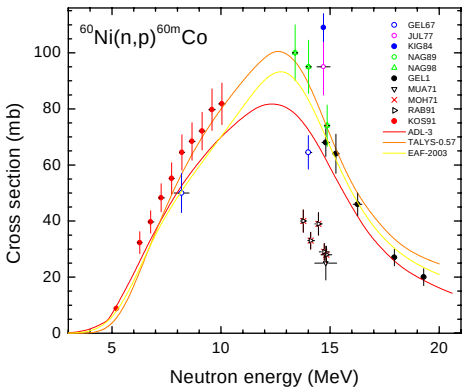

Figure 2.54: $^{60}Ni(n,p)^{60m}Co$ *reaction.*

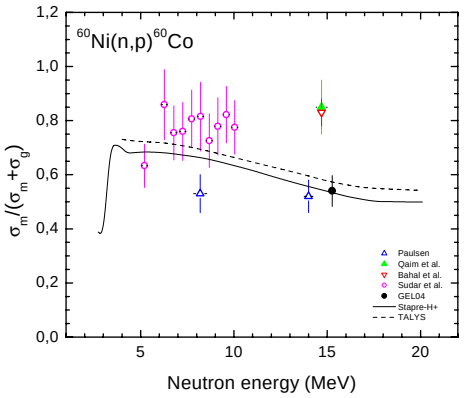

Figure 2.55: $^{60}Ni(n,p)^{60m,g}Co$ *reaction.*

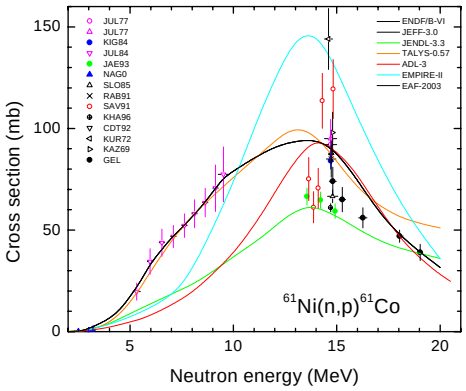

Figure 2.56: $^{61}Ni(n,p)^{61}Co$ *reaction.*

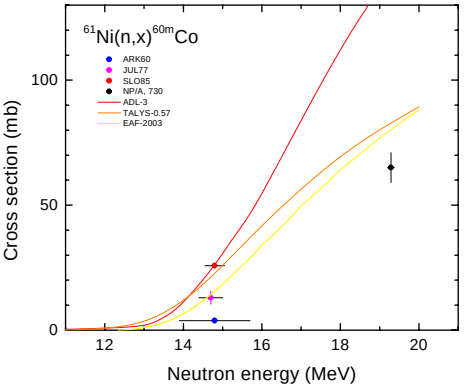

Figure 2.57: $^{61}Ni(n,x)^{60m}Co$ *reaction.*

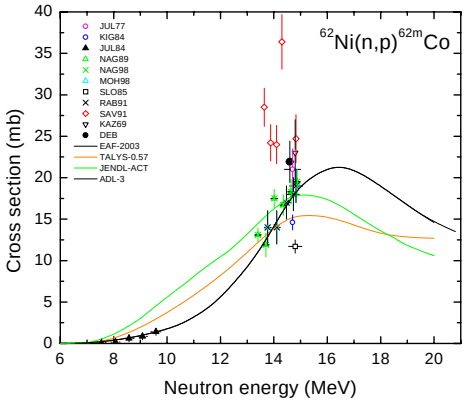

Figure 2.58: $^{62}Ni(n,p)^{62m}Co$ *reaction.*

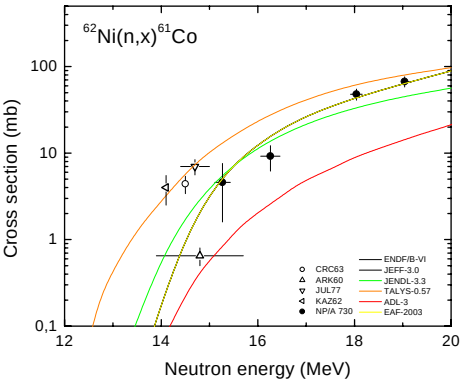

Figure 2.59: $^{62}Ni(n,x)^{61}Co$ *reaction.*

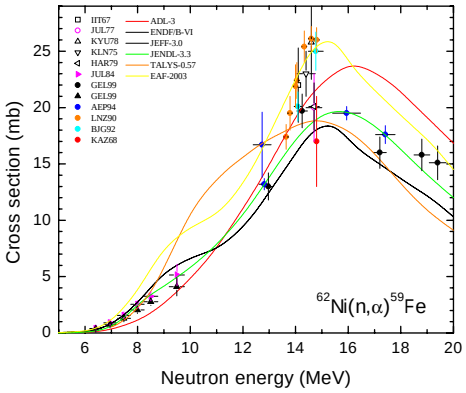

Figure 2.60: $^{62}Ni(n,\alpha)^{59}Fe$ *reaction.*

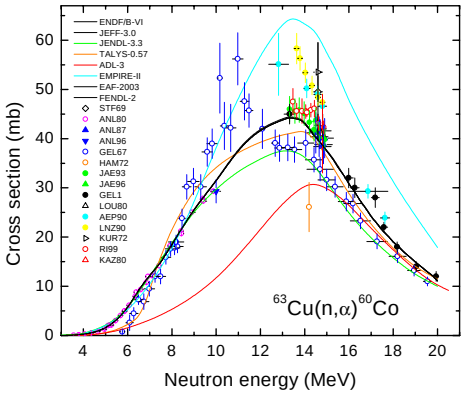

Figure 2.61: $^{63}Cu(n,\alpha)^{60}Co$ *reaction.*

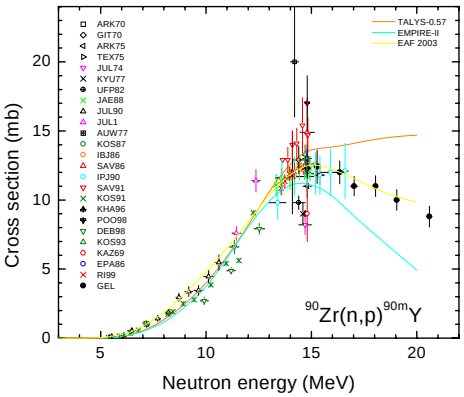

Figure 2.62: $^{90}Zr(n,p)^{90m}Y$ *reaction.*

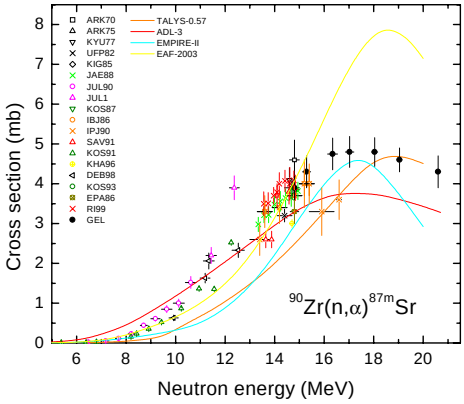

Figure 2.63: $^{90}Zr(n,\alpha)^{87m}Sr$ *reaction.*

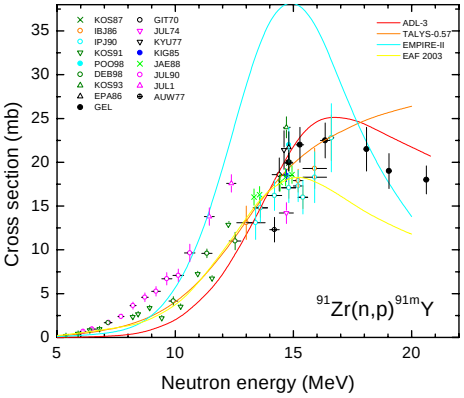

Figure 2.64: $^{91}Zr(n,p)^{91m}Y$ *reaction.*

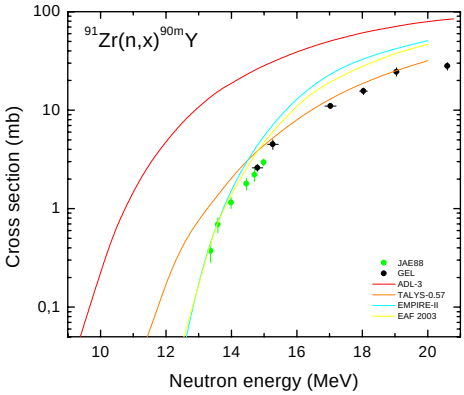

Figure 2.65: $^{91}Zr(n,x)^{90m}Y$ *reaction.*

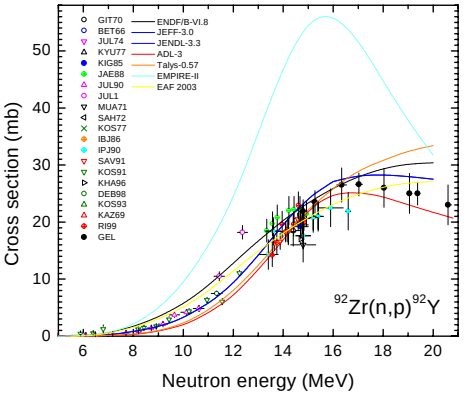

Figure 2.66: $^{92}Zr(n,p)^{92}Y$ *reaction.*

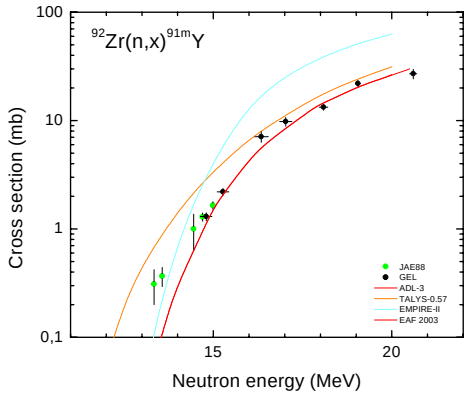

Figure 2.67: $^{92}Zr(n,x)^{91m}Y$ *reaction.*

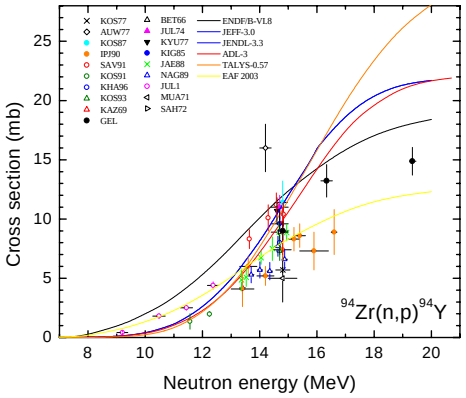

Figure 2.68: $^{94}Zr(n,p)^{94}Y$ *reaction.*

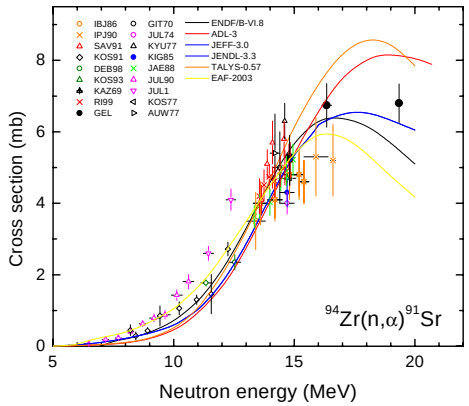

Figure 2.69: $^{94}Zr(n,\alpha)^{91}Sr$ *reaction.*

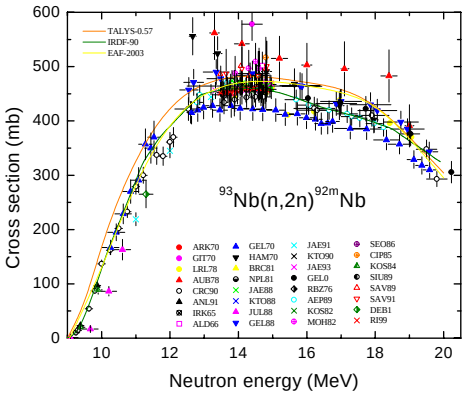

Figure 2.70: $^{93}Nb(n,2n)^{92m}Nb$ *reaction.*

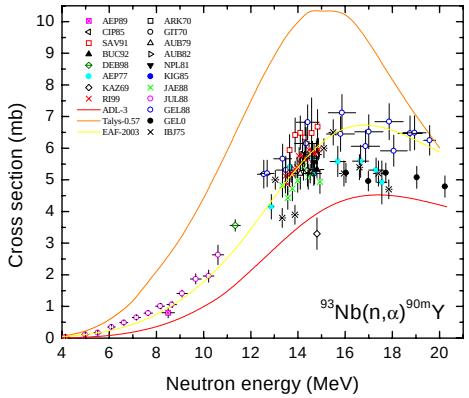

Figure 2.71: $^{93}Nb(n,\alpha)^{90m}Y$ *reaction.*

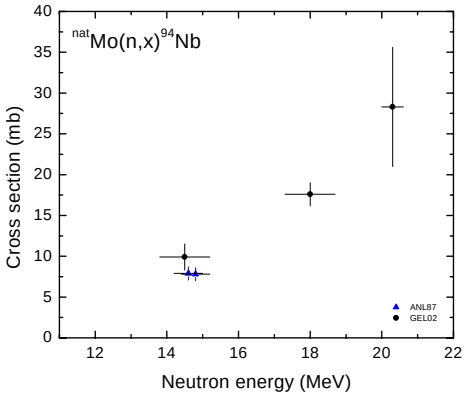

Figure 2.72: $^{nat}Mo(n,x)^{94}Nb$ *reaction.*

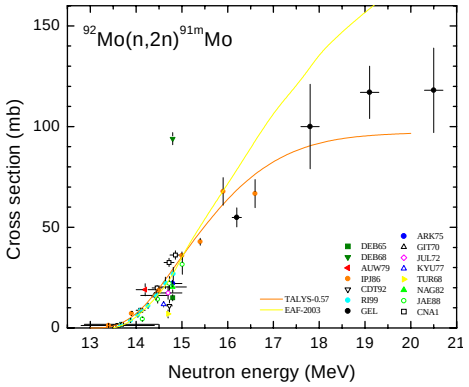

Figure 2.73: $^{92}Mo(n,2n)^{91m}Mo$ *reaction.*

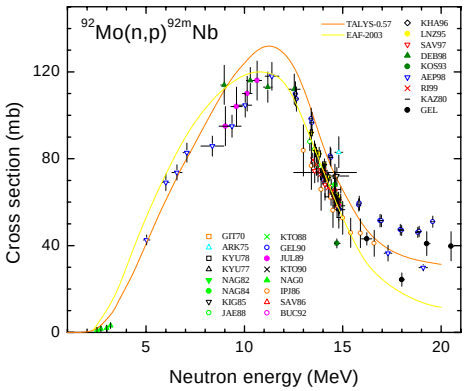

Figure 2.74: $^{92}Mo(n,p)^{92m}Nb$ *reaction.*

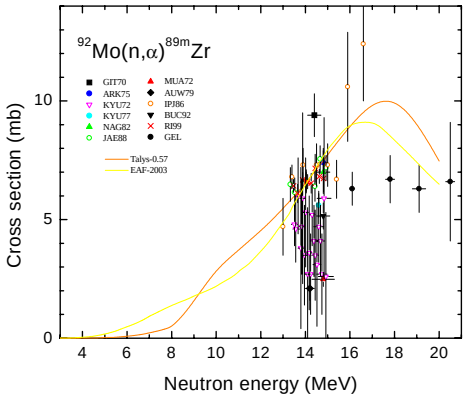

Figure 2.75: $^{92}Mo(n,\alpha)^{89m}Zr$ *reaction.*

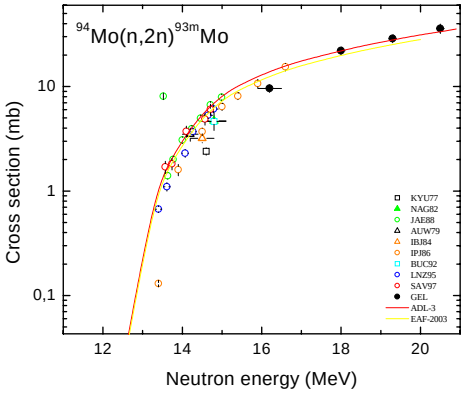

Figure 2.76: $^{94}Mo(n,2n)^{93m}Mo$ *reaction.*

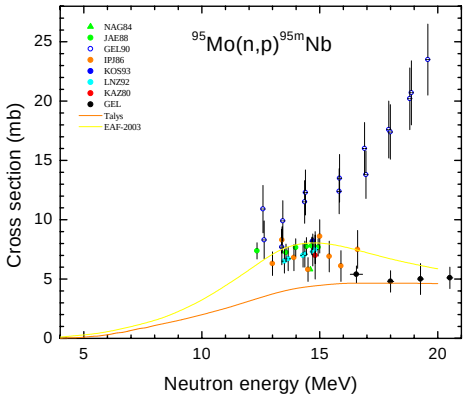

Figure 2.77: $^{95}Mo(n,p)^{95m}Nb$ *reaction.*

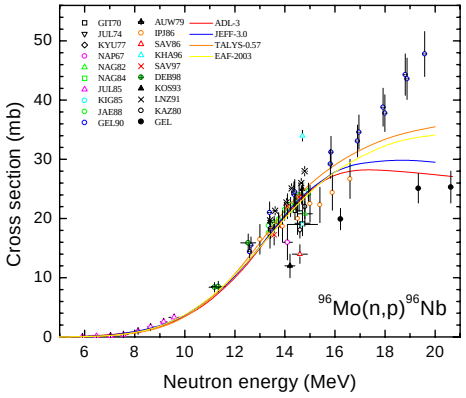

Figure 2.78: $^{96}Mo(n,p)^{96}Nb$ *reaction.*

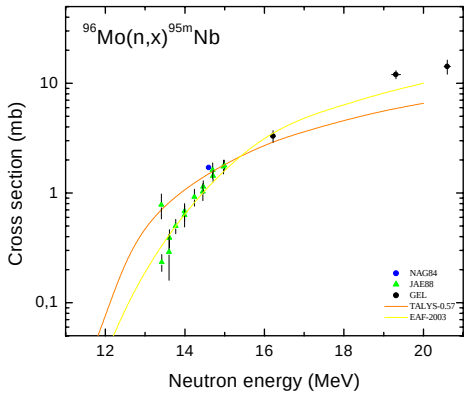

Figure 2.79: $^{96}Mo(n,x)^{95m}Nb$ *reaction.*

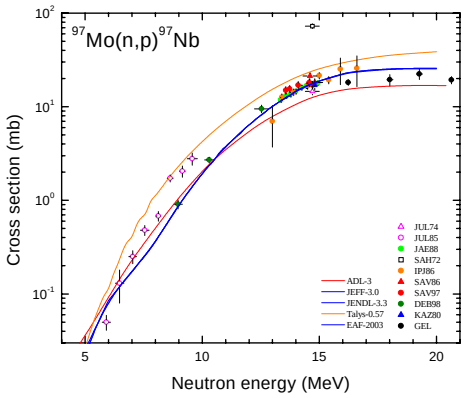

Figure 2.80: $^{97}Mo(n,p)^{97}Nb$ *reaction.*

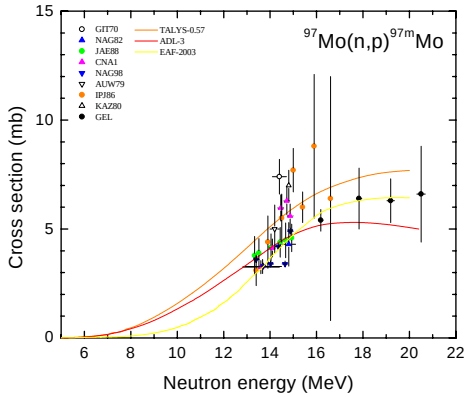

Figure 2.81: $^{97}Mo(n,p)^{97m}Nb$ *reaction.*

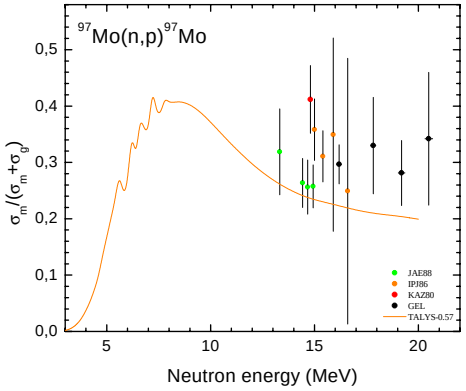

Figure 2.82: $^{97}Mo(n,p)^{97m,g}Nb$ *reaction.*

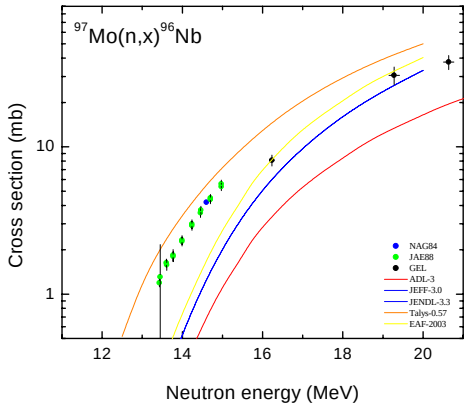

Figure 2.83: $^{97}Mo(n,x)^{96}Nb$ *reaction.*

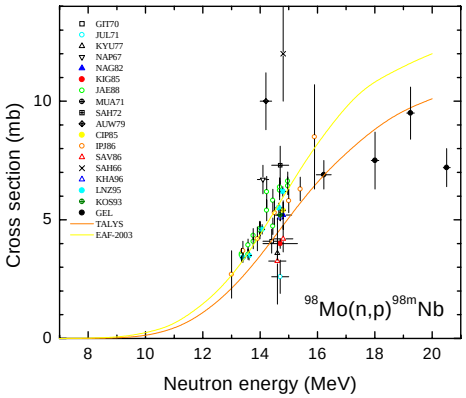

Figure 2.84: $^{98}Mo(n,p)^{98m}Nb$ *reaction.*

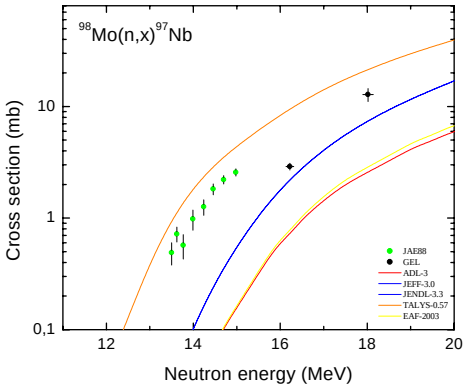

Figure 2.85: $^{98}Mo(n,x)^{97}Nb$ *reaction.*

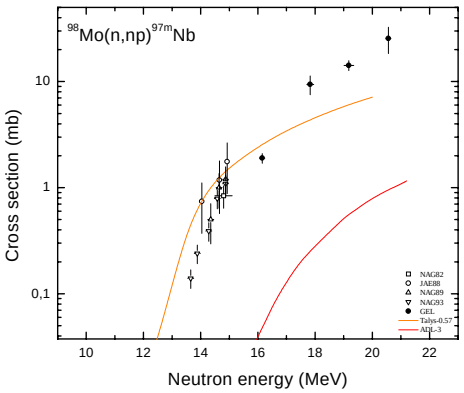

Figure 2.86: *The* $^{98}Mo(n,x)^{97m}Nb$ *reaction.*

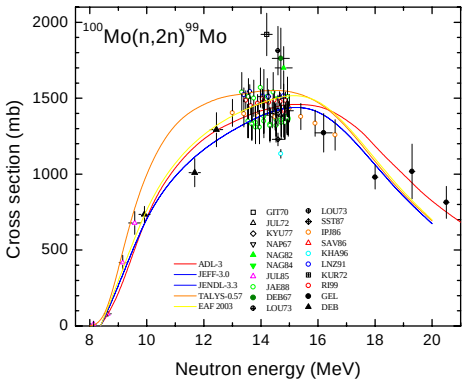

Figure 2.87: $^{100}Mo(n,2n)^{99}Mo$ *reaction.*

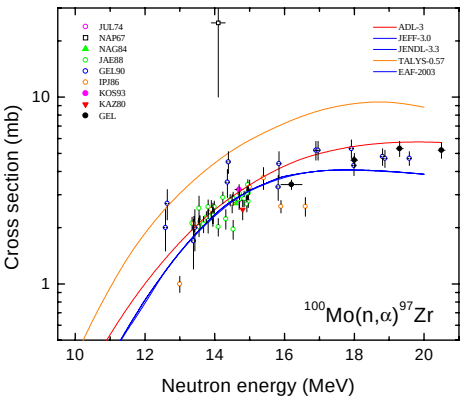

Figure 2.88: $^{100}Mo(n,\alpha)^{97}Zr$ *reaction.*

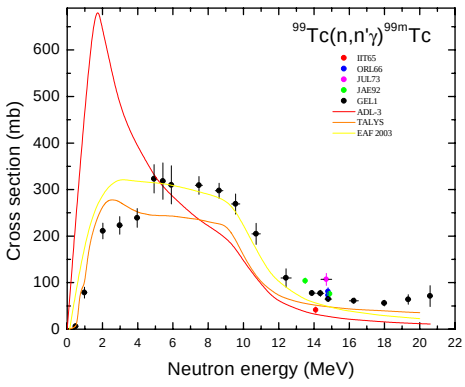

Figure 2.89: $^{99}Tc(n,n'\gamma)^{99m}Tc$ *reaction.*

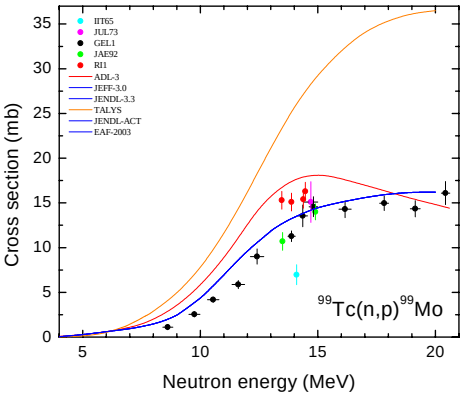

Figure 2.90: $^{99}Tc(n,p)^{99}Mo$ *reaction.*

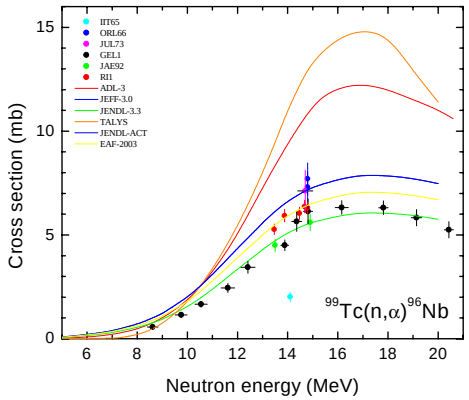

Figure 2.91: $^{99}Tc(n,\alpha)^{96}Nb$ *reaction.*

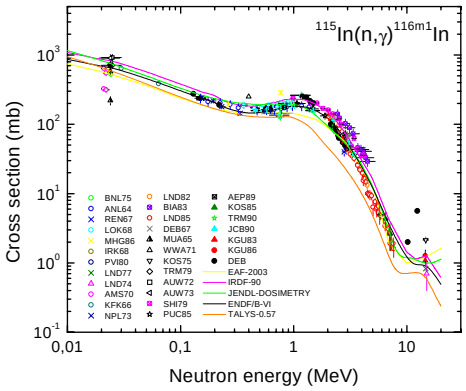

Figure 2.92: $^{115}In(n,\gamma)^{116}In$ *reaction.*

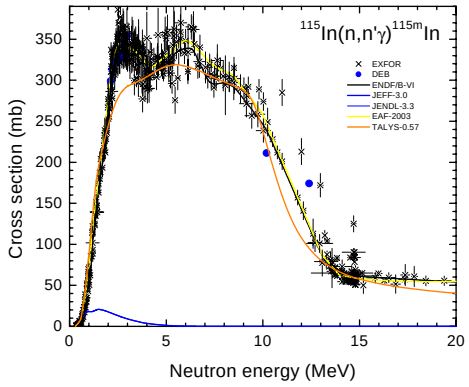

Figure 2.93: $^{115}In(n,n'\gamma)^{115m}In$ *reaction.*

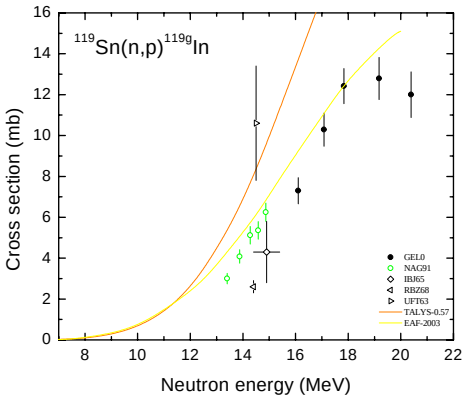

Figure 2.94: $^{119}Sn(n,p)^{119m}In$ *reaction.*

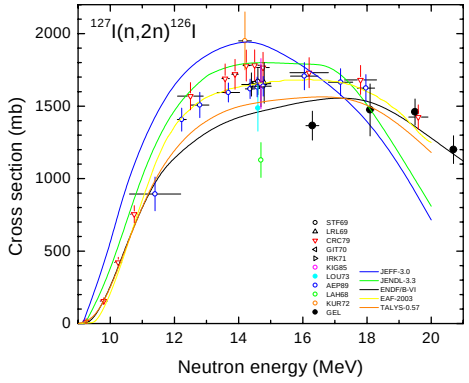

Figure 2.95: $^{127}I(n,2n)^{126}I$ *reaction.*

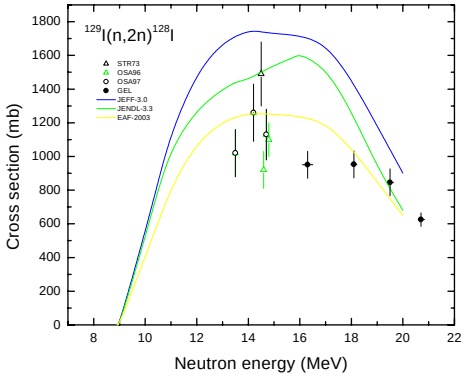

Figure 2.96: $^{129}I(n,2n)^{128}I$ *reaction.*

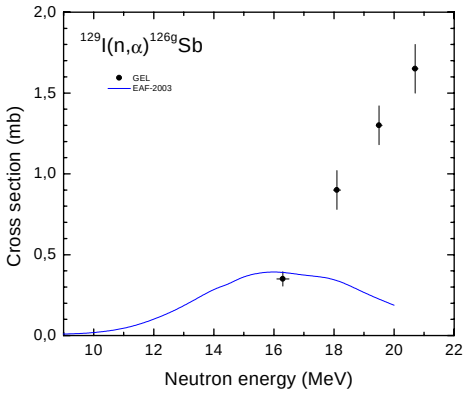

Figure 2.97: $^{129}I(n,\alpha)^{126g}$*Sb reaction.*

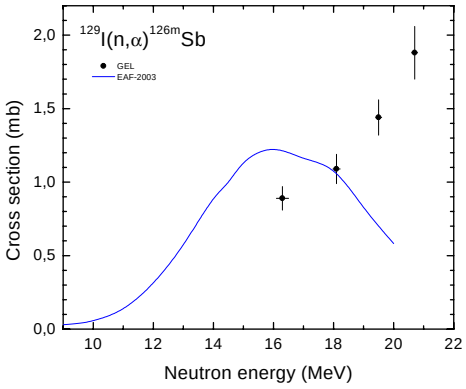

Figure 2.98: $^{129}I(n,\alpha)^{126m}$*Sb reaction.*

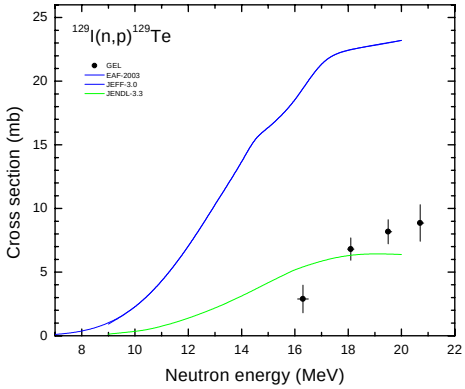

Figure 2.99: $^{129}I(n,p)^{129g}$*Te reaction.*

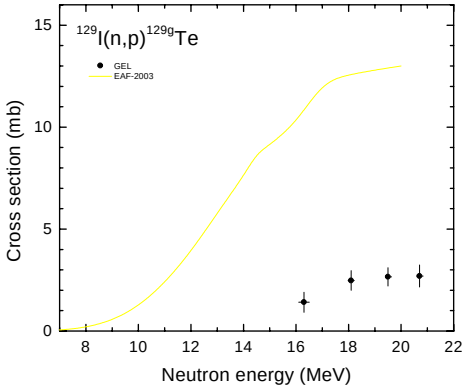

Figure 2.100: $^{129}I(n,p)^{129g}$*Te reaction.*

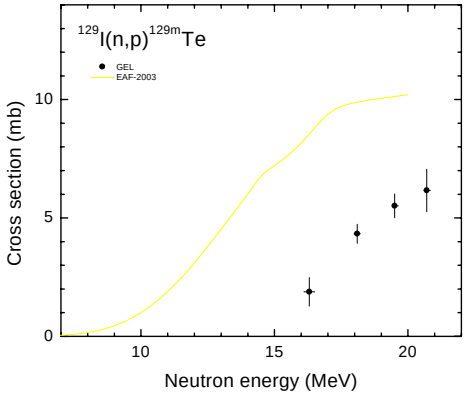

Figure 2.101: $^{129}I(n,p)^{129m}$*Te reaction.*

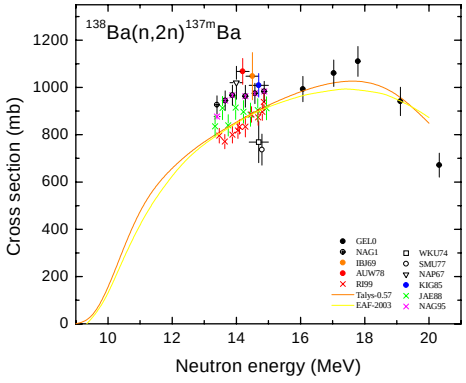

Figure 2.102: $^{138}Ba(n,2n)^{137m}$*Ba reaction.*

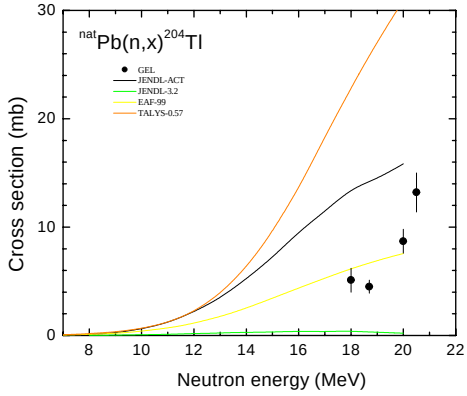

Figure 2.103: *$^{nat}Pb(n,x)^{204}Tl$ reaction.*

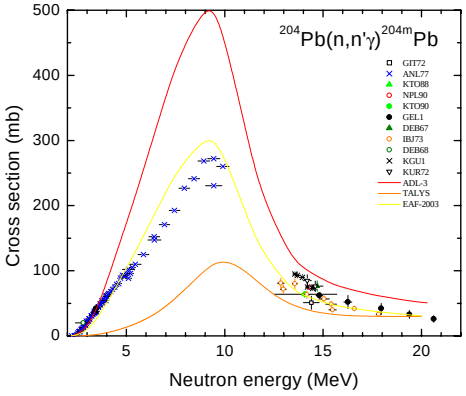

Figure 2.104: *$^{204}Pb(n,n'\gamma)^{204m}Pb$ reaction.*

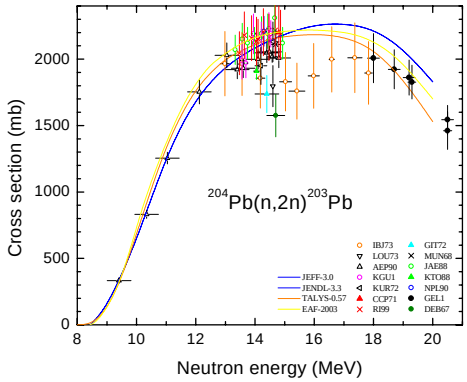

Figure 2.105: *$^{204}Pb(n,2n)^{203}Pb$ reaction.*

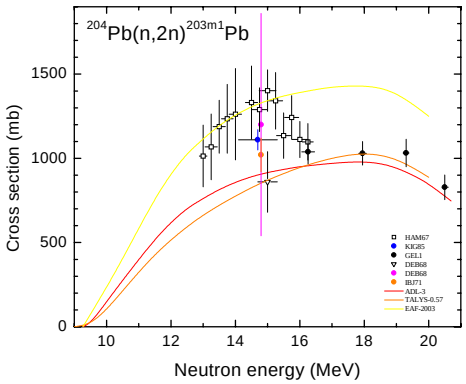

Figure 2.106: *$^{204}Pb(n,2n)^{203m}Pb$ reaction.*

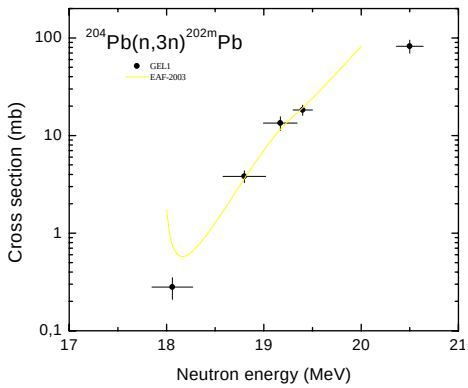

Figure 2.107: *$^{204}Pb(n,3n)^{202m}Pb$ reaction.*

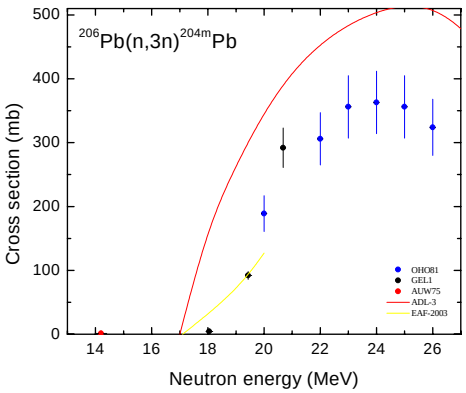

Figure 2.108: *$^{206}Pb(n,3n)^{204m}Pb$ reaction.*

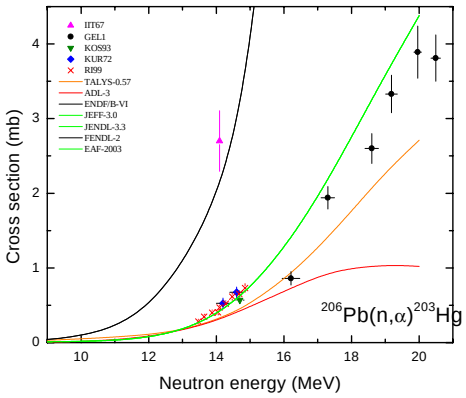

Figure 2.109: $^{206}Pb(n,\alpha)^{203}Hg$ *reaction.*

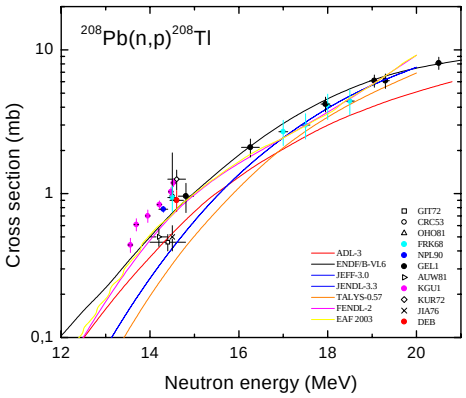

Figure 2.110: $^{208}Pb(n,p)^{208}Tl$ *reaction.*

3. Results of the model calculations with STAPRE

Below one finds the results of the calculations in the local approach with the STAPRE-H code for the ^{51}V, Ni, Co and Mo target nuclei.

Table 3.1: *Results of model calculations in the local approach.*

$^{51}\mathrm{V}(n,p)^{51}\mathrm{Ti}$					
E_n (MeV)	σ (mb)	E_n (MeV)	σ (mb)	E_n (MeV)	σ (mb)
2.6402	1.31E-06	2.9461	2.10E-05	3.2521	1.17E-04
3.5	2.96E-04	3.75	5.92E-04	4	9.37E-04
4.25	0.00133	4.5	0.00168	4.75	0.00207
5	0.00252	5.25	0.00296	5.5	0.0035
5.75	0.00414	6	0.00479	6.25	0.00562
6.5	0.00676	6.75	0.00789	7	0.00903
7.25	0.01026	7.5	0.01125	7.75	0.01209
8	0.01288	21	0.01337	8.25	0.01371
20.75	0.01386	20.5	0.01441	8.5	0.01455
20.25	0.01495	8.75	0.01539	20	0.01549
19.75	0.01608	9	0.01633	19.5	0.01672
9.25	0.01722	19.25	0.01741	19	0.01811
9.5	0.0182	18.75	0.01885	9.75	0.01924
18.5	0.01959	10	0.02033	18.25	0.02037
18	0.02126	10.25	0.02141	17.75	0.02215
10.5	0.02245	17.5	0.02304	10.75	0.02338
17.25	0.02403	11	0.02442	17	0.02491
11.25	0.02541	16.75	0.02575	16.5	0.02629
11.5	0.02634	16.25	0.02654	16	0.02674
15.75	0.02679	15.5	0.02684	15.25	0.02689
15	0.02694	14.75	0.02699	14.5	0.02723
11.75	0.02723	14.25	0.02782	12	0.02792
14	0.02842	12.25	0.02851	13.75	0.02881
12.5	0.02891	13.5	0.02916	12.75	0.02916
13.25	0.0293	13	0.0293		
$^{51}\mathrm{V}(n,\alpha)^{48}\mathrm{Sc}$					
E_n (MeV)	σ (mb)	E_n (MeV)	σ (mb)	E_n (MeV)	σ (mb)
6.01E+00	8.89E-06	6.31E+00	2.59E-05	6.62E+00	6.51E-05
6.92E+00	1.40E-04	7.23E+00	2.84E-04	7.54E+00	5.19E-04
7.75	7.67E-04	8	0.0011	8.25	0.00153
8.5	0.00199	8.75	0.00248	9	0.00301
9.25	0.00347	9.5	0.00396	9.75	0.00439
10	0.00481	10.25	0.00521	10.5	0.00564

Table 3.1: *Results of model calculations in the local approach.*

10.75	0.00613	11	0.00659	11.25	0.00718
11.5	0.00773	11.75	0.00837	12	0.00914
12.25	0.00987	12.5	0.0107	12.75	0.01147
13	0.01221	13.25	0.01294	13.5	0.01359
13.75	0.01429	14	0.015	14.25	0.0157
14.5	0.0165	14.75	0.0172	15	0.01791
15.25	0.01843	15.5	0.01895	15.75	0.01944
16	0.01987	16.25	0.0203	16.5	0.02067
16.75	0.02104	17	0.02131	17.25	0.02144
17.5	0.02144	17.75	0.02131	18	0.02101
18.25	0.02061	18.5	0.02012	18.75	0.01957
19	0.01901	19.25	0.0184	19.5	0.01782
19.75	0.01714	20	0.01647	20.25	0.01582
20.5	0.01518	20.75	0.01457	21	0.01395
$^{51}\mathrm{V}(n,x)^{50}\mathrm{Ti}$					
E_n (MeV)	σ (mb)	E_n (MeV)	σ (mb)	E_n (MeV)	σ (mb)
10.289	0.00417	10.594	0.00864	10.9	0.01528
11.206	0.02418	11.512	0.03538	11.818	0.04607
12.124	0.05491	12.25	0.05712	12.43	0.06201
12.5	0.06272	12.75	0.06645	13	0.06944
13.25	0.07112	13.5	0.07243	13.75	0.07317
14	0.07373	14.25	0.07448	14.5	0.07523
14.75	0.07653	15	0.07784	15.25	0.07952
15.5	0.08139	15.75	0.08344	16	0.08531
16.25	0.08755	16.5	0.08941	16.75	0.09109
17	0.09296	17.25	0.09483	17.5	0.09669
17.75	0.09837	18	0.10024	18.25	0.10173
18.5	0.10341	18.75	0.10491	19	0.10659
19.25	0.10827	19.5	0.10976	19.75	0.11125
20	0.11275	20.25	0.11424	20.5	0.11573
20.75	0.11723	21	0.11853		
$^{51}\mathrm{V}(n,x\alpha)^{47}\mathrm{Sc}$					
E_n (MeV)	σ (mb)	E_n (MeV)	σ (mb)	E_n (MeV)	σ (mb)
1.46E+01	2.42E-06	1.49E+01	8.01E-06	1.52E+01	2.27E-05
1.55E+01	5.76E-05	1.58E+01	1.23E-04	1.61E+01	2.62E-04

Table 3.1: *Results of model calculations in the local approach.*

1.66E+01	8.22E-04	1.70E+01	1.62E-03	1.74E+01	2.83E-03
1.78E+01	4.44E-03	1.82E+01	6.36E-03	1.87E+01	8.54E-03
1.91E+01	1.09E-02	1.95E+01	1.33E-02	1.99E+01	1.57E-02
2.03E+01	1.82E-02	2.07E+01	2.06E-02	2.11E+01	2.29E-02
$^{51}\mathrm{V}(n,2n)^{50}\mathrm{V}$					
E_n (MeV)	σ (mb)	E_n (MeV)	σ (mb)	E_n (MeV)	σ (mb)
12.25	0.1352	12.5	0.1856	12.75	0.2458
13	0.3032	13.25	0.3606	13.5	0.4124
13.75	0.4628	14	0.5048	14.25	0.5468
14.5	0.5818	14.75	0.6182	15	0.6434
15.25	0.6644	15.5	0.6826	15.75	0.698
16	0.7134	16.25	0.7274	16.5	0.7414
16.75	0.7568	17	0.7694	17.25	0.782
17.5	0.7932	17.75	0.8044	18	0.8114
18.25	0.8184	18.5	0.8254	18.75	0.831
19	0.8366	19.25	0.8408	19.5	0.845
19.75	0.8492	20	0.852		
$^{59}\mathrm{Co}(n,2n)^{58}\mathrm{Co}$					
E_n (MeV)	σ (mb)	E_n (MeV)	σ (mb)	E_n (MeV)	σ (mb)
11.3	104	11.6	178	11.9	259
12.21	326	12.52	402	12.82	472
13.13	535	13.43	591	13.74	640
14.04	684	14.35	722	14.65	755
14.96	784	15.27	809	15.57	831
15.87	849	16.18	865	16.38	875
16.79	888	17.20	897	17.60	903
18.01	905	18.42	903	18.82	898
20.04	888	20.45	875	20.86	859
21.27	840	21.67	818	22.08	792
22.49	763	22.89	733	23.30	700
$^{59}\mathrm{Co}(n,2n)^{58m}\mathrm{Co}$					
E_n (MeV)	σ (mb)	E_n (MeV)	σ (mb)	E_n (MeV)	σ (mb)
11.30	76.6	11.60	129	11.91	187
12.21	231	12.52	282	12.82	327

Table 3.1: *Results of model calculations in the local approach.*

13.13	367	13.43	401	13.74	431
14.04	457	14.35	489	14.65	498
14.96	515	15.27	529	15.57	542
15.88	552	16.18	561	16.38	566
16.79	572	17.20	577	17.60	579
18.01	580	18.42	578	18.82	574
20.05	566				
^{59}Co$(n,2n)^{58m,g}$Co					
E_n (MeV)	σ (mb)	E_n (MeV)	σ (mb)	E_n (MeV)	σ (mb)
11.6	0.729	11.9	0.722	12.2	0.713
12.5	0.705	12.8	0.696	13.1	0.688
13.4	0.681	13.7	0.676	14.0	0.671
14.3	0.666	14.7	0.663	15.0	0.66
15.3	0.657	15.6	0.655	15.9	0.653
16.2	0.649	16.4	0.648	16.8	0.646
17.2	0.645	17.6	0.644	18	0.643
18.4	0.642	18.4	0.642	18.8	0.642
19.2	0.642	19.6	0.641	20.0	0.64
20.5	0.64	20.9	0.64	21.3	0.64
21.7	0.641	22.1	0.641	22.5	0.641
^{58}Ni$(n,x)^{57}$Co					
E_n (MeV)	σ (mb)	E_n (MeV)	σ (mb)	E_n (MeV)	σ (mb)
10.1	22.1	10.4	49.5	10.7	84.7
11	126	11.3	171	11.6	221
11.9	272	12.2	323	12.5	374
12.8	422	13.1	468	13.4	512
13.7	551	14	590	14.3	627
14.7	662	14.9	687	15.3	727
15.7	762	16.1	791	16.5	815
16.9	834	17.3	849	17.7	860
18.1	867	18.5	872	18.9	873
19.3	872	20.6	837		

Table 3.1: *Results of model calculations in the local approach.*

^{58}Ni$(n,p)^{58}$Co					
E_n (MeV)	σ (mb)	E_n (MeV)	σ (mb)	E_n (MeV)	σ (mb)
0.14	7.53E-6	0.17	1.73E-5	0.19	2.28E-5
0.2	3.62E-5	0.3	3.44E-4	0.4	0.002
0.51	0.0104	0.605	0.0349	1.1	2.54
1.28	7.14	1.47	16	1.65	16
1.83	25.7	2.02	38.9	2.2	58.4
2.38	86.2	2.56	115	2.75	152
2.93	174	3.11	197	3.3	233
3.48	264	3.66	293	3.85	325
4.03	358	4.21	395	4.4	437
4.58	456	4.76	481	4.95	517
5.13	535	5.49	581	6.41	624
6.72	631	7.02	637	7.33	641
7.63	643	9.16	633	9.46	630
9.77	630	10.1	628	10.4	624
10.7	617	11	609	11.3	598
11.6	583	11.9	565	12.2	544
12.5	521	12.8	496	13.1	469
13.4	440	13.7	408	14	378
14.3	348	14.7	318	14.9	299
15.3	264	15.7	233	16.1	205
16.5	180	16.9	158	17.3	139
17.7	122	18.1	108	18.5	94.9
18.9	84	19.3	74.7	20.6	62.8
^{58}Ni$(n,p)^{58m}$Co					
E_n (MeV)	σ (mb)	E_n (MeV)	σ (mb)	E_n (MeV)	σ (mb)
0.3	1.11E-5	0.51	7.51E-4	0.917	0.124
1.1	0.541	1.28	1.66	1.47	3.84
1.65	4.51	1.83	6.81	2.02	10.2
2.2	15.4	2.38	23.1	2.56	29.7
2.75	39.7	2.93	48.3	3.11	58.7
3.3	72.1	3.48	85.2	3.66	97.7
3.85	110	4.03	125	4.21	140
4.4	156	4.58	165	4.76	175

Table 3.1: *Results of model calculations in the local approach.*

4.95	189	5.13	197	5.49	217
6.41	241	6.72	246	7.02	251
7.33	255	7.63	259	7.94	263
8.24	266	8.55	266	8.85	270
9.16	273	9.46	276	9.77	279
10.1	281	10.4	283	10.7	283
11	283	11.3	281	11.6	277
11.9	271	12.2	264	12.5	255
12.8	245	13.1	234	13.4	222
13.7	208	14	194	14.3	180
14.7	166	14.9	157	15.3	140
15.7	125	16.1	110	16.5	97.9
17.3	76.7	17.7	67.8	18.1	59.9
18.5	53.1	18.9	47.1	19.3	41.9
19.7	37.5	20.1	38	20.6	34.5
^{58}Ni$(n,p)^{58m,g}$Co					
E_n (MeV)	σ (mb)	E_n (MeV)	σ (mb)	E_n (MeV)	σ (mb)
0.3	0.0321	0.51	0.0715	0.917	0.177
1.1	0.213	1.28	0.233	1.47	0.241
1.65	0.282	1.83	0.266	2.02	0.266
2.2	0.264	2.38	0.268	2.56	0.257
2.75	0.261	2.93	0.277	3.11	0.297
3.3	0.309	3.48	0.323	3.66	0.333
3.85	0.339	4.03	0.348	4.21	0.353
4.4	0.358	4.58	0.361	4.76	0.363
4.95	0.365	5.13	0.369	5.49	0.373
6.41	0.386	6.72	0.39	7.02	0.394
7.33	0.399	7.63	0.403	7.94	0.408
8.24	0.414	8.44	0.42	9.16	0.431
9.46	0.437	9.77	0.443	10.1	0.448
10.4	0.454	10.7	0.459	11	0.465
11.3	0.47	11.6	0.475	11.9	0.48
12.2	0.485	12.5	0.49	12.8	0.495
13.1	0.5	13.4	0.504	13.7	0.509
14	0.514	14.3	0.518	14.7	0.522

Table 3.1: *Results of model calculations in the local approach.*

14.9	0.525	15.3	0.531	15.7	0.535
16.1	0.54	16.5	0.544	16.9	0.548
17.3	0.551	17.7	0.554	18.1	0.557
18.5	0.559	18.9	0.561	19.3	0.562
19.7	0.562	20.1	0.55		
^{58}Ni$(n,2n)^{57}$Ni					
E_n (MeV)	σ (mb)	E_n (MeV)	σ (mb)	E_n (MeV)	σ (mb)
13.43	12.9	13.74	17.9	14.04	23.9
14.35	29.8	14.65	35.1	14.85	37.9
15.67	47.9	16.48	55.7	17.30	62.9
18.11	69.77	18.92	76.0	19.74	79.7
20.55	84.7	21.37	89.1		
^{60}Ni$(n,p)^{60}$Co					
E_n (MeV)	σ (mb)	E_n (MeV)	σ (mb)	E_n (MeV)	σ (mb)
3.34	0.012	3.64	0.0861	3.95	0.422
4.25	41.41	4.56	3.28	4.86	6.15
5.17	10.2	5.47	15.3	5.78	21.1
6.08	27	6.39	33.1	6.69	39.5
7	46.3	7.3	53.4	7.61	60.6
7.91	66.8	8.22	74	8.52	81
8.83	88	9.13	94.8	9.44	102
9.74	108	10	115	10.4	121
10.7	127	11	133	11.3	139
11.6	145	11.9	150	12.2	155
12.5	159	12.8	161	13.1	162
13.4	161	13.7	158	14	155
14.3	150	14.6	144	14.9	137
15.2	130	15.5	122	16	107
16.5	96.9	16.9	87.1	17.3	78.1
18.5	62.2	18.9	56.2	19.3	50.9
19.7	46.1	20.1	41.9		
^{60}Ni$(n,p)^{60m}$Co					
E_n (MeV)	σ (mb)	E_n (MeV)	σ (mb)	E_n (MeV)	σ (mb)
3.34	8.41E-3	3.64	6.13E-2	3.95	0.299

Table 3.1: *Results of model calculations in the local approach.*

4.25	0.959	4.56	2.23	4.86	4.21
5.17	7	5.47	10.5	5.78	14.4
6.08	18.5	6.39	22.6	6.69	26.9
7	31.3	7.3	35.9	7.61	40.7
7.91	44.7	8.22	49.3	8.52	53.6
8.83	57.8	9.13	61.8	9.44	65.6
9.74	69.3	10	72.9	10.4	76.1
10.7	79.2	11	82	11.3	84.8
11.6	87.4	11.9	89.9	12.2	91.7
12.5	93	12.8	93.4	13.1	92.9
13.4	91.4	13.7	89.2	14	86.3
14.3	82.8	14.6	78.8	14.9	74.2
15.2	69.4	15.5	64.5	16	55.9
16.5	49.9	16.9	44.3	17.3	39.4
18.5	31.2	18.9	28.1	19.3	25.4
19.7	23	20.1	20.9		
^{60}Ni$(n,p)^{60m,g}$Co					
E_n (MeV)	σ (mb)	E_n (MeV)	σ (mb)	E_n (MeV)	σ (mb)
3.64	0.712	3.95	0.703	4.25	0.679
4.56	0.681	4.86	0.683	5.17	0.684
5.47	0.684	6.39	0.681	7.3	0.672
8.22	0.664	9.13	0.65	10	0.634
11	0.616	11.9	0.597	12.8	0.579
13.7	0.562	14.6	0.546	15.5	0.53
16	0.52	16.9	0.509	17.7	0.5
18.5	0.501	19.3	0.499	20.1	0.499
^{61}Ni$(n,p)^{61}$Co					
E_n (MeV)	σ (mb)	E_n (MeV)	σ (mb)	E_n (MeV)	σ (mb)
1.73	4.31E-3	2.04	3.54E-2	2.34	0.143
2.65	0.405	2.95	0.853	3.26	1.46
3.56	2.3	3.87	3.31	4.17	4.63
4.48	6.28	4.78	8.29	5.09	10.4
5.39	12.7	5.7	14.9	6	17
6.31	19.2	6.61	21.6	6.92	24.1
7.22	26.7	7.53	29.3	7.83	31.9

Table 3.1: *Results of model calculations in the local approach.*

8.14	34.6	8.44	37.5	8.75	40.4
9.66	51.3	9.97	54.1	10.3	56.7
10.6	59.5	10.9	62	11.2	64.5
11.5	66.9	11.8	69.3	12.1	71.7
12.4	73.9	12.7	75.7	13	76.9
13.2	77.1	13.6	77.4	14	76.6
14.4	75	14.8	72.5	15.3	69.5
15.7	65.9	16.1	62.2	16.5	58.4
16.9	54.7	17.3	51.1	17.7	47.9
18.1	44.9	18.5	41.9	18.9	39.2
19.3	36.6	19.7	34.1		
^{61}Ni$(n,x)^{60m}$Co					
E_n (MeV)	σ (mb)	E_n (MeV)	σ (mb)	E_n (MeV)	σ (mb)
9.05	6.92E-7	9.36	1.7E-5	9.66	1.79E-4
9.97	1.09E-3	10.3	4.55E-3	10.6	1.45E-2
10.9	3.73E-2	11.2	8.15E-2	11.5	0.157
11.8	0.276	12.1	0.466	12.4	0.769
12.7	1.59	13	2.43	13.2	3.09
13.6	5.01	14	7.58	14.4	10.8
14.8	14.5	15.3	18.8	15.7	23.5
16.1	28.5	16.5	33.8	16.9	39
17.3	44.7	17.7	50	18.1	55.2
18.5	60.7	18.9	65.6	19.3	70.2
19.7	74.4				
^{62}Ni$(n,x)^{61}$Co					
E_n (MeV)	σ (mb)	E_n (MeV)	σ (mb)	E_n (MeV)	σ (mb)
13.173	0.283	13.783	0.987	14.088	1.76
14.392	2.94	14.697	4.6	15.002	6.75
15.307	9.38	15.612	12.46	15.917	15.92
16.222	19.75	16.527	24.07	16.628	25.63
17.035	32.01	17.441	38.73	17.848	45.73
18.254	52.84	18.661	59.98	19.067	67.09
19.474	73.77	19.88	94.65	20.287	102.2
20.693	109.5	21.1	116.7		

Table 3.1: *Results of model calculations in the local approach.*

^{92}Mo$(n,2n)^{91m}$Mo					
E_n (MeV)	σ (mb)	E_n (MeV)	σ (mb)	E_n (MeV)	σ (mb)
14.588	0.01402	14.891	0.02178	15.195	0.0303
15.498	0.03946	15.7	0.04812	16.105	0.05856
16.509	0.07026	16.913	0.08001	17.318	0.08774
17.722	0.09362	18.127	0.09776	18.531	0.10049
18.935	0.10209	19.34	0.10264	19.744	0.10223
20.149	0.10167	20.553	0.10085	20.957	0.09982
^{92}Mo$(n,2n)^{91}$Mo					
E_n (MeV)	σ (mb)	E_n (MeV)	σ (mb)	E_n (MeV)	σ (mb)
13.982	0.11529	14.285	0.15747	14.588	0.19741
14.891	0.238	15.195	0.27745	15.498	0.31489
15.7	0.34769	16.105	0.37621	16.509	0.41726
16.913	0.45424	17.318	0.48671	17.722	0.51418
18.127	0.53683	18.531	0.55497	18.935	0.56911
19.34	0.57949	19.744	0.58409	20.149	0.58797
20.553	0.59046	20.957	0.59162		
^{92}Mo$(n,\alpha)^{89m}$Zr					
E_n (MeV)	σ (mb)	E_n (MeV)	σ (mb)	E_n (MeV)	σ (mb)
5.4895	1.82E-04	5.7928	2.51E-04	6.0961	3.39E-04
6.3994	4.48E-04	6.7027	5.81E-04	7.006	7.38E-04
7.3093	9.20E-04	7.6126	0.00112	7.9158	0.00135
8.2191	0.00159	8.5224	0.00183	8.8257	0.00204
9.129	0.00241	9.4323	0.00269	9.7356	0.00296
10.039	0.00323	10.342	0.0035	10.645	0.00376
10.949	0.00402	11.252	0.00425	11.555	0.00448
11.859	0.0047	12.162	0.00491	13.678	0.00645
13.982	0.00666	14.285	0.00685	14.588	0.00703
15.195	0.00733	15.8	0.00707	16.913	0.00695
17.318	0.00674	17.722	0.00646	18.127	0.0061
18.531	0.00571	19.542	0.00527	20.553	0.00503
20.957	0.00474				
^{92}Mo$(n,\alpha)^{89}$Zr					
E_n	σ	E_n	σ	E_n	σ

Table 3.1: *Results of model calculations in the local approach.*

(MeV)	(mb)	(MeV)	(mb)	(MeV)	(mb)
5.4895	7.90E-04	5.7928	0.00102	6.0961	0.00129
6.3994	0.00161	6.7027	0.00196	7.006	0.00234
7.3093	0.00275	7.6126	0.00318	7.9158	0.00365
8.2191	0.00416	8.5224	0.00473	8.8257	0.00524
9.129	0.00613	9.4323	0.00693	9.7356	0.0078
10.039	0.00872	10.342	0.00969	10.645	0.0107
10.949	0.01173	11.252	0.01277	11.555	0.01381
11.859	0.01487	12.162	0.01592	13.678	0.02306
13.982	0.0243	14.285	0.02553	14.588	0.02674
15.195	0.02907	15.8	0.03039	16.913	0.03241
17.318	0.03288	17.722	0.03302	18.127	0.03277
18.531	0.03214	19.54	0.0309	20.553	0.0287
20.957	0.02689				
^{92}Mo$(n,d)^{91m}$Nb					
E_n (MeV)	σ (mb)	E_n (MeV)	σ (mb)	E_n (MeV)	σ (mb)
7.9158	8.74E-08	8.2191	3.41E-07	8.5224	1.01E-06
8.8257	2.41E-06	9.129	5.07E-06	9.4323	9.66E-06
9.7356	1.72E-05	10.039	2.96E-05	10.342	4.97E-05
10.645	8.16E-05	10.949	1.31E-04	11.252	2.03E-04
11.555	3.75E-04	11.859	5.49E-04	12.162	7.73E-04
12.465	0.00105	12.768	0.00139	13.072	0.00179
13.375	0.00225	13.678	0.00276	13.982	0.00334
14.285	0.00397	14.588	0.00464	14.891	0.00537
15.195	0.00613	15.498	0.00693	15.7	0.00792
16.105	0.00904	16.509	0.01023	16.913	0.01145
17.318	0.01268	17.722	0.01392	18.127	0.01515
19.34	0.02516	19.744	0.02662	20.149	0.02799
20.553	0.02927	20.957	0.03044		
^{92}Mo$(n,d)^{91}$Nb					
E_n (MeV)	σ (mb)	E_n (MeV)	σ (mb)	E_n (MeV)	σ (mb)
7.6126	7.39E-08	7.9158	3.83E-07	8.2191	1.41E-06
8.5224	4.02E-06	8.8257	9.25E-06	9.129	1.90E-05
9.4323	3.51E-05	9.7356	6.06E-05	10.039	1.00E-04
10.342	1.61E-04	10.645	2.54E-04	10.949	3.94E-04

Table 3.1: *Results of model calculations in the local approach.*

11.252	5.97E-04	11.555	0.00107	11.859	0.00156
12.162	0.00221	12.465	0.00302	12.768	0.00402
13.072	0.00521	13.375	0.0066	13.678	0.00819
13.982	0.00998	14.285	0.01196	14.588	0.01412
14.891	0.01646	15.195	0.01896	15.498	0.02161
15.7	0.02351	16.105	0.02718	16.509	0.03125
16.913	0.03553	17.318	0.03998	17.722	0.04458
18.127	0.04929	19.34	0.09021	19.744	0.09651
20.149	0.10266	20.553	0.10866	20.957	0.11445
^{92}Mo$(n,np)^{91m}$Nb					
E_n (MeV)	σ (mb)	E_n (MeV)	σ (mb)	E_n (MeV)	σ (mb)
9.7356	1.18E-04	10.039	5.82E-04	10.342	0.00198
10.645	0.00509	10.949	0.01072	11.252	0.0194
11.555	0.03128	11.859	0.04603	12.162	0.06298
12.465	0.08124	12.768	0.10003	13.072	0.11806
13.375	0.13426	13.678	0.14809	13.982	0.1588
14.285	0.16661	14.588	0.17193	14.891	0.17466
15.195	0.17559	15.498	0.17524	15.7	0.17544
16.105	0.16595	16.509	0.16292	16.913	0.15935
17.318	0.15558	17.722	0.1519	18.127	0.14837
18.531	0.14506	18.935	0.14198	19.34	0.13891
19.744	0.13582	20.149	0.13328	20.553	0.13088
20.957	0.12857				
^{92}Mo$(n,np)^{91}$Nb					
E_n (MeV)	σ (mb)	E_n (MeV)	σ (mb)	E_n (MeV)	σ (mb)
9.7356	7.55E-04	10.039	0.00339	10.342	0.01082
10.645	0.02679	10.949	0.05482	11.252	0.09699
11.555	0.15348	11.859	0.22241	12.162	0.30057
12.465	0.3844	12.768	0.47071	13.072	0.54895
13.375	0.61062	13.678	0.65988	13.982	0.70045
14.285	0.73628	14.588	0.76862	14.891	0.79386
15.195	0.81328	15.498	0.82788	15.7	0.8364
16.105	0.81278	16.509	0.81513	16.913	0.81297
17.318	0.80765	17.722	0.80088	18.127	0.79328
18.531	0.7856	18.935	0.77813	19.34	0.7712

Table 3.1: *Results of model calculations in the local approach.*

19.744	0.76123	20.149	0.754	20.553	0.74765
20.957	0.74184				
^{92}Mo$(n,p)^{92m}$Nb					
E_n (MeV)	σ (mb)	E_n (MeV)	σ (mb)	E_n (MeV)	σ (mb)
2.1534	7.01E-04	2.4566	0.00178	2.7599	0.00396
3.0632	0.00715	3.3665	0.0102	3.6698	0.01547
3.9731	0.01969	4.2764	0.02511	4.5797	0.03424
4.883	0.04357	5.1862	0.04927	5.4895	0.05442
5.7928	0.05857	6.0961	0.06284	6.3994	0.06727
6.7027	0.07112	7.006	0.07417	7.3093	0.07723
7.6126	0.08049	7.9158	0.08356	8.2191	0.08626
9.129	0.09484	9.4323	0.09685	9.7356	0.09875
10.039	0.10056	10.342	0.10221	10.645	0.1036
10.949	0.10464	11.252	0.1051	11.555	0.10501
11.859	0.10429	12.162	0.10289	12.465	0.1007
12.768	0.09781	13.072	0.09416	13.375	0.08977
13.678	0.08473	13.982	0.07913	14.285	0.07304
14.588	0.06677	14.891	0.06078	15.195	0.05534
15.9	0.04835	16.913	0.04144	17.318	0.03815
17.722	0.03535	18.127	0.03293	18.531	0.03082
18.935	0.02897	19.34	0.02734	19.744	0.02584
20.149	0.02452	20.553	0.02334	20.957	0.02226
^{94}Mo$(n,2n)^{93m}$Mo					
E_n (MeV)	σ (mb)	E_n (MeV)	σ (mb)	E_n (MeV)	σ (mb)
13.171	5.29E-04	13.474	0.00112	13.777	0.002
14.08	0.0031	14.384	0.00438	14.687	0.00576
14.99	0.00677	15.293	0.00811	15.597	0.00945
15.9	0.01079	16.203	0.01215	16.405	0.01389
16.809	0.01578	17.214	0.01771	17.618	0.01968
18.022	0.02181	18.427	0.02383	18.831	0.02587
19.235	0.02782	19.64	0.02993	20.044	0.03184
20.448	0.03385	20.852	0.03591		
^{94}Mo$(n,2n)^{93}$Mo					
E_n (MeV)	σ (mb)	E_n (MeV)	σ (mb)	E_n (MeV)	σ (mb)

Table 3.1: *Results of model calculations in the local approach.*

10.745	0.27296	11.048	0.40326	11.352	0.52501
11.655	0.63601	11.958	0.7385	12.261	0.8326
12.564	0.92038	12.868	1.0007	13.171	1.0734
13.474	1.1374	13.777	1.193	14.08	1.2412
14.384	1.2828	14.687	1.318	14.99	1.29
15.293	1.3155	15.597	1.3363	15.9	1.3534
16.203	1.3673	16.405	1.3735	16.809	1.3857
17.214	1.3943	17.618	1.3997	18.022	1.3994
18.427	1.3973	18.831	1.3918	19.235	1.3774
19.64	1.3627	20.044	1.3402	20.448	1.3148
20.852	1.2852				
^{94}Mo$(n,d)^{93m}$Nb					
E_n (MeV)	σ (mb)	E_n (MeV)	σ (mb)	E_n (MeV)	σ (mb)
8.9258	1.39E-08	9.229	6.59E-08	9.5322	2.50E-07
9.8354	8.03E-07	10.139	2.24E-06	10.442	5.57E-06
10.745	1.25E-05	11.048	2.54E-05	11.352	6.26E-05
11.655	1.09E-04	11.958	1.77E-04	12.261	2.72E-04
12.564	3.97E-04	12.868	5.55E-04	13.171	7.47E-04
13.474	9.73E-04	13.777	0.00123	14.08	0.00153
14.384	0.00186	14.687	0.00223	14.99	0.00261
15.293	0.00303	15.597	0.00348	15.9	0.00395
16.203	0.00444	16.405	0.00449	16.809	0.00516
17.214	0.00586	17.618	0.00659	19.64	0.01353
20.044	0.01443	20.448	0.01529	20.852	0.01607
^{94}Mo$(n,d)^{93}$Nb					
E_n (MeV)	σ (mb)	E_n (MeV)	σ (mb)	E_n (MeV)	σ (mb)
8.6225	7.01E-09	8.9258	4.44E-08	9.229	2.06E-07
9.5322	7.63E-07	9.8354	2.39E-06	10.139	6.55E-06
10.442	1.60E-05	10.745	3.55E-05	11.048	7.23E-05
11.352	1.78E-04	11.655	3.12E-04	11.958	5.13E-04
12.261	7.97E-04	12.564	0.00118	12.868	0.00168
13.171	0.00229	13.474	0.00304	13.777	0.00391
14.08	0.00492	14.384	0.00605	14.687	0.00732
14.99	0.00866	15.293	0.01016	15.597	0.01177
15.9	0.01348	16.203	0.01529	16.405	0.0165

Table 3.1: *Results of model calculations in the local approach.*

16.809	0.01913	17.214	0.02191	17.618	0.02481
19.64	0.0573	20.044	0.06133	20.448	0.06519
20.852	0.06876				
^{94}Mo$(n,np)^{93m}$Nb					
E_n (MeV)	σ (mb)	E_n (MeV)	σ (mb)	E_n (MeV)	σ (mb)
11.048	3.05E-06	11.352	9.00E-06	11.655	2.48E-05
11.958	6.15E-05	12.261	1.38E-04	12.564	2.72E-04
12.868	4.66E-04	13.171	7.30E-04	13.474	0.00109
13.777	0.00156	14.08	0.00216	14.384	0.00289
14.687	0.00376	14.99	0.0045	15.293	0.00553
15.597	0.00662	15.9	0.00774	16.203	0.00885
16.405	0.00972	16.809	0.01107	17.214	0.01238
17.618	0.01363	18.022	0.01478	18.427	0.01589
18.831	0.01695	19.235	0.01792	19.64	0.01889
20.044	0.01968	20.448	0.02047	20.852	0.02125
^{94}Mo$(n,np)^{93}$Nb					
E_n (MeV)	σ (mb)	E_n (MeV)	σ (mb)	E_n (MeV)	σ (mb)
11.048	4.40E-05	11.352	1.35E-04	11.655	3.31E-04
11.958	6.84E-04	12.261	0.00127	12.564	0.00207
12.868	0.00305	13.171	0.00429	13.474	0.00593
13.777	0.00807	14.08	0.01083	14.384	0.01423
14.687	0.01829	14.99	0.02196	15.293	0.02696
15.597	0.03231	15.9	0.03787	16.203	0.04351
16.405	0.04885	16.809	0.05615	17.214	0.06349
17.618	0.0709	18.022	0.07817	18.427	0.08511
18.831	0.09194	19.235	0.09823	19.64	0.10485
20.044	0.11064	20.448	0.11659	20.852	0.12254
^{94}Mo$(n,p)^{94m}$Nb					
E_n (MeV)	σ (mb)	E_n (MeV)	σ (mb)	E_n (MeV)	σ (mb)
3.771	1.92E-05	4.0743	5.10E-05	4.3775	1.12E-04
4.6807	2.12E-04	4.9839	3.63E-04	5.2871	5.76E-04
5.5904	8.64E-04	5.8936	0.00124	6.1968	0.0017
6.5	0.00227	6.8032	0.00295	7.1064	0.00373
7.4097	0.00461	7.7129	0.00559	8.0161	0.00664

Table 3.1: *Results of model calculations in the local approach.*

8.3193	0.00857	8.6225	0.0098	8.9258	0.01112
9.229	0.01247	9.5322	0.01386	9.8354	0.0153
10.139	0.01681	10.442	0.01836	10.745	0.01993
11.048	0.02152	11.352	0.02312	11.655	0.02471
11.958	0.02625	12.261	0.02766	12.564	0.02904
12.868	0.03029	13.171	0.0313	13.474	0.03206
14.839	0.03458	16.203	0.03241	16.405	0.03081
16.809	0.02935	17.214	0.02807	17.618	0.02695
18.022	0.02591	18.427	0.02492	18.831	0.02401
19.235	0.02312	19.64	0.02233	20.044	0.02152
20.448	0.02077	20.852	0.02007		
^{94}Mo$(n,p)^{94}$Nb					
E_n (MeV)	σ (mb)	E_n (MeV)	σ (mb)	E_n (MeV)	σ (mb)
3.771	2.16E-05	4.0743	5.78E-05	4.3775	1.28E-04
4.6807	2.46E-04	4.9839	4.28E-04	5.2871	6.89E-04
5.5904	0.00105	5.8936	0.00151	6.1968	0.0021
6.5	0.00283	6.8032	0.00369	7.1064	0.00469
7.4097	0.00584	7.7129	0.00711	8.0161	0.0085
8.3193	0.01118	8.6225	0.01287	8.9258	0.01472
9.229	0.01662	9.5322	0.0186	9.8354	0.02067
10.139	0.02288	10.442	0.02517	10.745	0.02753
11.048	0.02994	11.352	0.0324	11.655	0.03487
11.958	0.0373	12.261	0.03952	12.564	0.04177
12.868	0.04388	13.171	0.04561	13.474	0.04698
14.839	0.0524	16.405	0.04652	16.809	0.04413
17.214	0.04203	17.618	0.04023	18.022	0.03855
18.427	0.03694	18.831	0.03546	19.235	0.03401
19.64	0.03277	20.044	0.03152	20.448	0.03038
20.852	0.02932				
^{95}Mo$(n,d)^{94}$Nb					
E_n (MeV)	σ (mb)	E_n (MeV)	σ (mb)	E_n (MeV)	σ (mb)
8.9399	1.24E-08	9.2431	8.05E-08	9.5463	3.86E-07
9.8495	1.46E-06	10.153	4.63E-06	10.456	1.26E-05
10.759	3.04E-05	11.062	6.59E-05	11.365	1.31E-04
11.669	2.39E-04	11.972	5.57E-04	12.275	8.83E-04

Table 3.1: *Results of model calculations in the local approach.*

12.578	0.00133	12.881	0.00191	13.185	0.00264
13.488	0.00352	13.791	0.00456	14.094	0.00577
14.397	0.00713	14.599	0.00812	15.004	0.01031
15.408	0.01276	15.812	0.01535	16.216	0.01822
16.621	0.02128	17.025	0.02451	17.429	0.02788
17.833	0.03136	18.238	0.03489	18.642	0.0384
20.663	0.07355	21.067	0.07551	21.472	0.07691
21.876	0.07774	22.28	0.07812		
^{95}Mo$(n,np)^{94}$Nb					
E_n (MeV)	σ (mb)	E_n (MeV)	σ (mb)	E_n (MeV)	σ (mb)
11.365	1.00E-05	11.669	3.23E-05	11.972	8.61E-05
12.275	1.97E-04	12.578	4.01E-04	12.881	7.46E-04
13.185	0.00127	13.488	0.00204	13.791	0.0031
14.094	0.00449	14.397	0.00623	14.599	0.00759
15.004	0.01069	15.408	0.01423	15.812	0.01768
16.216	0.02169	16.621	0.02574	17.025	0.02998
17.429	0.03443	17.833	0.03889	18.238	0.04342
18.642	0.04801	19.046	0.05265	19.45	0.05733
19.855	0.06204	20.259	0.06634	20.663	0.07095
21.067	0.07543	21.472	0.07966	21.876	0.08307
22.28	0.08632				
^{95}Mo$(n,p)^{95m}$Nb					
E_n (MeV)	σ (mb)	E_n (MeV)	σ (mb)	E_n (MeV)	σ (mb)
3.771	1.92E-05	4.0743	5.10E-05	4.3775	1.12E-04
4.6807	2.12E-04	4.9839	3.63E-04	5.2871	5.76E-04
5.5904	8.64E-04	5.8936	0.00124	6.1968	0.0017
6.5	0.00227	6.8032	0.00295	7.1064	0.00373
7.4097	0.00461	7.7129	0.00559	8.0161	0.00664
8.3193	0.00857	8.6225	0.0098	8.9258	0.01112
9.229	0.01247	9.5322	0.01386	9.8354	0.0153
10.139	0.01681	10.442	0.01836	10.745	0.01993
11.048	0.02152	11.352	0.02312	11.655	0.02471
11.958	0.02625	12.261	0.02766	12.564	0.02904
12.868	0.03029	13.171	0.0313	13.474	0.03206
14.839	0.03458	16.203	0.03241	16.405	0.03081

Table 3.1: *Results of model calculations in the local approach.*

16.809	0.02935	17.214	0.02807	17.618	0.02695
18.022	0.02591	18.427	0.02492	18.831	0.02401
19.235	0.02312	19.64	0.02233	20.044	0.02152
20.448	0.02077	20.852	0.02007		
^{95}Mo$(n,p)^{95}$Nb					
E_n (MeV)	σ (mb)	E_n (MeV)	σ (mb)	E_n (MeV)	σ (mb)
17.833	0.04193	17.429	0.04304	15.61	0.0415
14.094	0.03488	13.791	0.03404	13.488	0.03293
13.185	0.03165	12.881	0.03032	12.578	0.02859
12.275	0.02694	11.972	0.0254	11.669	0.02368
11.365	0.02197	11.062	0.0203	10.759	0.01866
10.456	0.01708	10.153	0.01556	9.8495	0.01411
9.5463	0.01278	9.2431	0.01154	8.9399	0.01035
8.0304	0.00493	7.7272	0.00412	7.424	0.00339
7.1208	0.00275	6.8176	0.00218	6.5144	0.00171
6.2113	0.00131	5.9081	9.89E-04	5.6049	7.19E-04
5.3017	5.13E-04	4.9985	3.55E-04	4.6953	2.37E-04
4.3921	1.53E-04	4.089	8.69E-05	3.7858	5.10E-05
3.4826	2.78E-05	3.1794	1.37E-05	2.8762	5.90E-06
2.573	2.09E-06	2.2698	5.89E-07		
^{96}Mo$(n,d)^{95m}$Nb					
E_n (MeV)	σ (mb)	E_n (MeV)	σ (mb)	E_n (MeV)	σ (mb)
9.7807	3.55E-09	10.084	2.41E-08	10.387	1.18E-07
10.69	4.55E-07	10.993	1.45E-06	11.296	4.63E-06
11.6	1.12E-05	11.903	2.41E-05	12.206	4.75E-05
12.509	8.62E-05	12.812	1.45E-04	13.115	2.30E-04
13.419	3.44E-04	13.722	4.91E-04	14.025	6.70E-04
14.328	8.81E-04	14.631	0.00112	14.934	0.0014
15.237	0.0017	15.541	0.00202	15.844	0.00237
16.147	0.00275	16.45	0.00314	16.753	0.00355
16.955	0.00409	17.359	0.0047	17.764	0.00532
18.976	0.00956	19.381	0.01042	19.785	0.01127
20.189	0.01211	20.593	0.01291	20.997	0.01354
^{96}Mo$(n,d)^{95}$Nb					
E_n	σ	E_n	σ	E_n	σ

Table 3.1: *Results of model calculations in the local approach.*

(MeV)	(mb)	(MeV)	(mb)	(MeV)	(mb)
9.4775	2.49E-09	9.7807	1.67E-08	10.084	8.40E-08
10.387	3.39E-07	10.69	1.15E-06	10.993	3.40E-06
11.296	1.03E-05	11.6	2.44E-05	11.903	5.25E-05
12.206	1.04E-04	12.509	1.91E-04	12.812	3.29E-04
13.115	5.34E-04	13.419	8.23E-04	13.722	0.00121
14.025	0.00171	14.328	0.00233	14.631	0.00309
14.934	0.00398	15.237	0.00502	15.541	0.00619
15.844	0.0075	16.147	0.00895	16.45	0.01053
16.753	0.01223	16.955	0.01335	17.359	0.0159
17.764	0.01865	18.976	0.03938	19.381	0.04381
19.785	0.04828	20.189	0.05275	20.593	0.05711
20.997	0.06101				
^{96}Mo$(n,np)^{95m}$Nb					
E_n (MeV)	σ (mb)	E_n (MeV)	σ (mb)	E_n (MeV)	σ (mb)
12.206	2.06E-06	12.509	6.69E-06	12.812	1.78E-05
13.115	4.08E-05	13.419	8.28E-05	13.722	1.52E-04
14.025	2.59E-04	14.328	3.89E-04	14.631	5.84E-04
14.934	8.33E-04	15.237	0.00114	15.541	0.00149
15.844	0.00188	16.147	0.00231	16.45	0.00275
16.753	0.00321	16.955	0.0035	17.359	0.0041
17.764	0.00469	18.168	0.00525	18.572	0.00579
18.976	0.00624	19.381	0.00668	19.785	0.00712
20.189	0.00753	20.593	0.00792	20.997	0.0083
^{96}Mo$(n,np)^{95}$Nb					
E_n (MeV)	σ (mb)	E_n (MeV)	σ (mb)	E_n (MeV)	σ (mb)
11.903	6.97E-06	12.206	2.39E-05	12.509	6.80E-05
12.812	1.66E-04	13.115	3.54E-04	13.419	6.80E-04
13.722	0.0012	14.025	0.00196	14.328	0.00291
14.631	0.00425	14.934	0.00591	15.237	0.00789
15.541	0.01015	15.844	0.01263	16.147	0.01527
16.45	0.018	16.753	0.02083	16.955	0.02274
17.359	0.02664	17.764	0.03057	18.168	0.03444
18.572	0.0383	18.976	0.04177	19.381	0.04511
19.785	0.04857	20.189	0.05194		

Table 3.1: *Results of model calculations in the local approach.*

^{96}Mo$(n,p)^{96}$Nb					
E_n (MeV)	σ (mb)	E_n (MeV)	σ (mb)	E_n (MeV)	σ (mb)
6.446	5.95E-05	6.7492	9.75E-05	7.0523	1.52E-04
7.3555	2.29E-04	7.6586	3.33E-04	7.9618	5.94E-04
8.2649	8.20E-04	8.5681	0.0011	8.8712	0.00145
9.1744	0.00187	9.4775	0.00236	9.7807	0.00294
10.084	0.00362	10.387	0.00439	10.69	0.00526
10.993	0.00623	11.296	0.00729	11.6	0.00846
11.903	0.00973	12.206	0.01103	12.509	0.01246
14.177	0.02311	15.844	0.02836	16.147	0.02815
16.45	0.02779	16.753	0.02746	16.955	0.02708
17.359	0.02663	17.764	0.02611	18.168	0.02559
18.572	0.02506	18.976	0.02446	19.381	0.02384
19.785	0.0233	20.189	0.02277	20.593	0.02223
20.997	0.0217	21.402	0.02113	21.806	0.02061
22.21	0.02009	22.614	0.01959	23.018	0.0191
23.423	0.01859	23.827	0.01814	24.231	0.0177
24.635	0.01728				
^{97}Mo$(n,d)^{96}$Nb					
E_n (MeV)	σ (mb)	E_n (MeV)	σ (mb)	E_n (MeV)	σ (mb)
9.4543	2.35E-09	9.7574	1.77E-08	10.061	9.60E-08
10.364	4.06E-07	10.667	1.41E-06	10.97	4.19E-06
11.273	1.09E-05	11.576	2.54E-05	11.879	6.73E-05
12.182	1.31E-04	12.485	2.38E-04	12.789	4.03E-04
13.092	6.46E-04	13.395	9.84E-04	13.698	0.00143
14.001	0.00201	14.304	0.00272	14.607	0.00358
14.91	0.00458	15.113	0.00534	15.517	0.00705
15.921	0.00902	16.325	0.01124	16.729	0.01369
17.133	0.01636	17.537	0.01922	17.942	0.02225
18.346	0.02541	18.75	0.02862	19.962	0.05309
20.367	0.05637	20.771	0.05913	21.175	0.06137
21.579	0.0631	21.983	0.06433	22.387	0.06511
22.792	0.06549				
^{97}Mo$(n,np)^{96}$Nb					
E_n	σ	E_n	σ	E_n	σ

Table 3.1: *Results of model calculations in the local approach.*

(MeV)	(mb)	(MeV)	(mb)	(MeV)	(mb)
11.879	1.36E-06	12.182	4.69E-06	12.485	1.31E-05
12.789	3.14E-05	13.092	6.56E-05	13.395	1.25E-04
13.698	2.21E-04	14.001	3.64E-04	14.304	5.67E-04
14.607	8.40E-04	14.91	0.00129	15.113	0.00161
15.517	0.00238	15.921	0.0033	16.325	0.00432
16.729	0.00551	17.133	0.00689	17.537	0.00836
17.942	0.00997	18.346	0.0117	18.75	0.01355
19.154	0.01552	19.558	0.01761	19.962	0.01968
20.367	0.02196	20.771	0.02429	21.175	0.02656
21.579	0.02895	21.983	0.03129	22.387	0.03369
22.792	0.0358				
^{97}Mo$(n,p)^{97m}$Nb					
E_n (MeV)	σ (mb)	E_n (MeV)	σ (mb)	E_n (MeV)	σ (mb)
6.7262	4.73E-05	7.0293	7.06E-05	7.3325	1.01E-04
7.6356	1.40E-04	7.9387	1.88E-04	8.8481	5.99E-04
9.1512	7.03E-04	9.4543	8.16E-04	9.7574	9.39E-04
10.061	0.00108	10.364	0.00123	10.667	0.00139
10.97	0.00156	11.273	0.00174	11.576	0.00192
11.879	0.00209	12.182	0.00229	12.485	0.0025
12.789	0.00273	13.092	0.00294	14.759	0.00509
16.729	0.00649	17.537	0.00645	17.942	0.0064
18.346	0.00633	18.75	0.00624	19.154	0.00615
19.558	0.00605	19.962	0.00592	20.367	0.0058
20.771	0.00568	21.175	0.00555	21.579	0.00542
21.983	0.0053	22.387	0.00519	22.792	0.00507
^{97}Mo$(n,p)^{97}$Nb					
E_n (MeV)	σ (mb)	E_n (MeV)	σ (mb)	E_n (MeV)	σ (mb)
6.7262	1.38E-04	7.0293	2.03E-04	7.3325	2.89E-04
7.6356	4.00E-04	7.9387	5.39E-04	8.394	0.0011
8.8481	0.00184	9.1512	0.0022	9.4543	0.00259
9.7574	0.00303	10.061	0.00351	10.364	0.00404
10.667	0.0046	10.97	0.00521	11.273	0.00584
11.576	0.00651	11.879	0.00716	12.182	0.00789
12.485	0.00864	12.789	0.00948	13.092	0.01025

Table 3.1: *Results of model calculations in the local approach.*

14.759	0.01849	16.729	0.02446	17.537	0.02457
17.942	0.02448	18.346	0.02431	18.75	0.02408
19.154	0.02379	19.558	0.02346	19.962	0.02304
20.367	0.02262	20.771	0.02218	21.175	0.02168
21.579	0.02121	21.983	0.02073	22.387	0.02028
22.792	0.01981				
^{98}Mo$(n,\alpha)^{95}$Zr					
E_n (MeV)	σ (mb)	E_n (MeV)	σ (mb)	E_n (MeV)	σ (mb)
6.4406	4.66E-05	6.7437	6.01E-05	7.0468	7.63E-05
7.3499	9.56E-05	7.653	1.15E-04	7.9561	1.42E-04
8.2591	1.76E-04	8.5622	2.19E-04	8.8653	3.24E-04
9.1684	4.13E-04	9.4715	5.24E-04	9.7746	6.57E-04
10.078	8.13E-04	10.381	9.93E-04	10.684	0.00119
10.987	0.00142	11.29	0.00166	11.593	0.00191
11.896	0.00218	12.805	0.00409	13.109	0.00453
13.412	0.00496	13.715	0.00526	14.018	0.00566
14.321	0.00603	14.624	0.00636	14.927	0.00665
15.23	0.00688	15.533	0.00707	15.836	0.0072
18.463	0.00834	21.09	0.00778		
^{98}Mo$(n,d)^{97m}$Nb					
E_n (MeV)	σ (mb)	E_n (MeV)	σ (mb)	E_n (MeV)	σ (mb)
10.684	4.42E-09	10.987	3.83E-08	11.29	1.92E-07
11.593	7.34E-07	11.896	2.28E-06	12.199	6.05E-06
12.502	1.41E-05	12.805	2.93E-05	13.109	5.57E-05
13.412	9.79E-05	13.715	1.61E-04	14.018	2.49E-04
14.321	3.68E-04	14.624	5.20E-04	14.927	7.10E-04
15.23	9.39E-04	15.533	0.00121	15.836	0.00152
16.139	0.00186	16.443	0.00224	16.746	0.00265
17.049	0.00309	17.352	0.00357	19.069	0.00955
19.473	0.01068	19.878	0.01167	20.282	0.01284
20.686	0.01386	21.09	0.01497		
^{98}Mo$(n,d)^{97}$Nb					
E_n (MeV)	σ (mb)	E_n (MeV)	σ (mb)	E_n (MeV)	σ (mb)
10.078	7.72E-10	10.381	4.91E-09	10.684	2.67E-08

Table 3.1: *Results of model calculations in the local approach.*

10.987	1.37E-07	11.29	5.56E-07	11.593	1.91E-06
11.896	5.66E-06	12.199	1.47E-05	12.502	3.43E-05
12.805	7.23E-05	13.109	1.40E-04	13.412	2.52E-04
13.715	4.23E-04	14.018	6.72E-04	14.321	0.00101
14.624	0.00146	14.927	0.00203	15.23	0.00273
15.533	0.00357	15.836	0.00455	16.139	0.00567
16.443	0.00694	16.746	0.00834	17.049	0.00986
17.352	0.01152	19.069	0.03223	19.473	0.03641
19.878	0.04019	20.282	0.04452		
^{98}Mo$(n,np)^{97m}$Nb					
E_n (MeV)	σ (mb)	E_n (MeV)	σ (mb)	E_n (MeV)	σ (mb)
13.109	9.28E-08	13.412	3.65E-07	13.715	1.06E-06
14.018	2.73E-06	14.321	6.14E-06	14.624	1.24E-05
14.927	2.33E-05	15.23	4.06E-05	15.533	6.73E-05
15.836	1.06E-04	16.139	1.60E-04	16.443	2.34E-04
16.746	3.28E-04	17.049	4.43E-04	17.352	5.85E-04
17.655	7.52E-04	17.857	8.90E-04	18.261	0.00118
18.665	0.0015	19.069	0.00186	19.473	0.00225
19.878	0.00267	20.282	0.00311	20.686	0.00357
21.09	0.00404				
^{98}Mo$(n,np)^{97}$Nb					
E_n (MeV)	σ (mb)	E_n (MeV)	σ (mb)	E_n (MeV)	σ (mb)
12.502	1.21E-06	12.805	4.19E-06	13.109	1.16E-05
13.412	2.77E-05	13.715	5.99E-05	14.018	1.14E-04
14.321	2.01E-04	14.624	3.29E-04	14.927	5.08E-04
15.23	7.42E-04	15.533	0.00104	15.836	0.00141
16.139	0.00183	16.443	0.00234	16.746	0.00292
17.049	0.00356	17.352	0.00426	17.655	0.00502
17.857	0.00558	18.261	0.00674	18.665	0.00796
19.069	0.00928	19.473	0.01068	19.878	0.01215
20.282	0.01367	20.686	0.01524	21.09	0.01686
^{98}Mo$(n,p)^{98m}$Nb					
E_n (MeV)	σ (mb)	E_n (MeV)	σ (mb)	E_n (MeV)	σ (mb)
8.8653	5.15E-05	9.1684	7.96E-05	9.4715	1.18E-04

Table 3.1: *Results of model calculations in the local approach.*

9.7746	1.68E-04	10.078	2.33E-04	10.381	3.14E-04
10.684	4.13E-04	10.987	5.30E-04	11.29	6.67E-04
11.593	8.26E-04	11.896	9.97E-04	12.199	0.0012
13.564	0.00349	14.927	0.00633	15.23	0.00668
15.533	0.00701	15.836	0.00731	16.139	0.00756
16.443	0.00781	16.746	0.00802	17.049	0.00822
17.352	0.00838	17.655	0.00852	17.857	0.00839
18.261	0.00853	18.665	0.0086	19.069	0.00866
19.473	0.00868	19.878	0.00868	20.282	0.00864
20.686	0.00858	21.09	0.00846		
^{100}Mo$(n,2n)^{99}$Mo					
E_n (MeV)	σ (mb)	E_n (MeV)	σ (mb)	E_n (MeV)	σ (mb)
9.3948	0.43335	9.6978	0.60303	10.001	0.75571
10.304	0.89119	10.607	1.0095	10.91	1.1113
11.213	1.1972	11.516	1.2679	11.819	1.325
12.122	1.3704	12.425	1.4069	13.334	1.421
13.637	1.4382	13.94	1.4529	14.243	1.4607
14.546	1.4696	14.849	1.4766	15.152	1.4799
15.455	1.4769	15.758	1.4626	16.061	1.4424
16.364	1.4155	16.667	1.3807	16.97	1.3383
17.273	1.2881	17.577	1.232	17.88	1.1712
18.183	1.1066	18.385	1.0594	18.789	0.97026
19.193	0.88517	19.597	0.80392	20.001	0.72843
20.405	0.65931	20.809	0.60443		
^{100}Mo$(n,\alpha)^{97}$Zr					
E_n (MeV)	σ (mb)	E_n (MeV)	σ (mb)	E_n (MeV)	σ (mb)
10.304	1.63E-04	10.607	2.18E-04	10.91	2.87E-04
11.213	3.70E-04	11.516	4.66E-04	12.274	9.66E-04
13.031	0.00166	13.334	0.0019	13.637	0.00215
13.94	0.00241	14.243	0.00265	14.546	0.00288
14.849	0.0031	15.152	0.0033	15.455	0.00348
16.061	0.00374	16.364	0.00384	16.97	0.00394
18.587	0.0047	19.597	0.00544	20.405	0.00523
20.809	0.0051				
^{100}Mo$(n,d)^{99m}$Nb					

Table 3.1: *Results of model calculations in the local approach.*

E_n (MeV)	σ (mb)	E_n (MeV)	σ (mb)	E_n (MeV)	σ (mb)
11.819	3.03E-08	12.122	1.58E-07	12.425	6.36E-07
12.728	2.08E-06	13.031	5.80E-06	13.334	1.41E-05
13.637	3.05E-05	13.94	5.98E-05	14.243	1.08E-04
14.546	1.79E-04	14.849	2.80E-04	15.152	4.13E-04
15.455	5.81E-04	15.758	7.82E-04	16.061	0.00102
16.364	0.00129	16.667	0.00159	16.97	0.00192
17.273	0.00229	17.577	0.00268	18.385	0.00506
18.789	0.00588	19.193	0.00675	19.597	0.00765
20.001	0.00844	20.405	0.00936	20.809	0.01017
^{100}Mo$(n,np)^{99m}$Nb					
E_n (MeV)	σ (mb)	E_n (MeV)	σ (mb)	E_n (MeV)	σ (mb)
14.243	6.22E-08	14.546	2.23E-07	14.849	6.56E-07
15.152	1.66E-06	15.455	3.71E-06	15.758	7.46E-06
16.061	1.38E-05	16.364	2.39E-05	16.667	3.88E-05
16.97	5.98E-05	17.273	8.81E-05	17.577	1.25E-04
17.88	1.70E-04	18.183	2.25E-04	18.385	2.67E-04
18.789	3.67E-04	19.193	4.85E-04	19.597	6.20E-04
20.001	7.71E-04	20.405	9.36E-04	20.809	0.00112
^{nat}Mo$(n,x)^{94}$Nb					
E_n (MeV)	σ (mb)	E_n (MeV)	σ (mb)	E_n (MeV)	σ (mb)
8.6	0.00118	8.7	0.00123	8.8	0.00129
8.9	0.00135	9	0.0014	9.1	0.00146
9.2	0.00152	9.3	0.00158	9.4	0.00164
9.5	0.0017	9.6	0.00176	9.7	0.00183
9.8	0.00189	9.9	0.00196	10	0.00202
10.1	0.00209	10.2	0.00216	10.3	0.00223
10.4	0.0023	10.5	0.00237	10.6	0.00244
10.7	0.00251	10.8	0.0026	10.9	0.00267
11	0.00274	11.1	0.00282	11.2	0.0029
11.3	0.00298	11.4	0.00305	11.5	0.00314
11.6	0.00322	11.7	0.00331	11.8	0.0034
11.9	0.0035	12	0.00359	12.1	0.00368
12.2	0.00376	12.3	0.00386	12.4	0.00396

Table 3.1: *Results of model calculations in the local approach.*

12.5	0.00407	12.6	0.00418	12.7	0.00428
12.8	0.0044	12.9	0.00452	13	0.00463
13.1	0.00475	13.2	0.00487	13.3	0.00499
13.4	0.00512	13.5	0.00525	13.6	0.0054
13.7	0.00555	13.8	0.00569	13.9	0.00587
14	0.00605	14.1	0.00622	14.2	0.00642
14.3	0.00662	14.4	0.00682	14.5	0.00704
14.6	0.00726	14.7	0.00751	14.8	0.00775
14.9	0.00796	15	0.00816	15.1	0.00837
15.2	0.00859	15.3	0.0088	15.4	0.00902
15.5	0.00924	15.6	0.00945	15.7	0.00967
15.8	0.00989	15.9	0.01014	16	0.01039
16.1	0.01064	16.2	0.01089	16.3	0.01104
16.4	0.01118	16.5	0.0114	16.6	0.01163
16.7	0.01186	16.8	0.0121	16.9	0.01235
17	0.01259	17.1	0.01285	17.2	0.0131
17.3	0.01337	17.4	0.01364	17.5	0.01391
17.6	0.01419	17.7	0.01446	17.8	0.01473
17.9	0.01501	18	0.01528	18.1	0.01557
18.2	0.01585	18.3	0.01613	18.4	0.01641
18.5	0.01669	18.6	0.01698	18.7	0.01726
18.8	0.01755	18.9	0.01783	19	0.01811
20.2	0.02456	20.3	0.02483	20.4	0.02508
20.5	0.02534	20.6	0.0256	20.7	0.02585
20.8	0.02607				

OECD PUBLICATIONS, 2 rue André-Pascal, 75775 PARIS CEDEX 16
Printed in France.